Calcined clays and marlstones as supplementary cementitious materials

Victor Poussardin

THÈSE DE DOCTORAT DE

L'ÉCOLE CENTRALE DE NANTES
Et l'UNIVERSITE DE SHERBROOKE

ECOLE DOCTORALE N° 602
Sciences pour l'Ingénieur
Spécialité : Génie civil

Par
Victor POUSSARDIN

Utilisation d'argiles et de marnes calcinées dans le développement de ciments composés

Thèse présentée et soutenue à l'Institut des Matériaux de Nantes, le 30 septembre 2022
Unité de recherche : Département GERS-GIE, Université Gustave Eiffel, Campus de Nantes

Rapporteurs avant soutenance :

Jean-Baptiste d'ESPINOSE de LACAILLERIE	Professeur, ESPCI Paris
Richard GAGNE	Professeur, Université de Sherbrooke, Canada

Composition du Jury :

Président :	Ahmed LOUKILI	Professeur des universités, Ecole Centrale de Nantes
Examinateurs :	Siham KAMALI-BERNARD	Maitre de conférences, HDR, INSA Rennes
	William WILSON	Professeur, Université de Sherbrooke, Canada
Dir. de thèse :	Dimitri DENEELE	Directeur de recherche, Université Gustave Eiffel, Bouguenais
Dir. de thèse :	Arezki TAGNIT-HAMOU	Professeur, Université de Sherbrooke, Canada
Co-encadrant :	Michael PARIS	Ingénieur de recherche, Nantes Université

Remerciements

« Les commencements ont des charmes inexprimables. » **Molière (Dom Juan)**

De par sa durée et l'investissement qu'elle implique, une thèse de doctorat constitue le fil conducteur d'une tranche de vie. Une période charnière, au crépuscule d'un jeune étudiant candide et à l'aube d'un scientifique plus raisonné. De nombreuses personnes se sont retrouvées impliquées, parfois de manière fortuite, dans cette belle aventure. Ce sont ces mêmes que je souhaite remercier aujourd'hui.

Merci tout d'abord à mes directeurs, Dimitri et Arezki pour leur confiance indéfectible dans la réalisation de cette thèse. Merci Dimitri pour ta disponibilité, ton écoute, ta franchise et ta bienveillance. Tes précieux conseils ont eu un rôle prépondérant dans la réussite de mon travail, tant pour l'aspect professionnel que personnel. Merci Arezki pour ton soutien, ta patience et l'attention portée à mes travaux.

Merci à mes encadrants, Michael et William pour la qualité de nos échanges, l'appréciation de mon travail, et les valeurs partagées. Merci Michael de m'avoir fait profiter de tes compétences et de m'avoir orienté dans la bonne direction. Merci William d'avoir su me motiver et de m'avoir aidé à progresser.

J'adresse tous mes remerciements à Monsieur d'Espinose et Monsieur Gagné pour l'honneur qu'ils m'ont fait en acceptant d'être rapporteurs de cette thèse. J'exprime ma gratitude à Madame Kamali-Bernard et Monsieur William Wilson qui ont accepté d'être examinateurs.

Enfin, ce projet n'aurait pu aboutir sans l'affection et l'implication de mes parents et mes proches. J'ai eu la chance de pouvoir compter sur leur soutien, tant affectueux que financier ainsi que leurs encouragements et la patience dont ils ont fait preuve, particulièrement lors des difficultés rencontrées et des moments de doute.

Sommaire

Résumés

Résumé en français

L'utilisation de Supplementary Cementitious Materials (SCMs) en substitution du clinker est une technologie aujourd'hui bien connue qui permet de réduire le coût environnemental du ciment. Parmi les SCMs largement utilisés aujourd'hui on retrouve les cendres volantes, les laitiers de hauts fourneaux ou encore la poudre de verre. Dans les dernières années, un intérêt grandissant s'est développé pour l'utilisation d'argiles calcinées comme ajouts cimentaires, notamment du fait de leur forte réactivité et de leur grande disponibilité. Ce projet de thèse s'intéresse à l'utilisation d'argiles et de marnes calcinées comme ajouts cimentaires. L'objectif principal est d'identifier de nouveaux échantillons susceptibles de présenter un intérêt pour une utilisation comme SCMs. Pour ce faire, une approche multi-échelle macro/micro est utilisée afin d'étudier de manière précise la calcination, la réactivité pouzzolanique et le comportement en système cimentaire de ces nouveaux échantillons. Il a été possible de démontrer que les marnes (malgré leur composition minéralogique complexe) sont des matériaux qui peuvent être utilisés comme ajout cimentaire après calcination, et ce, même s'ils contiennent une faible proportion d'argiles. Par la suite, il a été démontré que la palygorskite est une argile à haut potentiel pour une utilisation comme ajout cimentaire après calcination, et peut être considérée comme une alternative viable au métakaolin. L'étude poussée de l'utilisation de palygorskites calcinées comme ajouts cimentaires a également permis d'apporter de nouvelles connaissances fondamentales sur la compréhension des mécanismes impliqués lors de la calcination de ce type de matériaux.

Résumé en anglais

The use of Supplementary Cementitious Materials (SCMs) as a substitute for clinker is a well-known technology that can reduce the environmental cost of cement. Among the SCMs widely used today are fly ash, blast furnace slag and glass powder. In recent years, there has been a growing interest in the use of calcined clays as SCMs, particularly due to their high reactivity and availability. This thesis project focuses on the use of calcined clays and marls as supplementary cementitious materials. The main objective is to identify new samples that could be of interest for use as SCMs. To this end, a multi-scale macro/micro approach is used to study the calcination, pozzolanic reactivity and performance in cementitious systems of these new materials. It was possible to demonstrate that marlstones (despite their complex mineralogical composition) have the potential to be used as supplementary cementitious materials after calcination, even with a low proportion of clays. Subsequently, it was shown that palygorskite is a high potential clay for use as a supplementary cementitious material after calcination, and can be considered as a viable alternative to metakaolin. The extensive study of the use of calcined palygorskites as SCMs has also provided new fundamental insights into the understanding of the mechanisms involved in the calcination of this type of material.

Introduction

Contexte général

L'un des objectifs principaux de l'accord de Paris sur le climat est de parvenir à une diminution rapide des émissions de dioxyde de carbone tout en permettant aux différents signataires de répondre à leurs besoins économiques, industriels et humains. En effet, les générations présentes doivent pouvoir répondre aux enjeux actuels sans compromettre la capacité des générations futures à répondre aux leurs. L'urbanisation généralisée qui accompagne le développement économique se traduit par la construction rapide d'infrastructures industrielles et de transport, ce qui entraine une importante augmentation de la demande en ciment [1]. Le ciment Portland, constituant majeur du béton, est de loin le matériau de construction le plus utilisé du fait de sa facilité de fabrication et de sa simplicité d'usage. Au cours des 65 dernières années, la consommation mondiale en ciment a été décuplée [2]. Cela n'est pas sans conséquence puisqu'on estime que le ciment compte pour 36% des 7,7 milliards de tonnes de CO_2 émises annuellement par le secteur de la construction [3], ce qui représente environ 8% des émissions totales de CO_2 d'origine anthropique [4,5].

Pourtant, le béton (dont le ciment est le constituant principal) reste le matériau de construction le moins carboné, puisque 1kg de béton émet en moyenne 0,13 kg de CO_2. En comparaison, 1 kg de bois ou d'acier émettent respectivement 0,46 et 2,8 kg de CO_2 [6]. Le fait que l'industrie cimentière soit responsable d'autant d'émissions de CO_2 relève en réalité d'une question de quantités. En effet, on estime qu'en 2019 environ 4,2 milliards de tonnes de ciment ont été produites dans le monde [7]. Ce n'est donc pas le ciment en lui-même, mais son utilisation intensive et systématique qui en fait un matériau de construction polluant. Dans ce contexte, les industries cimentières se tournent vers la recherche et le développement d'innovations pouvant permettre de réduire le coût environnemental du ciment. Une baisse de quelques % de la quantité de CO_2 émise lors de la fabrication d'1kg de ciment aurait un impact significatif sur les émissions mondiales de CO_2 d'origine anthropique, à condition que ces innovations soient mises en place à grande échelle.

Le point critique de la fabrication du ciment en termes d'émissions de CO_2 est la calcination. Atteindre et maintenir une température de 1450°C n'est pas anodin puisque cela va nécessiter

l'utilisation d'une importante quantité d'énergie, qui provient majoritairement de combustibles d'origine fossile. On estime que 1/3 du CO_2 émis lors de la fabrication du ciment provient des combustibles utilisés pour alimenter les fours. Une première manière de diminuer l'empreinte environnementale de ciment consiste donc à substituer une partie des combustibles fossiles traditionnels (dont le charbon) utilisés dans les fours des cimenteries par des combustibles alternatifs, plus faibles en carbone et/ou issus de la valorisation de ressources secondaires considérées comme déchets [8]. Les 2/3 restants du CO_2 émis lors de la calcination proviennent de la décarbonatation du calcaire présent dans le mélange de base. Sous l'effet de la température le carbonate de calcium ($CaCO_3$) qui constitue très largement la roche calcaire va se décarbonater et former de la chaux vive (CaO) et émettre du CO_2 sous forme gazeuse directement dans l'atmosphère. Une autre innovation consiste donc à capturer le CO_2 émis lors de la décarbonatation du calcaire directement au niveau du four de la cimenterie. Mais la mise en place de cette technologie à l'ensemble des cimenteries représente un coût financier très important, sans oublier que ce système de capture ne répond pas à l'enjeu du stockage à long terme ou même de la réutilisation du CO_2 capturé [9]. Différentes technologies sont donc aujourd'hui à l'étude pour pouvoir diminuer l'empreinte environnementale du ciment telles que la diminution du taux de clinker, la substitution des combustibles fossiles ou encore les systèmes de capture et de stockage du CO_2. La figure 1-1 est extraite du plan de transition sectoriel de l'industrie cimentière en France. Elle liste une partie des technologies envisagées pour diminuer l'empreinte carbone de la production du ciment et les compare entre elles en fonction de leur temps de mise en place et de leur coût financier [10].

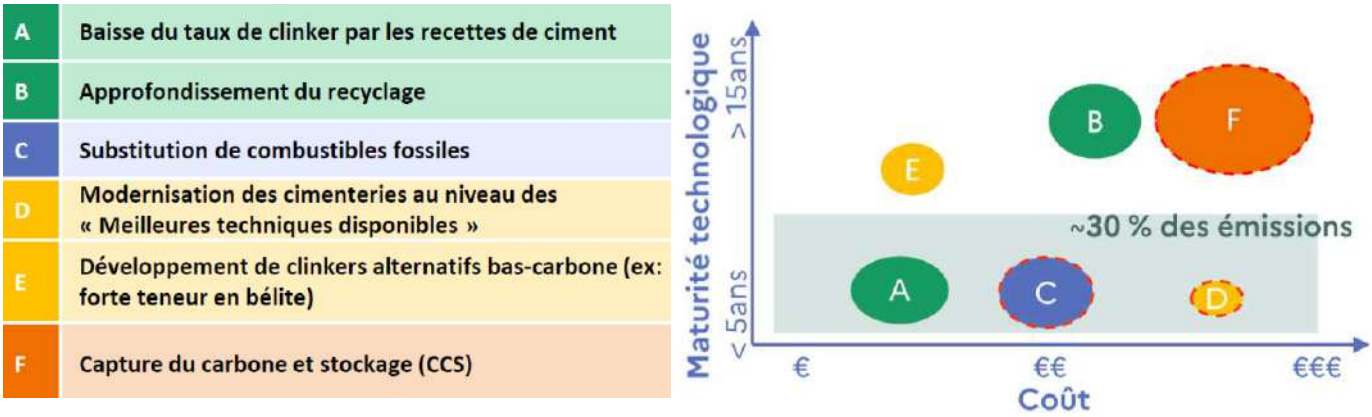

Figure 1: Comparaison des principales technologies de réduction des émissions de CO_2 de l'industrie cimentière [10].

La première information importante de cette figure est que la technologie de capture et de stockage du carbone ne semble pas être assez mature et représente un coût financier trop important pour être une vraie innovation de rupture à court terme. En revanche, la modernisation des installations existantes ainsi que la substitution des combustibles fossiles sont des choses qui peuvent être réalisées dès aujourd'hui et qui présentent un potentiel de réduction des émissions de CO_2 important. L'autre piste importante mise en avant est la baisse du taux de clinker dans le ciment, une technologie qui pourrait être mise en place dès aujourd'hui et qui présenterait un coût financier relativement faible.

L'utilisation de Supplementary Cementitious Materials (SCMs) en substitution du clinker est une technologie aujourd'hui bien connue. Ces ajouts cimentaires permettent de diminuer la proportion de clinker (constituant principal du ciment dont la fabrication entraine la majorité des rejets de CO_2) sans imputer de manière importante les propriétés mécaniques ou encore la durabilité du ciment. Parmi les SCMs largement utilisés, on retrouve les laitiers de hauts fourneaux [11], les cendres volantes de centrale électrique [12], ou encore les argiles calcinées. Les ressources en laitiers de hauts fourneaux ne sont pas assez abondantes pour être utilisées de manière durable et la transition énergétique limite à juste titre la disponibilité des ressources en cendres volantes provenant de la combustion du charbon [13]. En revanche, les réserves d'argiles avec un potentiel pour la calcination sont considérables et réparties de manière homogène [13], ce qui en fait une ressource de premier choix pour une utilisation comme SCM.

Originalité et objectifs

La majorité des études qui ont été menées ces dernières années sur la réactivité de différents types d'argiles calcinées dans des systèmes cimentaires s'est intéressée au métakaolin [14–16], aux smectites calcinées [17,18] et aux illites calcinées [19–21]. Il y a un manque d'intérêt significatif de la communauté scientifique pour l'étude d'autres types d'argiles. En cause, il y a la répartition de ces argiles qui est parfois très hétérogène et la concurrence industrielle qui peut limiter leur disponibilité. L'autre raison importante est que ces argiles sont souvent associées à d'autres minéraux tels que des carbonates, ce qui crée des systèmes à plusieurs phases relativement complexes. Cependant, l'étude de ces argiles dites « peu

conventionnelles » peut présenter un fort intérêt, notamment dans des contextes de valorisation de ressources dites secondaires et considérées comme déchets.

L'objectif général de ce projet de thèse est d'étudier l'utilisation d'échantillons argileux calcinés comme ajouts cimentaires dans des ciments composés, avec notamment un intérêt fort pour la valorisation d'échantillons naturels complexes contenant des phases argileuses dites peu conventionnelles. La réussite de ce projet de thèse amènera de nouvelles connaissances fondamentales sur la calcination et la réactivité en système cimentaire d'argiles peu ou pas étudiées à l'heure actuelle et permettra d'ouvrir de nouvelles voies de valorisation de ressources secondaires considérées comme déchets.

Fil conducteur du manuscrit de thèse

Après l'introduction, ce manuscrit de thèse va débuter avec un état de l'art explorant les bases du ciment Portland, son hydratation et les solutions existantes pour diminuer son empreinte environnementale. Un descriptif général des minéraux argileux, des marnes et de leur utilisation comme ajout cimentaire permettra de situer ce projet de thèse en comparaison de ce qui a déjà été fait sur le sujet. Le corps de cette thèse sera ensuite basé sur 5 articles scientifiques qui permettront de progressivement développer une compréhension des modifications physico-chimiques qui ont lieu lors de la calcination et de l'utilisation comme ajouts cimentaires de différents échantillons argileux. En premier, le chapitre 2 traite de la calcination d'une marne dolomitique naturelle contenant de la palygorskite et de la smectite. Il consiste en une description poussée des modifications physico-chimiques qui ont lieu lors du traitement thermique de ce matériau et démontre la formation de plusieurs phases potentiellement réactives en système cimentaire (palygorskite calcinée, smectite calcinée et C_2S). Le chapitre 3 est la continuité directe du chapitre 2 et il s'intéresse à l'auto-réactivité dans l'eau après calcination de ce même échantillon, en vue d'une utilisation comme ajout cimentaire. Il démontre que les phases argileuses calcinées (palygorskite et smectite) ainsi que les phases néoformées à l'issue de la calcination (C_2S) présentent un potentiel réactif en milieu cimentaire. Le chapitre 4 est une étude comparative de la marne dolomitique étudiée dans les chapitres 2 et 3 avec une autre marne dolomitique (issue du même site minier) contenant cette fois-ci uniquement de la smectite. La comparaison de la calcination, de l'auto-réactivité

et des performances mécaniques en système cimentaire permet de démontrer que la marne contenant de la palygorskite en plus de la smectite a une meilleure réactivité, comparativement à celle contenant uniquement de la smectite. Cela laisse présager que la palygorskite est une argile à haut potentiel réactif à tester pour une utilisation comme ajout cimentaire. Le chapitre 5 s'intéresse à des échantillons contenant des teneurs en palygorskite plus élevées que l'échantillon marneux étudié dans les chapitres 2, 3 et 4. Il permet de démontrer une importante amélioration des performances mécaniques (proportionnelle à la pureté des échantillons) sur des ciments composés incorporant ces palygorskites calcinées, ce qui confirme la forte réactivité pouzzolanique de cette argile calcinée. Le chapitre 6 a pour objectif de comprendre l'origine de cette forte réactivité en comparant la calcination, la réactivité pouzzolanique et les performances mécaniques en système cimentaire d'une palygorskite dite « modèle » à une kaolinite pure. Les résultats prouvent que la palygorskite peut effectivement être considérée comme une argile hautement réactive après calcination et permettent d'établir une corrélation entre les modifications physico-chimiques induites par la calcination, la réactivité pouzzolanique et les performances mécaniques en système cimentaire. Finalement, la conclusion résume les principales avancées et contributions de ce projet de thèse avant de suggérer de nouvelles pistes de réflexion.

Références

[1] Y. Cancio Díaz, S. Sánchez Berriel, U. Heierli, A.R. Favier, I.R. Sánchez Machado, K.L. Scrivener, J.F. Martirena Hernández, G. Habert, Limestone calcined clay cement as a low-carbon solution to meet expanding cement demand in emerging economies, Development Engineering. 2 (2017) 82–91. https://doi.org/10.1016/j.deveng.2017.06.001.

[2] P.J.M. Monteiro, S.A. Miller, A. Horvath, Towards sustainable concrete, Nature Mater. 16 (2017) 698–699. https://doi.org/10.1038/nmat4930.

[3] B. Bajželj, J.M. Allwood, J.M. Cullen, Designing Climate Change Mitigation Plans That Add Up, Environ. Sci. Technol. 47 (2013) 8062–8069. https://doi.org/10.1021/es400399h.

[4] S.A. Miller, V.M. John, S.A. Pacca, A. Horvath, Carbon dioxide reduction potential in the global cement industry by 2050, Cement and Concrete Research. 114 (2018) 115–124. https://doi.org/10.1016/j.cemconres.2017.08.026.

[5] D.N. Huntzinger, T.D. Eatmon, A life-cycle assessment of Portland cement manufacturing: comparing the traditional process with alternative technologies, Journal of Cleaner Production. 17 (2009) 668–675. https://doi.org/10.1016/j.jclepro.2008.04.007.

[6] G.P. Hammond, C.I. Jones, Embodied energy and carbon in construction materials, Proceedings of the Institution of Civil Engineers - Energy. 161 (2008) 87–98. https://doi.org/10.1680/ener.2008.161.2.87.

[7] Global Cement Magazine, (n.d.) 11.

[8] E. Mokrzycki, Alternative fuels for the cement industry, Applied Energy. (2003) 6.

[9] K. Vatopoulos, E. Tzimas, Assessment of CO2 capture technologies in cement manufacturing process, Journal of Cleaner Production. 32 (2012) 251–261. https://doi.org/10.1016/j.jclepro.2012.03.013.

[10] Rapport final du Plan de transition sectoriel de l'industrie cimentière en France - La librairie ADEME, (n.d.). https://librairie.ademe.fr/changement-climatique-et-energie/5234-rapport-final-du-plan-de-transition-sectoriel-de-l-industrie-cimentiere-en-france.html#/44-type_de_produit-format_electronique (accessed May 19, 2022).

[11] M. Behim, B. Redjel, R. Jauberthie, Réactivitié du laitier de hauts fourneaux d'Annaba (Algérie) en substitution partielle du ciment, (2002).

[12] Z.T. Yao, X.S. Ji, P.K. Sarker, J.H. Tang, L.Q. Ge, M.S. Xia, Y.Q. Xi, A comprehensive review on the applications of coal fly ash, Earth-Science Reviews. 141 (2015) 105–121. https://doi.org/10.1016/j.earscirev.2014.11.016.

[13] K. Scrivener, F. Martirena, S. Bishnoi, S. Maity, Calcined clay limestone cements (LC3), Cement and Concrete Research. 114 (2018) 49–56. https://doi.org/10.1016/j.cemconres.2017.08.017.

[14] R.S. Almenares, L.M. Vizcaíno, S. Damas, A. Mathieu, A. Alujas, F. Martirena, Industrial calcination of kaolinitic clays to make reactive pozzolans, Case Studies in Construction Materials. 6 (2017) 225–232. https://doi.org/10.1016/j.cscm.2017.03.005.

[15] A. Alujas, R. Fernández, R. Quintana, K.L. Scrivener, F. Martirena, Pozzolanic reactivity of low grade kaolinitic clays: Influence of calcination temperature and impact of calcination products on OPC hydration, Applied Clay Science. 108 (2015) 94–101. https://doi.org/10.1016/j.clay.2015.01.028.

[16] H. El-Diadamony, A.A. Amer, T.M. Sokkary, S. El-Hoseny, Hydration and characteristics of metakaolin pozzolanic cement pastes, HBRC Journal. 14 (2018) 150–158. https://doi.org/10.1016/j.hbrcj.2015.05.005.

[17] I.W.M. Brown, K.J.D. MacKenzie, R.H. Meinhold, The thermal reactions of montmorillonite studied by high-resolution solid-state 29Si and 27Al NMR, (1987) 3265–3275.

[18] N. Garg, J. Skibsted, Thermal Activation of a Pure Montmorillonite Clay and Its Reactivity in Cementitious Systems, The Journal of Physical Chemistry C. 118 (2014) 11464–11477. https://doi.org/10.1021/jp502529d.

[19] R. Fernandez, F. Martirena, K.L. Scrivener, The origin of the pozzolanic activity of calcined clay minerals: A comparison between kaolinite, illite and montmorillonite, Cement and Concrete Research. 41 (2011) 113–122. https://doi.org/10.1016/j.cemconres.2010.09.013.

[20] N. Garg, J. Skibsted, Pozzolanic reactivity of a calcined interstratified illite/smectite (70/30) clay, Cement and Concrete Research. 79 (2016) 101–111. https://doi.org/10.1016/j.cemconres.2015.08.006.

[21] S. Hollanders, R. Adriaens, J. Skibsted, Ö. Cizer, J. Elsen, Pozzolanic reactivity of pure calcined clays, Applied Clay Science. 132–133 (2016) 552–560. https://doi.org/10.1016/j.clay.2016.08.003.

Chapitre 1 – Etat de l'art

Dans ce projet de thèse portant sur l'utilisation de marnes et d'argiles calcinées en remplacement du ciment Portland, il apparaît important de définir clairement ces termes et de préciser les objectifs de l'étude en synthétisant ce qui existe déjà dans la littérature. La première partie de cet état de l'art sera consacrée à une description générale du matériau cimentaire, de sa fabrication, de son impact environnemental et des technologies permettant de réduire ce dernier. La seconde partie traitera des argiles en général avec notamment un focus sur deux minéraux argileux que sont la smectite et la palygorskite. La troisième partie traitera de l'utilisation d'argiles calcinées en remplacement du ciment, avec une description de l'étape de calcination, de la réactivité pouzzolanique et des récentes études réalisées sur le sujet. La quatrième partie s'intéressera aux marnes et à leur utilisation comme ajout cimentaire. Enfin la dernière partie présentera les verrous scientifiques actuels sur le sujet et les enjeux/problématiques auxquels ce projet de thèse tentera de répondre.

1.1. Le ciment

Selon la norme NF EN 197-1 [1] le ciment est un liant hydraulique, c'est-à-dire un matériau minéral finement moulu qui, gâché avec de l'eau, forme une pâte qui fait prise et durcit par suite de réactions et de processus d'hydratation. Après son durcissement, le ciment hydraté conserve sa résistance et sa stabilité, même sous l'eau.

1.1.1. Fabrication du clinker et du ciment

Le clinker est le principal constituant du ciment portland, il se présente sous la forme de nodules centimétriques durs et cristallisés. Sa fabrication est le fruit de la réaction de clinkérisation qui intervient lors de la cuisson d'un mélange contenant du calcaire et de l'argile, aussi appelé « cru », à très haute température (1450°C). Le mélange doit permettre de réunir les éléments principaux selon des dosages préétablis : la chaux (65%), la silice (20%), l'alumine (10%) et l'oxyde de fer (5%) [2]. Les différentes étapes de la fabrication du ciment sont présentées ci-dessous :

L'extraction et le concassage : Le calcaire et l'argile sont extraits de carrières et les blocs obtenus sont concassés.

La préparation de la matière première : Les grains de calcaire et d'argile sont mélangés après broyage dans des proportions définies (80% / 20% généralement) en un mélange très fin appelé le cru.

La cuisson du cru : Le cru est ensuite introduit en amont dans un four rotatif. Il va alors circuler grâce à un dispositif de conduite et va être progressivement chauffé jusqu'à atteindre la température de clinkérisation. Lors de cette cuisson quatre étapes se distinguent :

- Décarbonatation : Elle se produit à des températures comprises entre 700 et 1000°C, le calcaire se décompose pour former de l'oxyde de calcium ($CaCO_3$ ➔ $CaO + CO_2$). Cette réaction de décarbonatation est responsable d'environ les 2/3 des émissions de CO_2 associées à la fabrication du ciment [3]. Il est important de noter que dans les nouvelles installations, cette étape se fait dans un « preheater » en amont du four rotatif

- Phase de transition : L'oxyde de calcium (CaO) produit lors de l'étape précédente se combine avec le silicium et l'aluminium de l'argile pour former de la bélite (silicate bicalcique impur ou C_2S de formule Ca_2SiO_4) et une solution solide d'aluminates de calcium. Ces réactions ont lieu à l'état solide.

- Phase de cuisson : La température de la matière monte à 1450°C. A partir de 1300°C le silicate bicalcique (Ca_2SiO_4) réagit avec une partie de l'oxyde de calcium (CaO) non combiné pour former du silicate tricalcique (Alite, C_3S impur de formule Ca_3SiO_5). Cette réaction est très endothermique, c'est pourquoi elle nécessite de telles températures. Au même moment, le fer et l'alumine se combinent au CaO sous forme liquide, on appelle cette phase interstitielle le fondant.

- La trempe : La matière est brusquement refroidie à l'air de 1450°C à environ 100°C en quelques minutes, on obtient alors le clinker. Cette étape de trempe a pour but de figer les espèces minérales qui seraient susceptibles de se décomposer à température

ambiante. Par exemple, la phase C_3S se décomposerait en C_2S et CaO. Les aluminates (C_3A et C_4AF de formules génériques $Ca_3Al_2O_6$ et $Ca_4Al_2Fe_2O_{10}$ respectivement mais qui possèdent des rapports Al/Fe variables) qui étaient sous forme liquide (phase interstitielle) vont servir de liant aux cristaux de silicates lors de ce refroidissement brutal.

Lors de ces premières étapes de la fabrication du clinker, différentes réactions vont se produire afin de former les phases anhydres qui le composent. La figure 1-1 présente un diagramme de l'évolution des phases minérales durant l'étape de clinkérisation d'un ciment Portland :

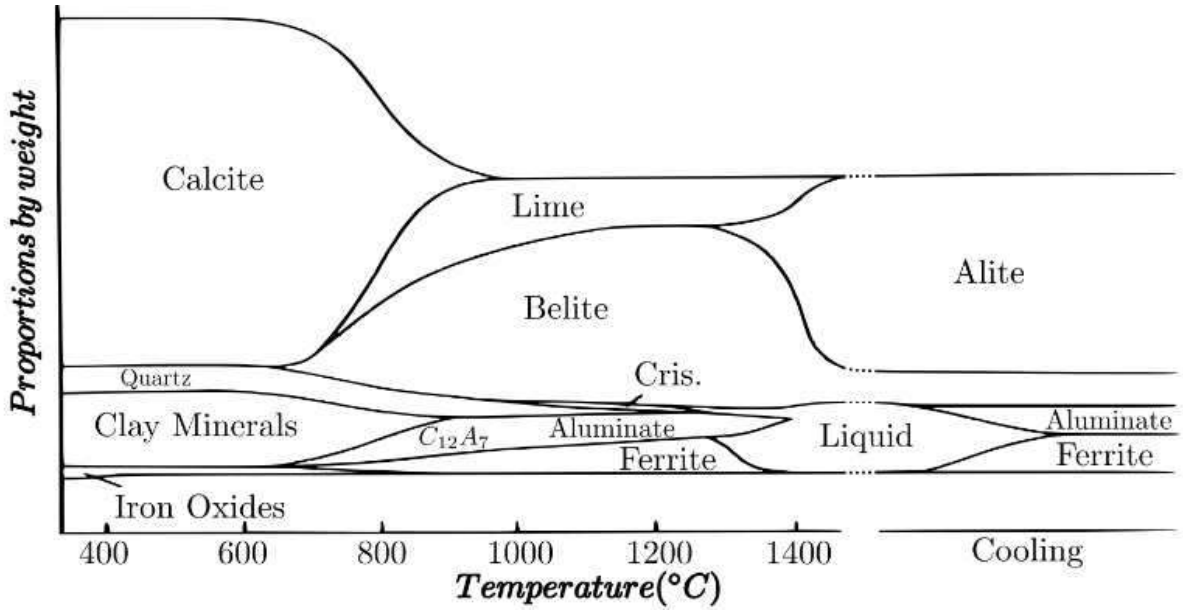

Figure 1-1 : Diagramme de l'évolution des phases minérales au cours de la clinkérisation [4].

Avec l'augmentation de la température, les phases minérales initiales (calcite, quartz, minéraux argileux, oxydes de fer) vont se recombiner pour former les nouvelles phases cimentaires anhydres (alite, bélite, aluminate, ferrite) qui composent le clinker.

Le produit obtenu (clinker) a généralement la composition chimique massique suivante : 67% CaO, 22% SiO_2, 5% Al_2O_3, 3% Fe_2O_3, et 3% d'autres composants. Il est composé de différentes phases présentes dans différentes proportions [5] :

- 50 à 65% d'alite

- 15 à 20% de bélite
- 5 à 15% d'aluminate tricalcique
- 5 à 10% d'aluminoferrite tétracalcique

L'hydratation de ces phases dites « majeures » va être à l'origine des propriétés du ciment durci. Il y a également la présence de phases en plus faibles proportions (3%) dites « mineures » telles que les sulfates alcalins et l'oxyde de calcium [5].

Les différentes phases anhydres ne vont pas avoir la même réactivité en fonction de leur composition chimique et de leur minéralogie. Leur hydratation va donc contribuer plus ou moins aux résistances finales. Le tableau 1-1 classifie les phases majeures du clinker en fonction de leurs caractéristiques et de leur contribution à la résistance une fois hydratées :

Phases	**C_3S**	**C_2S**	**C_3A**	**C_4AF**
Formule chimique idéale théorique	Ca_3SiO_5	Ca_2SiO_4	$Ca_3Al_2O_6$	$Ca_4Al_2Fe_2O_{10}$
Nom technique	Alite	Bélite	Phase aluminate	Phase ferrite
Réactivité	Elevée	Faible	Très élevée	Faible
Impuretés	Al_2O_3, Fe_2O_3, MgO	Al_2O_3, Fe_2O_3, Na_2O, K_2O, SO_3	Fe_2O_3, Na_2O, K_2O, MgO	MgO, SiO_2, TiO_2
Contribution à la résistance	Forte à jeune âge	Forte à un âge très avancé	Forte à jeune âge	Très faible

Tableau 1-1 : Phases majeures du ciment portland et leurs caractéristiques [6].

On peut voir que les deux phases les plus réactives sont l'alite et la phase aluminate. Elles vont toutes les deux contribuer aux résistances à jeune âge. La bélite en revanche va surtout participer aux résistances à long terme tandis que la phase ferrite n'aura qu'une très faible contribution de manière générale.

Le broyage : C'est la dernière étape de la fabrication, le clinker obtenu est broyé avec du sulfate de calcium (environ 5%) afin d'obtenir du ciment portland. L'ajout de gypse va permettre de ralentir la prise du ciment pour permettre la fabrication et le transport du béton sans influer sur le développement ultérieur des résistances mécaniques. Le ciment ensuite produit va avoir la capacité de former une pâte qui fait prise et durcit lors du processus d'hydratation.

Ces différentes étapes et notamment la décarbonatation du calcaire vont entrainer l'émission d'importantes quantités de dioxyde de carbone et participer grandement aux émissions mondiales de CO_2 puisqu'on estime que l'industrie cimentière est responsable de 5 à 8% de ces émissions mondiales [7,8].

1.1.2. Les ciments composés et les types d'ajouts cimentaires

Les ciments composés sont des ciments dont une partie du clinker est substituée par de nouvelles ressources que l'on appelle « Supplementary Cemetitious Materials » (SCMs). Parmi les principaux SCMs actuellement utilisés dans l'industrie cimentière, on retrouve les laitiers de hauts fourneaux, les cendres volantes de centrale électrique ou encore la poudre de verre.

1.1.2.1. Les laitiers de hauts fourneaux

Ce sont des sous-produits de l'élaboration de la fonte, on estime que la production d'une tonne de fonte brute entraine la production de 260 à 280 kg de laitiers de hauts fourneaux [9]. Ils sont principalement formés de constituants non ferreux, des fondants et des cendres de coke [10]. Il existe deux technologies différentes de traitement de ces laitiers de hauts fourneaux [11]. Ils peuvent être refroidis par air et être utilisés pour des applications de remplissage comme granulats pour bétons et bitumes par exemple [12,13], ou bien subir une trempe à l'eau puis être broyés afin d'obtenir des laitiers granulés de hauts fourneaux qui sont d'excellents SCMs. La figure 1-2 présente l'évolution de la résistance à la compression de différentes pâtes de ciments réalisées avec différents % de laitiers granulés de hauts fourneaux (ratio eau/ciment = 0.44) en fonction du temps d'hydratation [14] :

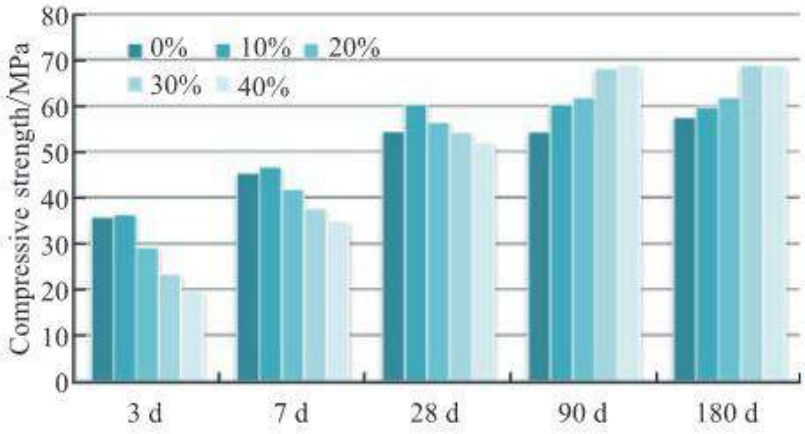

Figure 1-2 : Effet de l'ajout de laitiers de hauts fourneaux granulés sur les résistances à la compression de pâtes de ciments [14].

Le remplacement jusqu'à 40% du ciment Portland par du laitier granulé de hauts fourneaux permet une amélioration de la résistance à la compression à 90 et 180j. En revanche, même avec un taux de remplacement de seulement 20%, la résistance à la compression à 3 et 7 jours est inférieure à la référence 100% ciment. Cette inertie dans la réactivité des laitiers granulés de hauts fourneaux s'explique par le fait que la réaction pouzzolanique ne peut se mettre en place qu'une fois que les réactions d'hydratation du ciment ont eu lieu [15]. L'autre raison est qu'il peut y avoir formation d'un gel imperméable de silice et d'alumine amorphe autour des particules de laitiers, ralentissant ainsi leur dissolution et leur réaction [16]. La forte réactivité (hydraulique et pouzzolanique) des laitiers de hauts fourneaux a permis des taux de remplacements importants du ciment portland. On estime que l'utilisation de ces laitiers permets une réduction des émissions globales de CO_2 de la fabrication du ciment pouvant atteindre 48 % [11]. De plus, l'utilisation de laitiers de hauts fourneaux granulés comme SCM permet d'améliorer les propriétés techniques du ciment telles que la dureté, la perméabilité et la résistance à la corrosion et aux attaques chimiques (en particulier aux sulfates) [17,18].

L'utilisation de laitiers de hauts fourneaux en remplacement du ciment n'en est plus au stade de développement. Par exemple, la société ECOCEM qui est le premier producteur européen indépendant de laitier moulu de haut-fourneau a mis au point un ciment CEM III/C qui contient plus de 85% de laitier de haut-fourneau moulu [19]. De par sa forte proportion en laitier, ce ciment présente une très faible chaleur d'hydratation ainsi qu'une très haute résistance aux attaques chimiques et en particulier les sulfates [20].

Les réserves mondiales de laitiers de hauts fourneaux sont d'environ 330 Mt/an et la disponibilité de ce SCM devrait diminuer dans les prochaines années avec l'augmentation du recyclage de l'acier et l'introduction de nouvelles technologies de productions plus efficaces [21]. A l'heure actuelle plus de 90% des laitiers de hauts fourneaux conformes aux standards sont déjà utilisés comme SCM soit en remplacement du ciment, ou comme ajout dans le béton ou d'autres mélanges cimentaires [22,23]. Le potentiel de réduction des émissions mondiales de CO_2 par l'utilisation de laitiers de hauts fourneaux comme SCM est cependant relativement faible du fait de la limitation des ressources disponibles et il convient donc de s'intéresser à d'autres types d'ajouts cimentaires.

1.1.2.2. Les cendres volantes

Ce sont des déchets issus de la combustion du charbon dans les chaudières de centrales électriques [24] et leur utilisation comme substitut dans des ciments composés est aujourd'hui bien connue [25–27]. Elles permettent de diminuer l'empreinte environnementale du béton final tout en améliorant sa résistance, sa maniabilité et sa durabilité [28]. Généralement, les cendres volantes sont des particules sphériques de petite taille (entre 10 et 100 µm). Elles sont principalement constituées d'oxydes de silicium, d'aluminium, de fer et de calcium. Elles sont de classe C ou F en fonction de leur composition chimique [29]. Les cendres volantes de classe F viennent typiquement du charbon bitumineux et de l'anthracite, elles contiennent au maximum 10% de CaO [29]. Les cendres volantes de classe C sont souvent référées comme des cendres volantes à haute teneur en calcium [29]. Elles proviennent de la combustion du charbon sous-bitumineux et contiennent généralement au moins 20% de CaO [29].

Harison et al [30] se sont intéressés à l'influence de l'ajout de cendres volantes sur les résistances en compression du béton. Ils ont réalisé différents bétons à partir de ciments incorporant 10%, 20%, 30%, 40%, 50% et 60% de cendres volantes avec un ratio eau/ciment de 0.46 et ont réalisé des mesures de résistances à la compression. Les résultats sont présentés dans la figure 1-3 :

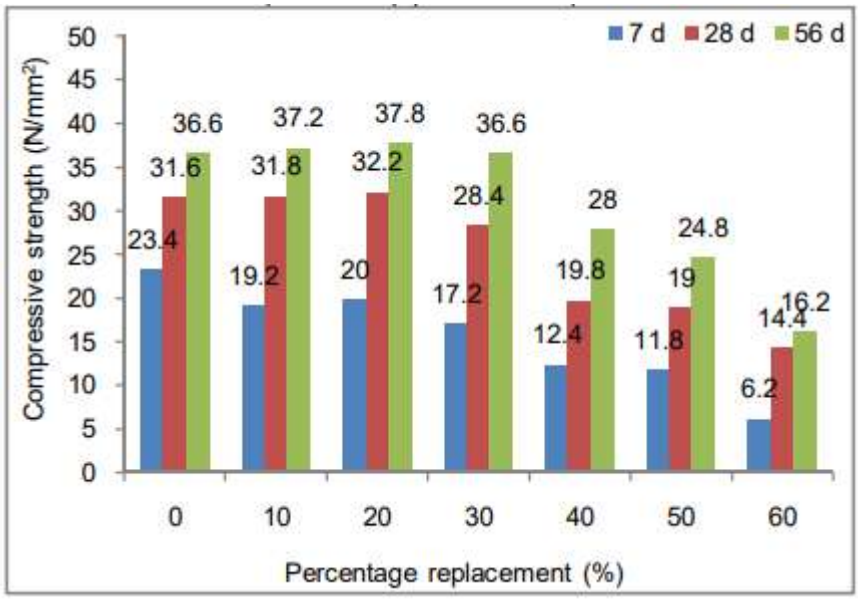

Figure 1-3 : Résistance à la compression de bétons en fonction du pourcentage de remplacement en cendres volantes [30].

Il apparaît que la résistance à la compression est similaire à la référence pour un taux de remplacement allant jusqu'à 30%, au-delà les valeurs commencent à diminuer. Un remplacement de 20% permet d'obtenir les valeurs de résistance à la compression les plus élevées. Il est important de noter que lors de l'addition de cendres volantes, la résistance à la compression à 7j diminue de manière importante. Fraay et al, [31] associent ce temps de latence au délai de déclenchement de la réaction pouzzolanique. La silice des cendres n'est attaquée qu'à partir du moment où le pH du liquide interstitiel du ciment atteint au moins 13,2. Or, l'alcalinité de ce liquide interstitiel croît en réponse à la réaction d'hydratation du ciment qui peut être plus ou moins longue. De plus, pendant cette période d'hydratation, les cendres volantes vont jouer un rôle de nucléus de germination des produits d'hydratation du ciment, la barrière ainsi formée par ces produits d'hydratation à la surface des cendres volantes retarde leur dissolution. C'est ce temps de latence qui diminue fortement la performance des cendres volantes comme SCM.

Les quantités disponibles de cendres volantes sont plus importantes que celles de laitiers de hauts fourneaux avec une production mondiale d'environ 900 Mt/an. Les principaux producteurs sont l'Inde, la Chine, les Etats-Unis et l'Allemagne. Cependant la qualité très variable des cendres volantes fait que seulement 1/3 est actuellement utilisé dans les ciments

et bétons [21]. Il apparaît également important de rappeler que la combustion du charbon pour produire de l'électricité est une importante source d'émission de CO_2 d'origine anthropique (environ 13% des émissions mondiales) [32]. La transition énergétique prévoit à juste titre une diminution de la quantité de cendres volantes disponibles (fermeture des centrales à charbon), par conséquent ce type de SCM ne pourra pas être utilisé indéfiniment.

1.1.2.3. La poudre de verre

Le recyclage du verre pose de nombreux problèmes sociétaux et environnementaux à cause de son caractère non-biodégradable et de la difficulté du tri du verre mixte. Il est donc important de développer de nouvelles voies de valorisation de ces déchets [33–35]. Le verre peut être broyé en une poudre très fine qui présentera alors des propriétés pouzzolaniques du fait de sa composition chimique riche en silicium, calcium, sodium et de son caractère amorphe [36]. Il a été démontré que le remplacement de 25% du ciment par de la poudre de verre permet une amélioration de la résistance à la compression et à la traction sur des mortiers [37]. La norme ASTM C1866/C1866M-20 régit l'utilisation de poudre de verre comme pouzzolane dans les bétons, elle couvre deux types de verres [38] :

- Le verre sodocalcique (GS) qui provient de la fabrication des bouteilles et des fenêtres.
- Le verre de type E (GE) qui provient de la fibre de verre qui est utilisée pour les renforts des matériaux composites.

La principale différence entre ces deux types de verres provient de la quantité de Na_2O. Le verre GS en contient 13% alors que le verre GE en contient moins de 1%.

La norme ASTM C1866 [38] stipule que le taux remplacement maximal est limité par la valeur de résistance à la compression sur mortiers et doit permettre d'obtenir un SAI (Strength Activity Index) d'au moins 75% à 7j et 85% à 28j. En général le taux de remplacement se situe donc entre 10 et 20%. La finesse (4000 cm^2/g ou plus) imposé par la norme ASTM C1866 permets également de s'affranchir de tout risque de réaction alcali-silice.

La poudre de verre est donc un excellent SCM et permet la valorisation de déchets qui sont non biodégradables et qui finissent la plupart du temps déversés dans des décharges [39]. Cependant, les volumes disponibles restent relativement faibles (environ 130 Mt/an mondialement) [40] et ne permettront pas d'avoir un réel impact sur les émissions mondiales de CO_2 d'origine anthropique.

1.1.2.4. Comparaison entre les principaux types de SCMs

La figure 1-4 [21] représente l'estimation des réserves mondiales en millions de tonnes par an des principaux SCMs et leur utilisation en remplacement du ciment.

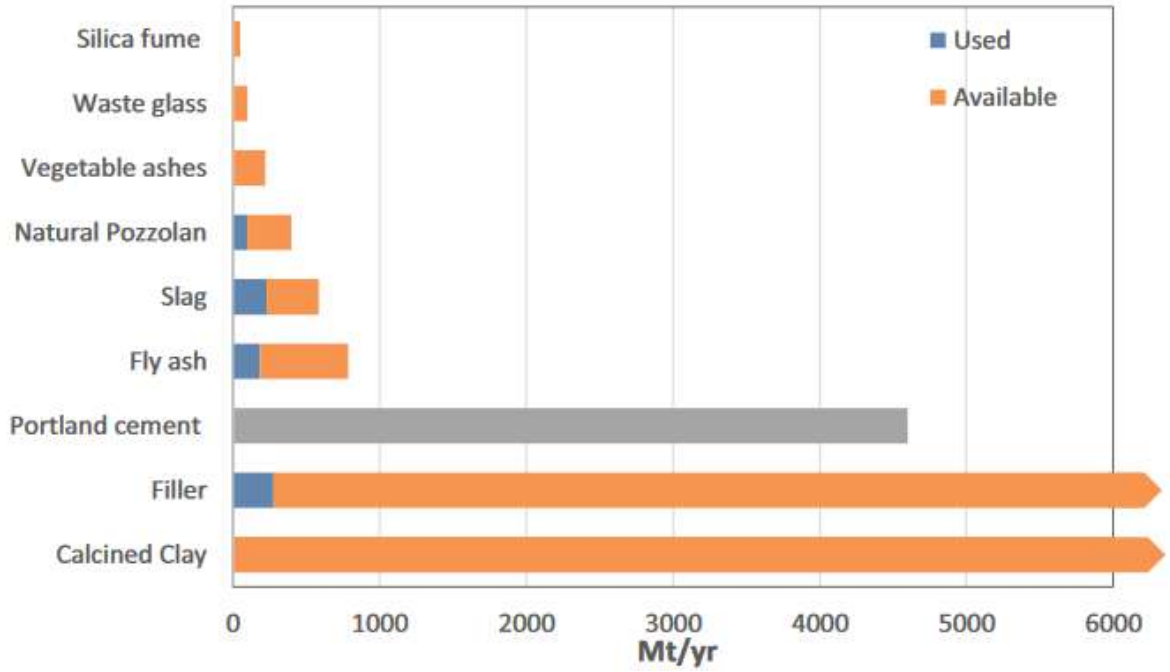

Figure 1-4 : Réserves et utilisation dans le ciment des principaux SCMs [21].

Comme précisé précédemment, on peut voir que les réserves utilisées comme SCM en poudre de verre, laitier de hauts fourneaux et cendre volante sont relativement faibles, notamment en comparaison de la production annuelle de ciment Portland qui est d'environ 4800 Mt/an. Il apparaît donc difficile d'imaginer que ces pouzzolanes puissent avoir un impact majeur sur les émissions mondiales de CO_2 d'origine anthropique.

La dernière ligne du graphique présente les réserves disponibles en argiles calcinées qui peuvent être utilisées en remplacement du ciment. Ces réserves sont très importantes et

pourraient permettre une importante diminution de l'empreinte environnementale de l'industrie cimentière à condition que cette innovation soit mise en place à grand échelle. La seconde partie de cet état de l'art s'intéresse donc à ces argiles.

1.2. Les argiles

Les argiles peuvent être définies de différentes manières, elles peuvent être :

- Une fraction de taille : tout ce qui est inférieure à 2 µm.
- Une famille de minéraux : les minéraux argileux.
- Une roche : composée de l'agrégation de minéraux argileux et d'autres composants.

Les minéraux argileux appartiennent à la famille des phyllosilicates. Ils sont constitués d'un empilement de feuillets tétraédriques et octaédriques séparés par un espace interfoliaire variable. Les feuillets tétraédriques sont constitués de tétraèdres d'oxygène entourant un atome de silicium ou d'aluminium. Les feuillets octaédriques sont constitués d'octaèdres d'oxygène entourant des atomes tels que : Al, Mg, Fe, Li, etc..

Les cations constituants le feuillet octaédrique vont selon leur valence définir le taux de remplissage de la couche tout entière. Ainsi, pour une couche octaédrique entièrement composée de cations divalents, tous les octaèdres sont occupés, on parle d'argile trioctaédrique. A l'inverse, pour une couche octaédrique composée de cations trivalents, seuls deux octaèdres sur trois seront occupés (du fait de l'excès de charge positive des cations trivalents en comparaison des cations divalents), on parle d'argile dioctaédrique. Des substitutions peuvent avoir lieu (appelées substitutions isomorphiques) au sein de la structure des minéraux argileux, dans le feuillet tétraédrique ou le feuillet octaédrique, entraînant un déficit de charge positive (appelé charge permanente). Ce déficit de charge positive est compensé notamment par l'incorporation de cations dans l'espace interfoliaire. Ces cations ont la capacité de s'hydrater, conférant ainsi des propriétés particulières aux minéraux argileux. Les minéraux argileux peuvent être répartis en plusieurs grandes familles (cf figure 1-5) en fonction de la combinaison des feuillets octaédriques et tétraédriques.

1.2.1. Structure des minéraux argileux

1.2.1.1. Les minéraux argileux dits 1:1 ou TO

Ils sont constitués d'une couche tétraédrique empilée sur une couche octaédrique et présentent une taille d'environ 7 Å (empilement TO + espace interfoliaire). Ils correspondent au groupe de la kaolinite qui regroupe différents minéraux dont la dickite, l'halloysite, la kaolinite (archétype) et la nacrite. Ils ont pour formule générale : $Al_2Si_2O_5(OH)_4$ et leur différence réside dans leur structure cristalline respective (polymorphes). Ils ont pour partcularité l'absence de substitutions isomorphiques, ce qui n'entraine pas de déficit de charge et ne nécessite donc pas la présence de cations compensateurs dans l'espace interfoliaire.

1.2.1.2. Les minéraux argileux dits 2:1 ou TOT

Ils sont constitués d'une couche octaédrique entourée de deux couches tétraédriques, ils présentent une taille pouvant varier de 10 à 18 Å en fonction du degré d'hydratation du cation interfoliaire (empilement TOT + espace interfoliaire). Des substitutions isomorphiques entraînent un déficit de charge, compensé par la présence de cations dans l'espace interfoliaire. En fonction de la nature de ces cations la fixation des molécules d'eau peut entraîner un gonflement.

Un premier exemple est le groupe des smectites, il regroupe différents minéraux dont la montmorillonite, la nontronite ou encore la saponite. La formule générale de la montmorillonite est : $(Na,Ca)_{0.3}(Al,Mg)_2Si_4O_{10}(OH)_2\ nH_2O$.

Un second exemple est le groupe des illites, qui ont une structure très proche de celle des micas (biotite, muscovite). La particularité des illites provient de la nature des cations compensateurs. En effet, le déficit de charge est compensé par la présence de potassium dans l'espace interfoliaire. Ce potassium à tendance à peu s'hydrater, ce qui explique l'absence de propriété de gonflement des illites. La formule générale des illites est : $(K,H_3O)(Al,Mg,Fe)_2(Si, Al)_4O_{10}[(OH)_2, (H_2O)$.

1.2.1.3. Les minéraux argileux dits 2:1:1 ou TOTO

Ils sont constitués de trois couches TOT et une couche d'octaèdres isolée (type brucite), ils présentent une taille d'environ 14 Å (TOT + O) Le groupe des chlorites est un exemple de minéraux argileux dits 2 :1 :1, il regroupe différents minéraux dont la chamosite ou encore la cookéite. La formule générale du groupe des chlorite est : $(Fe,Mg,Al)_6(Si,Al)_4O_{10}(OH)_8$.

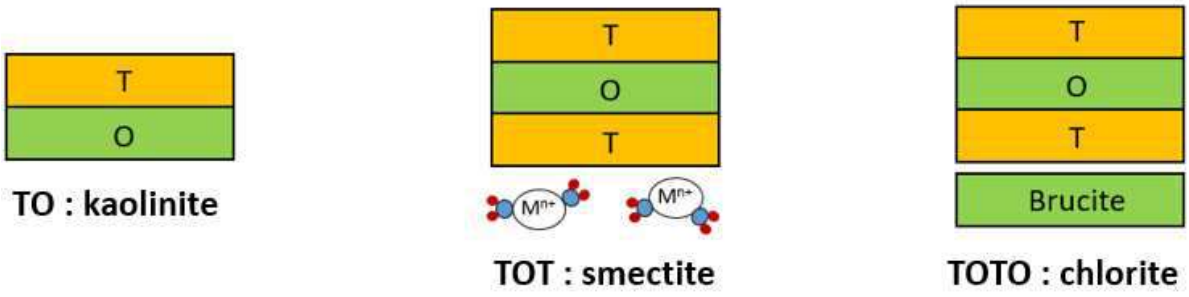

Figure 1-5 : Structures types des minéraux argileux.

Il y a donc une grande variabilité et un nombre important de minéraux argileux. Les smectites font parties des argiles les plus courantes [41] et il apparaît important de s'intéresser un peu plus en détail à leur minéralogie et à leur mode de formation.

1.2.2. Les smectites

1.2.2.1. Minéralogie et types de smectites

La composition type du groupe des smectites est la suivante : $\mathbf{A_{0,3}D_{2\text{-}3}T_4O_{10}Z_2 \cdot \mathit{n}\ H_2O}$ où D représente un cation octaédrique, T un cation tétraédrique, A un cation interfoliaire, Z un anion monovalent (généralement OH^-) et O un oxygène. Comme précisé précédemment les smectites appartiennent à la famille des argiles TOT. On distingue deux grands sous-groupes de smectites : le sous-groupe des smectites trioctaédriques (les saponites) qui ont trois cations dans la couche octaédrique et le sous-groupe des smectites dioactédriques (les montmorillonites) qui ont deux cations dans la couche octaédrique [42]. Chacun de ces sous-groupes contient ensuite une multitude de minéraux argileux. Les membres les plus communs du groupe des smectites sont :

- La montmorillonite ($\mathbf{(Na,Ca)_{0,3}(Al,Mg)_2Si_4O_{10}(OH)_2 \cdot n\ H_2O}$)
- La nontronite ($\mathbf{Na_{0,3}Fe^{III}_2(Si,Al)_4O_{10}(OH)_2 \cdot n\ H_2O}$)
- La saponite ($\mathbf{Ca_{0,25}(Mg,Fe)_3(Si,Al)_4O_{10}(OH)_2 \cdot n\ H_2O}$).

La figure 1-6 présente une micrographie par microscopie électronique à balayage d'une montmorillonite [43] :

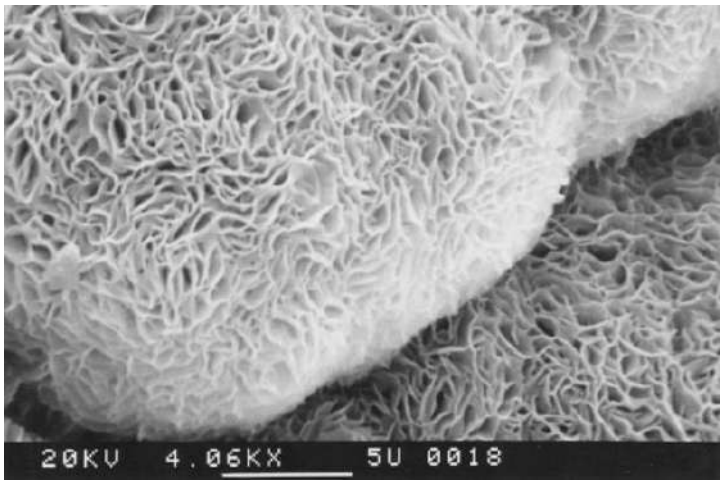

Figure 1-6 : Micrographie par microscopie électronique à balayage d'une montmorillonite [43].

La smectite présente des empilements en feuillets superposés et présentant des ondulations. Il est important de noter que les feuillets de smectites peuvent s'intercaler de manière régulière ou irrégulière avec d'autres feuillets argileux. Cet ensemble forme ce que l'on appelle des interstratifiés.

1.2.2.2. Modes de formation et ressources disponibles

Il existe trois grands modes de formations des smectites [44] :

L'altération diagénétique

Les smectites se forment par un processus d'altération diagénétique de feldspaths, de silicates mafiques, de verre volcanique ou encore d'autres minéraux alumineux-silicatés. En fonction du climat et du type de roche mère l'altération sera plus ou moins poussée et le type de

smectite formé sera différent. Par exemple, l'altération diagénétique de l'orthose (feldspath) va entraîner la formation de smectite potassique [45].

La néogénèse

Le second mode de formation est la néogénèse. Dans ce cas, les smectites se néoforment par précipitation directe dans une solution riche en ions. Il y aura une dissolution complète du minéral précurseur en solution (des silicates en principe) puis une re-précipitation. On obtient ainsi une nouvelle structure cristalline avec une réorganisation complète.

La transformation

Le dernier mode de formation est la transformation à partir d'autres minéraux argileux qui évoluent vers un nouvel état, en équilibre avec les nouvelles conditions dans lesquelles ils se trouvent. Il y aura transformation par dégradation (soustraction d'ions) ou par agradation (fixation d'ions) mais dans tous les cas il n'y a pas de dissolution complète comme pour la néogenèse. Généralement les smectites proviennent de la transformation d'illites, de chlorites ou encore de vermiculites.

On estime que la production mondiale de smectite était de 24.5 Mt/an en 2018, avec la Chine comme principal producteur mondial (environ ¼ de la production) suivi par les Etats-Unis et l'Inde [46,47].

L'une des particularités de ce projet de thèse est qu'il s'intéresse à l'utilisation d'une argile peu-conventionnelle comme ajout cimentaire : la palygorskite. La partie suivante va donc s'intéresser de plus près à ce type de minéral argileux.

1.2.3. La palygorskite

1.2.3.1. Minéralogie

La palygorskite (anciennement attapulgite mais ce terme n'est plus approuvé par l'Association Internationale Pour l'Etude des Argiles (AIPEA)) est un minéral argileux constitué de rubans de type TOT. La particularité est que les tétraèdres sont inversés quand on passe d'un ruban à l'autre. Cette alternance crée des canaux qui sont remplis d'eau zéolitique, donnant ainsi à la

palygorskite une structure creuse tridimensionnelle bien différente de la structure lamellaire classique des autres minéraux argileux (cf figure 1-7) :

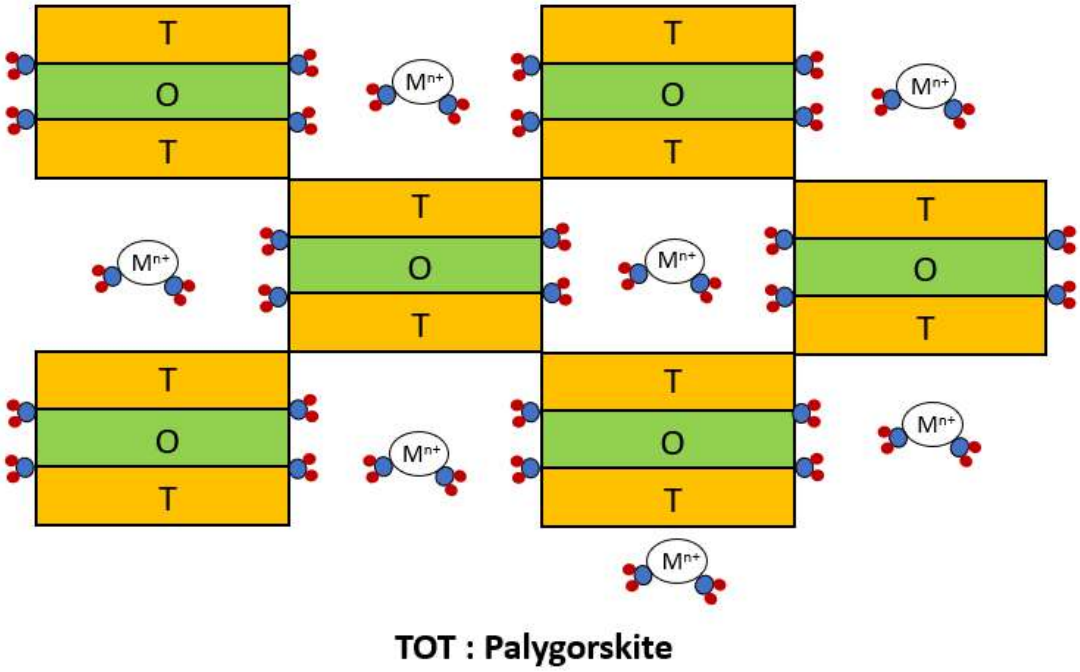

Figure 1-7 : Schéma structural d'une palygorskite.

La présence de ces canaux confère à la palygorskite une importante surface interne et par conséquent une importante surface spécifique (environ 150 m^2/g [48]), mais également de la microporosité et une grande capacité de sorption. Sa formule générale est $(Mg,Al)_2Si_4O_{10}(OH).4H_2O$, c'est une argile dioctaédrique et des substitutions isomorphiques sont possibles, notamment du silicium par de l'aluminium dans la couche tétraédrique. La figure 1- 8 présente une micrographie par microscopie électronique à balayage d'une palygorskite [49].

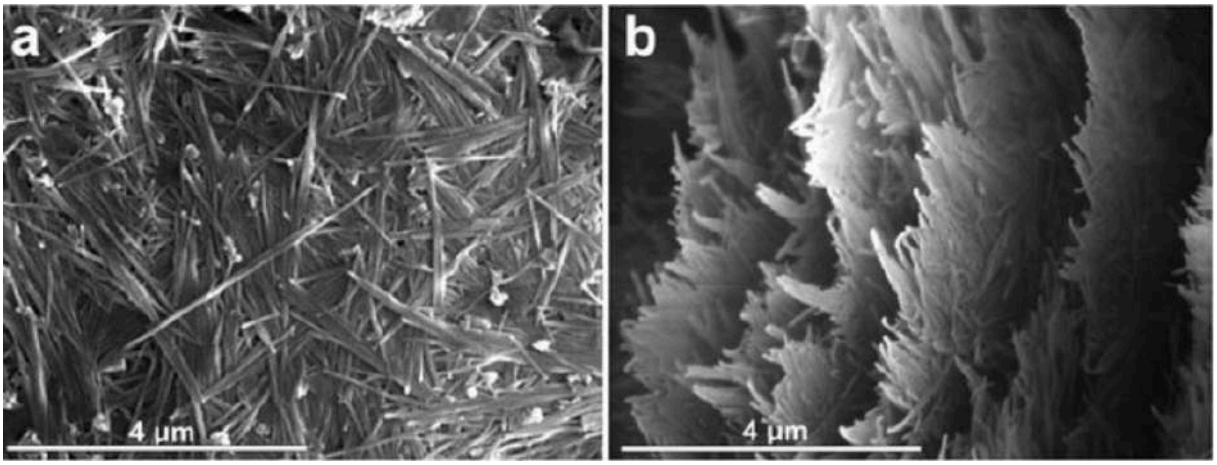

Figure 1-8 : Micrographie par microscopie électronique à balayage d'une palygorskite.

On peut voir qu'elle présente une morphologie allongée bien différente de celle de la smectite et forme des cristaux fibreux.

1.2.3.2. Modes de formation et ressources disponibles

Il existe différents types d'environnements géologiques dans lesquels la palygorskite peut se former. Elle est généralement formé par cristallisation à partir d'une solution dans des environnements lacustres [50] ou périmarins [51–53]. La formation de palygorskite peut également avoir une origine diagénétique [54] ou hydrothermale [55]. Il est important de noter que l'altération de précurseurs (tels que la smectite) peut également entrainer la formation de palygorskite [51,56]. La figure 1-9 présente les principaux dépôts de palygorskite à travers le monde. Les États-Unis sont les plus gros producteurs, en effet, ils détiennent environ 76% de la production mondiale de Palygorskite [57], notamment grâce au gisement du Meigs-Attapulgus-Quincy district.

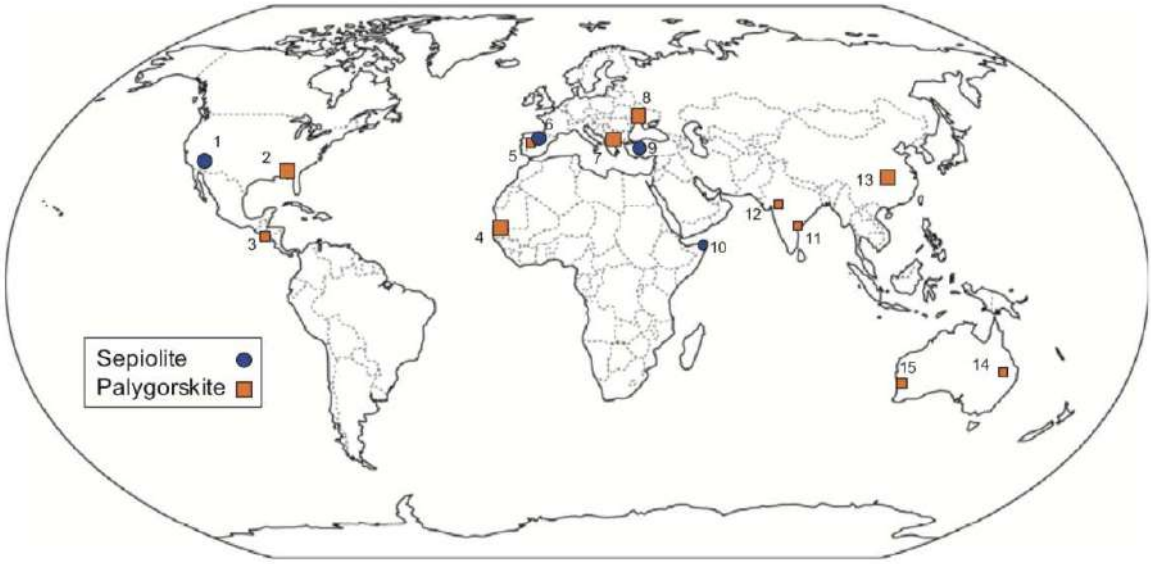

Sepiolite deposits: 1 Amargosa, Nevada (USA); 6. Vallecas-Vicálvaro-Yunclillos District and Mara (Spain); 9. Eskisehir (Turkey); 10. El-Bur (Somalia).

Palygorskite deposits: 2. Meigs-Attapulgus-Quincy District, South Georgia-North Florida (USA); 3. Guatemala; 4. Theis and Nianming (Senegal); 5. Torrejón and Bercimuel (Spain); 7. Ventzia, Grevena (Greece); 8. Cherkassy (Ukraine); 11. Timsampalli-Maripalli, Andhra Pradesh, and 12 Bhawnagar, Gujarat (India); 13. Guanshan, Anhui (China); **14.** Ipswich (Queensland) and15 Lake Nerramyne (Australia).

Figure 1-9 : Gisements de palygorskite à travers le monde [58].

La production mondiale annuelle en 2010 a été estimée à 1,3 Mt/an [58] bien en dessous des de la production de smectites (24 Mt/an), en revanche il n'a pas été possible de trouver des chiffres plus récents pour la palygorskite.

La troisième partie de cet état de l'art s'intéresse à l'utilisation d'argiles calcinées comme ajouts cimentaires. Cela passe dans un premier temps par une description de l'étape de calcination que subissent les minéraux argileux ainsi que la réaction pouzzolanique dans laquelle ils sont impliqués lors de leur ajout dans le ciment.

1.3. Les argiles calcinées comme ajouts cimentaires

1.3.1. La calcination

La calcination est un procédé important qui permet de modifier les propriétés des argiles et de leur conférer un caractère pouzzolanique. Elle permet le passage d'un état cristallisé stable à un état amorphe instable et donc plus réactif. 4 étapes se démarquent lors de ce processus [59] :

- **La déshydratation** qui correspond au départ des molécules d'eau du matériau et qui se fera à basse température, entre 80 et 250°C [60].

- **La déshydroxylation** au cours de laquelle on observe le départ des groupements hydroxyles. Cette étape se fera plus ou moins facilement en fonction du type de liaison du groupement hydroxyle avec le feuillet octaédrique. En effet, la résistance au traitement thermique de ces liaisons augmente de la manière suivante : Fe-OH < Al-OH < Mg-OH [60].

- **L'amorphisation** qui correspond à la perte de cristallinité totale du matériau et qui se déroule après la déshydroxylation complète du feuillet octaédrique.

- **La recristallisation** qui intervient si la température devient trop importante, généralement sous forme de mullite, cordierite, enstatite et cristobalite [61].

L'objectif de ce procédé est d'obtenir un matériau réactif déshydroxylé et amorphisé tout en évitant d'éventuelles recristallisations qui entraineraient alors une diminution de l'activité pouzzolanique. Il y a une température de calcination différente en fonction du type d'argile utilisée comme pouzzolane : Fernandez et al. [62] préconisent une température de calcination de l'ordre de 800°C pour un échantillon riche en kaolinite (48,76% de kaolinite ; impuretés de quartz et oxyhydroxide de fer). Hollanders et al. [63] ont calciné une illite pure à 900°C car une amorphisation complète ne peut être atteinte à des températures inférieures. Danner et al. [64] ont calciné un échantillon de montmorillonite (54% montmorillonite, 8% kaolinite, 4% illite, 25% calcite, et des impuretés) à 800°C. La figure 1-10 présente les courbes d'analyse thermo-différentielle de minéraux argileux communs et de la gibbsite :

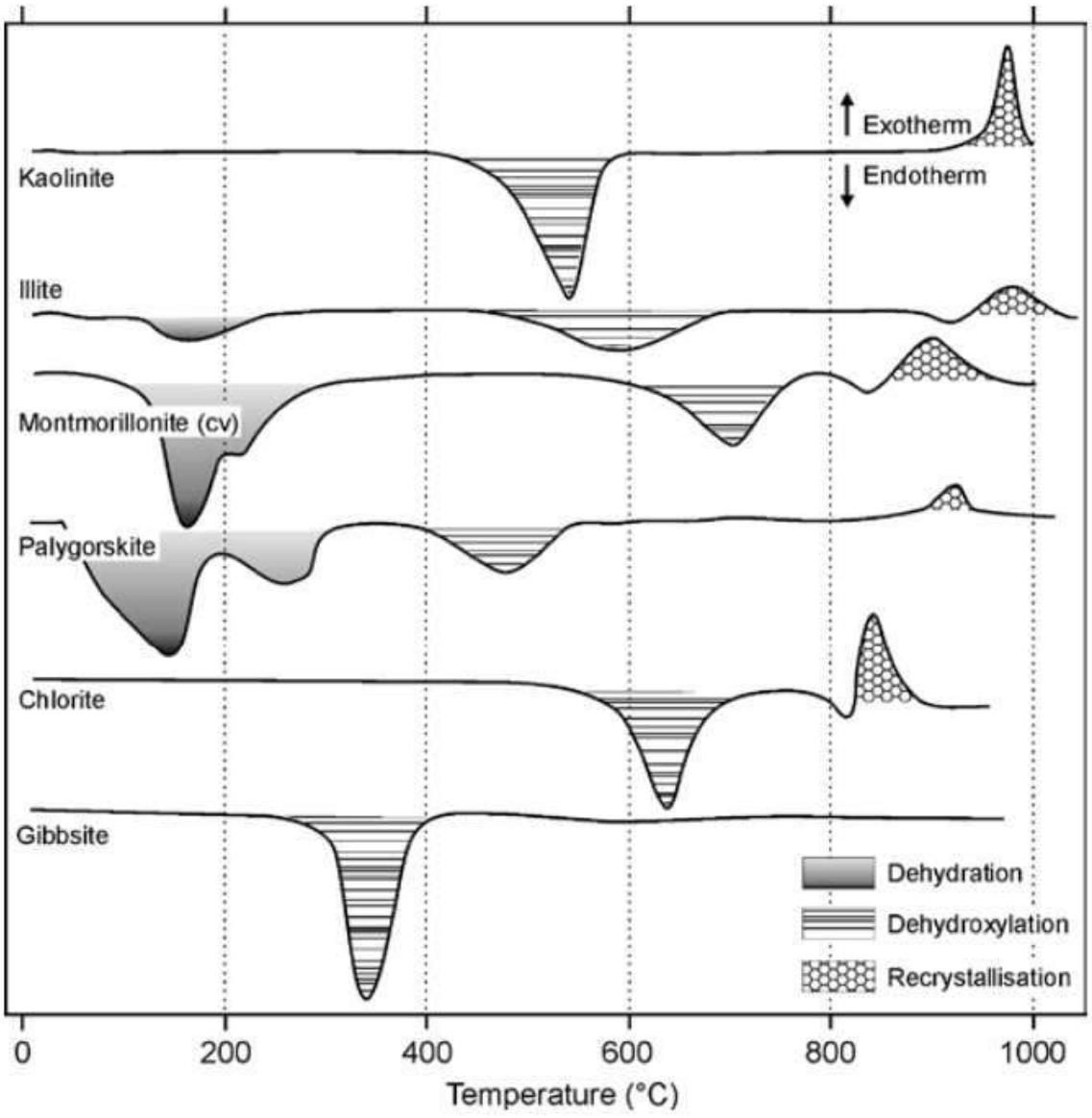

Figure 1-10 : Courbes d'analyse thermo-différentielle de minéraux argileux communs et de la gibbsite [60].

Nous allons nous intéresser aux comportements thermiques de 3 argiles en particulier : la kaolinite, la smectite et la palygorskite.

Il n'y a pas de phase de déshydratation pour la kaolinite (mis-à-part le départ de molécules d'eau qui peuvent s'adsorber à la surface), notamment du fait de sa structure TO et de l'absence de cations interfoliaires pouvant s'hydrater. La température de déshydroxylation va être régie par le degré d'ordre d'empilement des couches. Par exemple, une kaolinite désordonnée (qui possède des fautes d'empilement de ses feuillets) va se déshydroxyler entre

530 et 570°C alors qu'une kaolinite ordonnée va se déshydroxyler entre 570 et 630°C [60]. Avec l'augmentation de la température il y aura des phénomènes de recristallisation avec la formation de spinelle et de mullite. Les températures de calcination reportées pour la kaolinite varient entre 550 [65] et 850°C [66] pour différentes durées de traitement. D'une manière générale la plupart des valeurs de température de calcination de la kaolinite se situent entre 650 et 750°C [67–71].

Comme précisé précédemment les smectites sont des argiles TOT qui contiennent des cations interfoliaires et qui par conséquent ont la capacité de s'hydrater. Les substitutions isomorphiques ainsi que le type de cations interfoliaires vont influer la déshydratation et la déshydroxylation des smectites. La déshydratation va se faire à des températures avoisinant les 300°C et correspond à l'élimination des molécules d'eau liées à la surface externe ainsi qu'aux cations interfoliaires. Par la suite, la température de déshydroxylation va être fonction du type de cations qui sont présents dans les feuillets octaédriques (Fe < Al < Mg) ainsi que leur arrangement [60]. Pour les smectites dioactédriques (dont l'octaèdre contient essentiellement des cations trivalents (Al^{3+} et Fe^{3+}) il existe deux types de configurations : cis-vacante et trans-vacante. La figure 1-11 schématise ces deux configurations.

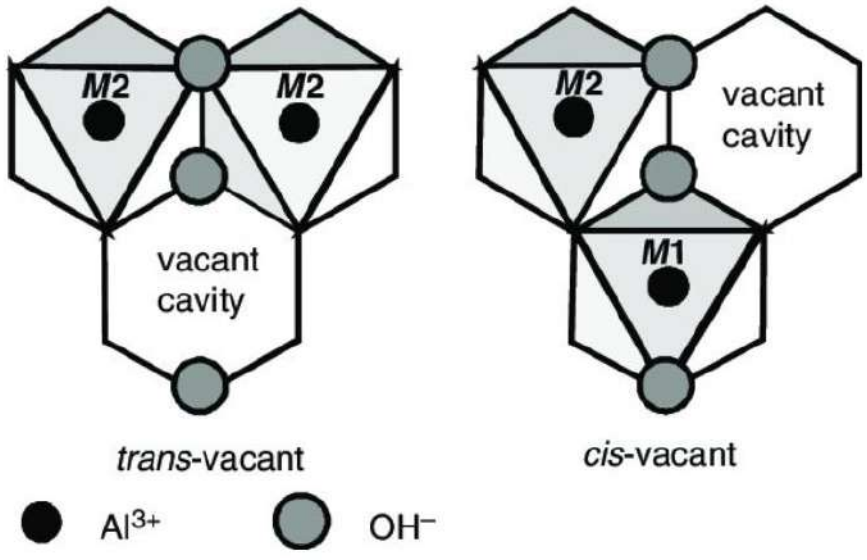

Figure 1-11 : Configurations trans et cis-vacantes d'un feuillet octaédrique [72].

Dans une configuration cis-vacante les OH- sont tous les deux du même côté du site vacant du feuillet octaédrique alors que dans une configuration trans-vacante les OH- sont de chaque côté du site vacant du feuillet octaédrique [73]. Ce type de configuration va avoir une influence sur la température de déshydroxylation. Ainsi, une smectite qui présente majoritairement des feuillets octaédriques cis-vacants se fera aux alentours de 700°C. Ceci est bien en dessous des 850°C nécessaires pour la déshydroxylation d'une smectite trans-vacante [74]. Les phénomènes de recristallisation débutent autour de 850°C en fonction de la composition chimique de la smectite. Les températures de calcination des smectites sont généralement plus élevées que les kaolinites et se situent entre 800 et 830°C [75–77].

La palygorskite, du fait de sa structure TOT si particulière (tétraèdres qui s'inversent alternativement créant des canaux remplis d'eau zéolitique) va avoir une déshydratation en deux temps. Dans un premier temps c'est l'eau zéolitique qui va être libérée aux alentours de 100°C suivi par l'eau liée au-dessus de 200°C [78]. La déshydroxylation se fait ensuite entre 400 et 600°C mais va être fonction de la chimie et notamment du ratio Mg/Al dans les feuillets octaédriques [60]. Il y a cependant très peu d'études qui traitent de la calcination de la palygorskite en vue d'une utilisation comme ajout cimentaire et il n'a pas été possible de trouver des valeurs de température de calcination de référence.

Dans tous les cas, le protocole de calcination est adapté à l'échantillon et est déterminé par des essais en laboratoire et notamment des mesures de surface spécifique, de spectroscopie infrarouge, de RMN MAS du solide et de diffraction des rayons X afin d'obtenir un échantillon combinant un haut degré d'amorphisation, une importante déshydroxylation des feuillets octaédriques et une surface spécifique élevée. L'objectif principal de cette étape de calcination est donc d'obtenir une argile calcinée qui présentera une réactivité pouzzolanique maximale.

1.3.2. La réaction pouzzolanique

L'argile calcinée ainsi produite peut ensuite, en présence d'eau, se dissoudre, et les éléments chimiques libérés se combiner avec la portlandite (CH) issue de la réaction d'hydratation du ciment afin de former des hydrates (C-(A)-S-H) : silicates de calcium et d'aluminium hydratés)

responsables du durcissement. Scrivener et al. [79] ont décrit la réaction (cf figure 1-12), où S représente la source de silicium et A la source d'aluminium issues de l'argile calcinée :

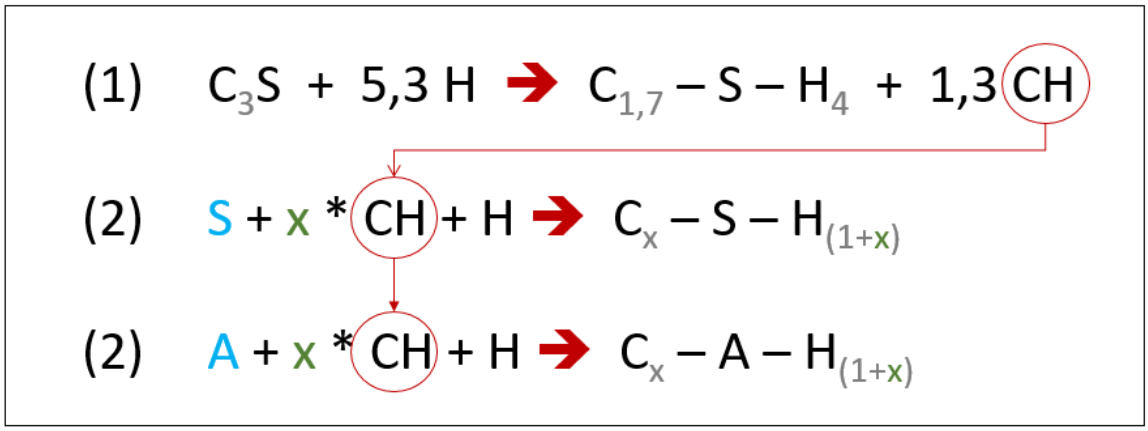

Figure 1-12 : Schéma réactionnel de la réaction pouzzolanique (adapté de Scrivener et al [79]).

La source de silicium (S) et la source d'aluminium (A) issues de l'argile calcinée vont réagir avec le calcium de la portlandite (CH) pour former des C-S-H, des C-A-H et des C-A-S-H. Les hydrates produits au cours de cette réaction pouzzolanique vont participer à la cohésion interne du ciment et permettre l'amélioration des propriétés mécaniques.

Cet ajout de pouzzolane permet de réduire la chaleur d'hydratation ce qui se traduit par une diminution de la fissuration. A l'état durci, la consommation de la portlandite et la formation de nouveaux hydrates permet une réduction de la porosité de la matrice et par conséquent une augmentation de la compacité du ciment. Le ciment produit sera plus durable d'une manière générale et particulièrement résistant contre les attaques de sulfates, chlorures et autres agressions chimiques.

1.3.3. Méthodes d'évaluation de la réactivité pouzzolanique

L'augmentation de la réactivité pouzzolanique engendrée par l'étape de calcination des minéraux argileux va être primordiale pour les performances mécaniques et la durabilité du ciment composé final. Il est donc important de pouvoir caractériser de manière précise la réactivité pouzzolanique d'une argile calcinée.

Il existe différentes méthodes normalisées pour l'évaluation de la réactivité pouzzolanique qui se basent sur différents paramètres tels que la consommation de $Ca(OH)_2$, la résistance à la compression ou encore la chaleur dégagée.

1.3.3.1. L'essai Chapelle modifié

L'essai Chapelle modifié provient de la norme française NF P18-513 [80]. La figure 1-13 présente le montage expérimental de ce test [81] :

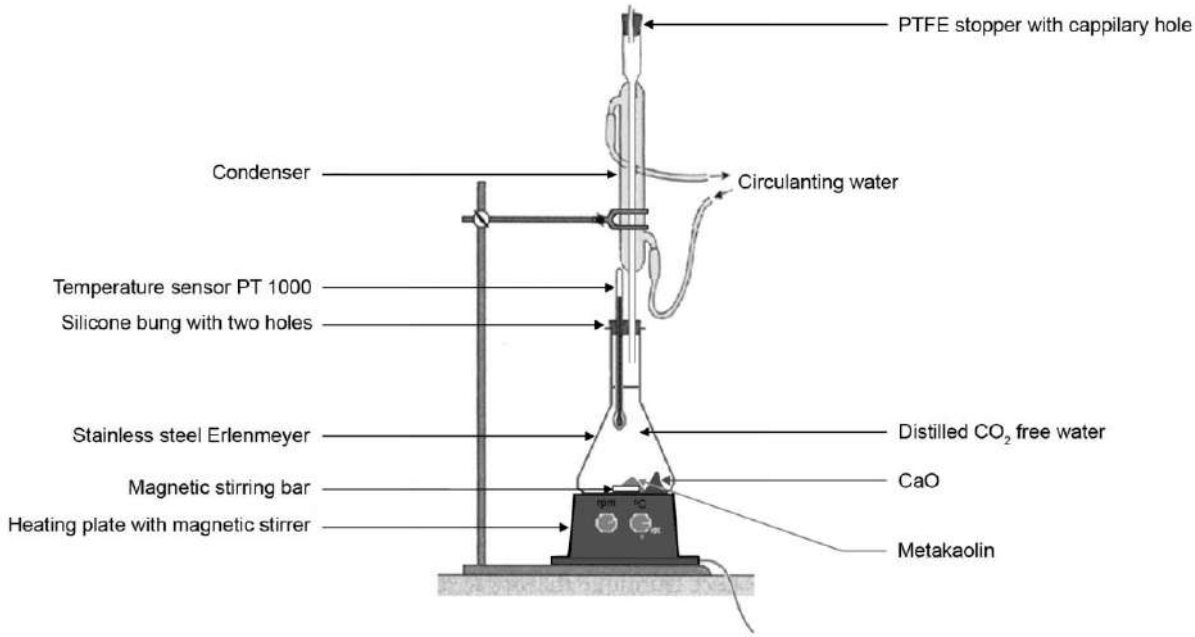

Figure 1-13 : Montage expérimental de l'essai Chapelle modifié [81].

Le principe consiste à mélanger 1g de pouzzolane avec 2g de de CaO dans 250 ml d'eau distillée. La suspension est ensuite placée sous agitation magnétique et chauffée à 85°C (+/- 5°C) durant 16h. Après 16h, la solution est refroidie et titrée à l'acide pour déterminer la quantité de $Ca(OH)_2$ restante. La quantité de $Ca(OH)_2$ consommée par la pouzzolane et les résultats sont exprimés en mg $Ca(OH)_2$ fixé /g de pouzzolane. La norme précise que pour être considérée comme active une pouzzolane doit obtenir une valeur d'au moins 700 mg $Ca(OH)_2$ fixé /g de pouzzolane. Ferraz et al [81] se sont intéressés à 6 métakaolins commerciaux et ont trouvés des valeurs comprises entre 920 et 1560 mg $Ca(OH)_2$ fixé /g de métakaolin. Ayati et al

[82] ont calciné une argile naturelle (contenant 31% de smectite et 11% d'illite) à 850°C et ont obtenu une valeur de 600 mg $Ca(OH)_2$ fixé/g de pouzzolane, ce qui est en dessous du seuil minimum fixé par la norme.

Le principal problème de ce test réside dans le fait qu'il se base sur la consommation de $Ca(OH)_2$ dans de l'eau distillée. Or les conditions en milieu cimentaire (là où va se dérouler la réaction pouzzolanique) sont différentes. La solution interstitielle riche en alcalins qui est présente en milieu cimentaire va avoir une influence sur la cinétique de cette réaction pouzzolanique, par conséquent, l'essai Chapelle modifié pourrait ne pas donner des résultats réalistes [83].

1.3.3.2. L'indice d'activité

L'indice d'activité (SAI pour « Strength Activity Index » en anglais) issu de la norme ASTM C311 [84] est une technique de détermination de la réactivité d'une pouzzolane très connue, qui se base sur des mesures de résistances à la compression. Le principe est très simple, un ciment composé est obtenu en mélangeant 80 % de ciment Portland avec 20 % de la pouzzolane testée. Un premier mortier référence est réalisé à partir d'un ciment pur (eau/liant de 0,484 et sable/liant de 2,75) et moulé dans des cubes de 50 x 50 x 50 mm^3. Ensuite, un second mortier à partir du ciment composé est réalisé avec le même ratio sable/liant et avec la quantité d'eau nécessaire pour avoir le même écoulement (+/- 5 mm). Des mesures de résistances à la compression à 7 et 28 jours sont faites puis les résultats du mortier test sont comparé à ceux du mortier référence par le biais du calcul de l'indice d'activité dont la formule est la suivante :

Indice d'activité = (A/B)*100

A = résistance à la compression du mortier test en MPa

B = résistance à la compression du mortier référence en MPa.

La norme ASTM C618 [29] stipule qu'une pouzzolane doit obtenir un indice d'activité d'au moins 75% à 28 jours pour être considérée comme active.

Le principal problème de cet indice d'activité réside dans le rapport eau/liant (e/l) utilisé pour le mortier test. En effet, en fonction du type de pouzzolane, la demande en eau pourrait être très différente et le e/l varierait considérablement, ce qui aurait pour conséquence de modifier les valeurs de résistance à la compression. Prenons l'exemple d'une argile calcinée d'une très grande finesse. Un e/l très grand est nécessaire en comparaison du mortier référence pour obtenir le même écoulement. Cette différence va entrainer une diminution importante des valeurs de résistances à la compression. Cette argile calcinée pourrait donc ne pas obtenir un indice d'activité >75% et serait considérée comme une pouzzolane inactive par la norme ASTM C618 malgré sa très forte réactivité pouzzolanique [85].

1.3.3.3. Le nouveau test ASTM C1897

Ce test normalisé par le comité RILEM TC-267 [83] se base sur les travaux de Avet et al. [86]. Le principe consiste à faire réagir une quantité donnée de pouzzolane avec du $Ca(OH)_2$ dans des conditions qui représentent un milieu cimentaire (présence de calcite et d'une solution interstitielle). Le tableau 1-2 présente les proportions de chaque constituants [87].

	SCM	$Ca(OH)_2$	$CaCO_3$	Potassium Solution
Mass (grams)	10.00	30.00	5.00	54.00

Tableau 1-2 : Proportions du mélange de la pâte [87].

Les différents constituants sont préchauffés à 40°C et mélangés jusqu'à l'obtention d'une pâte homogène qui est ensuite immédiatement transvasée dans une ampoule à calorimètre. La chaleur dégagée est ensuite mesurée à 40°C jusqu'à 3 et 7 jours. On obtient une valeur en J/g de pouzzolane. La chaleur dégagée sera directement proportionnelle à la réactivité pouzzolanique de l'échantillon. Ce test est à l'heure actuelle le meilleur test d'activité pouzzolanique en termes de prévisions des performances mécaniques en système cimentaire [88]. Cependant, comme pour l'essai Chapelle modifié, ce test se base sur une consommation de $Ca(OH)_2$ par la pouzzolane testée. Or si l'échantillon testé contient de la chaux, les proportions ne sont plus bonnes et le test devient difficile à réaliser (nécessité de quantifier la proportion de CaO dans l'échantillon pour adapter la quantité de $Ca(OH)_2$ à ajouter). Ce test

est donc efficace pour les kaolins dont la majorité des échantillons ne contiendront pas de carbonates de calcium en minéraux secondaires. Cependant pour les autres types d'argiles ainsi que les marnes les interprétations peuvent être faussées.

Il existe donc une multitude de tests d'activité pouzzolanique, ayant chacun des avantages et des inconvénients. Néanmoins, mesurer simplement la réactivité pouzzolanique n'est pas toujours suffisant et il apparait important d'essayer de déterminer s'il existe un lien entre la structure de base de l'argile, les modifications induites par la calcination sur cette structure et la réactivité pouzzolanique.

1.3.4. Lien structure - modifications physico-chimiques - réactivité pouzzolanique

Différents facteurs vont influencer la déshydroxylation et la réactivité pouzzolanique. Le premier est le type d'argile. Une argile TO telle que la kaolinite va avoir des groupements Al-OH octaédriques directement exposés, ce qui va avoir pour conséquence de faciliter la déshydroxylation. Pour les argiles TOT telles que les smectites et les illites, la déshydroxylation va être beaucoup plus difficile que pour les argiles TO. En effet, les groupements Al-OH sont bloqués par les deux feuillets tétraédriques, rendant beaucoup plus compliqué leur déshydroxylation. C'est cette différence structurale qui explique les différences de sensibilité au traitement thermique et de réactivité entre une argile TO et une argile TOT [62].

De plus, au sein d'une même famille d'argile, l'ordre d'empilement des feuillets structuraux va avoir une influence sur la déshydroxylation et la réactivité pouzzolanique. Une kaolinite désordonnée va se déshydroxyler à des températures comprises entre 530 et 570°C alors qu'une kaolinite ordonnée se déshydroxylera entre 570 et 630°C [60]. La réaction pouzzolanique va également être influencée par ce type d'empilement. En effet, une kaolinite désordonnée déshydroxylée va présenter une réactivité pouzzolanique plus importante qu'une kaolinite ordonnée déshydroxylée [70,89].

Lors du phénomène de calcination, il a été observé un changement de coordination des atomes d'aluminium octaédriques (conséquence directe de la déshydroxylation) qui passent

d'une coordination 6 à des coordinations 4 et 5 [62,90,91]. Fernandez et al, [92] ont tenté de démontrer qu'il existait un lien direct entre l'apparition d'aluminium 5 et la réactivité pouzzolanique par le biais de mesures de RMN du solide (^{27}Al) et de tests d'activité pouzzolanique. Cependant, leur étude se base sur l'appréciation qualitative des spectres RMN de ^{27}Al. Il est donc assez difficile de lier de manière certaine la réactivité pouzzolanique à l'apparition d'aluminium 5 sachant que l'aluminium 4 participe également au signal total observé. Une étude quantitative (par intégration spectrale) de la déshydroxylation de ces minéraux argileux associée à des mesures de réactivité pouzzolanique devrait permettre de vérifier cette hypothèse.

1.3.5. Les mélanges métakaolin / ciment

Maintenant que nous avons décrit les minéraux argileux, leur calcination et leur réactivité pouzzolanique il est temps s'intéresser de plus près à leur utilisation comme ajout cimentaire.

Dernièrement, de nombreuses études se sont intéressées à la substitution d'une partie du clinker par de l'argile calcinée afin de diminuer le coût environnemental du ciment. Une grande partie de ces travaux de recherche porte sur l'utilisation de métakaolin [62–64,93,94]. Le mode opératoire utilisé est similaire entre les différentes études à savoir la caractérisation des argiles brutes (diffraction des rayons X, analyses thermiques, infra-rouge, RMN du solide), leur calcination à la température appropriée dans un four de laboratoire et la caractérisation des produits calcinés. Les résultats sont comparés afin de mettre en évidence les différences structurales et chimiques induites par la calcination. Par la suite, la réactivité pouzzolanique des argiles calcinées est quantifiée à l'aide de tests d'activité pouzzolanique (Chapelle, ASTM C1897, etc..). Des pâtes de ciment et des mortiers sont réalisés avec différents taux de substitution (argile calcinée / ciment) et les phases formées sont ensuite caractérisées. Enfin, des tests de compression sont réalisés et les résultats comparés aux références afin de mettre en évidence l'influence de l'ajout sur les performances mécaniques. La figure 1-14 présente des mesures de résistance à la compression de mortiers confectionnés à partir d'un ciment composé contenant 20% de kaolinite calcinée à différentes températures (de 700 à 800°C) :

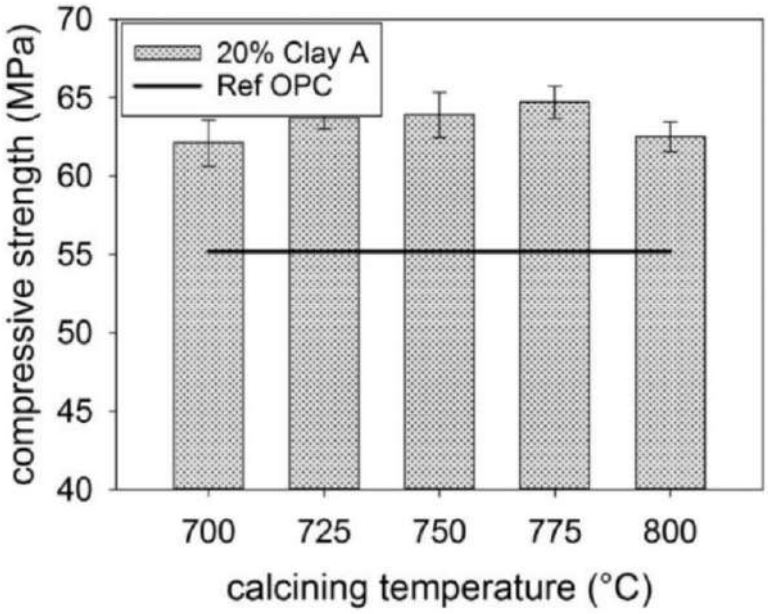

Figure 1-14 : Résistances à la compression de mortiers obtenus à partir de ciments incorporant 20% de métakaolin [64].

Les résultats de Danner et al. [64] démontrent que la substitution de 20% du ciment Portland par du métakaolin permet une nette augmentation de la résistance à la compression (par rapport à la référence 100% ciment) pour des températures de calcination allant de 700 à 800°C avec une valeur maximale obtenue à 775°C.

Cette hausse des performances mécaniques est due à la très forte réactivité pouzzolanique du métakaolin qui va consommer la portlandite issue de l'hydratation du ciment pour former des silicates de calcium et d'aluminates hydratés (C-S-H et C-(A)-S-H) [94]. De nombreuses études se sont donc intéressées à l'utilisation du métakaolin en remplacement du ciment [62,93–97] et les résultats sont unanimes. Le remplacement du ciment par du métakaolin dans des proportions allant jusqu'à 20% permet d'obtenir des performances mécaniques équivalentes voir supérieures à la référence 100% ciment. Ces excellents résultats ont donc amené au projet LC3 (Limestone Calcined Clay Cement) dont l'objectif est la normalisation d'un nouveau type de ciment ternaire à base d'argile calcinée et de calcaire.

1.3.6. Le projet LC3

Le projet LC3 (Limestone Calcined Clay Cement) initié par la professeure Karen Scrivener du Laboratoire des matériaux de construction de l'Ecole polytechnique fédérale de Lausanne vise à développer à l'échelle industrielle un nouveau type de ciment composé (50% clinker, 30% métakaolin, 15% calcaire, 5% gypse) à partir de métakaolin et de calcaire dit « low grade ». Lors de ce projet, différentes sources de carbonates ont été testées et il a été démontré qu'il est possible d'utiliser des calcaires dits impurs, mais également de la dolomite ou encore de la poudre de marbre dans la formulation de ce ciment composé ternaire [98]. L'ajout de calcaire permet d'améliorer les réactions d'hydratation des différentes phases du clinker en offrant une surface de nucléation supplémentaire pour les hydrates. Les carbonates issus du calcaire vont aussi réagir avec l'aluminium du clinker pour former des carbo-aluminates de calcium hydratés (hemi- et mono-carboaluminates [99]).

Le métakaolin utilisé est issu de la calcination de kaolin de qualité inférieure (proportion de kaolinite d'au moins 40%) qui est souvent considéré comme déchet par l'industrie. Plus de 46 sources de kaolins avec des proportions de kaolinite allant de 7,4% à 95% ont été testées [100]. Les argiles ont été calcinées à 800°C puis intégrées dans un mélange : 50% clinker, 30% métakaolin, 15% calcaire, 5% gypse (ciment LC3-50). Les résultats sont présentés dans la figure 1-15 [100] :

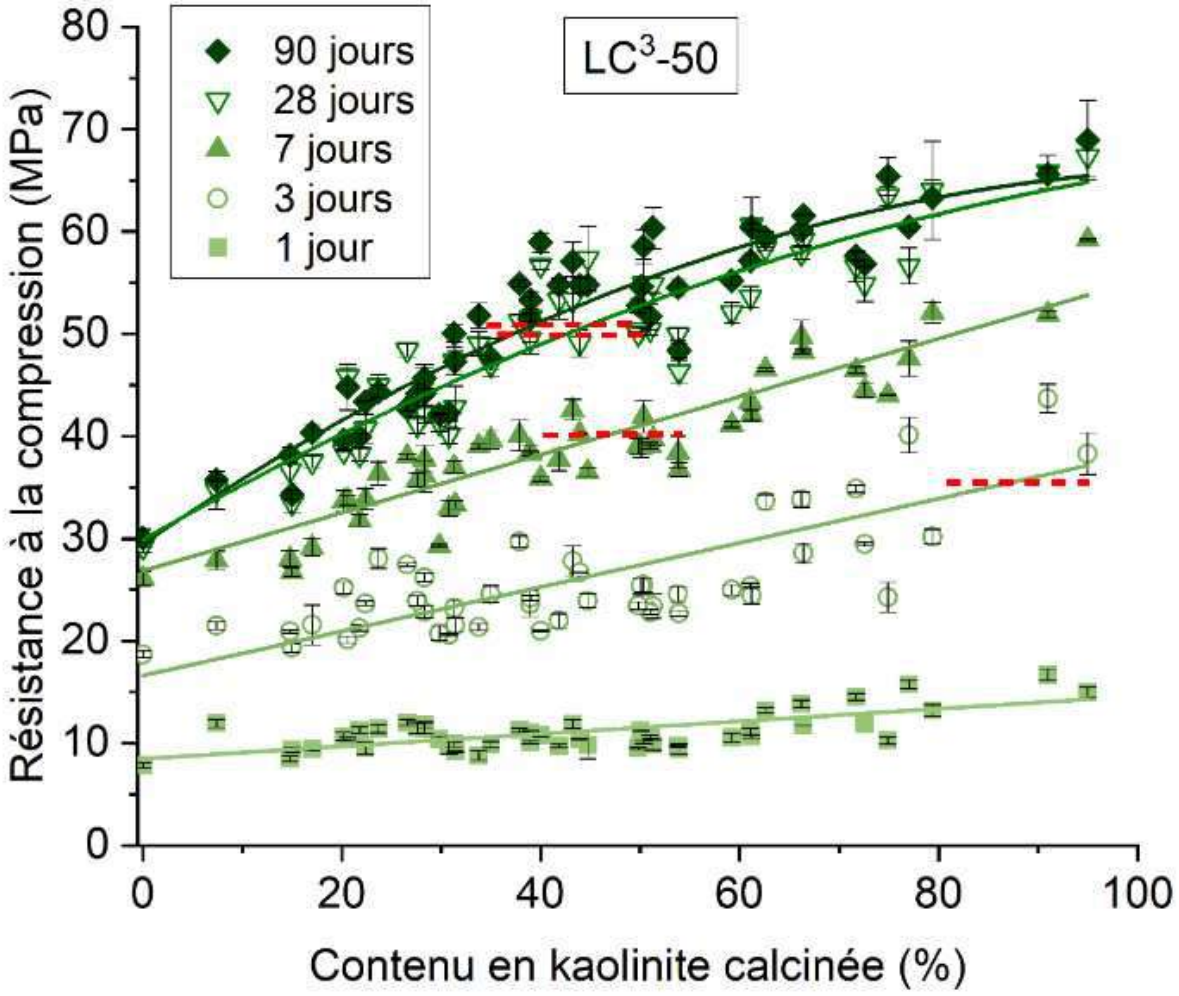

Figure 1-15 : Résistance à la compression sur mortier pour les systèmes LC3-50 avec différents contenus en kaolinite calcinée dans l'argile. Les lignes pointillées indiquent la résistance pour le système de ciment Portland de référence [100].

Les résultats démontrent que les argiles les plus susceptibles de présenter une bonne pouzzolanicité ne sont pas les argiles kaoliniques pures, mais les argiles contenant entre 40% et 70% de kaolinite [100]. Le gain en résistance mécanique pour des proportions de kaolinite plus élevées n'est pas significatif. L'ajout de calcaire, toujours dans une optique environnementale, permet d'augmenter le taux de substitution du clinker mais également les performances mécaniques. Le système final présente des résistances similaires au ciment Portland ordinaire à partir de 7 jours (figure 1-16).

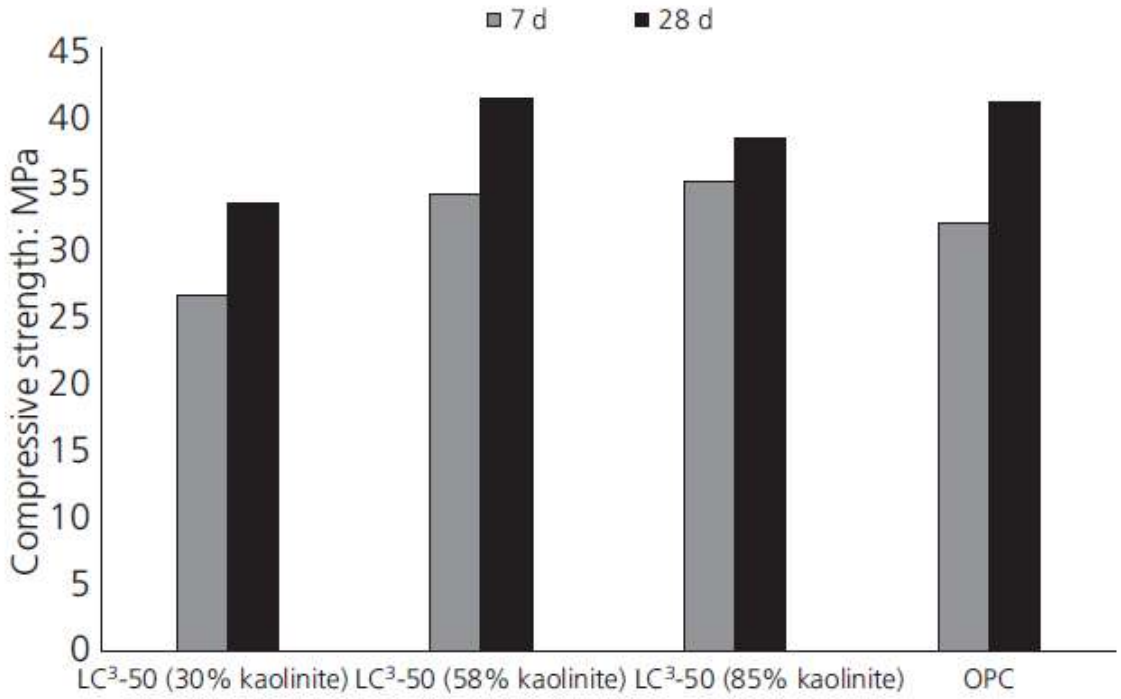

Figure 1-16 : Résultats des tests de compressions sur les ciments LC3 [100].

De plus, la durée de vie des structures faites en ciment LC3 peut être rallongée de manière significative en comparaison d'un ciment portland classique : résistance aux chlorures accrue du fait de la formation de C-(A)-S-H supplémentaires issus de la réaction pouzzolanique qui vont affiner la porosité, et par conséquent limiter la propagation des espèces chimiques au sein de la matrice [100]. Des essais à l'échelle industrielle ont été réalisés en Inde et à Cuba avec ensuite la réalisation de briques, de pavés, de blocs, et même de maisons

1.3.7. Les mélanges montmorillonite/illite - ciment

Différentes études ont tenté d'investiguer l'utilisation d'autres types d'argiles telles que des montmorillonites [62–64,101] et des illites [62,63]. D'une manière générale les montmorillonites calcinées présentent une meilleure activité pouzzolanique en comparaison des illites. La figure 1-17 présente les résultats de résistances à la compression de mortiers obtenus à partir de ciments incorporant 30% de métakaolin, de montmorillonite calcinée ou d'illite calcinée [62].

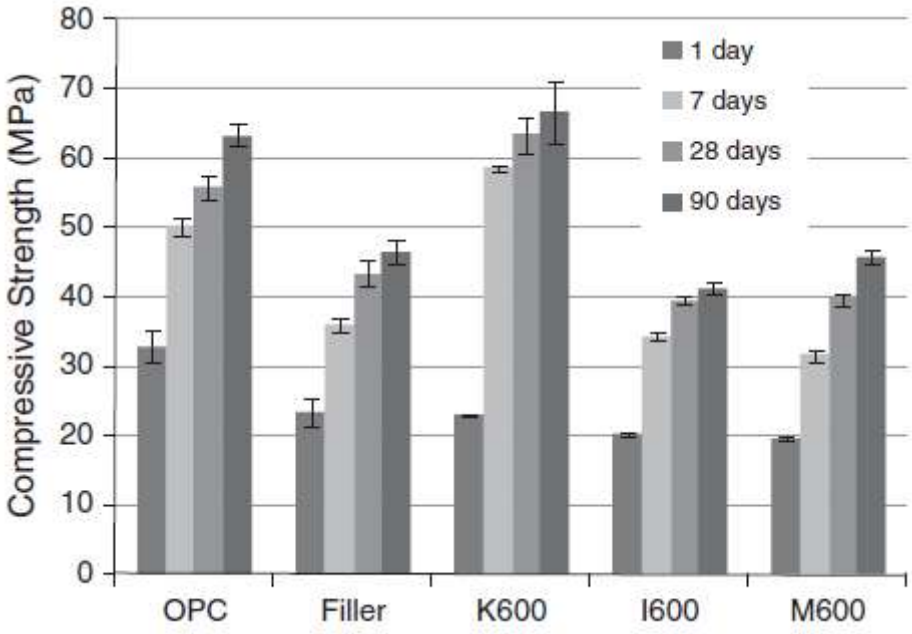

OPC = Ciment Portland
K600 = Ciment + métakaolin
I600 = Ciment + illite calcinée
M600 = Ciment + montmorillonite calcinée

Figure 1-17 : Résistances à la compression de mortiers obtenus à partir de ciments incorporant 30% de métakaolin, d'illite calcinée et de montmorillonite calcinée [62].

Les résultats démontrent que les mortiers réalisés à base de ciment substitué par de l'illite calcinée sont ceux qui présentent les moins bonnes performances mécaniques en comparaison de la montmorillonite calcinée et du métakaolin. D'une manière générale, les argiles riches en montmorillonite et illite vont donc présenter une réactivité pouzzolanique (indice d'activité) plus faible et une cinétique de réaction plus lente que les argiles riches en kaolinite [103]. En revanche, plusieurs autres études ont démontré que les résistances à la compression de mortiers contenant des illites et smectites calcinées peuvent être équivalentes à la référence 100% ciment après 28j tout en diminuant la perméabilité et en améliorant la résistance à l'attaque d'espèces chimiques telles que les chlorures [103–106]. Par exemple, une bentonite (argile riche en montmorillonite) provenant du Westervald en Allemagne et calcinée à 900°C a permis d'obtenir un indice d'activité (mesure de résistance à la compression) de 100% à 28 j [107]. Une autre argile du sud de l'Allemagne contenant 20-25% de kaolinite avec 40% de smectite a permis d'obtenir un indice d'activité supérieur à 100% à 28 j pour un taux de remplacement de 25% après calcination à 800°C [108]. Il apparait donc que des argiles naturelles avec un pourcentage de kaolinite inférieur à 30% mais contenant également une proportion élevée de smectite et/ou d'illite peuvent atteindre la pouzzolanicité élevée des SCM conventionnels [109–111].

Ce travail de recherche bibliographique a permis de comprendre de manière plus précise quels sont les facteurs qui vont influencer la réactivité des échantillons d'argiles tels que le type de minéraux argileux, la pureté ou encore la nature des minéraux accessoires. Le projet LC3 est très prometteur, cependant peu d'études se sont intéressées à la calcination et la réactivité en milieu cimentaire d'échantillons constitués notamment de mélanges d'argiles et de carbonates.

1.4. Les marnes calcinées comme pouzzolanes

Les marnes sont souvent négligées par les fabricants de terres cuites, notamment du fait de leur importante teneur en carbonates. Elles sont considérées comme des déchets par de nombreuses industries et les réserves ne cessent de croitre [112]. Pourtant ces matériaux peuvent contenir une quantité non négligeable de minéraux argileux, qui une fois calcinés présente un fort caractère pouzzolanique. L'utilisation de marnes calcinées comme pouzzolanes pourrait donc permettre de valoriser des ressources secondaires considérées comme déchets tout en réduisant l'empreinte environnementale de l'industrie cimentière. Dans cette partie, nous allons nous intéresser à la minéralogie particulière de ces matériaux ainsi que leur mode de formation, puis nous référencerons les connaissances actuelles sur leur calcination et leur utilisation comme ajout cimentaire.

1.4.1. Les marnes

Les marnes sont des roches sédimentaires composées d'un mélange d'argiles et de carbonates (généralement de la calcite ou de la dolomite). Dans les marnes, les pourcentages d'argiles et de carbonates varient généralement entre 25% et 75%. D'autres minéraux peuvent être présents tels que du quartz, des feldspaths et d'autres minéraux accessoires. Du fait de leur minéralogie, les marnes vont être majoritairement composées de SiO_2, CaO et Al_2O_3. La figure 1-18 [113] situe la composition chimique de plusieurs marnes dans un digramme ternaire SiO_2-CaO-Al_2O_3.

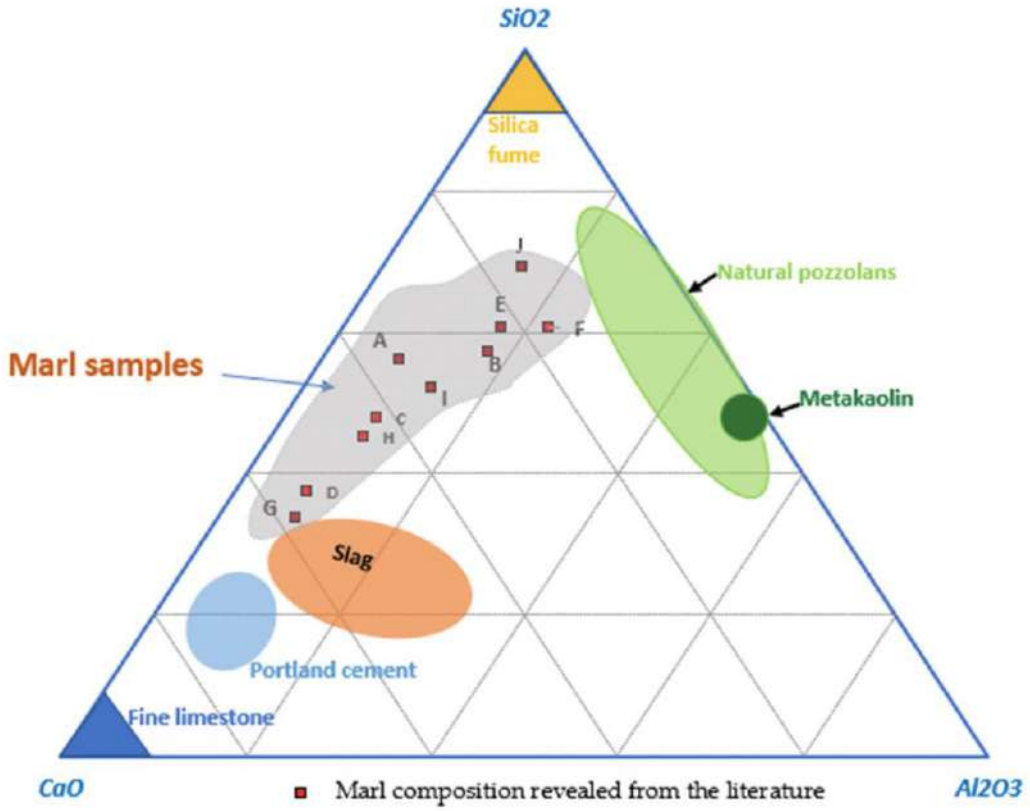

Figure 1-18 : Composition chimique de plusieurs marnes dans un digramme ternaire SiO_2-CaO-Al_2O_3 [113]. (A) : Bahhou et al. [114] ; (B) : Bullerjhan et al. [115] ; (C) : Kastis et al. [116] ; (D) : Soltani et al. [117] ; (E) : Danner et al. [64]; (F): Danner et al [118]. ; (G) : Weber et al. [119] ; (H) : Rakhimov et al. [120] ; (I) : Siline et al. [121] ; (J) : Akgun et al. [122].

Les marnes sont donc principalement situées sur l'axe SiO_2-CaO qui correspond en réalité à l'axe argile-carbonate. Certaines marnes en revanches possèdent également une quantité non négligeable d'aluminium qui s'explique par le type de minéraux argileux présent dans l'échantillon. Par exemple, l'échantillon (F) qui est le plus à droite du digramme contient de la kaolinite. Du fait de sa structure TO, la kaolinite présente un rapport Si/Al beaucoup plus faible que les montmorillonites, ce qui explique que la concentration en Al_2O_3 de l'échantillon (F) soit si importante en comparaison des autres. Tout cela donne un premier aperçu de la grande variabilité chimique et minéralogique des marnes. Plusieurs variables doivent être considérées lors de l'utilisation de marnes comme SCMs :

- **Le type de minéraux argileux :** kaolinite, palygorskite, smectite, illite, etc.

Ce sont ces minéraux argileux qui vont être responsables de la réactivité pouzzolanique et il est donc important de les identifier.

- **Le type de carbonate :** calcite, dolomite, ankerite, etc.

En fonction du type de carbonates présents, la température de calcination va différér car les carbonates ne se décomposent pas tous à la même température. De plus, il y aura formation de différentes phases après calcination qui pourront éventuellement avoir un impact important sur l'hydratation du système. Par exemple la calcination de calcite va entrainer la formation de CaO alors que la calcination de dolomite va entrainer la formation de MgO additionnel au CaO.

- **Les proportions relatives des minéraux argileux et des carbonates**

- **Les minéraux accessoires :** quartz, feldspath, etc.

Il est également important d'identifier ces minéraux accessoires pour savoir s'ils vont avoir un comportement inerte ou non.

Cette forte variabilité de la composition des marnes complexifie grandement l'étude de leur utilisation comme ajouts cimentaires. Il est donc parfois nécessaire d'avoir une étude spécifique pour chaque échantillon considéré.

1.4.2. Connaissances actuelles sur l'utilisation de marnes calcinées comme ajouts cimentaires

1.4.2.1. La calcination

La minéralogie des échantillons et notamment le type de minéraux argileux présents va dicter la température de calcination nécessaire. La figure 1-19 [113] présente les températures de

calcination en fonction du temps de résidence (temps à température maximale) pour différentes marnes contenants différents minéraux argileux.

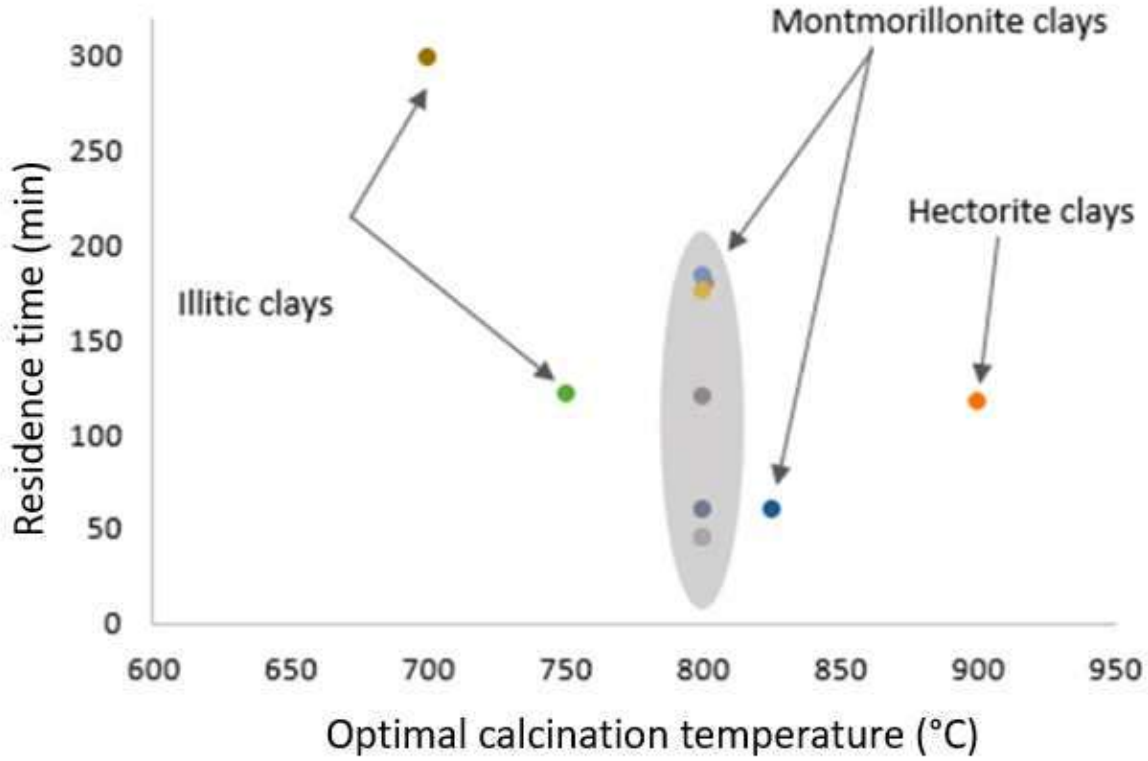

Figure 1-19 : Temps de résidence et températures utilisés pour différentes marnes [113].

Globalement, 800°C sera la température de calcination moyenne pour les marnes contenant de la montmorillonite par exemple alors que les échantillons riches en illite seront calcinés à des températures inférieures entre 700 et 750°C. L'autre facteur à prendre en compte est la nature des carbonates présents dans les échantillons. En effet, si l'échantillon contient de la calcite il y aura décarbonatation et formation de chaux. Si l'échantillon contient de la dolomite, il y aura alors formation de chaux et de périclase (qui est connu pour être responsable de problèmes de gonflement post-durcissement [123]). La formation de ces nouvelles phases potentiellement problématiques ainsi que les émissions de CO_2 dues à la décarbonatation des échantillons peuvent parfois suggérer d'utiliser une température de calcination inférieure. La détermination de la température de calcination doit se faire via des analyses physico-chimiques poussées afin d'obtenir le composé le plus réactif possible tout en limitant les problèmes de recristallisation et de néoformations de phases potentiellement néfastes pour l'hydratation du ciment composé final.

1.4.2.2. La réactivité

Différentes études se sont intéressées à l'étude de la réactivité de marnes calcinées [112,117,119,120,124]. Rakhimov et al, [120] se sont intéressés à l'utilisation d'une marne contenant de la kaolinite (7%), de la montmorillonite (12%), de la chlorite (4%), de la calcite (47%) et des minéraux accessoires (30% au total). Ils ont démontré que l'incorporation de cette marne calcinée entre 400 et 800°C dans des proportions allant de 5 à 20% de remplacement permettait une augmentation de la résistance à la compression variant de +5 à +37% par rapport à la référence. La meilleure formulation étant le remplacement de 10-15% du ciment par la marne calcinée à 800°C. Ils attribuent ce gain de résistance en compression à la réactivité pouzzolanique des phases argileuses calcinées d'une part, mais également à la réactivité des silicates de calcium néoformés durant la calcination qui vont participer à la formation de silicate de calcium hydraté lors de l'hydratation.

Danner et al, [125] se sont intéressés à une marne contenant de la smectite (54%), de la kaolinite (8%), de l'illite (4%), de la calcite (25%) et des minéraux accessoires (9%). Le tableau 1-3 présente les résistances à la compression de mortiers (e/l constant de 0,5) obtenus à partir de ciments incorporant différents pourcentages de cette marne calcinée à 800°C.

	Relative compressive strength (%)			
Time	REF	20%	35%	50%
1 day	100	81	64	43
3 day	100	88	77	58
7 days	100	95	92	84
28 days	100	107	106	95

Tableau 1-3 : Résistances en compression relatives de mortiers contenant une marne calcinée en fonction du pourcentage de remplacement [125].

Il est nécessaire d'attendre 28j avant d'avoir des résistances à la compression supérieures à la référence pour des pourcentages de remplacements allant de 20 à 35%, notamment du fait de la cinétique de la réaction pouzzolanique et de la dilution du clinker. Ces résultats démontrent que ce type de marne (riche en smectite) peut être utilisé comme ajout

cimentaire à des pourcentages de remplacement importants (un remplacement de 50% à 28j permet d'obtenir une résistance à la compression pratiquement équivalente à la référence).

L'une des principales difficultés lors de la caractérisation du potentiel d'utilisation comme ajout cimentaire d'une marne calcinée est la mesure de la réactivité pouzzolanique qui ne peut pas être faite par le biais des tests classiques tels que l'essai Chapelle [81] et la norme ASTM C1897 [87]. En effet, par leur minéralogie particulière et notamment par la présence de carbonate de calcium, il y a formation de chaux lors de la calcination des marnes si la température dépasse 700°C [126]. Or, l'essai Chapelle et la norme ASTM C1897 impliquent que l'échantillon testé ne contienne pas de calcium libre (car ils sont tous deux basés sur le principe de réactivité de l'échantillon avec une quantité définie de $Ca(OH)_2$). Par conséquent, la meilleure méthode actuelle pour caractériser la réactivité des marnes calcinées est de la tester en milieu cimentaire au travers de mesures de résistance à la compression.

1.5. Verrous scientifiques

Cette recherche bibliographique a permis de mettre en évidence plusieurs verrous scientifiques auxquels nous allons essayer de répondre dans ce manuscrit.

Le premier verrou scientifique concerne l'utilisation de marnes calcinées comme ajouts cimentaires. Il a été constaté que la grande variabilité chimique et minéralogique de ces matériaux complexifie leur étude. Même si des indices sur le choix de la température de calcination existent (notamment en fonction du type de minéraux argileux présents dans l'échantillon) il est parfois nécessaire de faire une étude spécifique pour chaque matériau considéré. De plus, la formation de chaux lors de la calcination rend imprécis la majorité des tests habituellement utilisés pour caractériser la réactivité pouzzolanique. L'un des objectifs de ce projet de thèse est donc de réaliser une étude spécifique de la calcination, de la réactivité et de l'utilisation comme ajout cimentaire de deux marnes dolomitiques considérées comme des déchets par l'industrie minière et qui contiennent notamment de la palygorskite et de la smectite comme phases argileuses. Au travers de cette étude, l'objectif est également de caractériser la réactivité pouzzolanique de ces matériaux calcinés en

utilisant un moyen détourné qui se base sur une étude multi-échelle à l'aide de la RMN du solide et de la diffraction des rayons X.

Le second verrou scientifique concerne l'utilisation d'une argile encore jamais étudiée à l'heure actuelle comme ajout cimentaire : la palygorskite, qui est présente dans l'une des deux marnes étudiées. En effet, les recherches bibliographiques réalisés sur le sujet ont permis de mettre en évidence un vide scientifique sur l'étude de la calcination et de la réactivité en système cimentaire de la palygorskite calcinée. Pourtant, l'étude de nouvelles argiles est primordiale pour pouvoir proposer des alternatives au métakaolin qui n'est pas réparti uniformément sur la planète. L'objectif de ce projet de thèse est donc de déterminer si la palygorskite calcinée présente un intérêt pour une utilisation comme SCM.

Le troisième verrou scientifique relève plus d'un aspect fondamental : Il a été mis en évidence que le lien entre les modifications physico-chimiques induites par la calcination, la réactivité pouzzolanique et les performances mécaniques en système cimentaire n'était pas encore bien établi. En effet, la majorité des explications restent hypothétiques et se basent sur une publication [62] dans laquelle aucun aspect quantitatif n'a été amené. Par conséquent, le dernier objectif de ce projet de thèse est d'amener de nouvelles données et notamment des aspects quantitatifs pour éventuellement mettre en évidence le lien entre les modifications physico-chimiques induites par la calcination, la réactivité pouzzolanique et les performances mécaniques en système cimentaire.

1.6. Références

[1] NF EN 197-1, Afnor EDITIONS. (n.d.). https://www.boutique.afnor.org/fr-fr/norme/nf-en-1971/ciment-partie-1-composition-specifications-et-criteres-de-conformite-des-ci/fa149898/1234 (accessed May 21, 2022).

[2] Fabrication du ciment. Processus de fabrication du ciment illustré étape par étape, (n.d.). https://www.febelcem.be/fr/ciment-applications/fabrication-du-ciment/ (accessed June 22, 2022).

[3] A. Hasanbeigi, L. Price, E. Lin, Emerging energy-efficiency and CO2 emission-reduction technologies for cement and concrete production: A technical review, Renewable and Sustainable Energy Reviews. 16 (2012) 6220–6238. https://doi.org/10.1016/j.rser.2012.07.019.

[4] T. Hanein, F.P. Glasser, M. Bannerman, Thermodynamics of Portland Cement Clinkering, (n.d.) 9.

[5] H.F.W. Taylor, Cement Chemistry, 2nd ed., Thomas Telford, London, 1997.

[6] G. Andreas, Cement-superplasticizer interactions at ambient temperatures: rheology, phase composition, pore water and heat of hydration of cementitious systems, ETH Zurich, 2002. https://doi.org/10.3929/ETHZ-A-004470198.

[7] S.A. Miller, V.M. John, S.A. Pacca, A. Horvath, Carbon dioxide reduction potential in the global cement industry by 2050, Cement and Concrete Research. 114 (2018) 115–124. https://doi.org/10.1016/j.cemconres.2017.08.026.

[8] D.N. Huntzinger, T.D. Eatmon, A life-cycle assessment of Portland cement manufacturing: comparing the traditional process with alternative technologies, Journal of Cleaner Production. 17 (2009) 668–675. https://doi.org/10.1016/j.jclepro.2008.04.007.

[9] J.G. Peacey, W.G. Davenport, The Iron Blast Furnace: Theory and Practice, Elsevier, 2016.

[10] M. Behim, B. Redjel, R. Jauberthie, Réactivitié du laitier de hauts fourneaux d'Annaba (Algérie) en substitution partielle du ciment, (2002).

[11] E. Crossin, The greenhouse gas implications of using ground granulated blast furnace slag as a cement substitute, Journal of Cleaner Production. 95 (2015) 101–108. https://doi.org/10.1016/j.jclepro.2015.02.082.

[12] B. K.C., G. Bir, S. Tamrakar, Utilization of Steel Slag as a Replacement for Filler Material in the Asphalt Concrete, (2020).

[13] M. Lagos-Varas, D. Movilla-Quesada, A.C. Raposeiras, D. Castro-Fresno, Á. Vega-Zamanillo, M. Cumian-Benavides, Use of Hydrated Ladle Furnace Slag as a filler substitute in asphalt mastics: Rheological analysis of filler/bitumen interaction, Construction and Building Materials. 332 (2022) 127370. https://doi.org/10.1016/j.conbuildmat.2022.127370.

[14] G. Xu, X. He, Y. He, Effect of Steel Slag and Granulated Blast-furnace Slag on the Mechanical Strength and Pore Structure of Cement Composites, J. Wuhan Univ. Technol.-Mat. Sci. Edit. 33 (2018) 1186–1192. https://doi.org/10.1007/s11595-018-1951-4.

[15] W.J. Johnson, The Effect of Chemical Composition of Blast-Furnace Slag on Compressive Strength and Durability Properties of Mortar Specimens, (n.d.) 97.

[16] M. Islam, M. Islam, M.A. Rahman, A. Das, Strength Behavior of Mortar Using Slag As Partial Replacement of Cement, MIST Journal: GALAXY (DHAKA). 3 (2011). https://doi.org/10.3329/mist.v3i0.8053.

[17] C. Shi, J. Qian, High performance cementing materials from industrial slags — a review, Resources, Conservation and Recycling. 29 (2000) 195–207. https://doi.org/10.1016/S0921-3449(99)00060-9.

[18] H.-W. Song, V. Saraswathy, Studies on the corrosion resistance of reinforced steel in concrete with ground granulated blast-furnace slag—An overview, Journal of Hazardous Materials. 138 (2006) 226–233. https://doi.org/10.1016/j.jhazmat.2006.07.022.

[19] Fiche-technique-CEM-III_C-32.5-N-LH_SR-FOS-04-2021-V.2.1.pdf, (n.d.). https://ecocem.fr/wp-content/uploads/2019/07/Fiche-technique-CEM-III_C-32.5-N-LH_SR-FOS-04-2021-V.2.1.pdf (accessed May 31, 2022).

[20] Z. Osmanovic, N. Haračić, J. Zelić, Properties of blastfurnace cements (CEM III/A, B, C) based on Portland cement clinker, blastfurnace slag and cement kiln dusts, Cement and Concrete Composites. 91 (2018) 189–197. https://doi.org/10.1016/j.cemconcomp.2018.05.006.

[21] K.L. Scrivener, V.M. John, E.M. Gartner, Eco-efficient cements: Potential economically viable solutions for a low-CO2 cement-based materials industry, Cement and Concrete Research. 114 (2018) 2–26. https://doi.org/10.1016/j.cemconres.2018.03.015.

[22] R. Snellings, Assessing, Understanding and Unlocking Supplementary Cementitious Materials, RILEM Technical Letters. 1 (2016) 50–55. https://doi.org/10.21809/rilemtechlett.2016.12.

[23] Cement Industry Energy and CO2 Performance: Getting the Numbers Right (GNR), World Business Council for Sustainable Development (WBCSD). (n.d.). https://www.wbcsd.org/mow8j (accessed June 3, 2022).

[24] Z.T. Yao, X.S. Ji, P.K. Sarker, J.H. Tang, L.Q. Ge, M.S. Xia, Y.Q. Xi, A comprehensive review on the applications of coal fly ash, Earth-Science Reviews. 141 (2015) 105–121. https://doi.org/10.1016/j.earscirev.2014.11.016.

[25] S.H. Lee, H.J. Kim, E. Sakai, M. Daimon, Effect of particle size distribution of fly ash–cement system on the fluidity of cement pastes, Cement and Concrete Research. 33 (2003) 763–768. https://doi.org/10.1016/S0008-8846(02)01054-2.

[26] E. Sakai, S. Miyahara, S. Ohsawa, S.-H. Lee, M. Daimon, Hydration of fly ash cement, Cement and Concrete Research. 35 (2005) 1135–1140. https://doi.org/10.1016/j.cemconres.2004.09.008.

[27] Y.M. Zhang, W. Sun, H.D. Yan, Hydration of high-volume fly ash cement pastes, Cement and Concrete Composites. 22 (2000) 445–452. https://doi.org/10.1016/S0958-9465(00)00044-5.

[28] A. Elahi, P.A.M. Basheer, S.V. Nanukuttan, Q.U.Z. Khan, Mechanical and durability properties of high performance concretes containing supplementary cementitious materials, Construction and Building Materials. 24 (2010) 292–299. https://doi.org/10.1016/j.conbuildmat.2009.08.045.

[29] ASTM C618-19, Standard Specification for Coal Fly Ash and Raw or Calcined Natural Pozzolan for Use in Concrete, ASTM International, West Conshohocken, PA, 2019, www.astm.org, (n.d.).

[30] A. Harison, V. Srivastava, A. Herbert, Effect of Fly Ash on Compressive Strength of Portland Pozzolona Cement Concrete, 2 (2014) 4.

[31] A.L.A. Fraay, J.M. Bijen, Y.M. de Haan, The Reaction of Fly Ash in Concrete, A critical Examination, (1989).

[32] O. US EPA, Sources of Greenhouse Gas Emissions, (2015). https://www.epa.gov/ghgemissions/sources-greenhouse-gas-emissions (accessed June 4, 2022).

[33] M. Pourabbas Bilondi, M.M. Toufigh, V. Toufigh, Experimental investigation of using a recycled glass powder-based geopolymer to improve the mechanical behavior of clay soils, Construction and Building Materials. 170 (2018) 302–313. https://doi.org/10.1016/j.conbuildmat.2018.03.049.

[34] K.H. Tan, H. Du, Use of waste glass as sand in mortar: Part I – Fresh, mechanical and durability properties, Cement and Concrete Composites. 35 (2013) 109–117. https://doi.org/10.1016/j.cemconcomp.2012.08.028.

[35] R. Xiao, P. Polaczyk, M. Zhang, X. Jiang, Y. Zhang, B. Huang, W. Hu, Evaluation of Glass Powder-Based Geopolymer Stabilized Road Bases Containing Recycled Waste Glass Aggregate, Transportation Research Record. 2674 (2020) 22–32. https://doi.org/10.1177/0361198119898695.

[36] I. Rachida, M. Cyr, A. Tagnit-Hamou, Pozzolanic properties of fine and coarse color-mixed glass cullet, Cement and Concrete Composites. 33 (2011) 19–29. https://doi.org/10.1016/j.cemconcomp.2010.09.013.

[37] Utilization of waste glass powder in the production of cement and concrete - ScienceDirect, (n.d.). https://www.sciencedirect.com/science/article/pii/S095006181631279X?casa_token=3cdVCiwKEjMAAAAA:OxXE13GcUw6TZX9tYgx2NPDgFLVxL9oswkPFJtYGfieij7ff09OiXVHD7j8jjaK19rL1u4dJVw (accessed May 10, 2022).

[38] ASTM International - ASTM C1866/C1866M-20 - Standard Specification for Ground-Glass Pozzolan for Use in Concrete | Engineering360, (n.d.). https://standards.globalspec.com/std/14182089/astm-c1866-c1866m-20 (accessed June 4, 2022).

[39] A.M. Rashad, Recycled waste glass as fine aggregate replacement in cementitious materials based on Portland cement, Construction and Building Materials. 72 (2014) 340–357. https://doi.org/10.1016/j.conbuildmat.2014.08.092.

[40] H. Du, K.H. Tan, Waste Glass Powder as Cement Replacement in Concrete, (n.d.). https://www.researchgate.net/publication/279287238_Waste_Glass_Powder_as_Cement_Replacement_in_Concrete (accessed March 21, 2021).

[41] N. Kumari, C. Mohan, Basics of Clay Minerals and Their Characteristic Properties, IntechOpen, 2021. https://doi.org/10.5772/intechopen.97672.

[42] S.W. Bailey, Structures of Layer Silicates, (1980). https://doi.org/10.1180/mono-5.1.

[43] Clay Mineralogy · Dr. Krakow Rohstoffconsult, (n.d.). https://www.geo-ceramic-laboratory.com/geo-ceramic-laboratory/clay-mineralogy/ (accessed June 6, 2022).

[44] S.P. Altaner, Smectite group, in: G.V. Middleton, M.J. Church, M. Coniglio, L.A. Hardie, F.J. Longstaffe (Eds.), Encyclopedia of Sediments and Sedimentary Rocks, Springer Netherlands, Dordrecht, 2003: pp. 675–677. https://doi.org/10.1007/978-1-4020-3609-5_216.

[45] Les réactions d'hydrolyse et la production d'argiles — Eduterre, (n.d.). https://eduterre.ens-lyon.fr/thematiques/hydro/erosion/hydrolyse (accessed June 8, 2022).

[46] T.J. Brown, R.A. Shaw, T.P. Bide, E. Petavratzi, A.S. Walters, E.R. Raycraft, British Geological Survey, World mineral production 2007-11, British Geological Survey, Nottingham, 2013.

[47] T.J. Brown, R.A. Shaw, T. Bide, E. Petravratzi, E.R. Raycraft, A.S. Walters, World mineral production 2014-18, British Geological Survey, Nottingham, UK, 2020.

[48] M. Rautureau, Sépiolite & palygorskite, (n.d.) 5.

[49] E. Garc, M. Suarez, J. Santaren, A. Álvarez, Crystallochemical Characterization of the Palygorskite and Sepiolite from the Allou Kagne Deposit, Senegal, Clays and Clay Minerals. 55 (2006). https://doi.org/10.1346/CCMN.2007.0550608.

[50] B.F. Jones, E. Galan, Chapter 16. SEPIOLITE AND PALYGORSKITE, in: Chapter 16. SEPIOLITE AND PALYGORSKITE, De Gruyter, 2018: pp. 631–674. https://doi.org/10.1515/9781501508998-021.

[51] A. Singer, Palygorskite in sediments: Detrital, diagenetic or neoformed — A critical review, Geol Rundsch. 68 (1979) 996–1008. https://doi.org/10.1007/BF02274683.

[52] B. Velde, Clay minerals, (1985). https://www.osti.gov/biblio/6904353 (accessed May 12, 2022).

[53] C.E. Weaver, K.C. Beck, Miocene of the S.E. United States: A model for chemical sedimentation in a peri-marine environment, Sedimentary Geology. 17 (1977) IX–234. https://doi.org/10.1016/0037-0738(77)90062-8.

[54] R.A. Couture, Composition and origin of palygorskite-rich and mont-morillonite-rich zeolite-containing sediments from the Pacific Ocean, Chemical Geology. 19 (1977) 113–130. https://doi.org/10.1016/0009-2541(77)90009-2.

[55] N. Imai, R. Otsuka, Sepiolite and Palygorskite in Japan, in: A. Singer, E. Galan (Eds.), Developments in Sedimentology, Elsevier, 1984: pp. 211–232. https://doi.org/10.1016/S0070-4571(08)70040-2.

[56] D.H. Yaalon, M. Wieder, Pedogenic palygorskite in some arid brown (calciorthid) soils of Israel, Clay Minerals. 11 (1976) 73–80. https://doi.org/10.1180/claymin.1976.011.1.08.

[57] H. Murray, Industrial Clays Case Study, (n.d.) 9.

[58] H.H. Murray, M. Pozo, E. Galán, Chapter 4 - An Introduction to Palygorskite and Sepiolite Deposits—Location, Geology and Uses, in: E. Galàn, A. Singer (Eds.), Developments in Clay Science, Elsevier, 2011: pp. 85–99. https://doi.org/10.1016/B978-0-444-53607-5.00004-9.

[59] N. Garg, J. Skibsted, Pozzolanic reactivity of a calcined interstratified illite/smectite (70/30) clay, Cement and Concrete Research. 79 (2016) 101–111. https://doi.org/10.1016/j.cemconres.2015.08.006.

[60] R. Snellings, G. Mertens, J. Elsen, Supplementary Cementitious Materials, Reviews in Mineralogy and Geochemistry. 74 (2012) 211–278. https://doi.org/10.2138/rmg.2012.74.6.

[61] K. Emmerich, Thermal Analysis in the Characterization and Processing of Industrial Minerals, (2010). https://doi.org/10.1180/EMU-notes.9.5.

[62] R. Fernandez, F. Martirena, K.L. Scrivener, The origin of the pozzolanic activity of calcined clay minerals: A comparison between kaolinite, illite and montmorillonite, Cement

and Concrete Research. 41 (2011) 113–122. https://doi.org/10.1016/j.cemconres.2010.09.013.

[63] S. Hollanders, R. Adriaens, J. Skibsted, Ö. Cizer, J. Elsen, Pozzolanic reactivity of pure calcined clays, Applied Clay Science. 132–133 (2016) 552–560. https://doi.org/10.1016/j.clay.2016.08.003.

[64] T. Danner, G. Norden, H. Justnes, Characterisation of calcined raw clays suitable as supplementary cementitious materials, Applied Clay Science. 162 (2018) 391–402. https://doi.org/10.1016/j.clay.2018.06.030.

[65] C. He, E. Makovicky, B. Osbæck, Thermal stability and pozzolanic activity of calcined kaolin, Applied Clay Science. 9 (1994) 165–187. https://doi.org/10.1016/0169-1317(94)90018-3.

[66] M. AYUB, M. YUSUF, M.A. BEG, F.A. FARUQI, Pozzolanic properties of burnt clays, Pak. J. Sci. Ind. Res. 31 (1988) 1–10.

[67] J. Ambroise, M. Murat, J. Péra, Hydration reaction and hardening of calcined clays and related minerals V. Extension of the research and general conclusions, Cement and Concrete Research. 15 (1985) 261–268. https://doi.org/10.1016/0008-8846(85)90037-7.

[68] M. Murat, Hydration reaction and hardening of calcined clays and related minerals. I. Preliminary investigation on metakaolinite, Cement and Concrete Research. 13 (1983) 259–266. https://doi.org/10.1016/0008-8846(83)90109-6.

[69] Pozzolanic activation of metakaolin | Advances in Cement Research, (n.d.). https://www.icevirtuallibrary.com/doi/10.1680/adcr.1992.4.16.167 (accessed June 6, 2022).

[70] G. Kakali, T. Perraki, S. Tsivilis, E. Badogiannis, Thermal treatment of kaolin: the effect of mineralogy on the pozzolanic activity, Applied Clay Science. 20 (2001) 73–80. https://doi.org/10.1016/S0169-1317(01)00040-0.

[71] A. Chakchouk, L. Trifi, B. Samet, S. Bouaziz, Formulation of blended cement: Effect of process variables on clay pozzolanic activity, Construction and Building Materials. 23 (2009) 1365–1373. https://doi.org/10.1016/j.conbuildmat.2008.07.015.

[72] G.E. Christidis, The concept of layer charge of smectites and its implications for important smectite-water properties, in: 2011.

[73] S.I. Tsipursky, V.A. Drits, The distribution of octahedral cations in the 2:1 layers of dioctahedral smectites studied by oblique-texture electron diffraction, Clay Miner. 19 (1984) 177–193. https://doi.org/10.1180/claymin.1984.019.2.05.

[74] An Improved Model for Structural Transformations of Heat-Treated Aluminous Dioctahedral 2:1 Layer Silicates | SpringerLink, (n.d.). https://link.springer.com/article/10.1346/CCMN.1995.0430608 (accessed June 6, 2022).

[75] R. Mielenz, L. Witte, O. Glantz, Effect of Calcination on Natural Pozzolans, in: 1950. https://doi.org/10.1520/STP39404S.

[76] C. He, E. Makovicky, B. Osbaeck, Thermal treatment and pozzolanic activity of Na- and Ca-montmorillonite, Applied Clay Science. 10 (1996) 351–368. https://doi.org/10.1016/0169-1317(95)00037-2.

[77] G. Habert, N. Choupay, G. Escadeillas, D. Guillaume, J.M. Montel, Clay content of argillites: Influence on cement based mortars, Applied Clay Science. 43 (2009) 322–330. https://doi.org/10.1016/j.clay.2008.09.009.

[78] W. Hirsiger, M. Müller-Vonmoos, H.G. Wiedemann, Thermal analysis of palygorskite, Thermochimica Acta. 13 (1975) 223–230. https://doi.org/10.1016/0040-6031(75)80083-9.

[79] K. Scrivener, R. Fernandez, Des argiles calcinées comme substitut au ciment, SA des éditions des associations techniques universitaires. (2011). https://doi.org/10.5169/seals-154199.

[80] NF P18-513, Afnor EDITIONS. (n.d.). https://www.boutique.afnor.org/fr-fr/norme/nf-p18513/addition-pour-beton-hydraulique-metakaolin-specifications-et-criteres-de-co/fa175740/39605 (accessed May 19, 2022).

[81] E. Ferraz, S. Andrejkovičová, W. Hajjaji, A. Velosa, A. Santos Silva, F. Rocha, Pozzolanic activity of metakaolins by the French standard of the modified Chapelle test: A direct methology, Acta Geodynamica et Geomaterialia. 12 (2015) 289–298. https://doi.org/10.13168/AGG.2015.0026.

[82] B. Ayati, D. Newport, H. Wong, C. Cheeseman, Low-carbon cements: Potential for low-grade calcined clays to form supplementary cementitious materials, Cleaner Materials. 5 (2022) 100099. https://doi.org/10.1016/j.clema.2022.100099.

[83] X. Li, R. Snellings, M. Antoni, N.M. Alderete, M. Ben Haha, S. Bishnoi, Ö. Cizer, M. Cyr, K. De Weerdt, Y. Dhandapani, J. Duchesne, J. Haufe, D. Hooton, M. Juenger, S. Kamali-Bernard, S. Kramar, M. Marroccoli, A.M. Joseph, A. Parashar, C. Patapy, J.L. Provis, S. Sabio, M. Santhanam, L. Steger, T. Sui, A. Telesca, A. Vollpracht, F. Vargas, B. Walkley, F. Winnefeld, G. Ye, M. Zajac, S. Zhang, K.L. Scrivener, Reactivity tests for supplementary cementitious materials: RILEM TC 267-TRM phase 1, Mater Struct. 51 (2018) 151. https://doi.org/10.1617/s11527-018-1269-x.

[84] ASTM C311 / C311M - 18 Standard Test Methods for Sampling and Testing Fly Ash or Natural Pozzolans for Use in Portland-Cement Concrete, (n.d.). https://www.astm.org/Standards/C311.htm (accessed November 18, 2021).

[85] M. Kasaniya, M.D.A. Thomas, E.G. Moffatt, Development of Rapid and Reliable Pozzolanic Reactivity Test Method, MJ. 116 (2019) 145–154. https://doi.org/10.14359/51716718.

[86] F. Avet, R. Snellings, A. Alujas Diaz, M. Ben Haha, K. Scrivener, Development of a new rapid, relevant and reliable (R3) test method to evaluate the pozzolanic reactivity of calcined kaolinitic clays, Cement and Concrete Research. 85 (2016) 1–11. https://doi.org/10.1016/j.cemconres.2016.02.015.

[87] Standard Test Methods for Measuring the Reactivity of Supplementary Cementitious Materials by Isothermal Calorimetry and Bound Water Measurements, (n.d.). https://www.astm.org/c1897-20.html (accessed March 24, 2022).

[88] R. Snellings, X. Li, F. Avet, K. Scrivener, Rapid, Robust, and Relevant (R3) Reactivity Test for Supplementary Cementitious Materials., ACI Materials Journal. 116 (2019) 155–163.

[89] Influence of degree of dehydroxylation on the pozzolanic activity of metakaolin - ScienceDirect, (n.d.).

https://www.sciencedirect.com/science/article/pii/S0169131709000283 (accessed June 6, 2022).

[90] H. Justnes, I. Meland, J.O. Bjoergum, J. Krane, T. Skjetne, Nuclear magnetic resonance (NMR) —a powerful tool in cement and concrete research, Advances in Cement Research. 3 (1990) 105–110. https://doi.org/10.1680/adcr.1990.3.11.105.

[91] J. Rocha, J. Klinowski, 29Si and 27Al magic-angle-spinning NMR studies of the thermal transformation of kaolinite, Phys Chem Minerals. 17 (1990) 179–186. https://doi.org/10.1007/BF00199671.

[92] Fernandez et al. - 2011 - The origin of the pozzolanic activity of calcined .pdf, (n.d.).

[93] R.S. Almenares, L.M. Vizcaíno, S. Damas, A. Mathieu, A. Alujas, F. Martirena, Industrial calcination of kaolinitic clays to make reactive pozzolans, Case Studies in Construction Materials. 6 (2017) 225–232. https://doi.org/10.1016/j.cscm.2017.03.005.

[94] A. Alujas, R. Fernández, R. Quintana, K.L. Scrivener, F. Martirena, Pozzolanic reactivity of low grade kaolinitic clays: Influence of calcination temperature and impact of calcination products on OPC hydration, Applied Clay Science. 108 (2015) 94–101. https://doi.org/10.1016/j.clay.2015.01.028.

[95] Z. Dai, T.T. Tran, J. Skibsted, Aluminum Incorporation in the C–S–H Phase of White Portland Cement–Metakaolin Blends Studied by 27Al and 29Si MAS NMR Spectroscopy, Journal of the American Ceramic Society. 97 (2014) 2662–2671. https://doi.org/10.1111/jace.13006.

[96] H. El-Diadamony, A.A. Amer, T.M. Sokkary, S. El-Hoseny, Hydration and characteristics of metakaolin pozzolanic cement pastes, HBRC Journal. 14 (2018) 150–158. https://doi.org/10.1016/j.hbrcj.2015.05.005.

[97] D. Zhao, R. Khoshnazar, Microstructure of cement paste incorporating high volume of low-grade metakaolin, Cement and Concrete Composites. 106 (2020) 103453. https://doi.org/10.1016/j.cemconcomp.2019.103453.

[98] S. Krishnan, A.C. Emmanuel, V. Shah, A. Parashar, G. Mishra, S. Maity, S. Bishnoi, Industrial production of limestone calcined clay cement: experience and insights, Green Materials. 7 (2019) 15–27. https://doi.org/10.1680/jgrma.18.00003.

[99] A. Ipavec, R. Gabrovšek, T. Vuk, V. Kaučič, J. Maček, A. Meden, Carboaluminate Phases Formation During the Hydration of Calcite-Containing Portland Cement, Journal of the American Ceramic Society. 94 (2011) 1238–1242. https://doi.org/10.1111/j.1551-2916.2010.04201.x.

[100] A. François, S. Karen, CIMENTS CALCAIRE ARGILES CALCINÉES – LIMESTONE CALCINED CLAY CEMENTS (LC3), (n.d.) 8.

[101] A. Trümer, H.-M. Ludwig, M. Schellhorn, R. Diedel, Effect of a calcined Westerwald bentonite as supplementary cementitious material on the long-term performance of concrete, Applied Clay Science. 168 (2019) 36–42. https://doi.org/10.1016/j.clay.2018.10.015.

[102] A. Trümer, H.-M. Ludwig, M. Schellhorn, R. Diedel, Effect of a calcined Westerwald bentonite as supplementary cementitious material on the long-term performance of

concrete, Applied Clay Science. 168 (2019) 36–42. https://doi.org/10.1016/j.clay.2018.10.015.

[103] R.C. Mielenz, K.T. Greene, N.C. Schieltz, Natural pozzolans for concrete, Economic Geology. 46 (1951) 311–328. https://doi.org/10.2113/gsecongeo.46.3.311.

[104] W. Price, Pozzolans—a review. J Am Concr Inst 72:225–232, (1975).

[105] L. Pepper, B. Mather, Effectiveness Of Mineral Admxtures In Preventing Excessive Expansion Of Concrete Due To Alkaliaggregate Reaction, SP. 223 (2004) 23–54. https://doi.org/10.14359/13494.

[106] S. De Souza, Industrial clays in Brazil: a review. Clay Odyssey 1:323, (2001).

[107] S.E. Schulze, J. Rickert, Suitability of natural calcined clays as supplementary cementitious material, Cement and Concrete Composites. 95 (2019) 92–97. https://doi.org/10.1016/j.cemconcomp.2018.07.006.

[108] N. Beuntner, R. Sposito, K.-C. Thienel, Potential of Calcined Mixed-Layer Clays as Pozzolans in Concrete, MJ. 116 (2019) 19–29. https://doi.org/10.14359/51716677.

[109] N.S. Msinjili, G.J.G. Gluth, P. Sturm, N. Vogler, H.-C. Kühne, Comparison of calcined illitic clays (brick clays) and low-grade kaolinitic clays as supplementary cementitious materials, Mater Struct. 52 (2019) 94. https://doi.org/10.1617/s11527-019-1393-2.

[110] Investigations into the application of calcined clays as composite material in cement - Cement Lime Gypsum, (n.d.). https://www.zkg.de/en/artikel/zkg_Investigations_into_the_application_of_calcined_clays_as_composite_material_2067804.html (accessed June 7, 2022).

[111] N. Beuntner, C. Thienel, Performance and Properties of Concrete made with Calcined Clays, in: 2017.

[112] H. Justnes, T. Østnor, K. De Weerdt, H. Vikan, CALCINED MARL AND CLAY AS MINERAL ADDITION FOR MORE SUSTAINABLE CONCRETE STRUCTURES CALCINED MARL AND CLAY AS MINERAL ADDITION FOR MORE SUSTAINABLE CONCRETE STRUCTURES, (2021).

[113] A. Bahhou, Y. Taha, Y.E. Khessaimi, R. Hakkou, A. Tagnit-Hamou, M. Benzaazoua, Using Calcined Marls as Non-Common Supplementary Cementitious Materials—A Critical Review, Minerals. 11 (2021) 517. https://doi.org/10.3390/min11050517.

[114] A. Bahhou, Y. Taha, Y. El Khessaimi, H. Idrissi, R. Hakkou, J. Amalik, M. Benzaazoua, Use of phosphate mine by-products as supplementary cementitious materials, Materials Today: Proceedings. 37 (2021) 3781–3788. https://doi.org/10.1016/j.matpr.2020.07.619.

[115] F. Bullerjahn, M. Zajac, J. Pekarkova, D. Nied, Novel SCM produced by the co-calcination of aluminosilicates with dolomite, Cement and Concrete Research. 134 (2020) 106083. https://doi.org/10.1016/j.cemconres.2020.106083.

[116] D. Kastis, G. Kakali, S. Tsivilis, M.G. Stamatakis, Properties and hydration of blended cements with calcareous diatomite, Cement and Concrete Research. 36 (2006) 1821–1826. https://doi.org/10.1016/j.cemconres.2006.05.005.

[117] A. Soltani, A. Tarighat, M. Varmazyari, Calcined Marl and Condensed Silica Fume as Partial Replacement for Ordinary Portland Cement, Int J Civ Eng. 16 (2018) 1549–1559. https://doi.org/10.1007/s40999-018-0289-9.

[118] T. Danner, H. Justnes, M. Geiker, R.A. Lauten, Phase changes during the early hydration of Portland cement with Ca-lignosulfonates, Cement and Concrete Research. 69 (2015) 50–60. https://doi.org/10.1016/j.cemconres.2014.12.004.

[119] J. Weber, N. Gadermayr, R. Kozłowski, D. Mucha, D. Hughes, D. Jaglin, W. Schwarz, Microstructure and mineral composition of Roman cements produced at defined calcination conditions, Materials Characterization. 58 (2007) 1217–1228. https://doi.org/10.1016/j.matchar.2007.04.025.

[120] R.Z. Rakhimov, N.R. Rakhimova, A.R. Gaifullin, V.P. Morozov, Properties of Portland cement pastes enriched with addition of calcined marl, Journal of Building Engineering. 11 (2017) 30–36. https://doi.org/10.1016/j.jobe.2017.03.007.

[121] S. Mohammed, G. Elhem, B. Mekki, Valorization of pozzolanicity of Algerian clay: Optimization of the heat treatment and mechanical characteristics of the involved cement mortars, Applied Clay Science. 132–133 (2016) 711–721. https://doi.org/10.1016/j.clay.2016.08.027.

[122] Dicle Üniversitesi Mühendislik Fakültesi Mühendislik Dergisi » Makale » Alternatif puzolan kalsine marn içeren sürdürülebilir katkılı çimentolar, (n.d.). https://dergipark.org.tr/tr/pub/dumf/issue/45282/492137 (accessed May 16, 2022).

[123] E.A. Cherney, R.D. Hooton, Cement Growth Failure Mechanism in Porcelain Suspension Insulators, IEEE Transactions on Power Delivery. 2 (1987) 249–255. https://doi.org/10.1109/TPWRD.1987.4308096.

[124] D.C. Hughes, D. Jaglin, R. Kozłowski, D. Mucha, Roman cements — Belite cements calcined at low temperature, Cement and Concrete Research. 39 (2009) 77–89. https://doi.org/10.1016/j.cemconres.2008.11.010.

[125] T. Danner, G. Norden, H. Justnes, Calcareous smectite clay as a pozzolanic alternative to kaolin, European Journal of Environmental and Civil Engineering. 25 (2021) 1647–1664. https://doi.org/10.1080/19648189.2019.1590741.

[126] V. Poussardin, M. Paris, A. Tagnit-Hamou, D. Deneele, Potential for calcination of a palygorskite-bearing argillaceous carbonate, Applied Clay Science. 198 (2020) 105846. https://doi.org/10.1016/j.clay.2020.105846.

Chapitre 2 – Calcination d'une marne dolomitique contenant de la palygorskite et de la smectite

2.1. Avant-propos

Note : Ce chapitre est basé sur un article publié dans un journal international à comité de lecture.

Titre de l'article : **Potential for calcination of a palygorskite-bearing argillaceous carbonate**

Victor Poussardin, Michael Paris, Arezki Tagnit-Hamou, Dimitri Deneele

Publié dans : Applied Clay Science

DOI : https://doi.org/10.1016/j.clay.2020.105846

Référence

V. Poussardin, M. Paris, A. Tagnit-Hamou, D. Deneele, *Potential for calcination of a palygorskite-bearing argillaceous carbonate*, Applied Clay Science. 198 (2020) 105846.

Contribution à la thèse

La recherche bibliographique réalisée dans l'état de l'art a mis en avant la nécessité de s'intéresser à l'utilisation de nouveaux échantillons argileux pour une utilisation comme ajout cimentaire après calcination. Le premier échantillon étudié est une marne dolomitique contenant de la palygorskite et de la smectite et étant considérée comme déchet par l'industrie minière. L'étape de calcination que subissent les échantillons avant leur ajout dans le ciment est primordiale car elle doit permettre de garantir une réactivité optimale en système cimentaire. C'est à cette première étape que s'intéresse cet article qui consiste en une étude poussée des modifications physico-chimiques qui ont lieu lors de la calcination de cette marne. L'étude de la calcination de cet échantillon peut permettre à terme d'envisager

son utilisation et donc la valorisation de cette ressource secondaire comme nouvel ajout cimentaire.

Résumé en français

L'utilisation intensive du ciment comme matériau de construction entraîne une pollution importante. La majorité des émissions de CO_2 provient du processus de fabrication et non du produit en lui-même. En effet, la décarbonatation du calcaire et l'utilisation de combustibles lors de la clinkérisation sont très polluantes. L'une des principales solutions pour réduire l'empreinte environnementale de l'industrie du ciment est l'utilisation de Supplementary Cementitious Materials (SCMs) en remplacement du clinker. Parmi eux, on trouve les poudres de verre, les cendres volantes, les laitiers de hauts fourneaux ou les argiles calcinées. Cet article se concentre sur la calcination d'une marne contenant de la palygorskite, de la smectite et de la dolomite. L'échantillon a été calciné à différentes températures et étudié par Résonance Magnétique Nucléaire du solide (RMN MAS), diffraction des rayons X (DRX) et microscopie électronique à balayage (MEB). L'augmentation de la température de calcination conduit à une amorphisation de la fraction argileuse de l'échantillon, ce qui entraîne un changement dans la coordination des atomes d'aluminium octaédriques. La transformation progressive des atomes d'aluminium 6 en aluminiums 4 et 5 a été quantifiée en fonction de la température de calcination. Par ailleurs, le calcium issu de la décarbonatation de la dolomite réagit avec le silicium issu de l'amorphisation des phases argileuses pour former un silicate dicalcique mal cristallisé (C_2S) potentiellement réactif. Ce double système (pouzzolanique et hydraulique) fait de cet échantillon un candidat prometteur pour une utilisation comme SCM dans des ciments composés. L'analyse multi-technique appliquée dans cette étude permet de mettre en évidence une corrélation directe entre la température de calcination et les modifications structurales induites.

Résumé en anglais

The intensive use of cement as a building material causes significant pollution. The majority of CO_2 emissions come from the manufacturing process and not from the product itself. Indeed, the decarbonation of limestone and the use of fuels during clinkerisation are very

polluting. One of the main solutions to reduce the environmental footprint of the cement industry is the use of Supplementary Cementitious Materials (SCMs) in substitution of clinker. Among them are glass powders, fly ashes, blast-furnace slags or calcined clays. This article focuses on the thermal reactivity of an argillaceous-carbonate sample containing palygorskite, smectite and Dolomite. The sample was calcined at different temperatures and investigated using Solid State Nuclear Magnetic Resonance (NMR), X-ray diffraction (XRD), and Scanning Electron Microscope (SEM). The increase in calcination temperature leads to an amorphisation of the clay fraction of the sample, resulting in a change in the coordination of the octahedral aluminium atoms. The progressive transformation of 6-fold aluminium atoms to 5-fold and 4-fold was quantified as a function of the calcination temperature. Furthermore, calcium issued from the decarbonation of Dolomite reacts with silicon from the amorphisation of clay phases to form poorly-crystallized Belite (C_2S). This dual system (pozzolanic and hydraulic) makes this sample a promising candidate as SCM in blended cements. The multi-technique analysis applied in this study allows to highlight a direct correlation between the calcination temperature and the induced structural modification.

2.2. Introduction

It is estimated that cement production is responsible for 5-8% of total anthropogenic CO_2 emissions [1]. In an international context promoting the reduction of CO_2 emissions, the cement industry appears to be a bad pupil. The fault resides in clinkerization, the process by which clinker, the basic product of Portland cement, is obtained. Both the use of mostly fossil fuels and the decarbonation of limestone during the process are contributing to the majority of CO_2 emissions [2]. Faced to this alarming observation, the cement industries are now turning to the research and development of new supplementary cementitious materials (SCMs) that can partially replace clinker in order to drastically reduce CO_2 release and the environmental cost of Ordinary Portland Cement (OPC) manufacture. These innovations include the use of additives from industry (blast furnace slags [3], fly ash from power plants [4]), natural additives (clays [5]) and artificial additives (calcined clays). The Limestone Calcined Clay Cement (LC^3) project [6] is a good example of the use of calcined clay as SCM. The substitution of 50% of the clinker with 20% limestone and 30% metakaolin reduces the environmental footprint of OPC by 20-23% while maintaining the delivery of cement with

satisfactory mechanical properties [2]. Numerous studies have shown that kaolinite dehydroxylation during calcination leads to the production of very reactive SCM metakaolin, [7]. In addition, the available kaolinite resources with potential for calcination are relatively well distributed on earth [8], making it possible to envisage large-scale use. In this context, the majority of scientific research has been focused on the calcination of kaolins, sometimes neglecting the study of less common clays. However, understanding the reactivity of other types of natural materials containing clays is essential to envisage the valorisation of secondary clayey resources, refine our knowledge and propose new innovative solutions to reduce the CO_2 emissions of the OPC production. Natural samples rich in palygorskite are one of these interesting materials to test as SCM.

Palygorskite is a clayey mineral consisting of TOT-type ribbons. Several studies have shown that TOT clays, mainly montmorillonites and illites, are not ideal as SCM [9,10], mainly due to the resistance of their structure to heat treatment. The particularity of palygorskite structure compared to montmorillonite and illite is that the tetrahedra are reversed when passing from one ribbon to the other. This alternation creates channels that are filled with zeolitic water, and confers to palygorskite a three-dimensional structure [11]. These channels provide to the palygorskite an important internal surface and hence large specific surface area, high sorption capacity, and microporosity. Its general formula is $(Mg,Al)_2Si_4O_{10}(OH).4H_2O$ but isomorphic substitutions are possible, in particular of silicon by aluminium in tetrahedral sheets [12].
As specified above, the latest studies on blended cement deal with the addition of metakaolin and calcium carbonate to the blended cement. Indeed, limestone will improve the hydration reactions of the different phases of the clinker by acting as a nucleation surface for the hydrates produced. It will also react with the active alumina (from calcined clay) to form carboaluminates. These carboaluminates will stabilize the Ettringite that forms at the early stages of hydration and prevent its transformation into monosulphate. The Ettringite thus stabilised can fill more space than in the monosulphate form, helping to improve the mechanical properties [13,14].

However, only few studies describe the addition of a calcined natural argillaceous-carbonate (Danner et al., 2018 ; Soltani et al.,2018). Then, we decided to progress by studying the potential for calcination of an argillaceous-carbonate containing palygorskite as a potential

SCM. The aim is to describe the physico-chemistry of the raw material, to identify and understand the physicochemical modifications induced by the calcination, and to define its optimum calcination temperature.

2.3. Materials and experimental methods

2.3.1. Material

The studied sample is a mining waste collected from a phosphate sedimentary deposit of a late Cretace-Eocene age. The series includes carbonates, marl, silex and clayey layers that are inserted between phosphate-rich layers, not exploited and considered as waste or a secondary resource to valorise. Sample was received in the form of loose blocks and was crushed and homogenized.

2.3.2. Calcination

The raw sample was calcined in alumina crucibles (about 3g of sample per crucible) using a laboratory furnace without atmosphere control. The furnace used was a silicon carbide laboratory chamber with a maximum operating temperature of 1500°C. The sample was heated from 20°C up to 600, 700, 800 and 900°C with a heating rate of 300°C/h and a maximum temperature time of 1h. The cooling rate was not controlled (inertia of the furnace door closed) and the sample was collected after cooled down to room temperature (20°C). The choice of this calcination protocol was made in accordance with the existing bibliography [10,15–18].

2.3.3. X-ray diffraction analysis

X-ray diffraction analysis were performed using a Bruker D5000 diffractometer with a Bragg-Brentano geometry. The source consists of a Cu anode tube (40 kV / 40 mA) that emits Cu Kα1 X-ray radiation (8 keV) of a wavelength λ = 1.5418 Å. The diffractograms of disoriented powders were recorded between 3° and 90° 2θ with a step size of 0.026° 2θ and a measurement time of 17s per step.

The diffractograms used for Rietveld quantification were acquired on a Bruker D8 diffractometer with a Bragg-Brentano geometry, using Cu anode tube, with Ni filter and without monochromator. The diffractograms were acquired between 4° and 90° 2θ with a step size of 0.018° 2θ and a measurement time of 6s per step. The quantification of the crystalline phases was made by Rietveld refinement using the open source Rietveld refinement program BGMN with Profex 4.0 interface [19], the amorphous phase was quantified by using corundum (alpha-phase, 99.95% min) as an internal standard (see supporting informations).

2.3.4. Nuclear magnetic resonance

The ^{27}Al NMR MAS spectra were acquired using a 2.5 mm MAS probe on a Bruker Avance III 500 MHz spectrometer. A π/13 excitation pulse length was used for a radio frequency field of 11 kHz. The MAS frequency was 30 kHz. The repetition time was 1s.

The MAS ^{29}Si spectra were acquired using a 7 mm MAS probe on a Bruker NEO 300 MHz spectrometer. The rotor rotation speed was 5 kHz and the pulse length was π/2. Different repetition times between scans were tested to ensure quantitative results and the choice was made to use a time of 10s. It is important to note that the repetition time of 10s chosen is too short to obtain a quantitative signal from the Quartz. Indeed, due to its high crystallinity, a longer repetition time would be mandatory. However, in the present study, Quartz is unreactive and shorter repetition time can be used to save spectrometer time.

^{1}H decoupling was performed during the acquisition on all spectra. ^{27}Al and ^{29}Si spectra are reference against an aqueous solution of $Al(NO_3)_3$ and TMS (Tetramethylsilane), respectively. Finally, spectral decompositions were realized using the dmfit software [20].

2.3.5. Scanning electron microscopy

The raw sample as well as changes induced by calcination were examined by scanning electron microscopy (SEM) using a Hitachi SU5000 microscope. The samples (raw fragment, raw powder, calcined powder) were subjected to a silver coating before observations.

2.4. Characterization of the raw material

A chemical analysis of the raw sample was carried out by X-Ray Fluorescence (XRF), the proportions of oxides (expressed in weight %) are presented in table 2-1.

Table 2-1: Chemical analysis of the raw argillaceous-carbonate.

Oxide	FeO	CaO	SiO_2	Al_2O_3	K_2O	TiO_2	Na_2O	V_2O_5	P_2O_5	MgO	LOI (1000°C)
wt.%	1.99	19.83	33.3	8.94	1.24	0.34	0.32	0.16	1.49	9.91	35.0

The oxides present in the highest quantity are SiO_2 (33.3 wt.%), CaO (19.83 wt.%), MgO (9.91 wt.%) and Al_2O_3 (8.94 wt.%). There is also a significant amount of FeO (1.99 wt.%), K_2O (1.24 wt.%) and P_2O_5 (1.49 wt.%).

Figure 2-1 displays the diffractograms of the raw argillaceous-carbonate samples. The characteristic peaks of palygorskite [21] ([110] 2θ=8.43°, [200] 2θ=13.73°, [130] 2θ =16.26°, [040] 2θ=19.92) are observed. There is also a wide peak at around 2θ=6.2° which is characteristic of the [001] peak of Ca-Smectite [22]. The width of this peak reflects the low crystallinity of this phase. palygorskite and Biotite, on the other hand, seem to be better crystallized because their peaks are much thinner. The other main crystalline phases composing this sample are Dolomite, Quartz, Biotite and Hydroxylapatite. Table 2-2 presents the results of the Rietveld refinement of the raw material (details in Supporting Information).

The sample is mainly composed of Dolomite (Dol = 53 wt.%) associated with palygorskite (Pal = 17.45 wt.%), Ca-smectite (Sm = 15.58 wt.%), Quartz (Qz = 8.00 wt.%), Hydroxylapatite (Hy = 3.00 wt.%) and biotite (Bio = 2.41 wt.%). The addition of corundum as an internal standard did

not reveal the presence of amorphous phases. Therefore, Ca-smectite, palygorskite and biotite are the only sources of aluminium. Ca-smectite, palygorskite, biotite and Quartz are the only sources of silicon in the material.

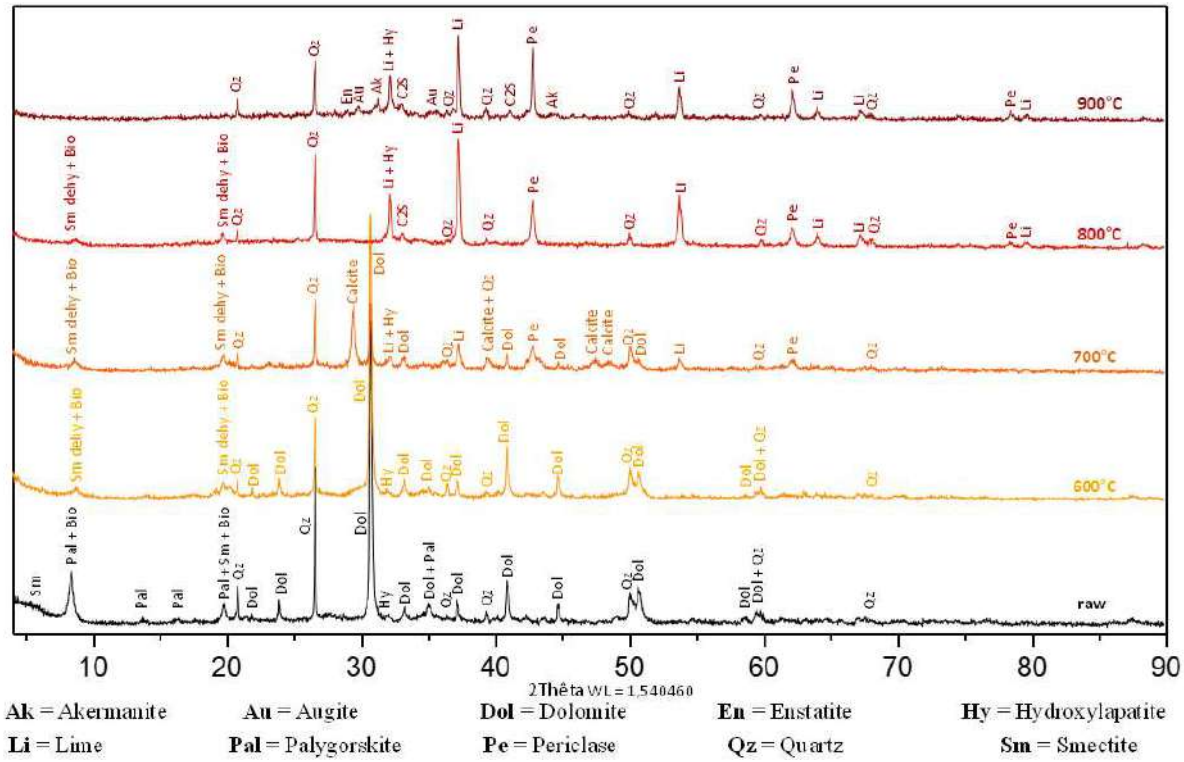

Figure 2-1: Evolution of the X-ray diffractograms of the samples as a function of the calcination temperature.

Table 2-2: Wt.% of the crystalline phases of the raw and 800°C argillaceous-carbonate samples. Dolomite (Dol), Biotite (Bio), Lime (Li), Periclase (Pe), Palygorskite (Pal), Ca-Smectite (Sm), Ca-Smectite dehydrated (Sm dehy), Quartz (Qz), Hydroxylapatite (Hy), Hematite (He), Belite (C_2S), Am (Amorphous).

Raw	Phase	Dol			Pal	Sm	Qz	Hy	Bio		
	wt.%	53.58 (+/- 0.48)			17.45 (+/- 0.35)	15.58 (+/- 0.54)	8.00 (+/- 0.24)	3.00 (+/- 0.14)	2.41 (+/- 0.22)		
800°C	Phase	Li	Pe	He	Pal	Sm dehy	Qz	Hy	Bio	C2S	Am
	wt.%	19.41 (+/- 0.43)	17.11 (+/-0.37)	1.45 (+/- 0.10)	0.00	13.48 (+/- 0.48)	11.19 (+/- 0.27)	4.07 (+/- 0.17)	1.00 (+/- 0.19)	4.45 (+/- 0.20)	27.90 (+/- 1.60)

Figure 2-2 displays two SEM images (A and B) of a fragment of the raw argillaceous-carbonate sample.

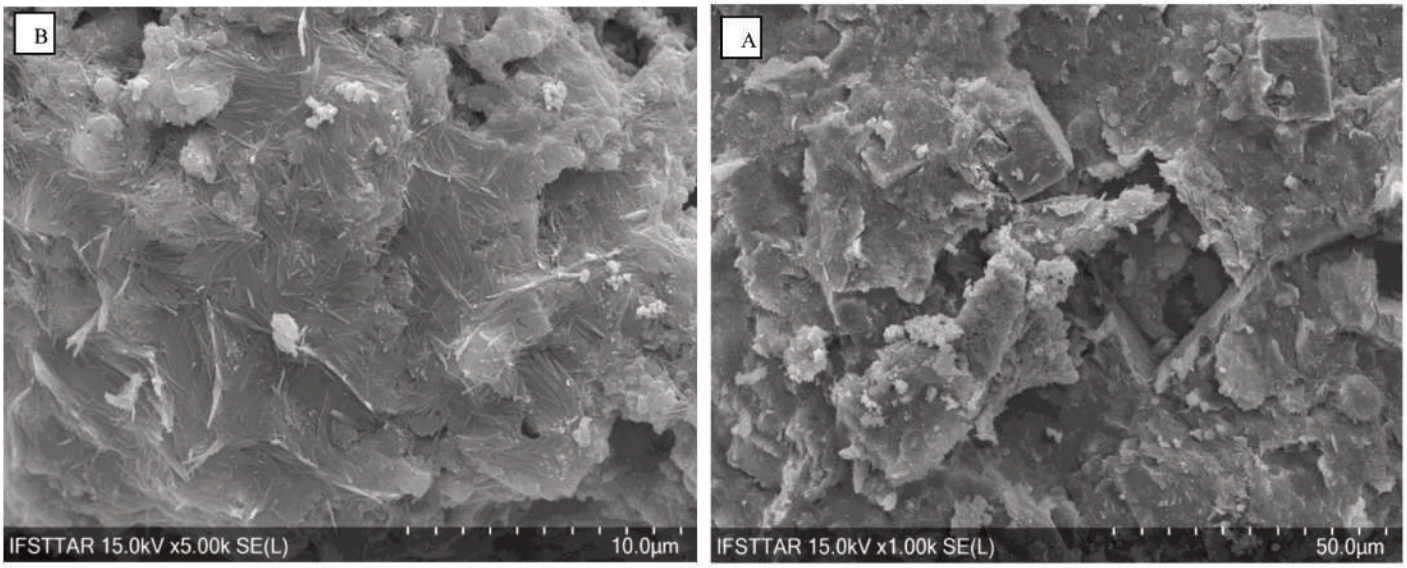

Figure 2-2: Scanning Electron Microscope images of the raw argillaceous-carbonate.

Figure 2-2A shows the global morphology of the raw sample. Dolomite rhombohedra are clearly visible as well as the presence of a coating covering the entire sample. Figure 2-2B displays another image of the surface of the sample at a higher magnification. The layer covering the sample consists of a veil and very fine needles which are respectively characteristic of smectite and palygorskite [23]. It therefore appears that palygorskite and smectite acts as a binder between the minerals in the sample and is present throughout the entire sample. This latter information completes the analysis made by XRD. Despite its average mass proportion (about 17 wt.%), the palygorskite is homogeneously distributed throughout the entire sample and is in contact with all phases.

The ^{27}Al MAS NMR spectrum of the raw argillaceous-carbonate sample is shown in Figure 2-3. It exhibits two main resonances at 3 and 70 ppm. The first intense resonance (3 ppm) corresponds to hexacoordinated aluminium [24] and can be associated with aluminium present in the palygorskite, Ca-smectite and biotite octahedra. The second resonance at 70 ppm corresponds to tetracoordinated aluminium [24] and can be associated with substitution of silicon atoms by aluminium atoms in the Ca-smectite and/or palygorskite tetrahedra [25], and to a lesser extent to aluminium present within the biotite tetrahedral sheets. There is also the presence of weak resonance at approximately 57 ppm which can be associated with AlO_4 $q^4(4Si)$ [26]. Aluminium present in the $q^4(4Si)$ configuration seems to be associated with a phase in very low quantity and/or composed of very small crystallites since the latter is not detectable by XRD.

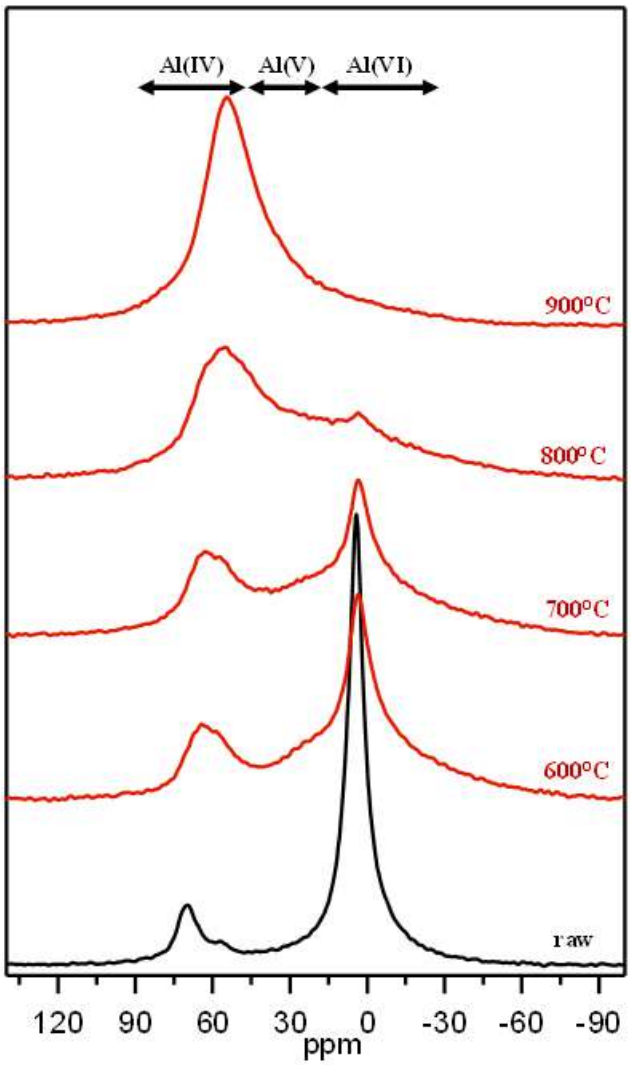

Figure 2-3: Evolution of the ^{27}Al MAS NMR spectra of the argillaceous-carbonate as function of the calcination temperature.

The two main resonances at -92 and -98 ppm are attributed to palygorskite. They correspond to silicon in Q3 configuration at the center and at the edges of the ribbons of tetrahedra, respectively [27]. The high intensity of resonances characteristic of palygorskite demonstrates its good crystallinity. In addition, Ca-smectite and biotite revealed by XRD analysis also contribute to the total ^{29}Si NMR signal. Indeed Q3 of Ca-smectite exhibit resonance at -93 ppm [28] and Q2(1Al) of biotite resonates at -86 ppm [29].

Figure 2-4 displays the ^{29}Si MAS NMR spectrum of the raw sample.

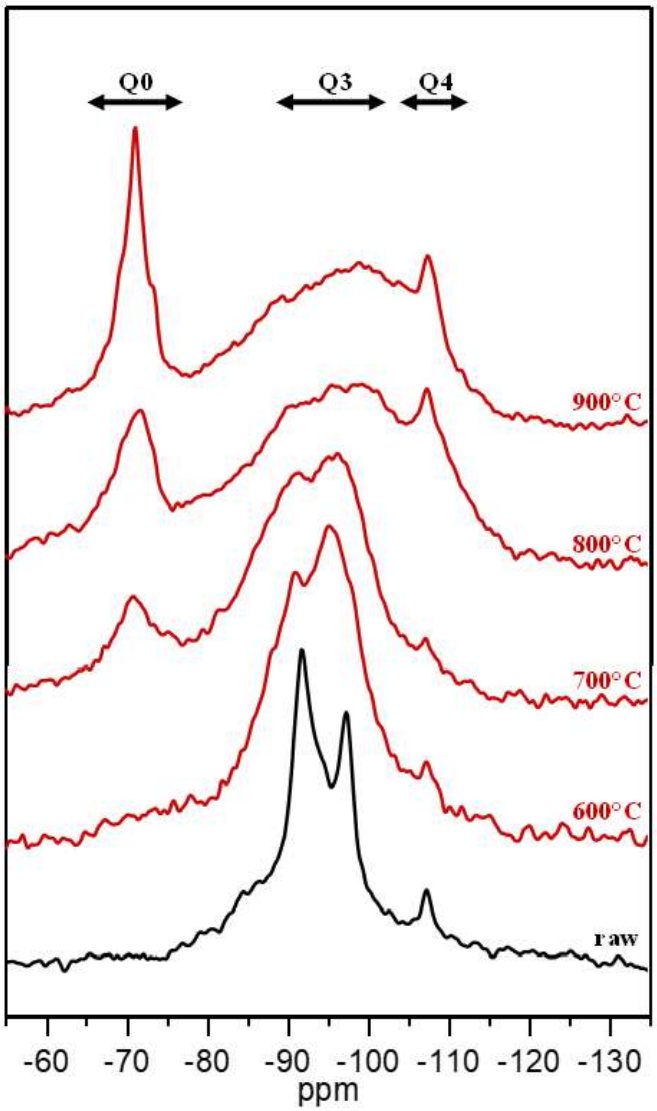

Figure 2-4: Evolution of the ^{29}Si MAS NMR spectra of the argillaceous-carbonate as a function of the calcination temperature.

The resonance observed at -108 ppm corresponds to the quartz in the sample [30]. The low resonance intensity at -93 ppm characteristic of smectite is explained by its very low crystallinity. Indeed, the existence of a local environment distribution for silicon atoms results in a broadening of the resonance, which is consistent with the observation made by XRD which suggests that Ca-smectite is very poorly crystallized.

2.5. Effects of calcination

Figure 2-1 displays the evolution of the X-ray diffractograms of the samples as a function of the calcination temperature. Above 600°C there is the disappearance of the peaks of palygorskite. This indicates a loss of crystallinity of the palygorskite phase in the sample. The shift of the [001] characteristic peak of the Ca-smectite from about 2θ = 6.2° to 2θ = 8.75° is caused by the decrease of the d001 value due to the removal of the water from the interfoliate space. This observation is in accordance with previous works on the dehydration of Ca-smectite [22,31]. Above 700° the intensities of the characteristic peaks of Dolomite decrease and new peaks attributed to Calcite, Periclase and Lime, appear. These results agree with the existing bibliography [32] describing the thermal decomposition of Dolomite as a two-stage process which proceeds as follows :

$$\mathbf{CaMg(CO_3)_2 \rightarrow CaCO_3 + MgO + CO_2}$$

$$\mathbf{CaCO_3 \rightarrow CaO + CO_2}$$

At 800°C all the characteristic peaks of Dolomite and Calcite have disappeared, demonstrating its full dissociation. On the other hand, we observe the appearance of a diffraction peak at 2θ = 33°. It is attributed to Belite, a dicalcium silicate common in anhydrous cement. The formation of Belite can be explained by a recombination phenomenon between the silicon from clayey phases and the calcium from Dolomite [33]. However, the low crystallinity of this new phase does not allow us to determine the type of polymorph. At 900°C all the peaks of dehydrated Ca-smectite and biotite disappeared, reflecting a complete loss of crystallinity of these two phases. This loss of crystallinity is correlated with recrystallization phenomena since the formation of new crystalline phases is observed. Among them we find Akermanite ($Ca_2MgSi_2O_7$), Augite $((Si,Al)_2O_6)(Ca,Mg,Fe,Ti,Al)_2$ and Enstatite ($Mg_2Si_2O_6$). Quartz and Hydroxylapatite ($Ca_5(PO_4)_3OH$) are not affected by the heat treatment since no relevant change is observed between the raw sample and the 900°C calcined samples. Thus, the argillaceous-carbonate material turned out to be sensitive to the heat treatment since loss of crystallinity of the clay phases, decomposition of Dolomite and recrystallization of new phases have been observed.

Figure 2-5 compares SEM images of raw (Figure 2-5A) and the 800°C calcined (Figure 2-5B) sample powders. Calcination at 800°C does not change the morphology of the material. Indeed, the shape of the mineral particle is almost identical before and after calcination. Yet the XRD analysis shows that at 800°C the Dolomite has transformed into Lime and Periclase and that palygorskite has lost its crystallinity. It therefore appears that the morphology of the material does not reflect changes in chemistry and structure induced by calcination. A deeper investigation of the changes in the structure of the clay phases as a function of the calcination temperature was performed by ^{27}Al and ^{29}Si MAS NMR.

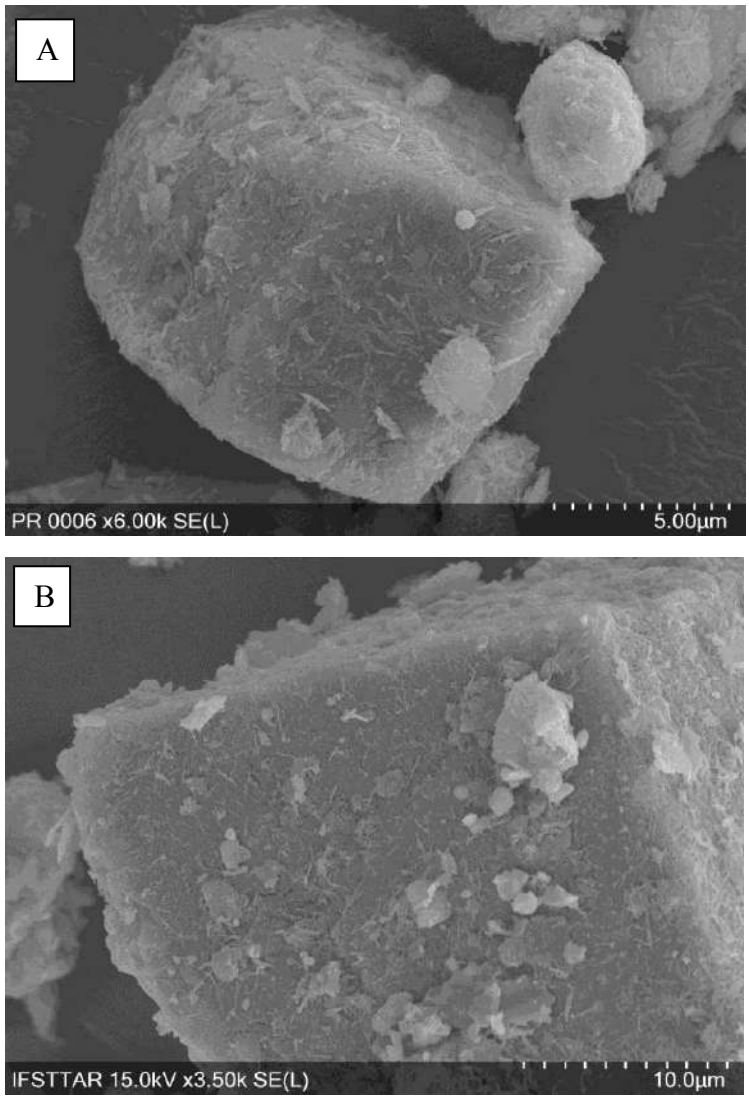

Figure 2-5: Scanning Electron Microscope images of the argillaceous-carbonate powder before (A) and after calcination at 800°C (B).

Aluminium NMR, through the observation of the change in coordination of aluminium atoms, allows us to characterize the dehydroxylation phenomenon of phyllosilicates induced by calcination.

Figure 2-3 displays the evolution of the ^{27}Al MAS NMR spectra of the argillaceous-carbonate samples as a function of the calcination temperature. The temperature increases leads to a diminution of the intensity of the resonance associated with hexacoordinated aluminium (3 ppm) and the appearance of two new resonances at around 59 and 27 ppm. These two new resonances can be associated with tetra and pentacoordinated aluminium, respectively [24]. The decrease in the proportion of 6-fold aluminium and the formation of 4 and 5-fold aluminium is a consequence of the dehydroxylation resulting from the calcination of the sample. The temperature increases leads to the release of hydroxyl groups linked to the clay octahedra, resulting in a decrease of the coordination number of the aluminium atoms.

Figure 2-6 gives the relative proportions of the 6-, 5- and 4-fold aluminium atoms having been quantified by spectral integration of the ^{27}Al NMR spectra (details in Supporting Information). At 600°C a significant dehydroxylation of the argillaceous phases is observed since Al (VI) evolves from 87% to 36%. By using the Rietveld quantification of the crystal phases and their ideal theoretical chemical compositions we can calculate the contribution of each phase to the total amount of aluminium in the sample: 62% of the total aluminium comes from Ca-smectite, 34% from palygorskite and 4% from biotite. It becomes clear that this decrease of more than half in the proportion of Al (VI) cannot be due to the dehydroxylation of palygorskite only. So it seems that Ca-smectite start to dehydroxylate at 600°C, without fully losing its crystallinity since its signal remains detectable by XRD up to 800°C. These results are in agreement with the observations made by Fernandez et al. [34] who suggested that the small amount of hydroxyl groups present in the smectite structure could explain the small effect of dehydroxylation on its cristallinity. On the other hand, as observed in Figure 2-1, there is a disappearance of the characteristic peaks of palygorskite from 600°C onwards. This strongest thermal reactivity of palygorskite compared to Ca-smectite could be explained by its particular TOT structure.

The hatched part of the total 6-fold aluminium in figure 2-6 corresponds to the component (see Supporting Information) close to the signature of the aluminium present in palygorskite and smectite octahedra. It can be explained by octahedral sheets that resisted calcination. On the other hand, the dotted part corresponds to the component associated with very distorted octahedra. It can be seen that their relative proportions do not vary in the same way with increasing temperature, specifically, the proportion of 6-fold aluminium belonging to distorted sheets decreases less rapidly with increasing temperature. It can be hypothesized that the passage of 6-fold to 5-fold aluminium is made through this intermediate state corresponding to distorted octahedral sheets.

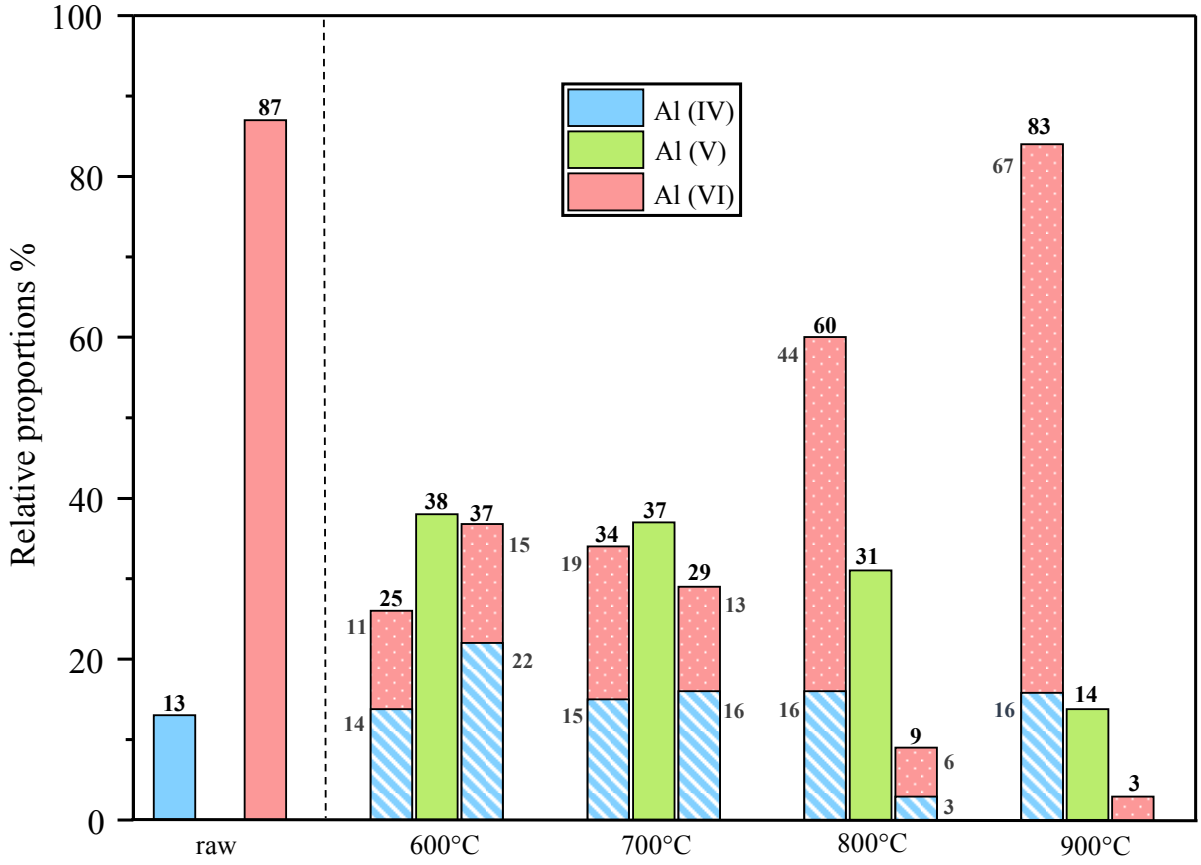

Figure 2-6: Relative proportions of the 6-, 5- and 4-fold aluminium atoms as a function of the calcination temperature.

From 600°C onwards 4-fold aluminium is formed (from 13 to 26 %). As for 6-fold aluminium, the 4-fold aluminium resonance is described by two components represented by hatched and dotted parts in figure 2-6. The isotropic chemical shift of the “hatched” component of the 4-fold aluminium is 69 ppm (see supporting information) and could be associated with 4-fold

aluminium in q3 configuration [35]. In contrast, the much lower isotropic chemical shift of the “dotted” component at 61 ppm can be associated with 4-fold aluminium in q4 configuration [26].

The “hatched” component appears as soon as the calcination temperature reaches 600°C and remains stable (around 15%) in spite of the temperature increase. Knowing that palygorskite becomes amorphous at 600°C (see figure 2-1), we can associate this “hatched” component of 4-fold aluminium with the dehydroxylation of palygorskite. Thereafter, only the "dotted” component of 4-fold aluminium increases with the increase of the calcination temperature, it would seem that this 4-fold aluminium is associated with the dehydroxylation of Ca-smectite and biotite.

Concerning the 5-fold aluminium, the highest proportion is reached from 600°C, and then decreases with increasing temperature. Up to 800°C its proportion remains stable because the dehydroxylation of 6-fold aluminium compensates for the transformation of 5-fold aluminium into 4-fold aluminium. Fernandez et al. [34] associated the pozzolanic activity of a calcined clay with the appearance of penta-coordinated aluminum within the structure of the clay. Indeed, penta-coordinated aluminum turns out to be the most unstable form and the most prone to react. However, it is important to remember that 4-fold aluminium is also reactive and could play an important role in the pozzolanic reaction.

Therefore, 800°C seems to be a good calcination temperature since it allows an almost total dehydroxylation of the clay phases (only 9% of 6-fold aluminium remains) while keeping a large proportion of 5-fold aluminium (31%).

Table 2-2 displays the result of the Rietveld refinement of the 800°C calcined argillaceous-carbonate. An amorphous phase is present and accounts for almost 28% of the total sample mass. This high proportion of amorphous is mainly due to the amorphisation of palygorskite as its signal is no longer observable at 800°C (figure 2-1). The formation of Hematite at 800°C shows that part of the Dolomite ($CaMg(CO_3)_2$) is actually Ankerite ($Ca(Fe,Mg)(CO_3)_2$). However, the proportion of Ankerite is very low in regards to the proportion of Hematite formed (1.45 wt.%), which confirms the low iron value in chemical analysis results (table 2-1).

Figure 2-4 displays the evolution of the ^{29}Si MAS NMR spectra of the argillaceous-carbonate sample as function of the calcination temperature. From 600°C, we can observe a broadening of the resonances characteristic of the Q3 of the clayey phases. This broadening of the lines reflects distribution of the silicon atoms environments and so indicates the increase in disorder within the clay phases. The characteristic resonances of palygorskite are now almost indistinguishable, which confirms the observations made by XRD and suggests that the disappearance of its XRD peaks is not only due to its loss of crystallinity but also to strong distortions within its structure.

At 700°C the broadening of the Q3 resonances continues, which shows that the loss of crystallinity of the clayey phases continues. The main information is the appearance of a new resonance at -71 ppm which is not common in the MAS NMR analysis of a calcined clay. Skibsted [36] associates it with the presence of monomeric Q0 orthosilicates typical of Belite (C_2S) one of the anhydrous phases of the clinker. That confirms the observations made by XRD and the possible reaction between silicon from clayey phases and calcium from Dolomite. The trend will continue at 800°C with a widening of the Q3 resonances and an increase in the proportion of Q0 associated with Belite. There is also the appearance of a new resonance at -74 ppm which can be associated with silicon in Q1 configuration [37] which is attributed to Akermanite detected by XRD. By crossing these results with XRD, we can highlight that recrystallization phenomena begin as early as 800°C, but the low crystallinity of these new phases prevents their characterization by XRD at this temperature.

Between 800 and 900°C the width of Q0 resonance of Belite decreases whereas its intensity increases. This means that the proportion and the level of crystallinity of the neo-formed Belite are increasing. The Q1 resonance of Akermanite is also more intense. The characteristic Q2 resonances of the Augite (-72 ppm) and the Enstatite (-84 ppm) cannot be observed because they overlap with the broader resonances from the calcined clay [38,39].

It is important to specify that the chosen repetition time does not allow to be quantitative for Quartz. Indeed, after several tests it seems that it is necessary to use a T_1 close to 3600 seconds to allow a complete relaxation, which complicates quantification. We have then calculated the

proportion of Belite formed at 800°C from the results of chemical analysis (XRF), quantification of crystal phases (XRD) and ^{29}Si MAS NMR. In order to carry out this calculation we made the hypothesis that Quartz does not react. Knowing the total amount of silicon (from XRF results) and the wt.% proportion of Quartz (from XRD Rietveld refinement) in the raw sample we re-calculated the total amount of silicon present in the system without Quartz. Then, by using the ^{29}Si MAS NMR spectrum of calcined sample, we quantified the relative repartition of silicon belonging to the Belite and to the rest of the system (without Quartz) at 800°C and we calculated their respective molar proportions. Subsequently, neglecting the minor phases, we used theoretical ideal formulas for palygorskite, smectite, and Belite to convert molar proportions of silicon to weight proportions of phases. Calculations give a proportion of ~8 wt.% of Belite in the sample calcined at 800°C. If we compare this value with the amount of crystalline Belite obtained by Rietveld refining (~4,5 wt.%), it appears that the low crystallinity of Belite causes the XRD to underestimate it by half.

The formation of Belite during the calcination of a mixture of palygorskite and Dolomite has already been observed [33]. Belite represents on average 15 to 20% of the total cement phases and is responsible of the long-term mechanical properties [40]. Its presence in the sample calcined at 800°C is therefore good news, assuming that it is reactive. However, the formation of Lime and Periclase could be troublesome for further use in cement systems (carbonation and post-hardening swelling).

2.6. Conclusion

The study of the thermal reactivity of this argillaceous carbonate highlighted its potential for a use as a SCM. Indeed, the palygorskite which composes this sample seems to be very sensitive to heat treatment and it dehydroxylated very easily from 600°C, certainly because of its so particular structure. Moreover, the calcination of the clay mixed with carbonate allowed to highlight the formation of Belite (C_2S) from 700°C. The chemistry of the system favours the reaction of calcium from Dolomite and silicon from clayey phases to form this cementitious phase. The calcined palygorskite associated with Belite formation make this carbonate-material a very interesting system for use as a cementitious addition because of its double reactivity (pozzolanic and hydraulic). For the rest, it would be interesting to study the influence

of the clay phase/carbonate ratio on the quality and quantity of neoformed Belite and finaly to test the reactivity of this sample.

ACKNOWLEGDMENTS

Dr. Bruno Lanson and Nathaniel Findling are thanked for their valuable help with the use of Profex software for Rietveld refinement.

2.7. References

[1] D.N. Huntzinger, T.D. Eatmon, A life-cycle assessment of Portland cement manufacturing: comparing the traditional process with alternative technologies, J. Clean. Prod. 17 (2009) 668–675. https://doi.org/10.1016/j.jclepro.2008.04.007.

[2] Y. Cancio Díaz, S. Sánchez Berriel, U. Heierli, A.R. Favier, I.R. Sánchez Machado, K.L. Scrivener, J.F. Martirena Hernández, G. Habert, Limestone calcined clay cement as a low-carbon solution to meet expanding cement demand in emerging economies, Dev. Eng. 2 (2017) 82–91. https://doi.org/10.1016/j.deveng.2017.06.001.

[3] J.I. Escalante, L.Y. Gómez, K.K. Johal, G. Mendoza, H. Mancha, J. Méndez, Reactivity of blast-furnace slag in Portland cement blends hydrated under different conditions, Cem. Concr. Res. 31 (2001) 1403–1409. https://doi.org/10.1016/S0008-8846(01)00587-7.

[4] E. Sakai, S. Miyahara, S. Ohsawa, S.-H. Lee, M. Daimon, Hydration of fly ash cement, Cem. Concr. Res. 35 (2005) 1135–1140. https://doi.org/10.1016/j.cemconres.2004.09.008.

[5] S. Horpibulsuk, W. Phojan, A. Suddeepong, A. Chinkulkijniwat, M.D. Liu, Strength development in blended cement admixed saline clay, Appl. Clay Sci. 55 (2012) 44–52. https://doi.org/10.1016/j.clay.2011.10.003.

[6] K. Scrivener, F. Martirena, S. Bishnoi, S. Maity, Calcined clay limestone cements (LC3), Cem. Concr. Res. 114 (2018) 49–56. https://doi.org/10.1016/j.cemconres.2017.08.017.

[7] H. El-Diadamony, A.A. Amer, T.M. Sokkary, S. El-Hoseny, Hydration and characteristics of metakaolin pozzolanic cement pastes, HBRC J. 14 (2018) 150–158. https://doi.org/10.1016/j.hbrcj.2015.05.005.

[8] M.S. Prasad, K.J. Reid, H.H. Murray, Kaolin: processing, properties and applications, Appl. Clay Sci. 6 (1991) 87–119. https://doi.org/10.1016/0169-1317(91)90001-P.

[9] S. Hollanders, R. Adriaens, J. Skibsted, Ö. Cizer, J. Elsen, Pozzolanic reactivity of pure calcined clays, Appl. Clay Sci. 132–133 (2016) 552–560. https://doi.org/10.1016/j.clay.2016.08.003.

[10] T. Danner, G. Norden, H. Justnes, Characterisation of calcined raw clays suitable as supplementary cementitious materials, Appl. Clay Sci. 162 (2018) 391–402. https://doi.org/10.1016/j.clay.2018.06.030.

[11] E. Galan, Properties and applications of palygorskite-sepiolite clays, Clay Miner. 31 (1996) 443–453. https://doi.org/10.1180/claymin.1996.031.4.01.

[12] C. Blanco, F. González, C. Pesquera, I. Benito, S. Mendioroz, J.A. Pajares, Differences Between One Aluminic Palygorskite and Another Magnesic by Infrared Spectroscopy, Spectrosc. Lett. 22 (1989) 659–673. https://doi.org/10.1080/00387018908053926.

[13] A. Ipavec, R. Gabrovšek, T. Vuk, V. Kaučič, J. Maček, A. Meden, Carboaluminate Phases Formation During the Hydration of Calcite-Containing Portland Cement: Carboaluminate Phase Formation, J. Am. Ceram. Soc. 94 (2011) 1238–1242. https://doi.org/10.1111/j.1551-2916.2010.04201.x.

[14] V.L. Bonavetti, V.F. Rahhal, E.F. Irassar, Studies on the carboaluminate formation in limestone filler-blended cements, Cem. Concr. Res. 31 (2001) 853–859. https://doi.org/10.1016/S0008-8846(01)00491-4.

[15] N. Garg, J. Skibsted, Thermal Activation of a Pure Montmorillonite Clay and Its Reactivity in Cementitious Systems, J. Phys. Chem. C. 118 (2014) 11464–11477. https://doi.org/10.1021/jp502529d.

[16] N. Garg, J. Skibsted, Pozzolanic reactivity of a calcined interstratified illite/smectite (70/30) clay, Cem. Concr. Res. 79 (2016) 101–111. https://doi.org/10.1016/j.cemconres.2015.08.006.

[17] S. Krishnan, A.C. Emmanuel, V. Shah, A. Parashar, G. Mishra, S. Maity, S. Bishnoi, Industrial production of limestone calcined clay cement: experience and insights, Green Mater. 7 (2019) 15–27. https://doi.org/10.1680/jgrma.18.00003.

[18] A. Trümer, H.-M. Ludwig, M. Schellhorn, R. Diedel, Effect of a calcined Westerwald bentonite as supplementary cementitious material on the long-term performance of concrete, Appl. Clay Sci. 168 (2019) 36–42. https://doi.org/10.1016/j.clay.2018.10.015.

[19] N. Doebelin, R. Kleeberg, *Profex* : a graphical user interface for the Rietveld refinement program *BGMN*, J. Appl. Crystallogr. 48 (2015) 1573–1580. https://doi.org/10.1107/S1600576715014685.

[20] D. Massiot, F. Fayon, M. Capron, I. King, S. Le Calvé, B. Alonso, J.-O. Durand, B. Bujoli, Z. Gan, G. Hoatson, Modelling one- and two-dimensional solid-state NMR spectra: Modelling 1D and 2D solid-state NMR spectra, Magn. Reson. Chem. 40 (2002) 70–76. https://doi.org/10.1002/mrc.984.

[21] W.F.Bradley, The structural scheme of attapulgite, in: 1940: pp. 405–410.

[22] P. Bala, B.K. Samantaray, S.K. Srivastava, Dehydration transformation in Ca-montmorillonite, Bull. Mater. Sci. 23 (2000) 61–67. https://doi.org/10.1007/BF02708614.

[23] L. Boudriche, R. Calvet, B. Hamdi, H. Balard, Effect of acid treatment on surface properties evolution of attapulgite clay: An application of inverse gas chromatography, Colloids Surf. Physicochem. Eng. Asp. 392 (2011) 45–54. https://doi.org/10.1016/j.colsurfa.2011.09.031.

[24] A.Á.B. Maia, R.S. Angélica, R. de Freitas Neves, H. Pöllmann, C. Straub, K. Saalwächter, Use of 29Si and 27Al MAS NMR to study thermal activation of kaolinites from Brazilian Amazon kaolin wastes, Appl. Clay Sci. 87 (2014) 189–196. https://doi.org/10.1016/j.clay.2013.10.028.

[25] J. Sanz, J.M. Serratosa, Silicon-29 and aluminum-27 high-resolution MAS-NMR spectra of phyllosilicates, J. Am. Chem. Soc. 106 (1984) 4790–4793. https://doi.org/10.1021/ja00329a024.

[26] D. Muller, W. Gessner, A. Samoson, E. Lippmaa, Solid-state Aluminium-27 Nuclear Magnetic Resonance Chemical Shift and Quadrupole Coupling Data for Condensed AIO4, Tetrahedra, J Chem Soc Dalton Trans. (1986) 5.

[27] P.F. Barron, R.L. Frost, N. Qlil, Solid state 29Si NMR examination of the 2:1 ribbon magnesium silicates, sepiolite and palygorskite, Am. Mineral. 70 (1985) 758–766.

[28] I.W.M. Brown, K.J.D. MacKenzie, R.H. Meinhold, The thermal reactions of montmorillonite studied by high-resolution solid-state 29Si and 27Al NMR, (1987) 3265–3275.

[29] K.J.D. Mackenzie, I.W.M. Brown, C.M. Cardile, R.H. Meinhold, The thermal reactions of muscovite studied by high-resolution solid-state 29-Si and 27-Al NMR, J. Mater. Sci. 22 (1987) 2645–2654. https://doi.org/10.1007/BF01082158.

[30] E. Lippmaa, M. Maegi, A. Samoson, G. Engelhardt, A.R. Grimmer, Structural studies of silicates by solid-state high-resolution silicon-29 NMR, J. Am. Chem. Soc. 102 (1980) 4889–4893. https://doi.org/10.1021/ja00535a008.

[31] S. Morodome, K. Kawamura, Swelling Behavior of Na- and Ca-Montmorillonite up to 150°C by in situ X-ray Diffraction Experiments, Clays Clay Miner. 57 (2009) 150–160. https://doi.org/10.1346/CCMN.2009.0570202.

[32] M. Olszak-Humienik, M. Jablonski, Thermal behavior of natural dolomite, J. Therm. Anal. Calorim. 119 (2015) 2239–2248. https://doi.org/10.1007/s10973-014-4301-6.

[33] J. Xie, T. Chen, B. Xing, H. Liu, Q. Xie, H. Li, Y. Wu, The thermochemical activity of dolomite occurred in dolomite–palygorskite, Appl. Clay Sci. 119 (2016) 42–48. https://doi.org/10.1016/j.clay.2015.07.014.

[34] R. Fernandez, F. Martirena, K.L. Scrivener, The origin of the pozzolanic activity of calcined clay minerals: A comparison between kaolinite, illite and montmorillonite, Cem. Concr. Res. 41 (2011) 113–122. https://doi.org/10.1016/j.cemconres.2010.09.013.

[35] X. Pardal, F. Brunet, T. Charpentier, I. Pochard, A. Nonat, 27Al and 29Si Solid-State NMR Characterization of Calcium-Aluminosilicate-Hydrate, Inorg. Chem. 51 (2012) 1827–1836. https://doi.org/10.1021/ic202124x.

[36] J. Skibsted, H.J. Jakobsen, C. Hall, Quantification of calcium silicate phases in Portland cements by 29Si MAS NMR spectroscopy, J. Chem. Soc. Faraday Trans. 91 (1995) 4423. https://doi.org/10.1039/ft9959104423.

[37] N. Janes, E. Oldfield, Prediction of silicon-29 nuclear magnetic resonance chemical shifts using a group electronegativity approach: applications to silicate and aluminosilicate structures, J. Am. Chem. Soc. 107 (1985) 6769–6775. https://doi.org/10.1021/ja00310a004.

[38] K.J.D. MacKenzie, R.H. Meinhold, The thermal reactions of talc studied by 29Si and 25Mg MAS NMR, Thermochim. Acta. 244 (1994) 195–203. https://doi.org/10.1016/0040-6031(94)80219-X.

[39] X. Huang, W. Ni, W. Cui, Z. Wang, L. Zhu, Preparation of autoclaved aerated concrete using copper tailings and blast furnace slag, Constr. Build. Mater. 27 (2012) 1–5. https://doi.org/10.1016/j.conbuildmat.2011.08.034.

[40] M.A. Bouzidi, A. Tahakourt, N. Bouzidi, D. Merabet, Synthesis and Characterization of Belite Cement with High Hydraulic Reactivity and Low Environmental Impact, Arab. J. Sci. Eng. 39 (2014) 8659–8668. https://doi.org/10.1007/s13369-014-1471-2.

2.8. Bilan scientifique du chapitre 2

Cette dernière partie dresse un bilan scientifique de ce chapitre 2 qui s'intéresse aux modifications physico-chimiques qui ont lieu lors de la calcination d'une marne dolomitique contenant de la palygorskite et de la smectite.

Ce type de marne, du fait de sa composition minéralogique particulière (association de palygorskite et de smectite avec de la dolomite), va subir d'importantes modifications lors de sa calcination. Il a été démontré qu'une température de calcination de 800°C permet une activation thermique optimale des phases argileuses (palygorskite et smectite) tout en évitant des phénomènes de recristallisation qui pourraient imputer de manière négative la réactivité pouzzolanique. Cependant, la calcination de cette marne à 800°C entraine la formation de chaux (CaO) et de périclase (MgO). Ces composés réactifs seront à contrôler lors de l'utilisation de ce type de matériaux en remplacement du ciment car ils pourraient avoir une influence sur l'hydratation et entraîner des désordres volumiques.

L'autre élément important est la formation de C_2S (silicate dicalcique) lors de la calcination à 800°C. Cette phase cimentaire se forme par réaction du silicium issu des phases argileuses calcinées avec le calcium issu de la décarbonatation de la dolomite. La formation de C_2S ajoute un caractère hydraulique à la réactivité pouzzolanique de cette marne calcinée et participera au développement des résistances lors de l'hydratation.

Ce chapitre 2 a donc permis d'identifier de manière précise les modifications qui ont lieu lors de la calcination d'une marne dolomitique contenant de la palygorskite et a démontré son potentiel intéressant pour une utilisation comme ajout cimentaire.

Chapitre 3 – Réactivité à l'eau après calcination d'une marne dolomitique contenant de la palygorskite et de la smectite

3.1. Avant-propos

Note : Ce chapitre est basé sur un article publié dans un journal international à comité de lecture.

Titre de l'article : **Self-reactivity of a calcined palygorskite-bearing marlstone for potential use as supplementary cementitious material**

Victor Poussardin, Michael Paris, William Wilson, Arezki Tagnit-Hamou, Dimitri Deneele

Publié dans : Applied Clay Science

DOI : https://doi.org/10.1016/j.clay.2021.106372

Référence

V. Poussardin, M. Paris, W. Wilson, A. Tagnit-Hamou, D. Deneele, *Self-reactivity of a calcined palygorskite-bearing marlstone for potential use as supplementary cementitious material*, Applied Clay Science. 216 (2022) 106372.

Contribution à la thèse

Le chapitre 2 a consisté en une étude poussée de la calcination d'une marne dolomitique contenant de la palygorskite et de la smectite. Cela a permis d'identifier que la température de calcination « optimale » est de 800°C et que le traitement thermique entraine la formation de plusieurs phases potentiellement réactives telles que du C_2S, de la chaux ou encore du périclase. La suite logique est donc de tester la réactivité de cette marne calcinée à 800°C. C'est dans ce sens-là que vient s'intégrer le chapitre 3 qui est la continuité directe du chapitre 2. L'objectif est de caractériser la réactivité dans l'eau de cette marne calcinée et de relier les observations faites avec les modifications physico-chimiques identifiées lors de la calcination.

Résumé en français

Cet article traite de l'étude de l'auto-réactivité d'une marne contenant de la palygorskite et calcinée à 800°C. Il s'agit d'un système multiphase complexe (contenant notamment du CaO et du MgO) dont la réactivité dans l'eau doit être étudiée avant d'être utilisée comme supplementary cementitious material (SCM). L'échantillon calciné a été hydraté (ratio eau/liant = 0,8) pendant 7, 14, 28 et 180 jours, puis étudié par diffraction des rayons X (DRX), résonance magnétique nucléaire du solide (RMN MAS) et microscope électronique à balayage (MEB). Le croisement des résultats des analyses de DRX et de RMN MAS (en particulier la quantification des phases par intégration spectrale des spectres ^{29}Si RMN MAS) a permis de mettre en avant la réactivité des phases argileuses calcinées avec la portlandite issue de l'hydratation du CaO qui conduit à la formation de C-(A)-S-H. Il a également été mis en évidence la réactivité du C_2S (néoformé pendant la calcination) dès 7 jours d'hydratation. L'hydratation de cet échantillon a montré une forte auto-réactivité (principalement pouzzolanique), ce qui en fait un échantillon prometteur pour une utilisation comme SCM.

Résumé en anglais

This article focuses on the study of the self-reactivity of a 800°C calcined palygorskite-bearing marlstone which is a complex multi-phase system (including CaO and MgO) whose reactivity in water must be studied before being used as Supplementary Cementitious Material (SCM). The sample was hydrated (w/s = 0.8) for 7, 14, 28 and 180 days and then investigated using X-ray diffraction (XRD), Solid State Nuclear Magnetic Resonance (MAS NMR), and Scanning Electron Microscope (SEM). Crossing the results of XRD and MAS NMR analyses (in particular the phase quantification by spectral integration of ^{29}Si MAS NMR spectra) have revealed the reactivity of the calcined clay phases with the portlandite which leads to the formation of C-(A)-S-H. It also highlighted the reactivity of C_2S (neoformed during calcination) within 7 days of hydration. Hydration of this sample showed high self-reactivity (mostly pozzolanic) making it a promising sample for use as SCM.

3.2. Introduction

The cement demand has been increasing over the past few decades [1], mainly as a result of the population and economic growth [2]. Countries and especially developing countries are rapidly building up industrial and transport infrastructures to cope with their economic development. It is estimated that the cement industry is responsible for 5 to 8% of the total anthropogenic CO_2 emissions [3] and 95% of this CO_2 is emitted during the manufacturing process [4]. In recent years, environmental legislation has become more drastic in order to reduce the amount of CO_2 emission of cement production, and the cement industries have turned to research and development of new innovations that can reduce the environmental footprint of cement.

The use of Supplementary Cementitious Materials (SCMs) as a substitute for clinker is one of the emerging technology that could significantly reduce the environmental footprint of cement manufacturing. Among the widely used SCMs there are industrial wastes which have hydraulic properties, and in the presence of water react to form hydrates responsible for setting and hardening (e.g. blast furnace slag [5,6] and fly ash [7,8]). However, blast furnace slag resources are not abundant enough to be used on a sustainable basis and the energetic transition rightly limits the availability of fly ash resources from coal combustion [9].

For several years now, the use of calcined clays as SCMs has been increasing. Indeed, the reserves of clays with potential for calcination are considerable and globally homogeneously distributed [9], making it a first choice resource for use as a SCM. Numerous studies have been carried out in recent years on the reactivity of different types of calcined clays in cementitious system and metakaolin resulting from the calcination of kaolin appeared the most promising [10–13], whereas the calcined smectites [14–16] and illites [17–19] show much less encouraging results. However, it is important to remember that clays are not limited to the kaolinite, smectite and illite families. Many mining wastes contain clay phases, particularly unconventional clays whose use as SCM has never been studied.

The present study takes place in a project targeting the valorization of secondary resources (mining waste) as SCM. The thermal reactivity of the sample has already been studied and a

temperature of 800°C has been determined as an optimum [20]. Upon calcination, the initial composition of this natural sample leads to the formation of reactive phases such as calcined clays, lime, periclase and C_2S. This composition is therefore very different from that of the classical SCMs currently in use. The presence of lime and periclase can be problematic factor for the use of this sample as SCM and should be considered. It is a very complex system whose reactivity cannot be directly studied in a cementitious system as usual.

This paper focuses on the reactivity of a mining waste from a phosphate mine initially composed of 17% of palygorskite and 16% of smectite [20]. The particularity of this material is that it contains palygorskite - a particular TOT clay whose pozzolanic reactivity after calcination has not yet been studied – as well as reactive free lime and C_2S neoformed [20].
The first step is to study its self-reactivity in presence of water in order to understand the contribution of each phases composing it, their evolution and the possible presence of synergies. In order to be able to accurately characterize the self-reactivity of this sample, different characterization techniques have been used, such as X-ray Diffraction, Nuclear Magnetic Resonance and Scanning Electron Microscopy.

3.3. Materials and experimental methods

3.3.1. Materials

The material used is a natural marlstone considered as waste by the mining industry which is looking for new ways of recovery. Table 3-1 shows the chemical analysis of the raw sample carried out by X-Ray Fluorescence (XRF), the proportions are given in oxides (expressed in weight %).

Table 3-1: Chemical analysis of the raw material.

Oxide	FeO	CaO	SiO_2	Al_2O_3	K_2O	TiO_2	Na_2O	V_2O_5	P_2O_5	MgO	LOI (1000°C)
wt.%	1.99	19.83	33.3	8.94	1.24	0.34	0.32	0.16	1.49	9.91	35.0

The physicochemical properties and the optimal calcination of this material have been investigated in a previous article [20].

The raw material is composed of a mixture of dolomite (54 wt.%), palygorskite (17 wt.%), Ca-smectite (16 wt.%), quartz (8 wt.%), hydroxylapatite (3 wt.%), and biotite (2 wt.%). A calcination temperature of 800°C has been selected to allow an important dehydroxylation of the clay phases while avoiding recrystallization phenomena. During the calcination process, different reactive phases were formed, such as lime (19 wt.%), periclase (17 wt.%) and C_2S (4 wt.%)".

3.3.2. Materials hydration

The raw natural sample has a high proportion of dolomite ($CaMg(CO_3)_2$) which, during calcination, led to the formation of lime (CaO). Therefore this sample is not suitable for the classical pozzolanic activity tests such as the R^3 screening [21], Frattini test or saturated lime test [22] since they all assume that the test sample does not contain free calcium. It was therefore decided to characterize the reactivity of the sample by a different approach: the reaction of the sample in water. During the hydration of this calcined material, the lime is hydrated into portlandite which becomes available to react pozzolanically with the calcined clay phases (palygorskite, smectite and biotite). In addition, hydration allows testing whether the C_2S neoformed during calcination is reactive. One gram of marlstone calcined at 800°C was manually mixed with water according to the selected water-to-solid ratios (w/s=0.8, 1, 2 and 4) until a homogeneous paste was obtained. The vials where then closed and left to react during 7, 14, 28 and 180 days at room temperature in sealed conditions (without atmosphere control). At the end of each curing time the samples were freeze-dried for 48h in order to stop hydration. Within 2 days, the dry samples were crushed and analyzed by XRD, MAS NMR, and SEM. Since the results are similar across all w/s ratios tested with respect to all ages, only the results for w/s = 0.8 are presented in this article.

3.3.3. Phases analyses

3.3.3.1. X-ray diffraction

The diffractograms were acquired on a Bruker D8 diffractometer based on a Bragg-Brentano geometry. The X-ray source consists of a copper anode tube (40 kV / 40 mA) that emits Cu Kα radiation. The X-ray diffractograms of disoriented powdered sample were acquired between 5° and 60° 2θ with a step size of 0.017° 2θ and a measurement time of 1s per step. The

identification of XRD peaks was done with the PROFEX software database (BGMN PROGRAM) [23].

3.3.3.2. Nuclear magnetic resonance

The ^{27}Al MAS NMR spectra were acquired on a Bruker Avance III 500 MHz spectrometer using a 2.5 mm MAS probe. The excitation pulse length used was π/13 for a radio frequency field of 11 kHz. The repetition time was 1s and the MAS frequency was 30 kHz.

The ^{29}Si MAS NMR spectra were acquired on a Bruker NEO 300 MHz spectrometer using a 7 mm MAS probe. A π/2 excitation pulse length was used, and the MAS frequency was 5 kHz. After several tests of different repetition times the choice was made to use a time of 10s in order to ensure quantitative results except for quartz. However, it has no consequences as quartz is non-reactive.^{1}H decoupling was performed during all the acquisitions. ^{27}Al spectra were referenced against an aqueous solution of $Al(NO_3)_3$ and ^{29}Si spectra against TMS (Tetramethylsilane). The spectral decompositions have been done using the dmfit software [24].

3.3.3.3. Scanning electron microscope

The morphological changes during the hydration were examined by scanning electron microscopy (SEM). The analysis was carried out using a Hitachi SU5000 microscope. The samples were subjected to a platine coating before SEM observations.

3.4. Results and discussions

3.4.1. X-ray diffraction analysis

Figure 3-1 displays the evolution of the diffractograms of the marlstone (labelled AC) calcined at 800°C (AC-800) and hydrated during 7 days (AC-800-7d), 14 days (AC-800-14d), 28 days (AC-800-28d), and 180 days (AC-800-180d).

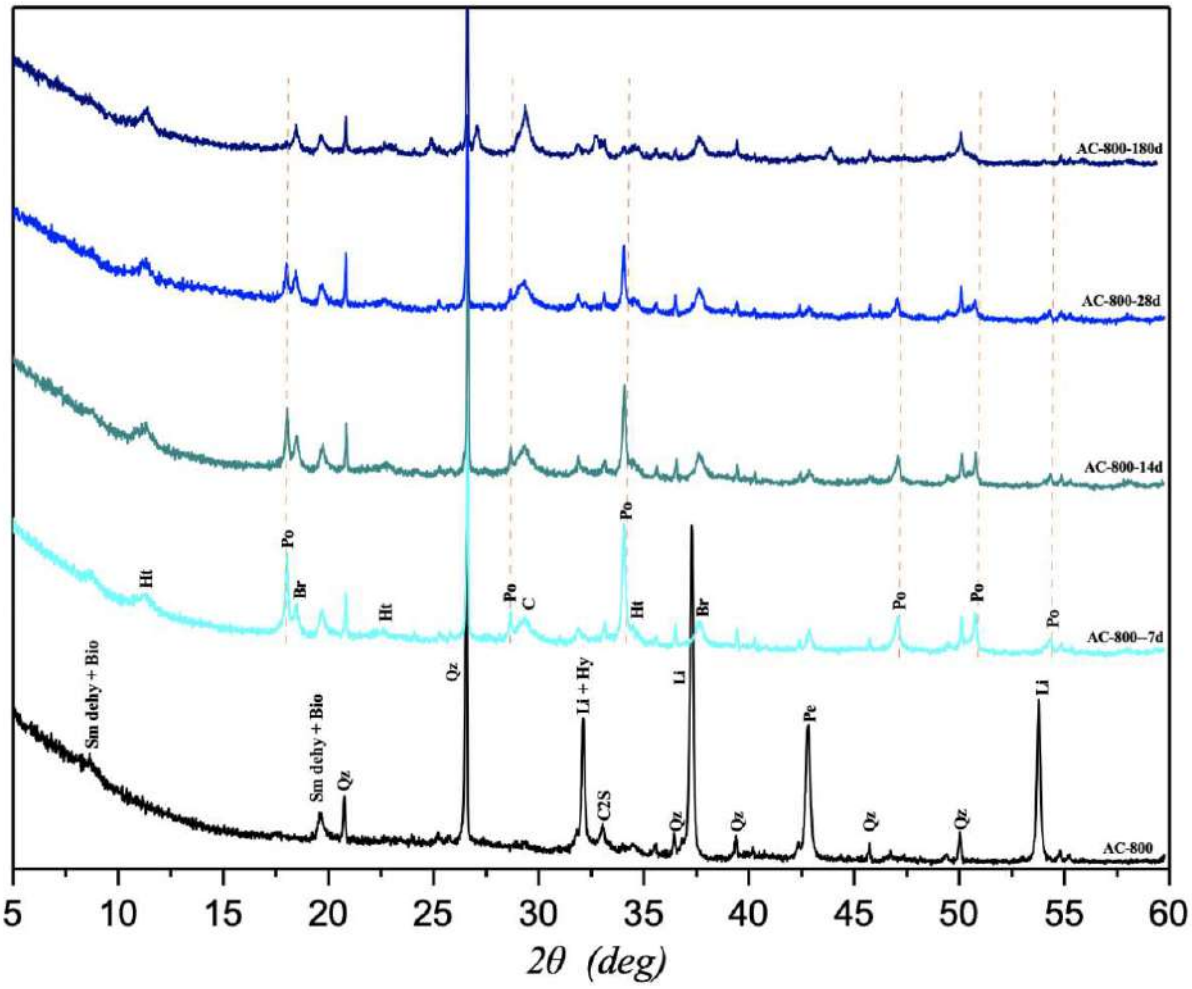

Figure 3-1: Evolution of the diffractogram of the marlstone calcined at 800°C and hydrated for 7, 14, 28 and 180 days, Sm = smectite ; Bio = biotite ; Ht = hydrotalcite ; Po = portlandite ; C = calcite ; Qz = quartz ; Hy = hydroxylapatite ; Br = brucite ; Li = lime ; Pe = periclase ; C_2S = dicalcium silicate.

The XRD pattern of the sample calcined at 800°C (AC-800) displays different peaks. The peaks associated with dehydrated smectite (Sm dehy) and biotite (Bio) are still detectable. In contrast, the peaks of palygorskite are no longer observable after the 800°C thermal treatment [20]. There are also peaks from quartz (Qz), lime (Li), periclase (Pe), hydroxylapatite (Hy) and C_2S.

Above 7 days of hydration (AC-800-7d) there is a significant decrease in the intensity of the peaks associated with lime and periclase. This decrease is correlated with the appearance of new peaks corresponding to portlandite (Po), hydrotalcite (Ht), brucite (Br) and calcite (C). The

formation of portlandite comes from the hydration of lime. The remaining signal of periclase in the hydrated sample could be explained by pockets of anhydrous periclase locked in a dense matrix of hydrates preventing water movement. The formation of calcite is due to the partial carbonation of the lime/portlandite [25]. The magnesium from periclase is incorporated into two new phases, brucite and hydrotalcite. However, the low intensity of the characteristic hydrotalcite peaks may suggests that most of the magnesium has been incorporated into brucite. ^{27}Al MAS NMR analysis will allow to characterize more precisely hydrotalcite formation during hydration.

The weak signals associated with the remaining clay phases (Sm dehy + bio) and C_2S remains present up to 180 days, demonstrating their non-reactivity. As the hydration time is increasing, the main change observed is the decrease in the intensity of the peaks associated with portlandite until they are no longer detectable after 180 days of hydration. The remaining signal associated with periclase does not evolve. On the other hand, the intensity of the peak associated with calcite is increasing. The diffractogram evolution as a function of the hydration time allowed to highlight a decrease in the intensity of the peaks associated with portlandite, which reflects a portlandite consumption. However, it is difficult to attribute this consumption to the pozzolanic reaction because C-S-H cannot be characterized by XRD, it was therefore decided to use solid state NMR to characterize them.

3.4.2. ^{29}Si and ^{27}Al MAS NMR analysis

Figure 3-2 displays the evolution of the ^{29}Si MAS NMR spectra of the calcined marlstone hydrated for 7, 14, 28 and 180 days.

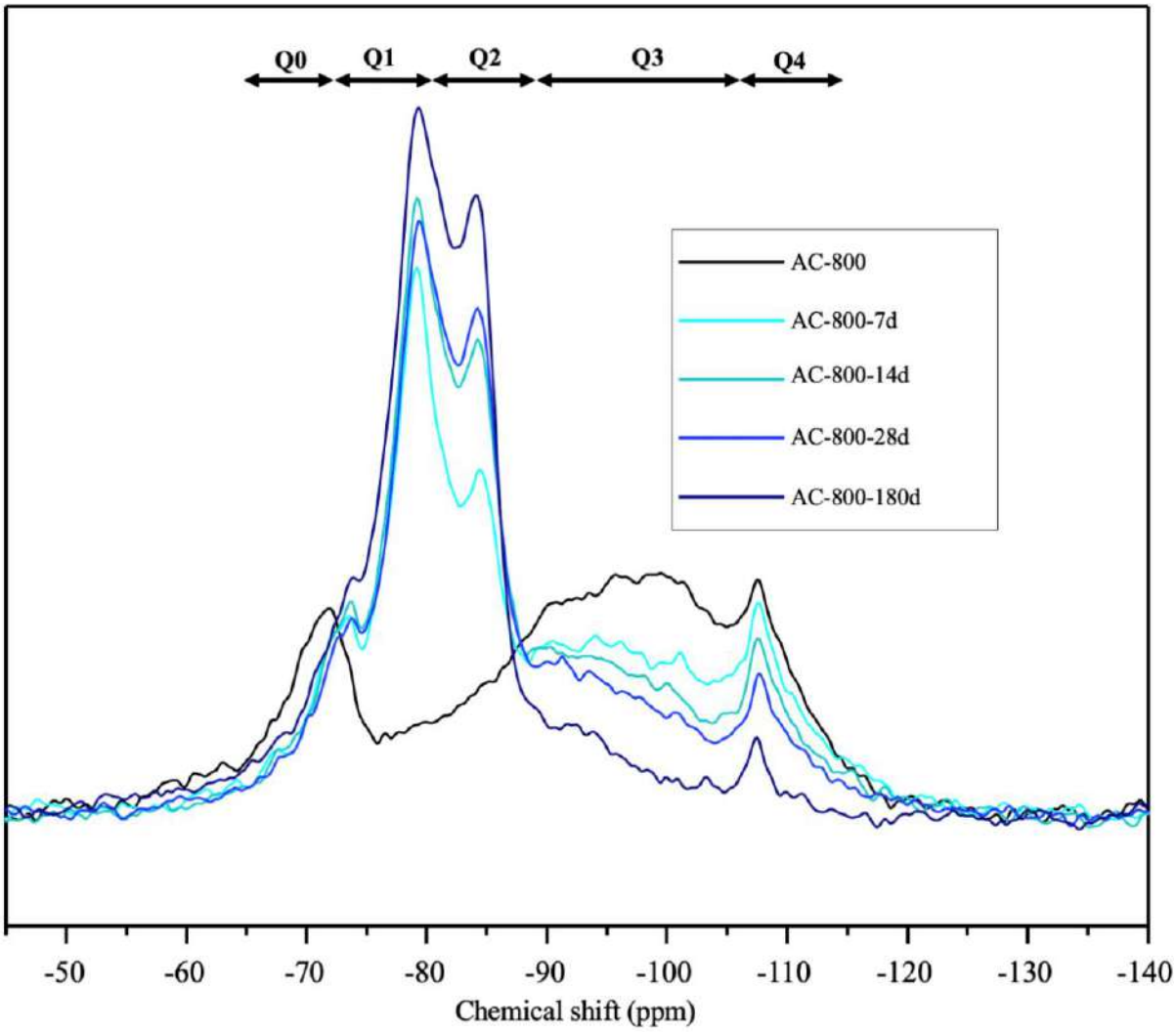

Figure 3-2: Evolution of ^{29}Si MAS NMR spectra of the calcined marlstone as function of the hydration time.

The AC-800 spectrum exhibits a resonance at -71 ppm which can be associated with monomeric Q^0 of C_2S [26] and a resonance at -108 ppm (Q^4) characteristic of quartz [27]. The broad signal of silicon in Q^3 configuration is composed of broad resonances of silicon in Q^3 configurations reflecting a distribution of their local environments and is characteristic of calcined palygorskite, and not fully calcined smectite and biotite [20]. As it is not possible to distinguish the respective contributions of calcined palygorskite and incompletely calcined smectite and biotite in this signal, the term "calcined clay phases" has been used to designate them hereafter.

After 7 days of hydration, the intensities of the broad resonances associated with the Q^3 of the calcined clays decrease. The consumption of the calcined clay phases is correlated with the appearance of two new resonances at -78 and -85 ppm which correspond to silicon in Q^1 and Q^2 configuration, respectively [28]. Silicon in Q^1 configuration can be associated with pairs of linked silicate tetrahedral (dimers) or with terminal silicate tetrahedral groups of C-S-H. Silicon in Q^2 configuration can be associated with silicate tetrahedral groups intermediates (Q^2-P) and/or bridging (Q^2-B) of C-S-H [29].

The C_2S resonance at -71 ppm decreases considerably and leaves a resonance at -73 ppm which can either be associated with Q^0 of non-reactive C_2S or Q^1 of akermanite / gehlenite phase. The weak but non zero XRD signal of C_2S is remaining with increasing hydration time (see figure 3-1), this observation supports the hypothesis that the resonance at -71 ppm can be associated with Q^0 of non-reactive C_2S. On the other hand, the study of calcination has demonstrated recrystallization phenomena in the form of akermanite from 900°C. This signal at -71 ppm, or a part of it, can therefore be associated with low-crystalline akermanite which is not yet observable by XRD at 800°C. Finally, numerous studies have also demonstrated the formation of gehlenite during calcination of a marlstone [30–32], this -71 ppm signal could therefore also be associated with gehlenite.

At 14 days the consumption of the calcined clay phases progresses while the intensities of the Q^1 and Q^2 resonances characteristics of C-S-H are increasing. There is appearance of a new resonance at -81 ppm corresponding to Q^2(1Al) [33] configuration in C-(A)-S-H [34]. The apparition of Q^2(1Al) shows the incorporation of aluminium into the C-(A)-S-H structure.

The trend goes on with the hydration time until 180 days. The remaining resonance centered at -89 ppm corresponds to remaining calcined clay phases that did not react. The consumption of the calcined clay phases associated with the formation of C-(A)-S-H confirms the intrinsic pozzolanic reactivity of this calcined marlstone. It is important to note that the neoformed brucite could have reacted with SiO_2 to form M-S-H. However, the ^{29}Si MAS NMR signature of M-S-H is clearly different from the one observed which is characteristic of C-S-H [35].

Figure 3-3 gives the evolution of the relative proportions (from the perspective of silicon content) of Q^n associated with C-(A)-S-H and Q^3 associated with calcined clay phases as function of the hydration time. This quantification was done by spectral integration of the ^{29}Si NMR spectra (details in supporting information). As the signal of Q^4 associated with quartz is not quantitative and the relative proportion of Q^0/Q^1 associated with C_2S and/or akermanite/gehlenite is constant with the increase in hydration time it was decided to display the relative evolution between Q^3 associated with calcined clay phases and Q^n associated with C-(A)-S-H only.

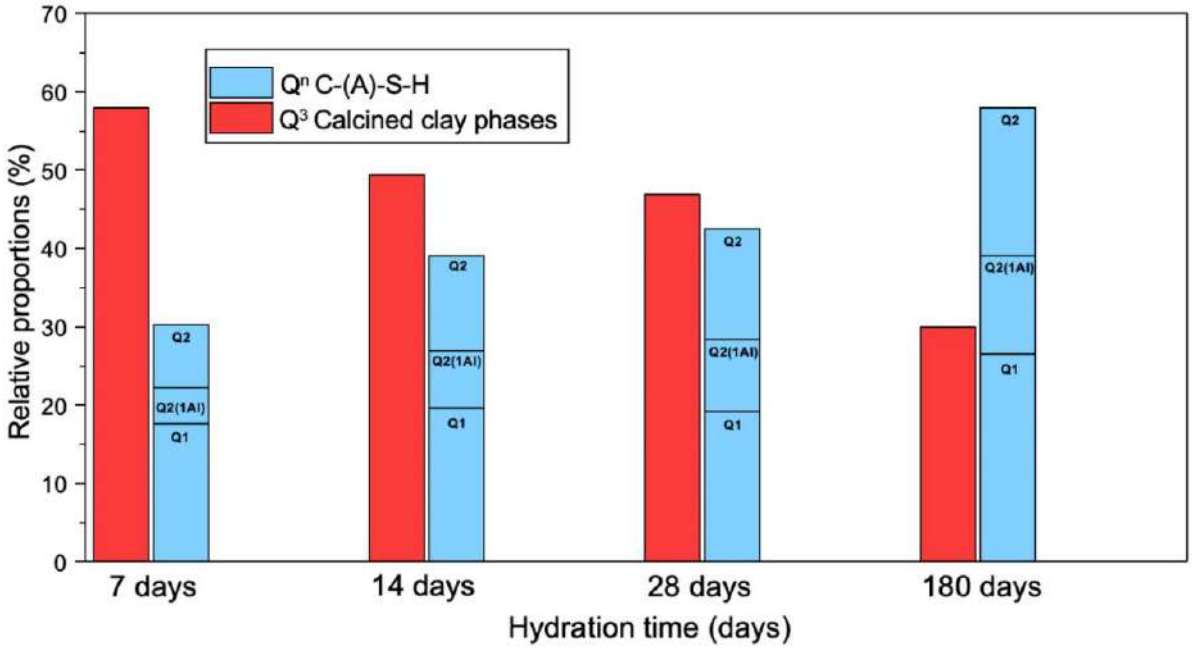

Figure 3-3: Relative proportions of silicon-containing phases (from the perspective of silicon content) as function of the hydration time obtained from ^{29}Si NMR spectra.

Between 7 and 180 days the relative proportion of silicon in Q^3 configuration associated with the calcined clay phases decreases from 58% to 30%. In parallel, the relative proportion of silicon associated with the C-(A)-S-H (Q^1 + Q^2(1Al) + Q^2) increases from 30% to 58%.

The mean chain length (MCL) of aluminosilicate chains, the mean chain length of pure silicate units (MCL_{Si}) and the Al/Si ratio of the formed C-(A)-S-H can be calculated from ^{29}Si MAS NMR spectral deconvolutions by using the substituted general model (SGM) of Richardson and Groves [36] :

$$MCL = \frac{2\left[Q^1 + Q^2 + \left(\frac{3}{2}\right)Q^2\ (1Al)\right]}{Q^1}$$

$$MCL_{Si} = \frac{2[Q^1 + Q^2 + Q^2\ (1Al)]}{Q^1 + \ Q^2\ (1Al)}$$

$$\left(\frac{Al}{Si}\right) = \frac{\left(\frac{1}{2}\right)Q^2(1Al)}{Q^1 + \ Q^2 + \ Q^2(1Al)}$$

Table 3-2 displays the evolution of these 3 values as function of the hydration time.

Table 3-2: MCL, MCL_{Si} and Al/Si values as function of the hydration time calculated by using SGM.

Non-cross-linked C-(A)-S-H structure : Substituted general model (SGM)			
Hydration time (days)	**MCL**	**MCL_{Si}**	**Al/Si**
7	3,69	2,72	0,076
14	4,37	2,90	0,094
28	4,91	2,99	0,108
180	4,86	2,97	0,109

The MCL, MCL_{Si} and Al/Si values are increasing with the hydration time between 7 and 14 days of hydration. After 14 days, the MCL_{Si} value does not evolve anymore. However, the MCL and Al/Si value still increase. This shows that the chains are lengthening by connecting silicate chains through AlO_4 units. Finally, the C-(A)-S-H structure remains stable after 28 days of hydration. It was not possible to find literature dealing with Al/Si, MCL and MCL_{Si} values in hydrated Metakaolin / CaO systems to undertake a comparative study. However, the Al/Si, MCL and MCL_{Si} values obtained are similar to those for C-(A)-S-H phases formed in hydrated white Portland cement-Metakaolin blends [37]. This demonstrates that the C-(A)-S-H formed in this system are similar to those of Metakaolin-based blended cements. Knowing that

Metakaolin blended cements are the most promising in terms of mechanical performance, this observation bodes well for the future use of this calcined marlstone as SCM.

It is important to note that the -89 ppm signal previously associated with remaining Q^3 of the calcined clay phases (figure 3-2) could also be associated with silicon in $Q^3(1Al)$ configuration related to cross-linking within the C-(A)-S-H structure [34]. In this case, another model can be used to calculate MCL and Al/Si : a full cross-linked tobermorite model [38]. Using this model, higher values were obtained for MCL and Al/Si (see supporting information). However, the evolution over the hydration time is similar to the one obtained from the SGM model. That clearly confirms that the C-(A)-S-H structure does not strongly depend on the hydration time. Figure 3-4 displays the evolution of the ^{27}Al MAS NMR spectra of the 800°C calcined argillaceous carbonate hydrated for 7, 14, 28 and 180 days.

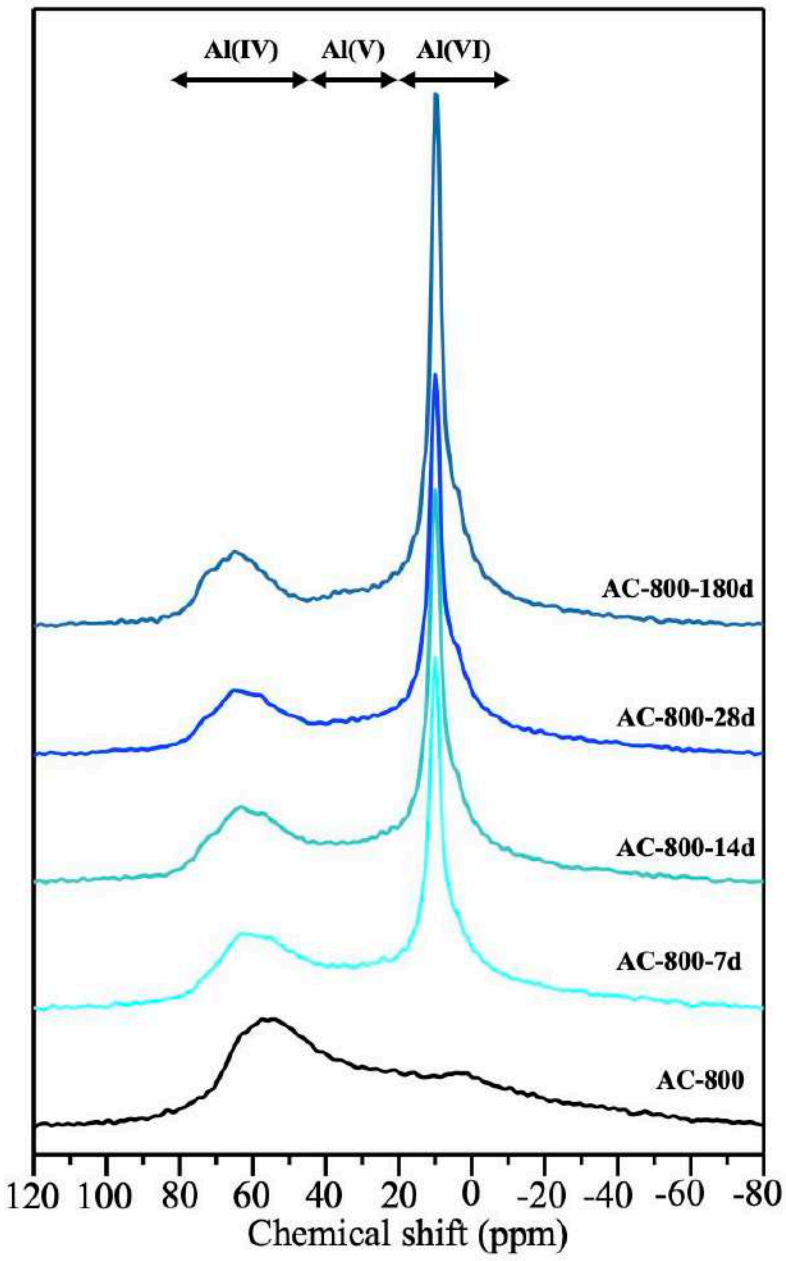

Figure 3-4: Evolution of ^{27}Al MAS NMR spectra of the calcined marlstone as function of the hydration time.

It was previously shown [20] that the AC-800 ^{27}Al MAS NMR spectrum is composed of 5 lines at 3.8, 6.5, 35, 61 and 69 ppm. The two former lines are associated with 6-fold aluminium whereas the 35 ppm line is associated with 5-fold aluminium. Finally, the 4-fold aluminium resonances at 61 and 69 ppm was attributed q4 to q3, respectively. 4-fold aluminium in q4 configuration and 5-fold aluminium are associated with the calcined clay phases. On the other hand, 4-fold aluminium in q3 configuration is close to what can be found in the gehlenite

structure [39], which supports the hypothetical attribution of a part of the ^{29}Si NMR signal at -73 ppm to gehlenite-like Q^1 configuration.

After 7 days of hydration, an intense and narrow resonance appears at 10 ppm, which can be associated with aluminium found within the hydrotalcite previously detected by XRD [40]. The detection of this characteristic hydrotalcite NMR signal confirms the hypothesis that part of the magnesium from periclase is incorporated directly into hydrotalcite in addition to brucite. This phenomenon has already been observed, notably during the hydration of alkali-activated blast-furnace slag [41][42]. Monocarboaluminates also resonate at 10 ppm in ^{27}Al MAS NMR, and their diffraction peaks at 11.6° 2θ and 23,5° 2θ overlap with those of hydrotalcite (figure 3-1) [43]. Therefore, the possibility of formation of monocarboaluminate in addition to hydrotalcite cannot be excluded.

At 14 days of hydration there is appearance of a shoulder at 72 ppm which can be associated with 4-fold aluminium in q2 configuration [44] characteristic of aluminium incorporated into C-(A)-S-H chains, confirming the ^{29}Si NMR results. The shoulder at 5 ppm suggests the presence of the third aluminate hydrate (TAH) formed at the surface of the C-(A)-S-H [45] and/or can be explained by 6-fold aluminium within the structure of C-(A)-S-H [46].

With the increase in hydration time there is a decrease in the intensity of the resonances previously associated with q4 Al(IV) and Al(V) thus reflecting the consumption of the calcined clay phases with time. On the other hand, the intensity of the resonance associated with q3 Al(IV) is not decreasing, suggesting that gehlenite potentially neoformed during calcination is not reactive. After 180 days it remains signal of q4 Al(IV) and Al(V) which correspond to the unreacted calcined clay phases whose Q^3 are still observable in ^{29}Si NMR (figure 3-2), due to the lack or portlandite.

3.4.3. Scanning electron microscope analysis

Figure 3-5 displays the SEM images of powder of the marlstone calcined at 800°C (Figure 3-5A) and hydrated during 28 days (figure 3-5B, and 3-5C).

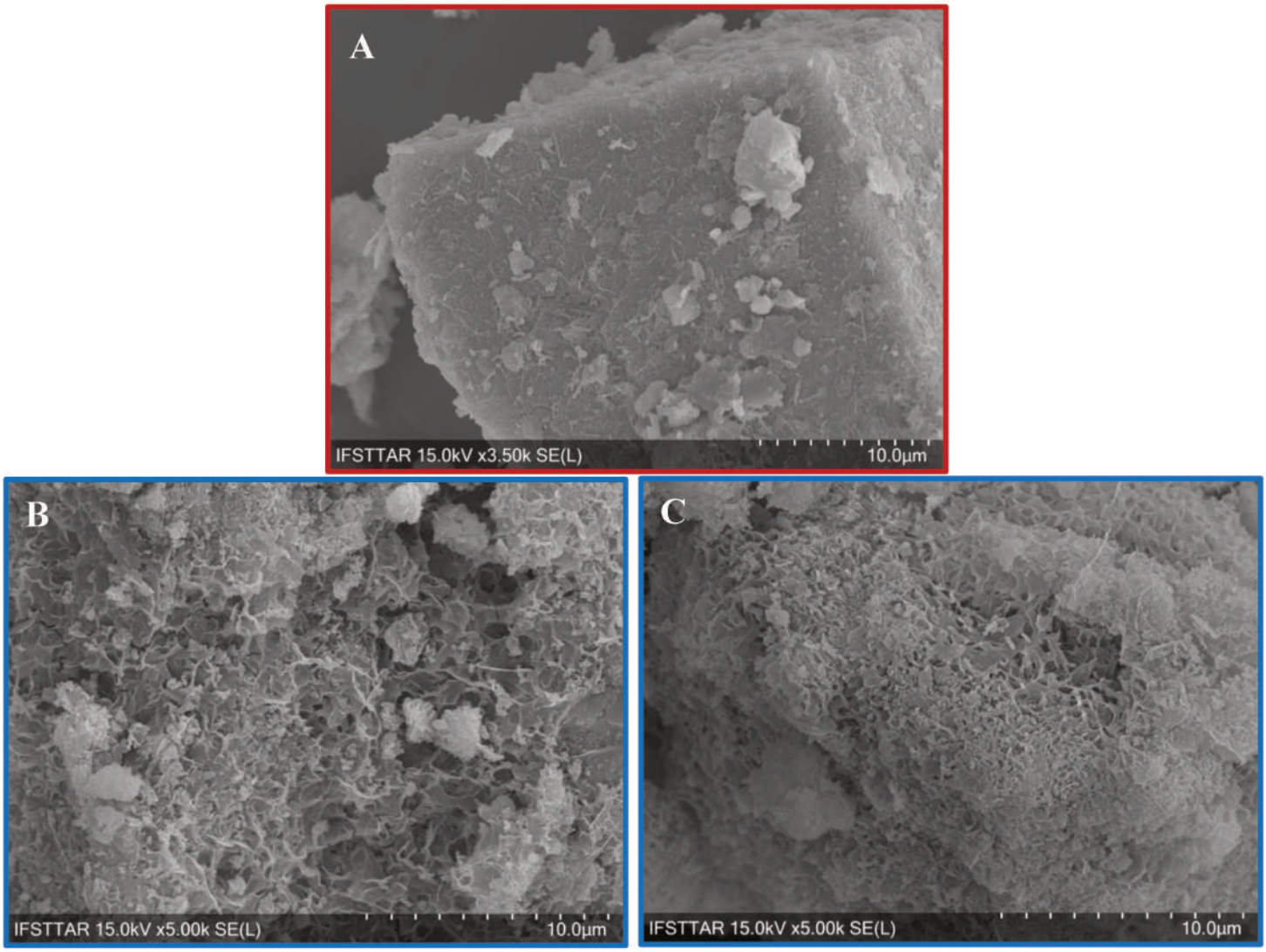

Figure 3-5: SEM images of the marlstone calcined at 800°C (A) and hydrated for 28 days (B and C).

On the figure 3-5A it can be distinguished a covering which consists of needles and a veil that covers the entire surface of the sample. These types of morphology are respectively typical of calcined palygorskite and smectite [47]. Even calcined, palygorskite and smectite morphology is conserved [20]. After 28-day hydration, there is the apparition of a new coating (figure 3-5B and 5C) which is mainly composed of flocs. This morphology is characteristic of flocs-like C-(A)-S-H phases [48]. This new C-(A)-S-H phase is covering/replacing the calcined clay phases supporting previous results suggesting C-(A)-S-H formation from pozzolanic reaction. It seems that reaction takes place at the interface between the calcined clay phases and the portlandite.

3.4.4. Potential use as supplementary cementitious material

As explained in the abstract, the objective of this study is not to obtain mechanical performance on cements incorporating the calcined material. The composition of this kind of material (marlstone) clearly differs from the classical SCMs currently in use. Consequently, it requires the use of an intermediate investigation step (self-reactivity under hydration) before mixing it with cement. The aim is to understand the evolution of the reactive phases (lime and periclase) neoformed during calcination and to characterize the pozzolanic reactivity of the calcined clay phases (palygorskite, smectite and biotite).

ASTM C618 standard states that a calcined clay is suitable for use as SCM if the sum of SiO_2, Al_2O_3 and Fe_2O_3 composing it is greater than or equal to 70% of the total oxide content. The 800°C calcined marlstone studied in this article has a CaO content of 19.5% and a MgO content of 17% [20], therefore the sum SiO_2, Al_2O_3 and Fe_2O_3 composing it is lower than 70% of its total oxide content and it does not meet the recommendations given by this standard.

The problem of MgO comes from its hydration into $Mg(OH)_2$ which leads to a potential swelling phenomenon. As the formation of $Mg(OH)_2$ has slow kinetics compared to the hydration of the anhydrous phases of the clinker, a post-hardening swelling can occur and lead to the formation of cracks and therefore loss of resistance [49]. XRD results reveal $Mg(OH)_2$ formation during hydration. On the other hand, XRD and ^{27}Al MAS NMR showed the formation of hydrotalcite after 7d of hydration. It thus appears that magnesium from MgO is found incorporated into both brucite and hydrotalcite and there is no swelling phenomenon related to the formation of hydrotalcite in the existing literature.

Free lime (CaO) content in cement has to be controlled in order to avoid undesirable effects such as reduced strength, expansion phenomenon or increased setting time. XRD results showed that the majority of the free lime is hydrated into portlandite from 7 days of hydration (the remaining lime being trapped in dense matrices of portlandite and C-(A)-S-H). The neoformed portlandite is then consumed by the pozzolanic reaction of the calcined clay phases until 180 days of hydration. The presence of free lime does not seem to be problematic in this particular hydrated system. However, its kinetics of hydration and consumption from

the pozzolanic reaction can be affected by the cementitious medium when using this calcined material as SCM.

3.5. Conclusion

This step of study of the hydration of this calcined palygorskite-bearing marlstone highlighted its self-reactivity. The reaction of the calcined clay phases and portlandite (from the hydrated decarbonated dolomite) lead to the formation of C-(A)-S-H, demonstrating the pozzolanic reactivity of this sample. C_2S neoformed during calcination reacts during the first 7 days of hydration. The self-reactivity of this calcined palygorkiste-bearing marlstone is therefore mainly due to its pozzolanic reactivity. The synergy of the phases that compose this sample leads to the consumption of the neoformed portlandite and the incorporation of magnesium from periclase into hydrotalcite and brucite. Now that the reactivity of this calcined material, as well as the evolution of the reactive phases of which it is composed, has been described, the next step will consist of a study of the mechanical and volumetric properties of cementitious blends incorporating this calcined material.

3.6. References

[1] Y.H.M. Amran, R. Alyousef, H. Alabduljabbar, M. El-Zeadani, Clean production and properties of geopolymer concrete; A review, Journal of Cleaner Production. 251 (2020) 119679. https://doi.org/10.1016/j.jclepro.2019.119679.

[2] H. Mikulčić, J.J. Klemeš, M. Vujanović, K. Urbaniec, N. Duić, Reducing greenhouse gasses emissions by fostering the deployment of alternative raw materials and energy sources in the cleaner cement manufacturing process, Journal of Cleaner Production. 136 (2016) 119–132. https://doi.org/10.1016/j.jclepro.2016.04.145.

[3] D.N. Huntzinger, T.D. Eatmon, A life-cycle assessment of Portland cement manufacturing: comparing the traditional process with alternative technologies, Journal of Cleaner Production. 17 (2009) 668–675. https://doi.org/10.1016/j.jclepro.2008.04.007.

[4] Y. Cancio Díaz, S. Sánchez Berriel, U. Heierli, A.R. Favier, I.R. Sánchez Machado, K.L. Scrivener, J.F. Martirena Hernández, G. Habert, Limestone calcined clay cement as a low-carbon solution to meet expanding cement demand in emerging economies, Development Engineering. 2 (2017) 82–91. https://doi.org/10.1016/j.deveng.2017.06.001.

[5] M. Behim, B. Redjel, R. Jauberthie, Réactivitié du laitier de hauts fourneaux d'Annaba (Algérie) en substitution partielle du ciment, (2002).

[6] H. Yazıcı, M.Y. Yardımcı, H. Yiğiter, S. Aydın, S. Türkel, Mechanical properties of reactive powder concrete containing high volumes of ground granulated blast furnace slag, Cement and Concrete Composites. 32 (2010) 639–648. https://doi.org/10.1016/j.cemconcomp.2010.07.005.

[7] Z.T. Yao, X.S. Ji, P.K. Sarker, J.H. Tang, L.Q. Ge, M.S. Xia, Y.Q. Xi, A comprehensive review on the applications of coal fly ash, Earth-Science Reviews. 141 (2015) 105–121. https://doi.org/10.1016/j.earscirev.2014.11.016.

[8] X. Hu, C. Shi, Z. Shi, L. Zhang, Compressive strength, pore structure and chloride transport properties of alkali-activated slag/fly ash mortars, Cement and Concrete Composites. 104 (2019) 103392. https://doi.org/10.1016/j.cemconcomp.2019.103392.

[9] K. Scrivener, F. Martirena, S. Bishnoi, S. Maity, Calcined clay limestone cements (LC3), Cement and Concrete Research. 114 (2018) 49–56. https://doi.org/10.1016/j.cemconres.2017.08.017.

[10] R.S. Almenares, L.M. Vizcaíno, S. Damas, A. Mathieu, A. Alujas, F. Martirena, Industrial calcination of kaolinitic clays to make reactive pozzolans, Case Studies in Construction Materials. 6 (2017) 225–232. https://doi.org/10.1016/j.cscm.2017.03.005.

[11] A. Alujas, R. Fernández, R. Quintana, K.L. Scrivener, F. Martirena, Pozzolanic reactivity of low grade kaolinitic clays: Influence of calcination temperature and impact of calcination products on OPC hydration, Applied Clay Science. 108 (2015) 94–101. https://doi.org/10.1016/j.clay.2015.01.028.

[12] H. El-Diadamony, A.A. Amer, T.M. Sokkary, S. El-Hoseny, Hydration and characteristics of metakaolin pozzolanic cement pastes, HBRC Journal. 14 (2018) 150–158. https://doi.org/10.1016/j.hbrcj.2015.05.005.

[13] D. Zhao, R. Khoshnazar, Microstructure of cement paste incorporating high volume of low-grade metakaolin, Cement and Concrete Composites. 106 (2020) 103453. https://doi.org/10.1016/j.cemconcomp.2019.103453.

[14] I.W. Brown, K.J.D. MacKenzie, R.H. Meinhold, The thermal reactions of montmorillonite studied by high-resolution solide-state 29Si and 27Al NMR, (1987).

[15] N. Garg, J. Skibsted, Thermal Activation of a Pure Montmorillonite Clay and Its Reactivity in Cementitious Systems, The Journal of Physical Chemistry C. 118 (2014) 11464–11477. https://doi.org/10.1021/jp502529d.

[16] R. Kaminskas, R. Kubiliute, B. Prialgauskaite, Smectite clay waste as an additive for Portland cement, Cement and Concrete Composites. 113 (2020) 103710. https://doi.org/10.1016/j.cemconcomp.2020.103710.

[17] N. Garg, J. Skibsted, Pozzolanic reactivity of a calcined interstratified illite/smectite (70/30) clay, Cement and Concrete Research. 79 (2016) 101–111. https://doi.org/10.1016/j.cemconres.2015.08.006.

[18] R. Fernandez, F. Martirena, K.L. Scrivener, The origin of the pozzolanic activity of calcined clay minerals: A comparison between kaolinite, illite and montmorillonite, Cement and Concrete Research. 41 (2011) 113–122. https://doi.org/10.1016/j.cemconres.2010.09.013.

[19] S.C. Taylor-Lange, F. Rajabali, N.A. Holsomback, K. Riding, M.C.G. Juenger, The effect of zinc oxide additions on the performance of calcined sodium montmorillonite and illite shale supplementary cementitious materials, Cement and Concrete Composites. 53 (2014) 127–135. https://doi.org/10.1016/j.cemconcomp.2014.06.008.

[20] V. Poussardin, M. Paris, A. Tagnit-Hamou, D. Deneele, Potential for calcination of a palygorskite-bearing argillaceous carbonate, Applied Clay Science. 198 (2020) 105846. https://doi.org/10.1016/j.clay.2020.105846.

[21] F. Avet, R. Snellings, A. Alujas Diaz, M. Ben Haha, K. Scrivener, Development of a new rapid, relevant and reliable (R3) test method to evaluate the pozzolanic reactivity of calcined kaolinitic clays, Cement and Concrete Research. 85 (2016) 1–11. https://doi.org/10.1016/j.cemconres.2016.02.015.

[22] A. Tironi, M.A. Trezza, A.N. Scian, E.F. Irassar, Assessment of pozzolanic activity of different calcined clays, Cement and Concrete Composites. 37 (2013) 319–327. https://doi.org/10.1016/j.cemconcomp.2013.01.002.

[23] N. Doebelin, R. Kleeberg, *Profex* : a graphical user interface for the Rietveld refinement program *BGMN*, Journal of Applied Crystallography. 48 (2015) 1573–1580. https://doi.org/10.1107/S1600576715014685.

[24] D. Massiot, F. Fayon, M. Capron, I. King, S. Le Calvé, B. Alonso, J.-O. Durand, B. Bujoli, Z. Gan, G. Hoatson, Modelling one- and two-dimensional solid-state NMR spectra: Modelling 1D and 2D solid-state NMR spectra, Magn. Reson. Chem. 40 (2002) 70–76. https://doi.org/10.1002/mrc.984.

[25] K. Van Balen, D. Van Gemert, Modelling lime mortar carbonation, Materials and Structures. 27 (1994) 393–398. https://doi.org/10.1007/BF02473442.

[26] J. Skibsted, H.J. Jakobsen, C. Hall, Quantification of calcium silicate phases in Portland cements by 29Si MAS NMR spectroscopy, Journal of the Chemical Society, Faraday Transactions. 91 (1995) 4423. https://doi.org/10.1039/ft9959104423.

[27] E. Lippmaa, M. Maegi, A. Samoson, G. Engelhardt, A.R. Grimmer, Structural studies of silicates by solid-state high-resolution silicon-29 NMR, Journal of the American Chemical Society. 102 (1980) 4889–4893. https://doi.org/10.1021/ja00535a008.

[28] M. Magi, E. Lippmaa, A. Samoson, G. Engelhardt, A.R. Grimmer, Solid-state high-resolution silicon-29 chemical shifts in silicates, The Journal of Physical Chemistry. 88 (1984) 1518–1522. https://doi.org/10.1021/j150652a015.

[29] M.D. Andersen, H.J. Jakobsen, J. Skibsted, Characterization of white Portland cement hydration and the C-S-H structure in the presence of sodium aluminate by 27Al and 29Si MAS NMR spectroscopy, Cement and Concrete Research. 34 (2004) 857–868. https://doi.org/10.1016/j.cemconres.2003.10.009.

[30] D.C. Hughes, D. Jaglin, R. Kozłowski, D. Mucha, Roman cements — Belite cements calcined at low temperature, Cement and Concrete Research. 39 (2009) 77–89. https://doi.org/10.1016/j.cemconres.2008.11.010.

[31] A. Verganelaki, N.-P. Maravelaki, M. Budak, CALCINED CLAYS AND LIMESTONE AS HYDRAULIC BINDERS, (n.d.) 9.

[32] S. Shoval, Mineralogical changes upon heating calcitic and dolomitic marl rocks, Thermochimica Acta. 135 (1988) 243–252. https://doi.org/10.1016/0040-6031(88)87393-3.

[33] M.D. Andersen, H.J. Jakobsen, J. Skibsted, Incorporation of Aluminum in the Calcium Silicate Hydrate (C−S−H) of Hydrated Portland Cements: A High-Field ^{27} Al and ^{29} Si MAS NMR Investigation, Inorganic Chemistry. 42 (2003) 2280–2287. https://doi.org/10.1021/ic020607b.

[34] X. Gao, Q.L. Yu, H.J.H. Brouwers, Apply 29Si, 27Al MAS NMR and selective dissolution in identifying the reaction degree of alkali activated slag-fly ash composites, Ceramics International. 43 (2017) 12408–12419. https://doi.org/10.1016/j.ceramint.2017.06.108.

[35] E. Bernard, B. Lothenbach, D. Rentsch, I. Pochard, A. Dauzères, Formation of magnesium silicate hydrates (M-S-H), Physics and Chemistry of the Earth, Parts A/B/C. 99 (2017) 142–157. https://doi.org/10.1016/j.pce.2017.02.005.

[36] I.G. Richardson, G.W. Groves, The incorporation of minor and trace elements into calcium silicate hydrate (C-S-H) gel in hardened cement pastes, Cement and Concrete Research. 23 (1993) 131–138. https://doi.org/10.1016/0008-8846(93)90143-W.

[37] Z. Dai, T.T. Tran, J. Skibsted, Aluminum Incorporation in the C–S–H Phase of White Portland Cement–Metakaolin Blends Studied by 27Al and 29Si MAS NMR Spectroscopy, Journal of the American Ceramic Society. 97 (2014) 2662–2671. https://doi.org/10.1111/jace.13006.

[38] R.J. Myers, S.A. Bernal, R. San Nicolas, J.L. Provis, Generalized Structural Description of Calcium–Sodium Aluminosilicate Hydrate Gels: The Cross-Linked Substituted Tobermorite Model, Langmuir. 29 (2013) 5294–5306. https://doi.org/10.1021/la4000473.

[39] P. Florian, E. Veron, T.F.G. Green, J.R. Yates, D. Massiot, Elucidation of the Al/Si Ordering in Gehlenite Ca2Al2SiO7 by Combined 29Si and 27Al NMR Spectroscopy/Quantum Chemical Calculations, Chem. Mater. 24 (2012) 4068–4079. https://doi.org/10.1021/cm3016935.

[40] R.V. Prikhod'ko, M.V. Sychev, I.M. Astrelin, K. Erdmann, A. Mangel', R.A. van Santen, Synthesis and Structural Transformations of Hydrotalcite-like Materials Mg-Al and Zn-Al, 74 (2001) 6.

[41] M.B. Haha, B. Lothenbach, G. Le Saout, F. Winnefeld, Influence of slag chemistry on the hydration of alkali-activated blast-furnace slag — Part I: Effect of MgO, Cement and Concrete Research. 41 (2011) 955–963. https://doi.org/10.1016/j.cemconres.2011.05.002.

[42] A. Cherki El Idrissi, M. Paris, E. Rozière, D. Deneele, S. Darson, A. Loukili, Alkali-activated grouts with incorporated fly ash: From NMR analysis to mechanical properties, Materials Today Communications. 14 (2018) 225–232. https://doi.org/10.1016/j.mtcomm.2018.01.012.

[43] A. Ipavec, R. Gabrovšek, T. Vuk, V. Kaučič, J. Maček, A. Meden, Carboaluminate Phases Formation During the Hydration of Calcite-Containing Portland Cement: Carboaluminate Phase Formation, Journal of the American Ceramic Society. 94 (2011) 1238–1242. https://doi.org/10.1111/j.1551-2916.2010.04201.x.

[44] X. Pardal, F. Brunet, T. Charpentier, I. Pochard, A. Nonat, 27Al and 29Si Solid-State NMR Characterization of Calcium-Aluminosilicate-Hydrate, Inorganic Chemistry. 51 (2012) 1827–1836. https://doi.org/10.1021/ic202124x.

[45] M.D. Andersen, H.J. Jakobsen, J. Skibsted, A new aluminium-hydrate species in hydrated Portland cements characterized by 27Al and 29Si MAS NMR spectroscopy, Cement and Concrete Research. 36 (2006) 3–17. https://doi.org/10.1016/j.cemconres.2005.04.010.

[46] A. Kunhi Mohamed, P. Moutzouri, P. Berruyer, B.J. Walder, J. Siramanont, M. Harris, M. Negroni, S.C. Galmarini, S.C. Parker, K.L. Scrivener, L. Emsley, P. Bowen, The Atomic-Level Structure of Cementitious Calcium Aluminate Silicate Hydrate, J. Am. Chem. Soc. 142 (2020) 11060–11071. https://doi.org/10.1021/jacs.0c02988.

[47] L. Boudriche, R. Calvet, B. Hamdi, H. Balard, Effect of acid treatment on surface properties evolution of attapulgite clay: An application of inverse gas chromatography, Colloids and Surfaces A: Physicochemical and Engineering Aspects. 392 (2011) 45–54. https://doi.org/10.1016/j.colsurfa.2011.09.031.

[48] O. Cizer, K.V. Balen, D.V. Gemert, J. Elsen, Carbonation and hydration of mortars with calcium hydroxide and calcium silicate binders, (n.d.) 13.

[49] E.A. Cherney, R.D. Hooton, Cement Growth Failure Mechanism in Porcelain Suspension Insulators, IEEE Transactions on Power Delivery. 2 (1987) 249–255. https://doi.org/10.1109/TPWRD.1987.4308096.

3.7. Bilan scientifique du chapitre 3

Cette dernière partie dresse un bilan scientifique de ce chapitre 3 qui s'intéresse à l'auto-réactivité après calcination d'une marne dolomitique contenant de la palygorskite et de la smectite.

L'étude de la réactivité dans l'eau de cette marne calcinée a donc permis de confirmer son fort potentiel pour une utilisation en remplacement du ciment. Du fait de sa composition minéralogique particulière (phases argileuses calcinées, chaux, périclase et C_2S) ce type de marne calcinée est auto-réactive dans l'eau. Il a été démontré que cette réactivité dans l'eau est principalement pouzzolanique et conduit à la formation de C-(A)-S-H (réaction des phases argileuses calcinées avec l'hydroxyde de calcium issu de l'hydratation de la chaux). Le périclase néoformé lors de la calcination (mis en avant dans le chapitre 2) est également réactif puisqu'une partie du magnésium va être incorporé dans de l'hydrotalcite et une seconde partie dans de la brucite. Cette formation de brucite devra être surveillée puisque des teneurs trop élevées (supérieures à 6%) pourraient conduire à des désordres volumiques délétères.

Il a été possible de relier la réactivité dans l'eau aux modifications physico-chimiques qui ont été induites lors de la calcination. Cela a permis de déterminer que les phases argileuses calcinées ne seront pas les seules à avoir un impact sur l'hydratation du ciment. Il est donc nécessaire de suivre de manière précise l'apparition de ces phases secondaires (chaux, périclase, C_2S) lors de la calcination de ce type de marnes en vue d'une utilisation comme ajout cimentaire.

Chapitre 4 – Utilisation de marnes calcinées comme ajouts cimentaires : influence de la présence de palygorskite

4.1. Avant-propos

Note : Ce chapitre est basé sur un article publié dans un journal international à comité de lecture.

Titre de l'article : **Calcined marlstones as supplementary cementitious materials : a comparison between palygorskite and smectite bearing marlstones**

Victor Poussardin, Michael Paris, William Wilson, Arezki Tagnit-Hamou, Dimitri Deneele

Publié dans : Materials and structures

DOI : https://doi.org/10.1617/s11527-022-02053-0

Contribution à la thèse

Les chapitres 2 et 3 se sont intéressés à la calcination et l'auto-réactivité d'une marne dolomitique contenant de la palygorskite et de la smectite. Il a été possible de se procurer un autre échantillon de marne, provenant du même site et ayant une composition minéralogique très proche de la marne étudiée précédemment. La seule différence notable étant l'absence de palygorskite dans ce nouvel échantillon. Ce chapitre consiste donc en une étude comparative de la calcination, de l'auto-réactivité lors de l'hydratation et de la réactivité en système cimentaire de ces deux marnes. L'objectif est double, déterminer si ces marnes peuvent être utilisées comme ajouts cimentaires une fois calcinées mais également évaluer le rôle de la palygorskite dans la réactivité totale de cette marne.

Résumé en français

Ce chapitre porte sur l'utilisation de deux marnes calcinées comme ajouts cimentaires, l'une avec de la palygorskite et de la smectite (MS1) comme phases argileuses et l'autre avec de la smectite uniquement (MS2). La calcination et la réactivité de ces deux matériaux ont d'abord été analysées par diffraction des rayons X (DRX) et par résonance magnétique nucléaire du solide (RMN MAS). Les deux marnes calcinées ont été mélangées avec du ciment Portland pour produire des ciments composés puis des mortiers ont été confectionnés afin de mesurer les résistances à la compression. Les résultats de DRX et de ^{27}Al RMN MAS ont montré que 800°C est une température de calcination optimale et que les deux marnes calcinées peuvent être utilisées comme ajouts cimentaires. La réactivité de MS1 s'est avérée plus élevée que celle de MS2. Ceci a été confirmé par les mesures de résistance à la compression sur mortiers qui ont montré des performances mécaniques supérieures pour les mortiers incorporant MS1 calcinée plutôt que MS2 calcinée. Cette différence entre MS1 et MS2 est due à la présence de palygorskite dans MS1, qui améliore considérablement la réactivité et les performances mécaniques finales. Par conséquent, les marnes contenant de la palygorskite sont appropriées pour une utilisation en tant que SCM et cela suggère que la palygorskite présente une réactivité pouzzolanique significative.

Résumé en anglais

This article focusses on the use of two calcined marlstones as supplementary cementitious materials, one with palygorskite and smectite (MS1) as clay phases and the other with smectite only (MS2). The calcination and the reactivity of these two materials were first analysed by X-ray diffraction (XRD) and Magic Angle Spinning Solid State Nuclear Magnetic Resonance (MAS NMR). The two calcined marlstones were combined with Portland cement to produce mortars and measure compressive strength. The XRD and ^{27}Al MAS NMR results showed that 800°C is an optimal calcination temperature and that both calcined marlstones can be used as supplementary cementitious materials. The reactivity of MS1 was found to be higher than that of MS2. This was confirmed with compressive strength measurements which showed superior performance for mortars blended with calcined MS1 rather than calcined

MS2. This difference between MS1 and MS2 is due to the presence of palygorskite in MS1, which greatly improves the reactivity and final mechanical performances. Therefore, palygorskite bearing marlstones are suitable for a use as SCM and this suggests that palygorskite exhibits a significant pozzolanic reactivity.

4.2. Introduction

In order to comply with the Paris climate agreements, and to limit the global temperature increase below +1.5°C compared to pre-industrial levels, the most polluting industrial sectors needs to reduce significantly their greenhouse gas emissions (may their CO_2 emissions). It is estimated that 5 to 8% of global anthropogenic CO_2 emissions comes from the cement industry [1]. In this context, cement producers are seeking to reduce their carbon footprint.

The use of Supplementary Cementitious Materials (SCMs) to replace part of the clinker is now seen as one of the major solutions to reduce the environmental footprint of the cement industry [2]. Blast furnace slag [3,4] and power plant fly ash [5–7] are the main examples of SCMs used today that reduce the environmental footprint of cement. However, blast furnace slag resources remain limited, preventing large-scale deployment of this technology, and fly ash reserves from coal combustion will continue to decline in the coming years as the energy transition legitimately limits their availability [2].

Among alternative SCMs, calcined clays are gaining in popularity. The resources of clays potentially viable as SCMs after calcination are abundant and well distributed around the world, especially in developing countries where the demand for cement is constantly growing [2]. The numerous studies carried out on the subject have shown that metakaolin (from the calcination of kaolin) has the highest reactivity in cementitious media [8–11], whereas calcined smectites [12–14] and illites [15–17] are much less reactive. These results led to a growing interest in the use of calcined kaolins (rock composed of kaolinite, quartz and minor accessory minerals) as SCMs, and to the development of Limestone Calcined Clay Cements (LC3) [18,19].

Only few studies have looked at other types of clays than kaolinites, smectites and illites [20,21], mainly because of industrial competition (which leads to higher prices) and lower availability. Furthermore, the majority of studies focused on relatively "pure" samples, which are mainly composed of clay minerals, quartz and other accessory minor minerals. Yet it is common to find clay minerals associated with other compounds, especially carbonates. If the proportion of carbonates is high, this mixture of clay minerals and carbonates is named marlstone.

Marlstones are often neglected by manufacturers of fired clay materials such as bricks because of their high content of calcium carbonate. They are considered as waste by many industries and supplies are increasing [22]. However, these materials contain a significant proportion of clay minerals, which can become pozzolans upon calcination. The use of marlstones as SCMs could therefore make it possible to recover mining wastes (and/or overburdens) while reducing the environmental footprint of cement production. Numerous studies looked at the use of marlstones as SCMs [23–27] , but the great variability of this type of material limits the possibility of global analyses. For each type of marlstones considered as a potential SCM, it is imperative to understand the evolution of each phase (clay minerals and carbonates) composing the marlstones during its calcination, as well as its influence on the reactivity and the final mechanical performances of calcined marlstone-cement blends.

This study focuses on the use as SCMs of two marlstones considered as waste by the mining industry. The first objective is to determine whether these materials can be used as SCMs. The second objective is to study the physico-chemical changes taking place during the calcination and the reaction of these new pozzolans and to correlate this information with the final mechanical performances. The last objective is to determine how palygorskite (an unconventional clay contained in one of the two materials) contributes to the pozzolanic reactivity.

4.3. Materials and experimental methods

4.3.1. Materials

The materials studied (MS1 and MS2) are two marlstones considered as waste by the mining industry. The samples were received as loose blocks and mechanically crushed before analysis. Table 4-1 shows the results of the chemical analysis (performed by X-Ray Fluorescence (XRF). The proportions of each element are expressed in weight percent.

Table 4-1: Chemical analysis of MS1 and MS2.

	Element	O	Ca	Si	Mg	Al	Fe	K	P	Na	Ti	V
MS1	wt. %	55.5	**14.2**	**15.6**	**6.0**	**4.7**	1.5	1.0	0.6	0.2	0.2	0.1
MS2	wt. %	56.0	**16.4**	**16.2**	**5.5**	**3.8**	1.2	0.2	0.2	0.2	0.2	0

MS1 and MS2 have a very close chemical composition, especially regarding the proportions of silicon, calcium, magnesium and aluminium. These similarities in the chemistry of MS1 and MS2 are not surprising as both materials originate from the same sedimentary deposit.

X-ray diffraction analysis (XRD) was performed to highlight the mineralogical composition MS1 and MS2 and the different phases were quantified using the Rietveld refinement technique (see supporting information). Table 4-2 shows the results of the quantitative phases analysis for MS1 and MS2.

Table 4-2 : wt.% of the crystalline phases of MS1 and MS2.

	Phase	Dolomite	Palygorskite	Smectite	Biotite	Hydroxylapatite	Quartz
MS1	wt.%	54	17	16	2	3	8
MS2	wt.%	59		27	1	2	11

MS1 and MS2 have a relatively close mineralogy, they are both mainly composed of dolomite associated with clay phases (smectite and biotite), quartz and hydroxylapatite. The main difference is the occurrence of palygorskite in MS1, which replaces part of the smectite.

4.3.2. Marlstones calcination

MS1 and MS2 were calcined at 600, 800 and 900°C in alumina crucibles using a laboratory furnace. The materials were heated at a heating rate of 300°C/h and then maintained for 1 hour at maximum temperature. They were then left to cool until room temperature with the furnace door closed.

4.3.3. Hydration of calcined marlstones

The calcination and hydration of MS1 have already been the subject of two previous studies [28,29] which demonstrated the formation of several reactive phases after calcination, notably CaO. As MS2 has a very close mineralogy to MS1, it is very likely to have the same reactive phases formed. Therefore, the pozzolanic activity of calcined MS1 and MS2 could not be measured using the classical pozzolanic activity tests (Chapelle test [30] and R^3 [31]), which requires the material tested not to contain free calcium. It was therefore decided to characterise the reactivity of these calcined materials by carrying out hydration tests. For both MS1 and MS2, 1g of 800°C calcined material was manually mixed with water according to the chosen water to binder ratios (w/b = 0.8; 1; 2 and 4). The mixtures were left to react in sealed conditions for 7, 14, 28 and 180 days. At the end of each time period, they hydration was stopped by freezing (24h) and freeze-drying (48h). The dried materials were crushed and analysed by X-ray diffraction (XRD) and solid state nuclear magnetic resonance (MAS NMR). As the result analysis did not reveal any significant differences between the different w/b, only the hydration results for w/b = 0.8 are reported.

4.3.4. X-ray diffraction analysis (XRD)

Measurements were made with a Bruker D8 diffractometer using a Bragg-Brentano geometry with a copper anode tube X-ray source (40 kV/40 mA) emitting Cu Kα radiation. The acquisitions of the diffractograms were made between 4° and 60° 2θ with a step size of 0.017° 2θ and a measurement time of 1s per step. The Rietveld quantification of MS1 and MS2 was performed using the Profex Rietveld refinement program [32].

4.3.5. Solid state nuclear magnetic resonance (MAS NMR)

^{27}Al MAS NMR spectra were acquired in a 2.5 mm MAS probe using a Bruker Avance III 500 MHz spectrometer with the following parameters : MAS frequency of 30 kHz, excitation pulse length of π/13, radio frequency field of 11 kHz and repetition time of 1s. ^{29}Si MAS NMR spectra were acquired in a 7 mm MAS probe using a Bruker NEO 300 MHz spectrometer with the following parameters : MAS frequency of 5 kHz, excitation pulse length of π/2 and repetition time of 10s. The chosen 10s repetition time is too short to obtain a quantitative signal from the quartz, but as quartz is unreactive shorter repetition time can be used to save spectrometer time. All the acquisitions were performed with ^{1}H decoupling. An aqueous solution of $Al(NO_3)_3$ was used to referenced ^{27}Al spectra while ^{29}Si spectra were referenced against TMS (Tetramethylsilane). The Dmfit sotftware [33] was used to perform the spectral decompositions (see supporting information).

4.3.6. Calcined marlstone-cement blends and compressive strength measurements

The compressive strength was assessed on mortar cubes (50 x 50 x 50 mm^3) made with graded standard (supports ASTM C109) sand (sand to cement ratio = 2.75) and a constant water to binder ratio (w/b = 0.484). Blended cement was obtained by mixing 80 wt.% of general use Portland cement (GU) with 20 wt.% of 800°C calcined MS1 (for M-MS1 mortar) or MS2 (for M-MS2 mortar). The particle size distributions of the GU cement and MS1 and MS2 (before and after calcination) are shown in table 4-3

.

Table 4-3 : Particle size distributions of GU cement and marlstones (MS1 and MS2) before and after calcination at 800°C.

Label	d10 (μm)	d50 (μm)	d90 (μm)
MS1	3.5	19.5	64.1
800°C-MS1	4.0	24.5	91.6
MS2	2.4	14.8	53.1
800°C-MS2	3.6	28.2	66.3
GU cement	3.5	20.5	59.7

Both 800°C-MS1 and 800°C-MS2 have a particle size distribution close to that of GU cement, which ensures homogeneous blends.nControl mortars cubes (labelled M-ref) were prepared using 100% GU cement. A polycarboxylate (PC) superplasticizer was used to obtain a flow equivalent to that of the control mixture (+/- 5 mm). Table 4-4 shows the proportions of the investigated mortars.

Table 4-4 : Mix proportions of mortars.

Label	Cement (g)	Pozzolan (g)	Sand (g)	Water (g)
M-Ref	500	0	1375	242
M-MS1	400	100	1375	242
M-MS2	400	100	1375	242

Mortars were mixed and specimens were molded according to the standard procedure ASTM C109) [34]. After molding, the specimens were placed in plastic bags for 20-24h until demolding. The demolded mortar cubes were stored in saturated lime water until testing. At 7 and 28 days the compressive strength was assessed according to the ASTM C109 loading procedure [34].

4.4. Results and discussion

4.4.1. Calcination

Figure 4-1 displays the evolution of MS1 (figure 4-1A) and MS2 (Figure 4-1B) X-ray diffractograms as a function of the calcination temperature.

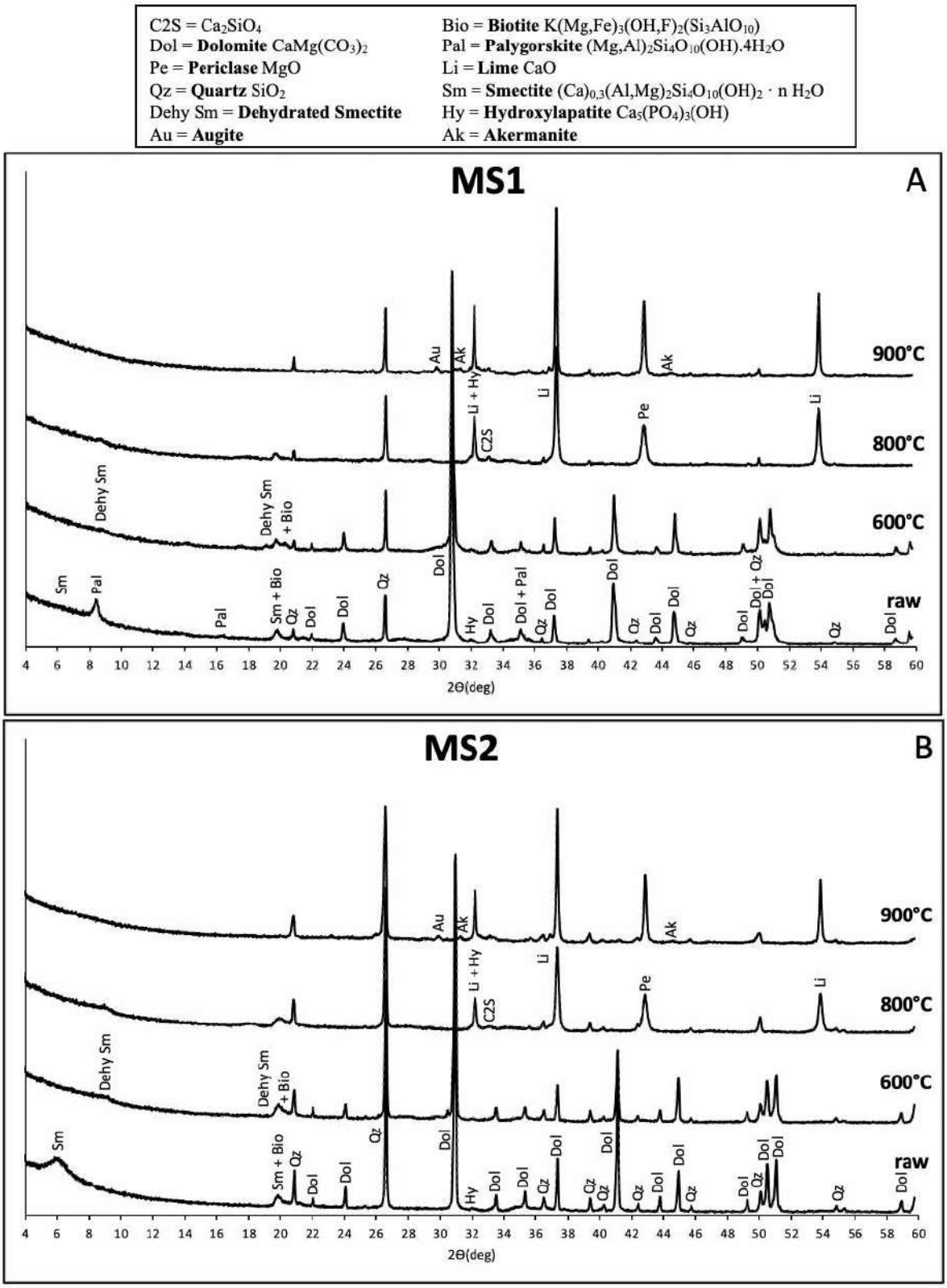

Figure 4-1 : Evolution of the X-ray diffractograms of MS1 (A) and MS2 (B) as a function of the calcination temperature.

At 600°C, for both MS1 and MS2 the 001 peak of smectite (Sm) is shifted from 6.2°(2θ) to 8.75°(2θ). This shift is explained by the dehydration of the smectite during the heat treatment (the removal of the interlayer water leads to a decrease in d001 basal spacing) [35,36]. Concerning MS1, the characteristic peaks of palygorskite disappears at 600°C, reflecting its loss of crystallinity.

At 800°C, for both MS1 and MS2 the dolomite ($CaMg(CO_3)_2$) decarbonates into lime (CaO) and periclase (MgO) and a peak associated with dicalcium silicate (C_2S) appears. However, the low intensity of the C_2S peaks (possibly due to low crystallinity of the phase) hinders the determination of the type of polymorph. The fact that this C_2S is formed at the same temperature as the lime supports the hypothesis that it results from a recombination phenomenon between the calcium from the decarbonated dolomite and the silicon from calcined clay phases [37].

At 900°C, for both MS1 and MS2 the characteristic peaks of dehydrated smectite and biotite disappear, indicating a complete loss of crystallinity of these two phyllosilicates. Quartz and hydroxylapatite are not sensitive to heat treatment since their peaks remain detectable up to 900°C. Finally, there are recrystallisation phenomena in the form of augite and akermanite at 900°C.

Based on these XRD results, 800°C seems to be a suitable calcination temperature as it allows the loss of crystallinity of the clay phases without causing recrystallisation phenomena (that could reduce the reactivity) for both MS1 and MS2.

Figure 4-2. displays the evolution of the ^{27}Al MAS NMR spectra of MS1 (Figure 4-2A) and MS2 (Figure 4-2B) as a function of the calcination temperature.

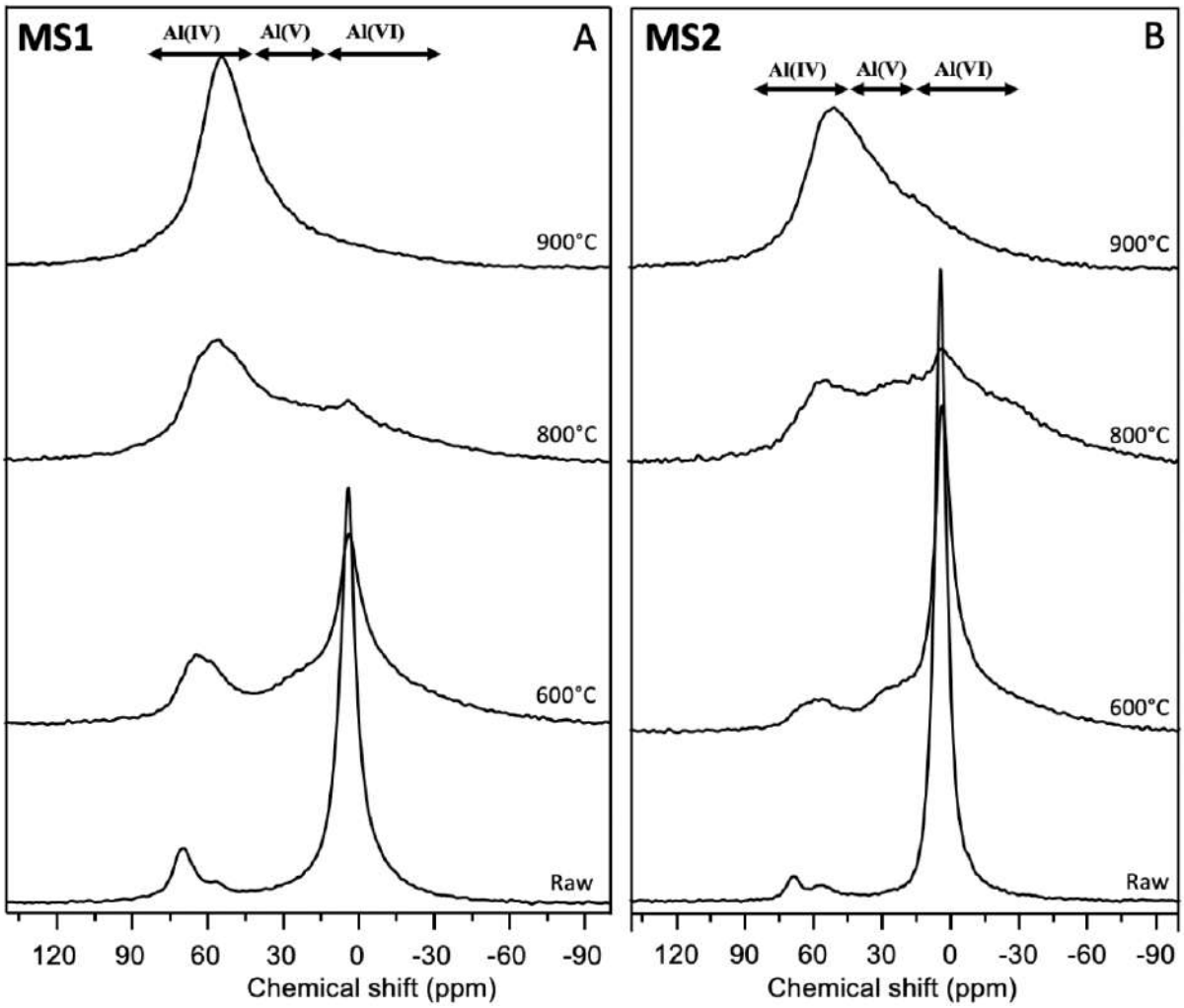

Figure 4-2: Evolution of the ^{27}Al MAS NMR spectra of MS1 (A) and MS2 (B) as function of the calcination temperature.

Both spectra of raw MS1 and MS2 exhibit two main resonances at 3 and 70 ppm which correspond to 6-fold and 4-fold aluminium, respectively [38]. The 6-fold aluminium resonance (3 ppm) can be associated with aluminium in palygorskite, smectite and biotite for MS1 and with aluminium in smectite and biotite for MS2 [39]. The 4-fold aluminium resonance (70 ppm) can be associated with the isomorphic substitution of silicon by aluminium atoms into silicate layers of palygorskite, smectite and biotite structures for MS1 and into smectite and biotite structures for MS2 [39].

A weak resonance at 57 ppm is detected in both MS1 and MS2 spectra, which corresponds to aluminium in $q^4(4Si)$ configuration [40] possibly associated with an additional phase occurring in low quantity and/or with low crystallinity, undetectable by XRD.

With the increasing calcination temperature, the 6-fold aluminium resonance intensity decreases while two new resonances appear at 27 and 59 ppm, which correspond to 5-fold and 4-fold aluminium, respectively [38]. During the calcination of MS1 and MS2, the calcination leads to a departure of hydroxyl groups from the clay phases (the dehydroxylation phenomenon). The octahedral (6-fold) aluminium atoms to which these hydroxyl groups were bonded have changed their coordination to 5- and 4-fold aluminium atoms. The pozzolanic activity of a calcined clay could be directly related to the relative proportion of 5- and 4-fold aluminium. These sites, in particular at the 5-fold one, are the starting point of the dissolution and the initiation of the pozzolanic reaction [15]. For both MS1 and MS2, the highest relative proportion of aluminium 5 and 4 (without recrystallization) is reached at 800°C, which suggests that this calcination temperature should allow the highest pozzolanic reactivity.

By comparing the evolution of MS1 and MS2 it is clear that the dehydroxylation occurs more easily in MS1 (which contains smectite and palygorskite) than in MS2 (which contains only smectite). At 800°C, a significantly higher relative proportion of 6-fold aluminium is still remaining in MS2 than in MS1. This difference can be explained by the occurrence of palygorskite in MS1, which was found to dehydroxylate more efficiently (at lower temperature) than smectite and biotite.

Figure 4-3 displays the evolution of the ^{29}Si MAS NMR spectra of MS1 (Figure 4-3A) and MS2 (Figure 4-3B) as a function of the calcination temperature.

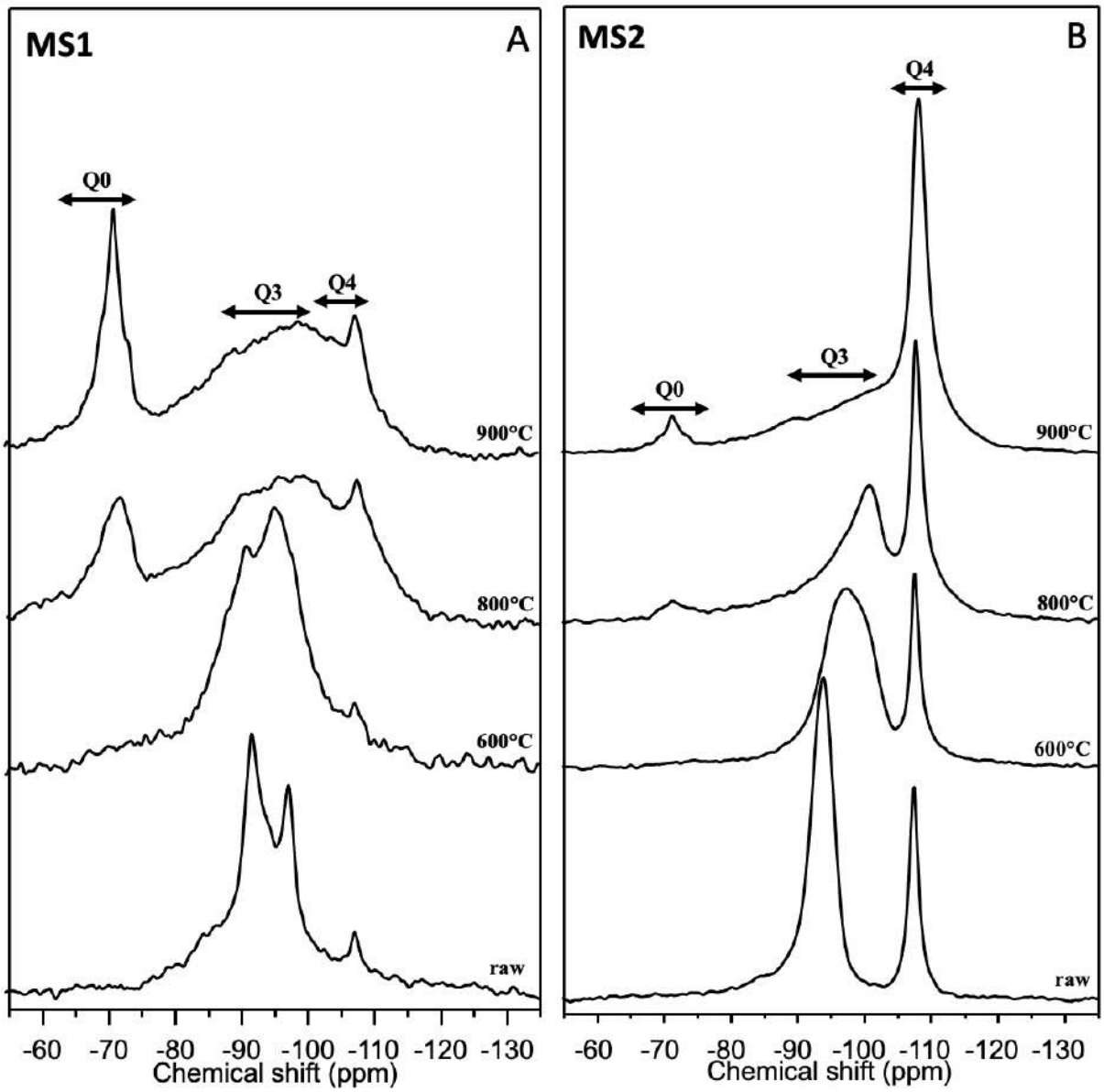

Figure 4-3: Evolution of the ^{29}Si MAS NMR spectra of MS1 (A) and MS2 (B) as function of the calcination temperature.

Both spectra of raw MS1 and MS2 exhibit a resonance at -108 ppm which correspond to Q^4 silicon atoms and which can be associated with silicon in the quartz structure [41]. For MS1, the total signal between -84 and -100 ppm is composed of Q^3 silicon atoms of smectite (-93 ppm) [12], Q^3(1Al) silicon atoms of biotite (-86 ppm) [42], Q^2 silicon atoms of palygorskite (-84 ppm) [43] and two Q^3 silicon sites of palygorskite at -98 and -92 ppm which correspond to SiO_4 at the edges and at the centre of the ribbons of tetrahedra, respectively [44]. For MS2, the total signal is only composed of Q^3 silicon atoms of smectite and Q^3(1Al) silicon atoms of biotite and smectite. For both MS1 and MS2, the increase of the calcination temperature leads

to a broadening of the resonances associated with the Q^3 of the clay phases. This broadening is explained by a distribution of the environments of the silicon atoms and indicates a structural loss of the clay phases upon calcination [45]. At 800°C a new resonance appears at -71 ppm in MS1 and MS2 spectra. This new resonance corresponds to Q^0 silicon atoms and can be associated with the silicon contained in the C_2S structure [46], in accordance with XRD results. With increasing the calcination temperature there is a low-frequency shift of the Q^3 resonances for MS2, which is explained by the condensation of the Q^3 into Q^4 silica [17].

By comparing MS1 and MS2 it is evident that the C_2S formation is facilitated in MS1 compared to MS2 (a higher relative proportion is observed). This could be explained by the occurrence of palygorskite as it is the only main difference between both materials. However, this difference of C_2S formation between MS1 and MS2 is not observable by XRD, meaning that the main part of this C_2S is amorphous.

Overall, the results of XRD and MAS NMR indicates that 800°C is probably the best calcination temperature for both MS1 and MS2. Moreover, MS1 seems to be more sensitive to the calcination, which leads to higher dehydroxylation of the clay phases and to higher relative amount of C_2S. The major difference between MS1 and MS2 being the occurrence of palygorskite in MS1, it seems clear that smectite and palygorskite have different responses to calcination.

4.4.2. Self-reactivity of calcined marlstones in water

The calcination study of MS1 and MS2 revealed the formation of different reactive phases such as lime, periclase and C_2S as well as the loss of crystallinity of the clay phases. MS1 and MS2 where thus hydrated in water in order to study their reactivity, the contribution of each phases, their evolution and the possible presence of synergies.

Figure 4-4 displays the evolution of the X-ray diffractograms of MS1 (figure 4-4A) and MS2 (figure 4-4B) calcined at 800°C and hydrated in water for 7, 14, 28 and 180 days.

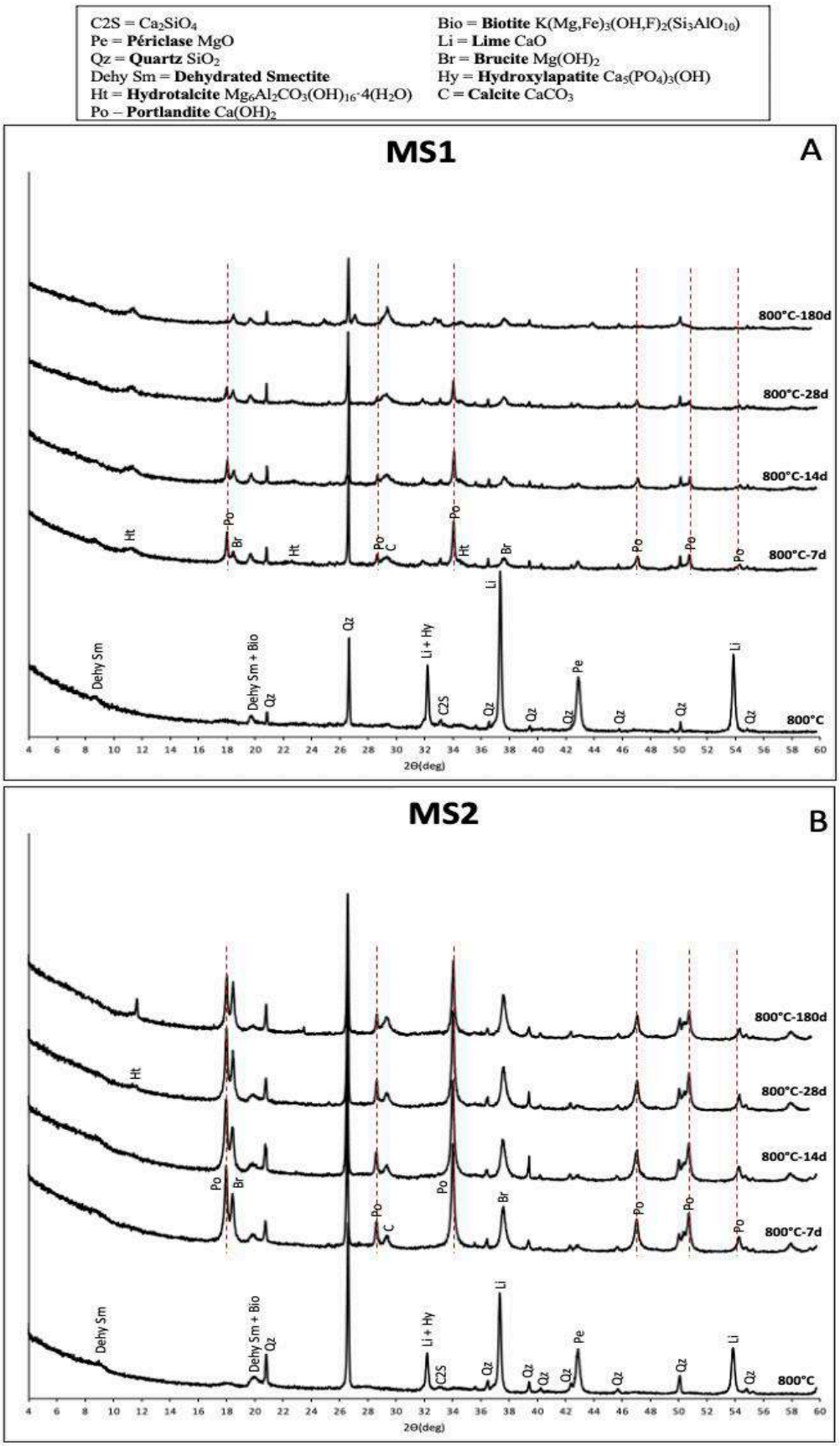

Figure 4-4: Evolution of the X-ray diffractograms of MS1 (A) and MS2 (B) calcined at 800°C and hydrated (w/b = 0.8) during 7, 14, 28 and 180 days.

After 7 days of hydration, for both MS1 and MS2, diffraction peaks characteristic of portlandite, calcite, hydrotalcite and brucite appear on the diffractograms. The formation of portlandite comes from the hydration of lime and calcite comes from its carbonation. The magnesium from the periclase is incorporated into two phases: brucite and hydrotalcite.

The formation of brucite can be problematic in cements. The hydration of periclase into brucite is a phenomenon that has relatively long kinetic compared to the hardening kinetic of cement. This post-hardening swelling can lead to cracking problems and therefore a loss of mechanical performance if there is not enough space available in the matrix [47]. Studies are currently underway to determine whether neoformed brucite leads to cracking in this system. However, there is no post-hardening swelling phenomenon associated with hydrotalcite (the second magnesian phase neoformed in our system) formation in the existing literature and the possible existence of synergies with the cement phases could enhance the formation of hydrotalcite instead of brucite in calcined marlstone-cement system.

The amount of neoformed brucite and portlandite is higher for MS2 than for MS1 (larger area under the peaks), therefore it is difficult to compare the evolution of these two phases between MS1 and MS2. With the increasing hydration time, the intensity of the peaks characteristic of portlandite decrease for MS1 and MS2. However, after 180 days of hydration the portlandite diffraction peaks are no longer detectable in MS1. This total consumption of portlandite in MS1 could be a first indication of a possible stronger pozzolanic reactivity compared to MS2. However, this apparent consumption of portlandite may also be due to its carbonation into calcite as we observe an increase in the intensity of the peak associated with calcite with increasing hydration time.

Figure 4-5 shows the evolution of the ^{29}Si MAS NMR spectra of MS1 (figure 4-5A) and MS2 (figure 4-5B) calcined at 800°C and hydrated in water during 7, 14, 28 and 180 days.

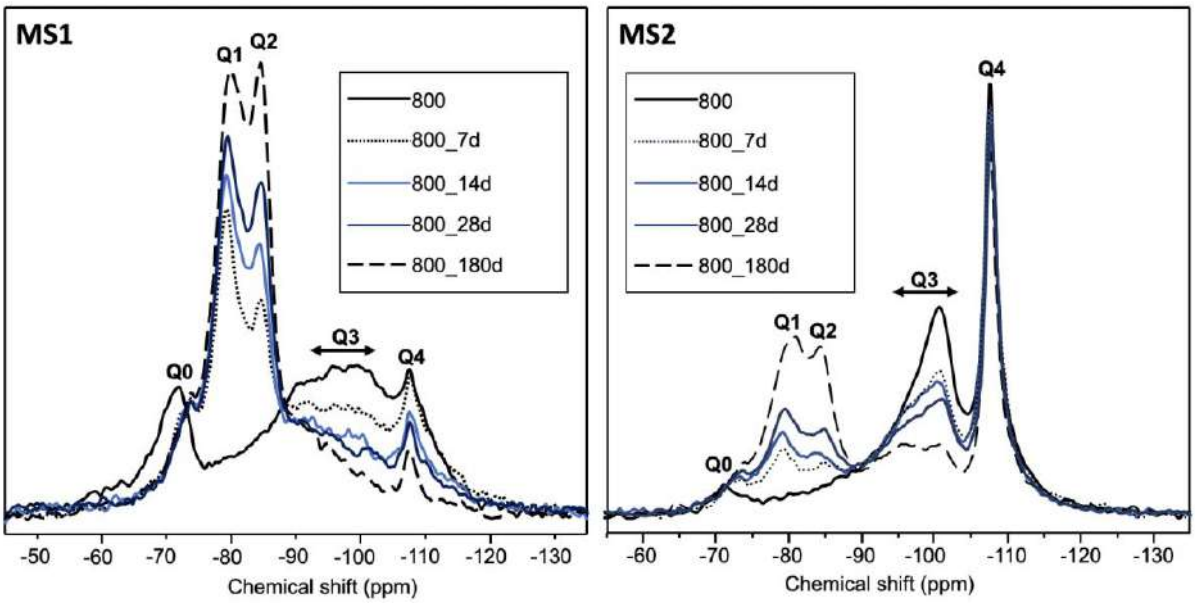

Figure 4-5: Evolution of the ^{29}Si MAS NMR spectra of MS1 (A) and MS2 (B) calcined at 800°C and hydrated (w/b = 0.8) during 7, 14, 28 and 180 days.

After 7 days of hydration for both MS1 and MS2, a decrease is observed for the intensity of the broad Q^3 resonances previously associated with the calcined clay phases. This decrease is correlated with the appearance of two new resonances at -78 and -85 ppm which corresponds to Q^1 and Q^2 silicon atoms, respectively [48]. Q^1 silicon atoms can be associated with pairs of linked silicate tetrahedral (dimers) and/or terminal tetrahedral silicate groups of C-S-H. Q^2 silicon atoms can be associated with C-S-H tetrahedral silicate groups in bridging (Q^2-B) and/or intermediates (Q^2-P) configurations [49].

The -71 ppm resonance corresponding to Q^0 atoms (associated previously with C_2S neoformed during calcination) decreases considerably after 7 days of hydration and leaves a resonance at -73 ppm for both MS1 and MS2. This -73 ppm resonance can either be associated with the Q^1 atoms of akermanite/gehlenite and/or Q^0 of non-reactive C_2S. The fact that the C_2S XRD signal remains detectable even after 180 days of hydration supports the hypothesis that some of the C_2S is non-reactive (the crystallised one). However, during the calcination of MS1 and MS2, the formation of akermanite was observed at 900°C (figure 4-1). The -73 ppm signal can thus also be associated with akermanite which is not yet crystallised enough to be detectable by XRD at 800°C. Finally, several studies have highlighted the formation of gehlenite during

the calcination of marlstones [50,51] and this signal at -73 ppm could therefore be associated with this phase.

After 14 days of hydration, for both MS1 and MS2, the intensity of the Q^3 calcined clay phases resonances continues to decrease while the intensity of the Q^1 + Q^2 resonances associated with C-S-H increases. A new resonance at -81 ppm appears after 14 days for MS1 and 28 days for MS2, which corresponds to silicon in $Q^{2(}$1Al) configuration and confirms the incorporation of aluminium into the C-A-S-H structure, which is characteristic of the pozzolanic reaction of calcined clays. The trend will continue up to 180 days for MS1 and MS2, validating the intrinsic pozzolanic reactivity of these two calcined materials.

The comparison of the series of spectra indicates that the formation of C-A-S-H and the consumption of calcined clay phases is significantly higher for MS1 than MS2. Spectral integration quantification was thus carried out to precisely compare the difference between MS1 and MS2 in terms of the consumption of calcined clay phases and the formation of C-A-S-H.

Figure 4-6 displays the evolution of the relative proportions (from the perspective of silicon content) of the Qn (C-A-S-H) and the Q^3 (calcined clay phases) for hydrated 800°C-MS1 (figure 4-6A) and 800°C-MS2 (figure 4-6B). Details of this quantification by spectral integration are given in the supporting information. The Q^4 signal associated with quartz is not quantitative and the Q^0-Q^1 signal associated with C_2S and/or akermanite/gehlenite is constant from 7 days and onward. Therefore, figure 5-6. includes only the evolution of the Q^3 (and Q^3-Q^4 for MS2) of the calcined clay phases and Q^n of the C-A-S-H.

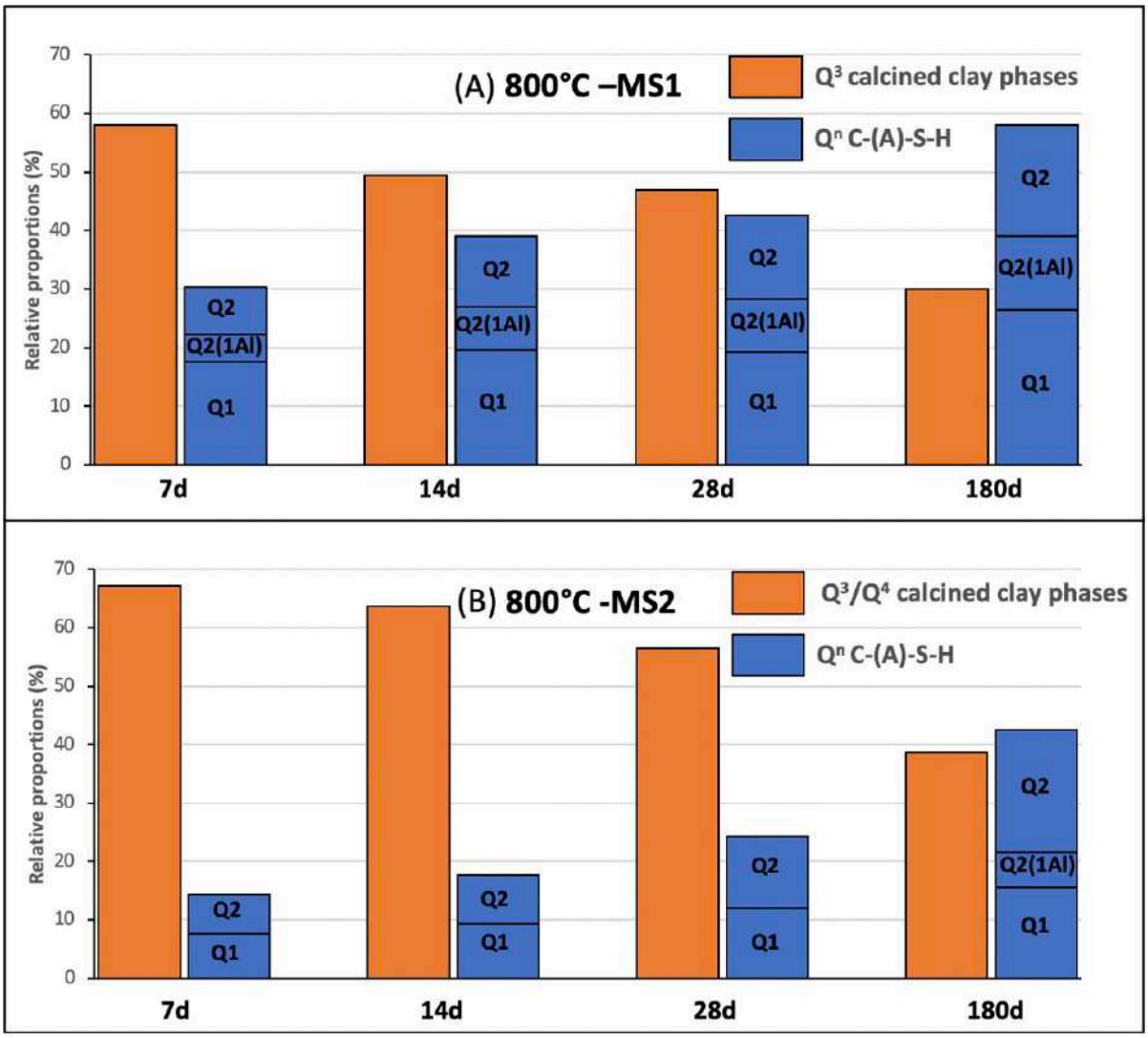

Figure 4-6: Relative proportions of silicon-containing phases of MS1 (A) and MS2 (B) calcined at 800°C (from the perspective of silicon content) as function of the hydration time obtained from ^{29}Si MAS NMR spectra.

For MS1, after only 7 days of hydration, the relative proportion of silicon in Q^n configuration associated with C-A-S-H is already 30%. From 7 to 180 days of hydration, the relative proportion of silicon in Q^3 configuration associated with the calcined clay phases decreases from 58% to 30%. In parallel, the relative proportion of Q^1, $Q^2(1Al)$ and Q^2 silicon associated with the C-(A)-S-H increases from 30% to 58%.

For MS2, after 7 days of hydration, the relative proportion of silicon in Q^n configuration associated with C-A-S-H is only 14%, which is much lower than for MS1 (30%). From 7 to 180 days of hydration the relative proportion of silicon in Q^3-Q^4 configuration associated with the

calcined clay phases decreases from 67% to 39%. In parallel, the relative proportion Q^1, Q^2(1Al) and Q^2 silicon associated with the C-(A)-S-H increases from 14% to 43%. The consumption of the calcined clay phases, associated with the formation of C-A-S-H and the consumption of portlandite during hydration confirms the pozzolanic reactivity of MS1 and MS2 calcined at 800°C. However, this pozzolanic reactivity is more important for MS1 (which contains palygorskite) than for MS2 ($\frac{Q^n\ (CASH)}{Q^3}$ = 1,93 for MS1 and $\frac{Q^n\ (CASH)}{Q^3+Q^4}$ = 1,13 for MS2 after 180 days of hydration). Compressive strengths were measured on mortars incorporating the two marlstones calcined at 800°C to confirm their different reactivity.

4.4.3. Calcined marlstone-cement blends

Figure 4-7 displays the compressive strength of M-ref, M-MS1 and M-MS2 after 7 and 28d of hydration. The error bars indicate the standard deviation for each set of 3 compression measurements.

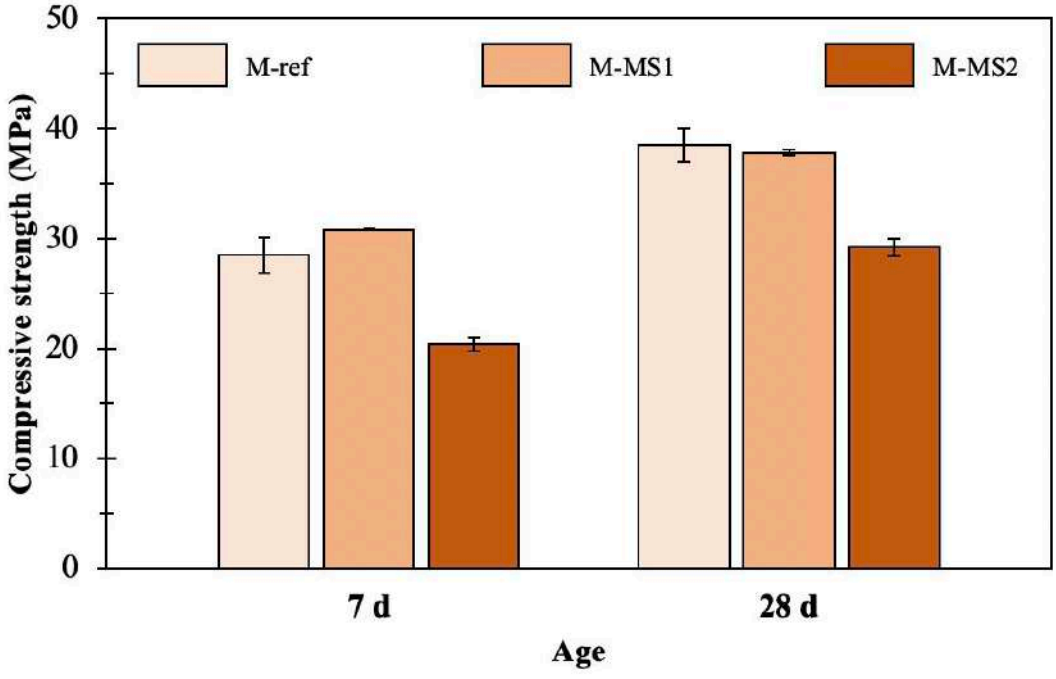

Figure 4-7: Compressive strengths at 7 and 28 days of M-ref, M-MS1 and M-MS2.

After 7 days M-MS1 shows a compressive strength slightly higher to that of the reference (M-ref) whereas M-MS2 shows a significant lower strength. At 28 days the trend continues for M-

MS1 which shows an equivalent compressive strength to that of the reference whereas M-MS2 still shows significant lower compressive strength.

The better mechanical performance of M-MS1 confirms the previous results assessed by ^{27}Al and ^{29}Si MAS NMR. The occurrence of palygorskite in MS1 leads to a higher degree of dehydroxylation at 800°C in comparison to MS2 (figure 4-2). This enhances the pozzolanic reactivity of 800°C-MS1 in comparison to 800°C-MS2 (figure 4-6) and results in higher compressive strengths at 7 and 28 days (figure 4-7). These results suggest that the palygorskite has a higher pozzolanic activity after calcination at 800°C than smectite. To a lesser extent, the higher mechanical performance of M-MS1 compared to M-MS2 could also be attributed to the greater amount of C_2S neoformed during the calcination (facilitated by the occurrence of palygorskite).

4.5. Conclusion

This paper compares the use of two calcined marlstones as SCMs in terms of calcination, self-reactivity in water and mechanical performance in cementitious blends. The two marlstones differ mainly by the presence of palygorskite (MS1) or not (MS2). Based on the results presented, the following conclusions can be drawn:

1. The calcination of MS1 and MS2 leads to the dehydroxylation of the clay phases associated with the formation of lime, periclase and C_2S. A calcination temperature of 800°C resulted in the highest expected reactivity for both MS1 and MS2. The degree of dehydroxylation and the amount of C_2S neoformed are higher for MS1 than MS2, which was attributed to the occurence of palygorskite in MS1.

2. Both MS1 and MS2 calcined at 800°C exhibit significant self-reactivity in water, mainly pozzolanic. The comparative study shows that MS1 calcined at 800°C exhibits a higher self-reactivity than MS2 confirming the results of the calcination analysis.

3. The comparative study shows that mortars made from cement blended with 20% of MS1 calcined at 800°C have much better compressive strength than those made with MS2 after 7

and 28 days. Once again, this confirms the results of the calcination (higher dehydroxylation of MS1 than MS2) and self-reactivity in water analysis (higher reactivity of 800°C-MS1 than 800°C-MS2).

4. Calcination, self-reactivity in water and compressive strength results indicate that calcined palygorskite-bearing marlstones have higher potential use as SCMs in cementitious systems than calcined smectite-bearing marlstones. These results open up new applications for this type of marlstones and suggest that palygorskite is a clay that could be used as SCM once calcined.

4.6. References

[1] D.N. Huntzinger, T.D. Eatmon, A life-cycle assessment of Portland cement manufacturing: comparing the traditional process with alternative technologies, Journal of Cleaner Production. 17 (2009) 668–675. https://doi.org/10.1016/j.jclepro.2008.04.007.

[2] K.L. Scrivener, V.M. John, E.M. Gartner, Eco-efficient cements: Potential economically viable solutions for a low-CO2 cement-based materials industry, Cement and Concrete Research. 114 (2018) 2–26. https://doi.org/10.1016/j.cemconres.2018.03.015.

[3] J.I. Escalante, L.Y. Gómez, K.K. Johal, G. Mendoza, H. Mancha, J. Méndez, Reactivity of blast-furnace slag in Portland cement blends hydrated under different conditions, Cement and Concrete Research. 31 (2001) 1403–1409. https://doi.org/10.1016/S0008-8846(01)00587-7.

[4] H. Yazıcı, M.Y. Yardımcı, H. Yiğiter, S. Aydın, S. Türkel, Mechanical properties of reactive powder concrete containing high volumes of ground granulated blast furnace slag, Cement and Concrete Composites. 32 (2010) 639–648. https://doi.org/10.1016/j.cemconcomp.2010.07.005.

[5] E. Sakai, S. Miyahara, S. Ohsawa, S.-H. Lee, M. Daimon, Hydration of fly ash cement, Cement and Concrete Research. 35 (2005) 1135–1140. https://doi.org/10.1016/j.cemconres.2004.09.008.

[6] Z.T. Yao, X.S. Ji, P.K. Sarker, J.H. Tang, L.Q. Ge, M.S. Xia, Y.Q. Xi, A comprehensive review on the applications of coal fly ash, Earth-Science Reviews. 141 (2015) 105–121. https://doi.org/10.1016/j.earscirev.2014.11.016.

[7] X. Hu, C. Shi, Z. Shi, L. Zhang, Compressive strength, pore structure and chloride transport properties of alkali-activated slag/fly ash mortars, Cement and Concrete Composites. 104 (2019) 103392. https://doi.org/10.1016/j.cemconcomp.2019.103392.

[8] A. Alujas, R. Fernández, R. Quintana, K.L. Scrivener, F. Martirena, Pozzolanic reactivity of low grade kaolinitic clays: Influence of calcination temperature and impact of calcination

products on OPC hydration, Applied Clay Science. 108 (2015) 94–101. https://doi.org/10.1016/j.clay.2015.01.028.

[9] R.S. Almenares, L.M. Vizcaíno, S. Damas, A. Mathieu, A. Alujas, F. Martirena, Industrial calcination of kaolinitic clays to make reactive pozzolans, Case Studies in Construction Materials. 6 (2017) 225–232. https://doi.org/10.1016/j.cscm.2017.03.005.

[10] H. El-Diadamony, A.A. Amer, T.M. Sokkary, S. El-Hoseny, Hydration and characteristics of metakaolin pozzolanic cement pastes, HBRC Journal. 14 (2018) 150–158. https://doi.org/10.1016/j.hbrcj.2015.05.005.

[11] D. Zhao, R. Khoshnazar, Microstructure of cement paste incorporating high volume of low-grade metakaolin, Cement and Concrete Composites. 106 (2020) 103453. https://doi.org/10.1016/j.cemconcomp.2019.103453.

[12] I.W. Brown, K.J.D. MacKenzie, R.H. Meinhold, The thermal reactions of montmorillonite studied by high-resolution solide-state 29Si and 27Al NMR, (1987).

[13] N. Garg, J. Skibsted, Thermal Activation of a Pure Montmorillonite Clay and Its Reactivity in Cementitious Systems, The Journal of Physical Chemistry C. 118 (2014) 11464–11477. https://doi.org/10.1021/jp502529d.

[14] R. Kaminskas, R. Kubiliute, B. Prialgauskaite, Smectite clay waste as an additive for Portland cement, Cement and Concrete Composites. 113 (2020) 103710. https://doi.org/10.1016/j.cemconcomp.2020.103710.

[15] R. Fernandez, F. Martirena, K.L. Scrivener, The origin of the pozzolanic activity of calcined clay minerals: A comparison between kaolinite, illite and montmorillonite, Cement and Concrete Research. 41 (2011) 113–122. https://doi.org/10.1016/j.cemconres.2010.09.013.

[16] S.C. Taylor-Lange, F. Rajabali, N.A. Holsomback, K. Riding, M.C.G. Juenger, The effect of zinc oxide additions on the performance of calcined sodium montmorillonite and illite shale supplementary cementitious materials, Cement and Concrete Composites. 53 (2014) 127–135. https://doi.org/10.1016/j.cemconcomp.2014.06.008.

[17] N. Garg, J. Skibsted, Pozzolanic reactivity of a calcined interstratified illite/smectite (70/30) clay, Cement and Concrete Research. 79 (2016) 101–111. https://doi.org/10.1016/j.cemconres.2015.08.006.

[18] Y. Cancio Díaz, S. Sánchez Berriel, U. Heierli, A.R. Favier, I.R. Sánchez Machado, K.L. Scrivener, J.F. Martirena Hernández, G. Habert, Limestone calcined clay cement as a low-carbon solution to meet expanding cement demand in emerging economies, Development Engineering. 2 (2017) 82–91. https://doi.org/10.1016/j.deveng.2017.06.001.

[19] K. Scrivener, F. Martirena, S. Bishnoi, S. Maity, Calcined clay limestone cements (LC3), Cement and Concrete Research. 114 (2018) 49–56. https://doi.org/10.1016/j.cemconres.2017.08.017.

[20] C. He, E. Makovicky, B. Osbæck, Thermal treatment and pozzolanic activity of sepiolite, Applied Clay Science. 10 (1996) 337–349. https://doi.org/10.1016/0169-1317(95)00035-6.

[21] C. He, B. Osbaeck, E. Makovicky, Pozzolanic reactions of six principal clay minerals: Activation, reactivity assessments and technological effects, Cement and Concrete Research. 25 (1995) 1691–1702. https://doi.org/10.1016/0008-8846(95)00165-4.

[22] H. Justnes, T. Østnor, K. De Weerdt, H. Vikan, CALCINED MARL AND CLAY AS MINERAL ADDITION FOR MORE SUSTAINABLE CONCRETE STRUCTURES CALCINED MARL AND CLAY AS MINERAL ADDITION FOR MORE SUSTAINABLE CONCRETE STRUCTURES, (2021).

[23] T. Danner, G. Norden, H. Justnes, Characterisation of calcined raw clays suitable as supplementary cementitious materials, Applied Clay Science. 162 (2018) 391–402. https://doi.org/10.1016/j.clay.2018.06.030.

[24] F. Bullerjahn, M. Zajac, J. Pekarkova, D. Nied, Novel SCM produced by the co-calcination of aluminosilicates with dolomite, Cement and Concrete Research. 134 (2020) 106083. https://doi.org/10.1016/j.cemconres.2020.106083.

[25] S. Mohammed, G. Elhem, B. Mekki, Valorization of pozzolanicity of Algerian clay: Optimization of the heat treatment and mechanical characteristics of the involved cement mortars, Applied Clay Science. 132–133 (2016) 711–721. https://doi.org/10.1016/j.clay.2016.08.027.

[26] T. Danner, G. Norden, H. Justnes, Calcareous smectite clay as a pozzolanic alternative to kaolin, European Journal of Environmental and Civil Engineering. 25 (2021) 1647–1664. https://doi.org/10.1080/19648189.2019.1590741.

[27] A. Bahhou, Y. Taha, Y.E. Khessaimi, R. Hakkou, A. Tagnit-Hamou, M. Benzaazoua, Using Calcined Marls as Non-Common Supplementary Cementitious Materials—A Critical Review, Minerals. 11 (2021) 517. https://doi.org/10.3390/min11050517.

[28] V. Poussardin, M. Paris, A. Tagnit-Hamou, D. Deneele, Potential for calcination of a palygorskite-bearing argillaceous carbonate, Applied Clay Science. 198 (2020) 105846. https://doi.org/10.1016/j.clay.2020.105846.

[29] V. Poussardin, M. Paris, W. Wilson, A. Tagnit-Hamou, D. Deneele, Self-reactivity of a calcined palygorskite-bearing marlstone for potential use as supplementary cementitious material, Applied Clay Science. 216 (2022) 106372. https://doi.org/10.1016/j.clay.2021.106372.

[30] E. Ferraz, S. Andrejkovičová, W. Hajjaji, A. Velosa, A. Santos Silva, F. Rocha, Pozzolanic activity of metakaolins by the French standard of the modified Chapelle test: A direct methology, Acta Geodynamica et Geomaterialia. 12 (2015) 289–298. https://doi.org/10.13168/AGG.2015.0026.

[31] F. Avet, R. Snellings, A. Alujas Diaz, M. Ben Haha, K. Scrivener, Development of a new rapid, relevant and reliable (R3) test method to evaluate the pozzolanic reactivity of calcined kaolinitic clays, Cement and Concrete Research. 85 (2016) 1–11. https://doi.org/10.1016/j.cemconres.2016.02.015.

[32] N. Doebelin, R. Kleeberg, *Profex* : a graphical user interface for the Rietveld refinement program *BGMN*, Journal of Applied Crystallography. 48 (2015) 1573–1580. https://doi.org/10.1107/S1600576715014685.

[33] D. Massiot, F. Fayon, M. Capron, I. King, S. Le Calvé, B. Alonso, J.-O. Durand, B. Bujoli, Z. Gan, G. Hoatson, Modelling one- and two-dimensional solid-state NMR spectra: Modelling

1D and 2D solid-state NMR spectra, Magn. Reson. Chem. 40 (2002) 70–76. https://doi.org/10.1002/mrc.984.

[34] C01 Committee, Test Method for Compressive Strength of Hydraulic Cement Mortars (Using 2-in. or [50-mm] Cube Specimens), ASTM International, n.d. https://doi.org/10.1520/C0109_C0109M-16A.

[35] P. Bala, B.K. Samantaray, S.K. Srivastava, Dehydration transformation in Ca-montmorillonite, Bulletin of Materials Science. 23 (2000) 61–67. https://doi.org/10.1007/BF02708614.

[36] S. Morodome, K. Kawamura, Swelling Behavior of Na- and Ca-Montmorillonite up to 150°C by in situ X-ray Diffraction Experiments, Clays and Clay Minerals. 57 (2009) 150–160. https://doi.org/10.1346/CCMN.2009.0570202.

[37] J. Xie, T. Chen, B. Xing, H. Liu, Q. Xie, H. Li, Y. Wu, The thermochemical activity of dolomite occurred in dolomite–palygorskite, Applied Clay Science. 119 (2016) 42–48. https://doi.org/10.1016/j.clay.2015.07.014.

[38] A.Á.B. Maia, R.S. Angélica, R. de Freitas Neves, H. Pöllmann, C. Straub, K. Saalwächter, Use of 29Si and 27Al MAS NMR to study thermal activation of kaolinites from Brazilian Amazon kaolin wastes, Applied Clay Science. 87 (2014) 189–196. https://doi.org/10.1016/j.clay.2013.10.028.

[39] J. Sanz, J.M. Serratosa, Silicon-29 and aluminum-27 high-resolution MAS-NMR spectra of phyllosilicates, Journal of the American Chemical Society. 106 (1984) 4790–4793. https://doi.org/10.1021/ja00329a024.

[40] D. Muller, W. Gessner, A. Samoson, E. Lippmaa, Solid-state Aluminium-27 Nuclear Magnetic Resonance Chemical Shift and Quadrupole Coupling Data for Condensed AIO4, Tetrahedra, J. Chem. Soc. Dalton Trans. (1986) 5.

[41] E. Lippmaa, M. Maegi, A. Samoson, G. Engelhardt, A.R. Grimmer, Structural studies of silicates by solid-state high-resolution silicon-29 NMR, Journal of the American Chemical Society. 102 (1980) 4889–4893. https://doi.org/10.1021/ja00535a008.

[42] K.J.D. Mackenzie, I.W.M. Brown, C.M. Cardile, R.H. Meinhold, The thermal reactions of muscovite studied by high-resolution solid-state 29-Si and 27-Al NMR, Journal of Materials Science. 22 (1987) 2645–2654. https://doi.org/10.1007/BF01082158.

[43] W. Kuang, G.A. Facey, C. Detellier, Dehydration and rehydration of palygorskite and the influence of water on the nanopores, Clays Clay Miner. 52 (2004) 635–642. https://doi.org/10.1346/CCMN.2004.0520509.

[44] P.F. Barron, R.L. Frost, N. Qlil, Solid state 29Si NMR examination of the 2:1 ribbon magnesium silicates, sepiolite and palygorskite, American Mineralogist. 70 (1985) 758–766.

[45] K.J.D. MacKenzie, M.E. Smith, Multinuclear Solid-State NMR of Inorganic Materials, Pergamon Materials Series, n.d.

[46] J. Skibsted, H.J. Jakobsen, C. Hall, Quantification of calcium silicate phases in Portland cements by 29Si MAS NMR spectroscopy, Journal of the Chemical Society, Faraday Transactions. 91 (1995) 4423. https://doi.org/10.1039/ft9959104423.

[47] E.A. Cherney, R.D. Hooton, Cement Growth Failure Mechanism in Porcelain Suspension Insulators, IEEE Transactions on Power Delivery. 2 (1987) 249–255. https://doi.org/10.1109/TPWRD.1987.4308096.

[48] M. Magi, E. Lippmaa, A. Samoson, G. Engelhardt, A.R. Grimmer, Solid-state high-resolution silicon-29 chemical shifts in silicates, The Journal of Physical Chemistry. 88 (1984) 1518–1522. https://doi.org/10.1021/j150652a015.

[49] M.D. Andersen, H.J. Jakobsen, J. Skibsted, Characterization of white Portland cement hydration and the C-S-H structure in the presence of sodium aluminate by 27Al and 29Si MAS NMR spectroscopy, Cement and Concrete Research. 34 (2004) 857–868. https://doi.org/10.1016/j.cemconres.2003.10.009.

[50] S. Shoval, Mineralogical changes upon heating calcitic and dolomitic marl rocks, Thermochimica Acta. 135 (1988) 243–252. https://doi.org/10.1016/0040-6031(88)87393-3.

[51] D.C. Hughes, D. Jaglin, R. Kozłowski, D. Mucha, Roman cements — Belite cements calcined at low temperature, Cement and Concrete Research. 39 (2009) 77–89. https://doi.org/10.1016/j.cemconres.2008.11.010.

4.7. Bilan scientifique du chapitre 4

Cette dernière partie dresse un bilan scientifique de ce chapitre 4 qui s'intéresse à l'utilisation de deux marnes calcinées comme ajouts cimentaires. Les deux marnes ont une composition minéralogique similaire (dolomite + smectite). La différence majeure est la présence de palygorskite en plus de la smectite dans l'une d'entre elle. La première marne contient 17% de palygorskite et 16% de smectite comme phases argileuses alors que l'autre contient 27% de smectite uniquement. L'étude comparative de la calcination, de l'auto-réactivité dans l'eau et des performances mécaniques en système cimentaire a permis de mettre en avant l'influence positive de la présence de palygorskite sur la réactivité totale du matériau.

Il a été démontré que les deux marnes étudiées ne présentent pas la même auto-réactivité dans l'eau ni la même réactivité en système cimentaire après calcination à 800°C. La présence de palygorskite dans l'une des deux marnes entraine une augmentation importante de sa réactivité pouzzolanique totale et *in fine* des performances mécaniques en système cimentaire. Ces résultats permettent de faire deux constats différents, le premier est que ce type de marne dolomitique contenant de la palygorskite présente un intérêt de valorisation comme ajout cimentaire dans des ciments composés après calcination. Le second est que la

palygorskite est une argile possédant une importante réactivité pouzzolanique après calcination, ce qui en fait une argile d'intérêt pour une utilisation comme ajout cimentaire.

Chapitre 5 – Utilisation de palygorskites calcinées comme ajouts cimentaires

5.1. Avant-propos

Note : Ce chapitre est basé sur un article soumis dans un journal international à comité de lecture.

Titre de l'article : **Calcined palygorskites as supplementary cementitious materials**

Victor Poussardin, Valentin Roux, William Wilson, Michael Paris, Arezki Tagnit-Hamou, Dimitri Deneele

Soumis à : Materials Today : Proceedings

Contribution à la thèse

Le chapitre 4 a permis de démontrer que la palygorskite est une argile qui présente une importante réactivité pouzzolanique après calcination. Cependant ces résultats se basent sur l'étude d'un échantillon naturel complexe puisqu'il s'agit d'une marne dont la teneur en palygorskite est limitée (17%) mais qui suffit à présenter des propriétés supérieures à la même marne ne contenant pas de palygorskite.. Pour la poursuite de l'expérimentation nous avons donc décidé de nous procurer deux argiles contenant une forte proportion de palygorskite afin d'évaluer la réactivité d'échantillons avec diverses teneurs en palygorskite. Le premier objectif est de comparer les résultats obtenus avec ces échantillons plus riches en palygorskite avec ceux décrits dans le chapitre 5. Le second objectif est d'évaluer comment la teneur en palygorskite influence la réactivité des échantillons après calcination.

Résumé en français

La diminution de l'empreinte environnementale du ciment est une nécessité absolue pour respecter les engagements de la COP26 et notamment la limitation du réchauffement climatique à +1,5°C par rapport au niveau préindustriel. Dans ce contexte, un intérêt particulier s'est développé ces dernières années pour l'utilisation d'argiles calcinées comme ajouts cimentaires. En effet, en raison de leur grande réactivité, de leurs importantes réserves et de leur répartition homogène à la surface de la terre, les argiles calcinées représentent une alternative viable aux ajouts cimentaires plus classiques déjà utilisés de nos jours. Les minéraux argileux sont très variables et il en existe un grand nombre, chacun ayant ses propres caractéristiques. Par conséquent, ils n'ont pas tous un potentiel de calcination et d'utilisation en tant qu'ajout cimentaire. Cet article étudie l'utilisation de la palygorskite (une argile qui est actuellement peu étudiée) comme ajout cimentaire. Pour ce faire, deux palygorskites commerciales ont été sélectionnées et leur calcination étudiée par diffraction des rayons X et par des tests d'activité pouzzolanique. Des ciments composés incorporant 20% de chacune des palygorskites calcinées ont ensuite été préparés et les performances mécaniques et la résistivité sur mortiers ont été mesurées. Les résultats ont montré que la température optimale de calcination est de 800°C (permettant une amorphisation complète de la fraction argileuse et la plus grande réactivité pouzzolanique) pour les deux argiles. Les mortiers confectionnés à partir de ciment incorporant 20% de palygorskite calcinée à 800°C ont permis une augmentation significative de la résistance à la compression et de la résistivité par rapport à la référence (100% ciment). En outre, c'est l'échantillon commercial avec le pourcentage le plus élevé de palygorskite qui présente la réactivité pouzzolanique et la résistance à la compression en système cimentaire la plus élevées, confirmant que la palygorskite est un minéral argileux avec un potentiel élevé pour une utilisation en tant qu'ajout cimentaire.

Résumé en anglais

Reducing the environmental footprint of cement is an absolute necessity in order to meet the commitments of COP26 and in particular to limit global warming to +1.5°C compared to the pre-industrial level. In this context, particular interest has developed in recent years in the use of calcined clays as supplementary cementiiousg materials (SCMs). Indeed, due to their high reactivity, large reserves and homogeneous distribution on the earth's surface, calcined clays represent a viable alternative to the SCMs already used nowadays. Clay minerals are highly variable and there are a large number of them, each with its own characteristics. As a result, not all of them have potential for calcination and use as SCM. This paper investigates the use of palygorskite (a clay that is currently poorly studied) as a supplementary cementitious material. For this purpose, two commercial palygorskites were selected and their calcination studied by X-ray diffraction and pozzolanic activity tests. Blended cements incorporating 20% of each of the calcined palygorskites were then prepared and the mechanical performance and resistivity of the mortars measured. The results showed that the optimum calcination temperature is 800°C (allowing complete amorphisation of the clay fraction and the highest pozzolanic reactivity) for both clays. Mortars made from cement blended with 20% de 800°C calcined palygorskite allowed a significant increase of compressive strength and electrical resistivity compare to the reference (100% OPC). Furthermore, it is the commercial sample with the highest percentage of palygorskite that exhibits the higher pozzolanic reactivity and mechanical performance in cementitious system, confirming that palygorskite is a clay mineral with a high potential for a use a SCM.

5.2. Introduction

The extensive urbanization that comes with economic development results in a significant increase in the cement demand [1]. Since 1955, cement demand has increased tenfold [2], resulting in significant CO_2 emissions. It is estimated today that the cement industry is responsible for about 8% of global CO_2 emissions [3,4], which represents about 2.7 billion tons of CO_2 emitted each year [5]. In this context, the cement industry is working to reduce its carbon footprint by modernizing existing plants to make them more efficient and by developing new technologies [6]. These include the substitution of fossil fuels in cement kilns by alternative fuels [7], CO_2 capture and storage systems (CCS) [8], and the development of alternative low-carbon clinkers (e.g. with high belite content [9]). However, all these innovations represent a significant financial cost and/or a long time of development [6]. The reduction of clinker content (by substituting it with other compounds), on the other hand, is a technology that can be implemented today and represents a low financial cost compared to others [6].

In this context, new types of cements incorporating blast furnace slag [10] or fly ash [11] have been developed. Unfortunately, the available quantities of blast furnace slag are not large enough to allow a significant reduction of CO_2 emissions and the energy transition rightly limits the available resources of fly ash from coal combustion [12]. The use of calcined clays as SCMs is a technology that is growing in interest. In particular because the available reserves of clays with potential for calcination and use as SCM are large and evenly distributed over the earth's surface [12]. This led to the development of the Limestone Calcined Clay Cements (LC^3) which are based on the use of metakaolin [1,12]. However, there is a scientific gap on the use of clays different than kaolinite or the other main clays studied such as smectite and illite [13,14].

A previous study that investigated the use of a dolomitic marlstone containing palygorskite (17 %) and smectite (16 %) as SCM demonstrated the high potential of palygorskite [15]. In this context, the aim of this paper is to investigate the use of calcined palygorskite as a new type of SCM by comparing two samples (Pal-1 and Pal-2) containing large amount of palygorskite. The main objectives are to determine whether these palygorskites can be used

as SCMs once calcined, and whether the percentage of palygorskite in the sample has an influence on the total reactivity. The final objective being to determine whether it is possible to use so-called low grade palygorskites. This involves a multi-scale study of the calcination, the pozzolanic reactivity, and the mechanical performances in cementitious systems of these two palygorskites.

5.3. Materials and experimental methods

5.3.1. Materials

The materials studied (Pal-1 and Pal-2) are two commercial palygorskites supplied by an industrial partner. Table 5-1 displays the results of the chemical analysis of the two materials (performed by X-Ray Fluorescence (XRF)).

Table 5-1: Chemical analysis of Pal-1 and Pal-2

	Oxydes	**SiO_2**	**Al_2O_3**	**MgO**	**Fe_2O_3**	**CaO**	**P_2O_5**	**K_2O**	**TiO_2**	**LOI (1050°C)**
Pal-1	wt. %	54.1	9.4	9.4	3.2	2.9	0.8	0.8	0.4	19.8
Pal-2	wt. %	52.8	9.8	10.5	3.3	2.6	0.9	0.7	0.4	19.5

The two materials have a very similar chemical composition, especially in terms of SiO_2, Al_2O_3, MgO, Fe_2O_3 and CaO contents. The quantification of the crystalline phases was carried out using the Rietveld method (see supporting informations) on the diffractograms of the raw Pal-1 and the raw Pal-2. Table 5-2 shows the mineralogical composition of each of these two materials.

Table 5-2: Mineralogical composition of Pal-1 and Pal-2

	Phases	**Palygorskite**	**Smectite**	**Quartz**	**Ankerite**
Pal-1	wt. %	61	25	10	4
Pal-2	wt. %	73	21	4	2

Pal-1 and Pal-2 have a relatively similar mineralogy, they are both mainly composed of palygorskite, associated with smectite, quartz and ankerite. The occurrence of smectite in

both materials is explained by the fact that palygorskite is mainly formed by the alteration of smectite [16,17]. It is therefore very common to find smectite associated with palygorskite in natural samples.

The particle size distributions (obtained by laser granulometry) of the GU-white, GU-grey, Pal-1 and Pal-2 (before and after calcination at 800°C) are shown in Table 5-3.

Table 5-3. Particle size distributions of the palygorskites (Pal-1 and Pal-2) before and after calcination at 800°C.

Label	d10 (μm)	d50 (μm)	d90 (μm)
Pal-1	5	22	67
800°C-Pal-1	4	20	72
Pal-2	4	11	23
800°C-Pal-2	3	9	20

5.3.2. Calcination

Pal-1 and Pal-2 were calcined using a laboratory furnace in flat alumina crucibles (to ensure a homogeneous calcination) under atmospheric conditions. They were heated from room temperature up to 600, 700, 800 and 900°C with a heating rate of 5°C/min and a residence time at maximum temperature of 1h. After calcination, the materials were left to cool down to room temperature into the oven overnight (with the door closed). The choice of this calcination protocol was made on the basis of the existing literature on the subject [18–22].

5.3.3. X-ray diffraction analysis

X-ray diffraction analysis were performed using a PANalytical X'Pert pro MPD diffractometer equipped with a PIXcel 1D detector (active length of 3.347°2θ). The X-ray tube consisted of a copper anode tube (40 kV / 50 mA) that emits Cu Kα radiation (λ = 1.5418 Å). Measurements were based on a Bragg-Brentano geometry with 0.04 rad Soller slits. Anti-scatter and incident

divergence slits were 1/8° and 1/16° respectively. The diffractograms were acquired between 3° and 70° 2θ, with a step size of 0.0131° 2θ and a measurement time of 0.75 second per step.

5.3.4. Nuclear magnetic resonance

The ^{27}Al MAS NMR spectra were acquired on a Bruker Avance III 500 MHz spectrometer using a 2.5 mm MAS probe. The excitation pulse length used was π/13 for a radio frequency field of 11 kHz. The repetition time was 1s and the MAS frequency was 30 kHz. The 29Si MAS NMR spectra were acquired on a Bruker NEO 300 MHz spectrometer using a 7 mm MAS probe.

A π/2 excitation pulse length was used, and the MAS frequency was 5 kHz. After several tests of different repetition times, the choice was made to use a time of 10s in order to ensure quantitative results (except for quartz). However, this has no consequences as quartz is non-reactive. ^{1}H decoupling was performed during all the acquisitions. ^{27}Al spectra were referenced against an aqueous solution of $Al(NO_3)_3$ and ^{29}Si spectra against TMS (Tetramethylsilane). The spectral decompositions have been done using the dmfit software [23].

5.3.5. Pozzolanic activity: isothermal calorimetry

The pozzolanic activity of Pal-1 and Pal-2 calcined at different temperatures was evaluated according to ASTM C1897 [24] by measuring the cumulative heat release. 10g of dry SCM was mixed with 30g of calcium hydroxide, 10g of calcium carbonate and 54g of potassium solution. Then, 15g of the paste was cast into calorimeter ampoules and placed into the calorimeter measurement chamber. The cumulative heat release was recorded for 7 days (168 h) after mixing and expressed in J/g of SCM.

5.3.6. Calcined palygorskite-cement blends and compressive strength measurements

Two different blended cements were obtained by mixing 80 wt.% of grey general use Portland cement (GU-grey) or white general use Portland cement (GU-white) with 20 wt.% of 800°C

calcined Pal-1 or 20% wt.% of 800°C calcined Pal-2. The objective of blending with GU-grey and GU-white cements is to evaluate the influence of the addition on the mechanical performance in a conventional system (GU-grey cement) but also to be able to perform solid state NMR measurements to evaluate the influence of the palygorskite on the hydration kinetics (GU-white cement).

Table 5-4. Particle size distributions of GU-grey and GU-white

Label	d10 (μm)	d50 (μm)	d90 (μm)
GU-grey	4	21	60
GU-white	2	14	42

The particle size distribution of the calcined palygorskites (table 5-3) and the two types of cements (table 5-4) are in the same order of magnitude, which ensures a homogeneous blend.

Table 5-5 gives the chemical analysis (performed by XRF) of the two cements: GU-grey and GU-white.

Table 5-5: Chemical analysis of GU-grey and GU-white

	Oxydes	CaO	SiO_2	Al_2O_3	SO_3	MgO	K_2O	TiO_2	Fe_2O_3	Cr_2O_3	SrO	P_2O_5	Na_2O	BaO	LOI
GU-grey	wt. %	61.9	20.7	4.5	3.6	2.1	0.8	0.2	2.5	0	0.1	0.1	0.2	0	2.8
GU-white	wt. %	64.8	21.7	5.1	3.1	0.9	0.2	0.2	0.2	0.2	0	0	0.1	0.1	3.2

The main differences concern the proportion of Fe_2O_3 which is very low for GU-white and the proportion of alkali which is higher for GU-grey.

Mortar cubes (50 x 50 x 50 mm^3) were then prepared with a constant water to binder ratio of 0.484 and with graded ASTM C109 [25] standard sand (sand/binder = 2.75). Molds were then placed in plastic bags for 20 h until demolding. The demolded mortar cubes were stored in CaO saturated water until the age of testing. Compressive strength was assessed according to

the ASTM C109 loading procedure [25] after 7 and 28 days of hydration. Control mortar cubes were made using 100% GU-grey and 100% GU-white. A polycarboxylate (PC) superplasticizer was used for mortars made with the blended cements to obtain a slump flow equivalent to that of the control mortars.

5.3.7. Electrical resistivity

The electrical bulk resistivity was used to assess the influence of the SCMs on the durability of mortars. The electrical resistivity was evaluated on 50 x 50 x 50 cm^3 mortars cubes at 28 days of curing. All measurements were made directly after removing the samples from the lime solution and after wiping the surface with a wet towel to remove the excess of water. This was done to ensure equivalent moisture state. Two electrodes were placed on opposite surfaces of the cubes, a voltage was applied, and the potential difference (resistance **R**) was measured. The electrical resistivity (in Ω.m) was calculated as $\rho = R.(A/l)$ with **R** being the electrical resistance (in Ω), **A** the area of the cross section of the specimen (in m^2) and **l** the length of the specimen (in m).

5.4. Results and discussion

5.4.1. Calcination and reactivity

Figure 5-1 displays the evolution of the X-ray diffractograms of the Pal-1 and Pal-2 samples as a function of the calcination temperature.

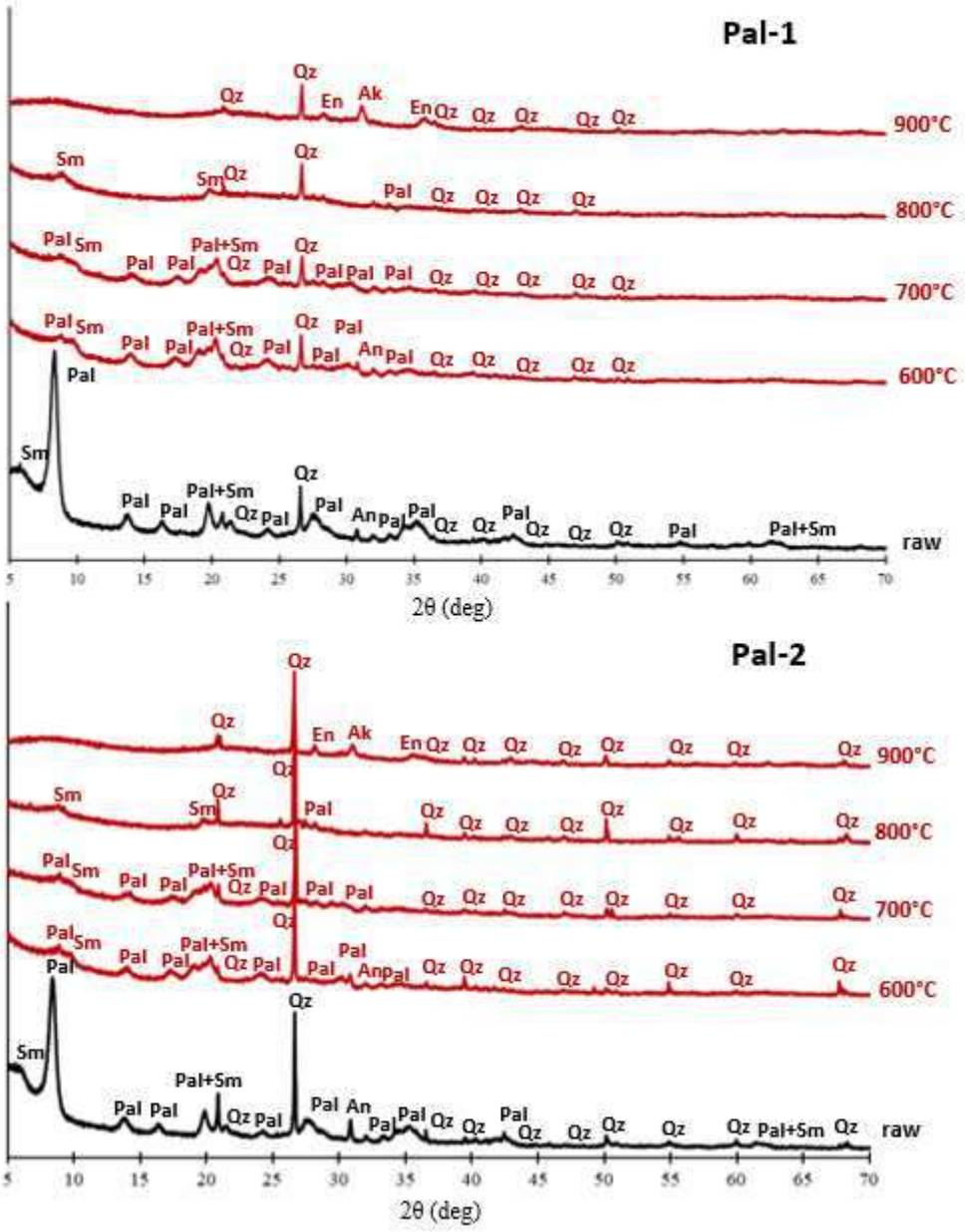

Figure 5-1: Evolution of the X-ray diffractograms of Pal-1 and Pal-2 samples as a function of the calcination temperature. Pal = palygorskite ; Sm smectite ; Qz = quartz ; An = ankerite ; Ak = akermanite ; En = enstatite.

Both diffractograms of the raw Pal-1 and Pal-2 samples exhibit the characteristic peaks of palygorskite (Pal), smectite (Sm), quartz (Qz) and ankerite (An). Already at 600°C there is a shift of the [001] characteristic peak of the smectite from about 2θ = 6° to 2θ = 9°, which is caused by the decrease of the d001 value due to the removal of the water from the interfoliate space [26].

With increasing calcination temperature, the intensity of the characteristic peaks of palygorskite and smectite are decreasing gradually. They are no longer detectable at 900°C while the characteristics peaks of akermanite (Ak) and enstatite (En) appear. Quartz is not affected by the thermal treatment as its characteristic peaks are still observable after calcination at 900°C. The evolution of the diffractograms of Pal-1 and Pal-2 is similar, and based on the XRD results, 800°C seems to be the best calcination temperature as it allows an important amorphization of the clay phases while avoiding recrystallization phenomena.

Pozzolanic activity measurements were then carried out at each temperature to accurately determine the optimum calcination temperature of Pal-1 and Pal-2. Figure 5-2 displays the evolution of the pozzolanic activity (7 days cumulative heat release, ASTM C1897 [24]) as a function of the calcination temperature for Pal-1 and Pal-2.

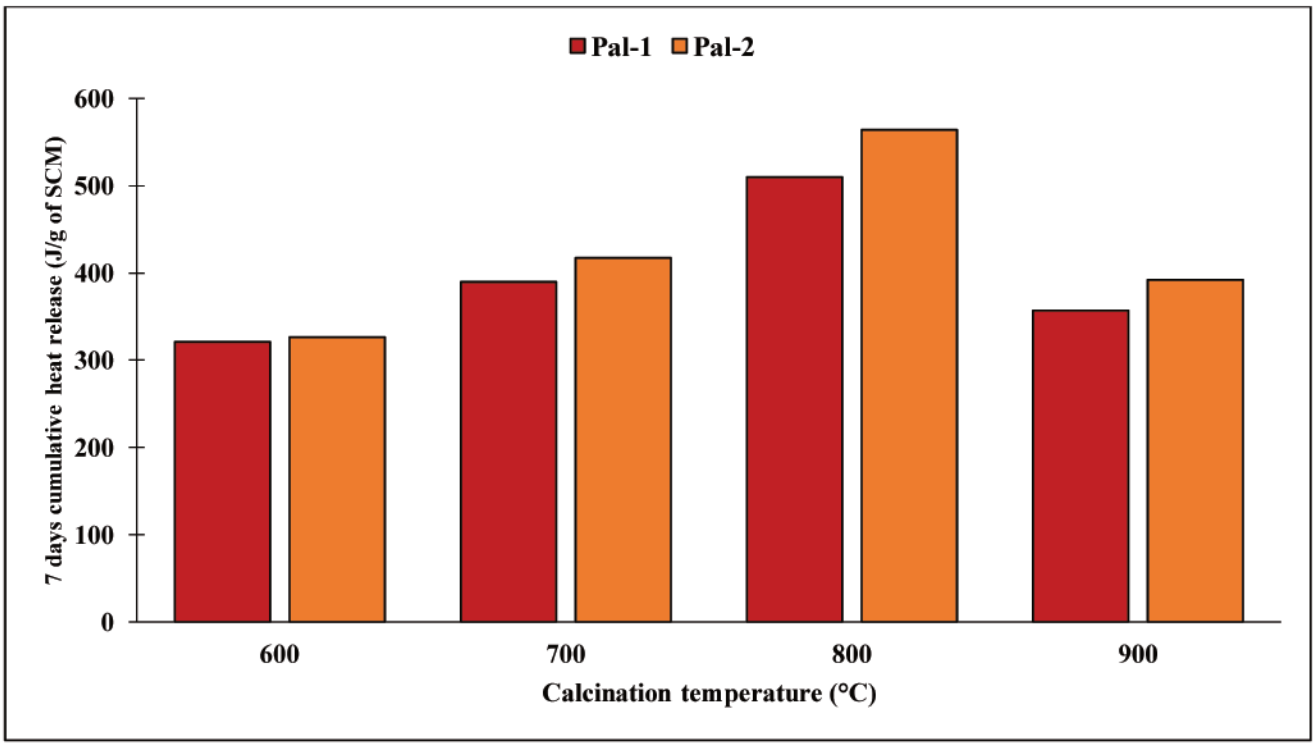

Figure 5-2: Evolution of the pozzolanic activity (cumulative heat release) of Pal-1 and Pal-2 samples as a function of the calcination temperature.

For both Pal-1 and Pal-2 the pozzolanic reactivity increases with the increasing calcination temperature up to a maximum of 510 J/g of SCM (Pal-1) and 564 J/g of SCM (Pal-2) at 800°C.

In a previous study [27], a reference palygorskite (containing 79 % of palygorskite and 11 % of smectite) supplied by the clay mineral society was tested and obtained a pozzolanic activity value of 528 J/g SCM after calcination at 800°C. Pal-1 and Pal-2 (which contain lower percentages of palygorskite : 73 and 69 % respectively) exhibits a pozzolanic reactivity equivalent to that of the reference palygorskite provided by the clay mineral society (79 % of palygorskite).

Londono-Zuluaga et al. [28] tested 10 types of metakaolins varying in purity and other constituent minerals and obtained pozzolanic reactivity values ranging from 250 to 960 J/g of SCM at 7 days. These pozzolanic reactivity values of palygorskite are therefore typical for this type of clay and very interesting as they are in the range of metakaolin which is the current reference for calcined clays.

The pozzolanic reactivity decreases after calcination at 900°C for both Pal-1 and Pal-2 because of the recrystallization phenomena, as highlighted with the XRD analyses. Pozzolanic reactivity measurements correlate well with the XRD analysis (figure 5-1), the increase in pozzolanic reactivity follows the loss of crystallinity of the calcined clay phases highlighted by XRD. Pal-2 exhibits a higher pozzolanic activity than Pal-1 at each calcination temperature which could be explained either by the higher total proportion of clay phases (94% for Pal-2 against 86% for Pal-1) or the higher proportion of palygorskite (73% for Pal-2 against 61% for Pal-1). It is also possible that the superior reactivity of Pal-2 is due to its greater finesse (table 5-3) which favors its dissolution and pozzolanic reactivity.

Based on the XRD analysis and the pozzolanic activity test it appears that 800°C is the appropriate calcination temperature for both Pal-1 and Pal-2. This temperature is in agreement with temperatures determined in previous studies on a palygorskite-bearing marlstone [29] and on a reference palygorskite [27]. Blended cements incorporating 20 wt.% Pal-1 and Pal-2 calcined at 800°C were then produced to make mortars and measure the compressive strength and resistivity.

5.4.2. Calcined palygorskite-cement systems

5.4.2.1. Compressive strength on calcined palygorskite grey and white cement mortars

The hydration of blended cements incorporating these two materials was then studied by solid state NMR. In this case, the replacements are made in white cement to avoid that the iron distorts the NMR signal. Therefore, it is necessary to access the compressive strengths on both systems : grey and white cement blends mortars

Figure 5-3 displays the compressive strength at 7 and 28 days for mortars M-G-GU (grey Portland cement), M-G-Pal-1 and M-G-Pal-2 (grey Portland cement incorporating 20 wt.% of Pal-1 and Pal-2 calcined at 800°C respectively), M-W-GU (white Portland cement), M-W-Pal-1 and M-W-Pal-2 (white Portland cement incorporating 20 wt.% of Pal-1 and Pal-2 calcined at 800°C respectively).

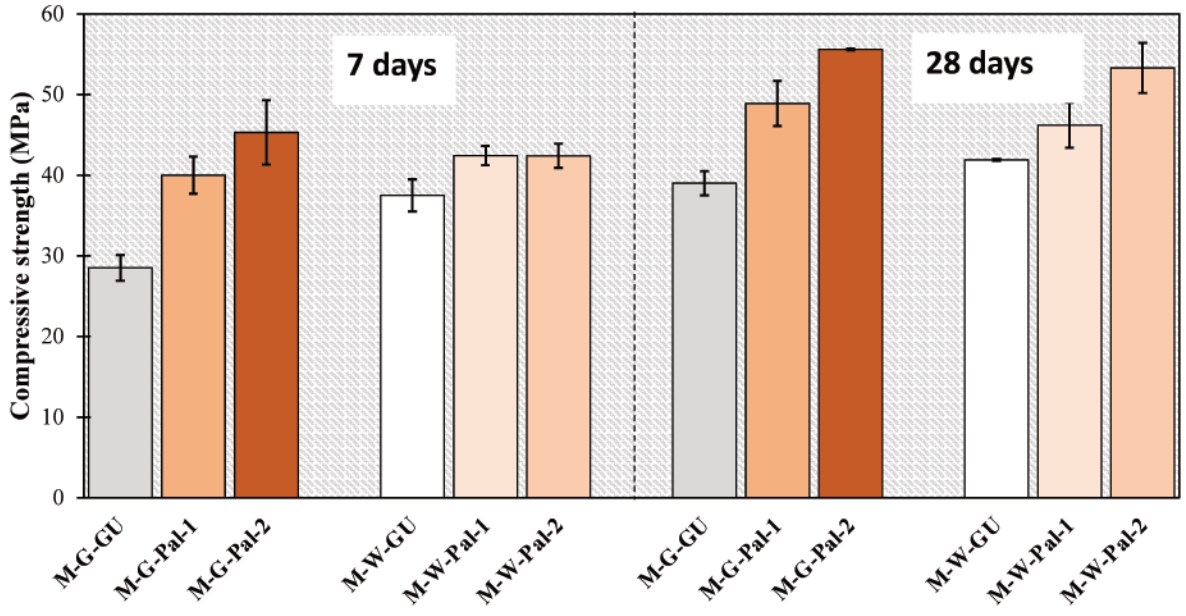

Figure 5-3: Compressive strength at 7 and 28 days of M-G-GU, M-G-Pal-1, M-G-Pal-2, M-W-GU, M-W-Pal-1 and M-W-Pal-2.

After 7 and 28 days of hydration, M-G-Pal-1, M-G-Pal-2, M-W-Pal-1 and M-W-Pal-2 exhibits higher compressive strength values than their respective reference (M-G-GU and M-W-GU). Mortars that incorporate Pal-1 and Pal-2 systematically have higher compressive strength values than the reference in both systems (white and grey Portland cement based mortars).

M-G-Pal-2 exhibit higher compressive strength values than M-G-Pal-1 at both 7 days (45 MPa against 40 Mpa) and 28 days (56 Mpa against 49 Mpa). These results agree with the pozzolanic activity test results which showed a higher pozzolanic reactivity of Pal-2 compared to Pal-1 after calcination at 800°C. These results are confirmed in the white Portland cement system as M-W-Pal-2 exhibit equivalent and higher compressive strength values than M-W-Pal-1 at 7 and 28 days respectively. The equivalent values at 7 days could be explained the low alkali content (see table 5-4) of the white cement in comparison to the grey cement. This will decrease the alkali content in the pore solution and will lead to a decrease of the rate of dissolution of the calcined SCM, thus delaying the pozzolanic reaction [30].

The partial cement replacement by Pal-1 or Pal-2 calcined at 800°C lead to a significant increase in compressive strengths, which confirms the high pozzolanic reactivity of these two materials. Based on these results, it appears that even with a lower percentage of palygorskite (as for Pal-1), this type of clay shows a significant pozzolanic reactivity.

^{29}Si and ^{27}Al MAS NMR analysis were then carried out on white portland cement blends pastes after 7 and 28 days of hydration to highlight the influence of the SCM on the hydration of white cement.

5.4.2.2. MAS NMR Analysis

Figure 5-4 displays the evolution of the ^{27}Al MAS NMR spectra obtained for the cement pastes P-W-GU (GU white cement), P-W-Pal-1 (GU white cement blended with 20% of 800°C-Pal-1) and P-W-Pal-2 (GU white cement blended with 20% of 800°C-Pal-2) hydrated during 7 and 28 days.

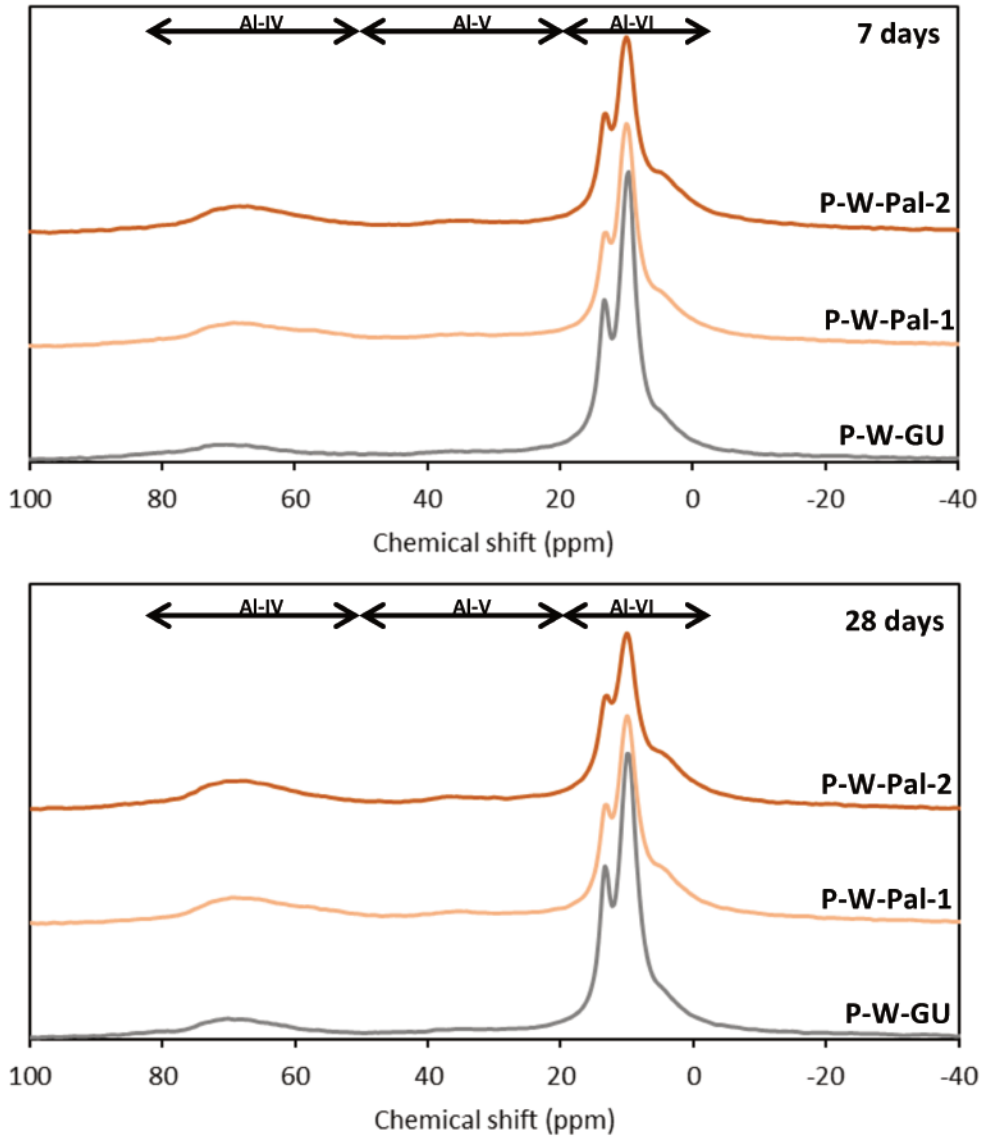

Figure 5-4: Evolution of the ^{27}Al MAS NMR spectra for the cement pastes P-GU (GU white cement), P-W-Pal-1 (GU white cement blended with 20% of 800°C-Pal-1) and P-W-Pal-2 (GU white cement blended with 20% of 800°C-Pal-2) hydrated during 7 and 28 days.

The spectrum of P-GU (at 7 and 28 days) exhibits 2 mains resonances in the spectral region for the 6-fold aluminium at 13.1 and 9.8 ppm which can be associated with aluminium in ettringite [31] and monosulfate [32], respectively. The shoulder at 4.5 ppm can be associated with 6-fold aluminium from the C-(A)-S-H as described by Mohamed et al [33]. The spectrum of P-GU exhibits also a broad resonance at 70 ppm which correspond to 4-fold aluminium and which can be associated with aluminium incorporated into the C-(A)-S-H chains [34,35].

Finally, the low intensity resonance at 35 ppm corresponds to 5-fold aluminium and can be associated with AlO_5 that have replaced calcium in the interlayer space of the C-(A)-S-H [36].

For the P-W-Pal-1 and P-W-Pal-2, the same characteristic resonances of ettringite (13.1 ppm), monosulphate (9.8 ppm) and aluminium incorporated in the chains (70 ppm) and interlayers (35 ppm) of C-(A)-S-H are observed. The 35 ppm resonance can also be associated with 5-fold aluminium from the un-reacted calcined clay phases. The addition of PFl-1 and PFl-2 calcined at 800°C does not seem to have much influence on the relative proportions of ettringite and monosulphate (at 7 and 28 days), apart from the dilution effect. However, it appears that the addition of Pal-1 and Pal-2 calcined at 800°C leads to an increase in the relative proportion of 4- and 5-fold aluminium which are associated with aluminium into the C-(A)-S-H chains and interlayers, respectively. The addition of calcined palygorskite will therefore lead to an increase in the incorporation of aluminium in C-(A)-S-H through pozzolanic reaction. The comparison of P-W-Pal-1 and P-W-Pal-2 indicates that the phenomenon is more pronounced for P-W-Pal-2, which correlates well with the higher pozzolanic reactivity for Pal-2.

Figure 5-5 displays the evolution of the ^{29}Si MAS NMR spectra for the cement pastes P-W-GU (GU white cement), P-W-Pal-1 (GU white cement blended with 20% of 800°C-Pal-1) and P-W-Pal-2 (GU white cement blended with 20% of 800°C-Pal-2) hydrated during 7 and 28 days.

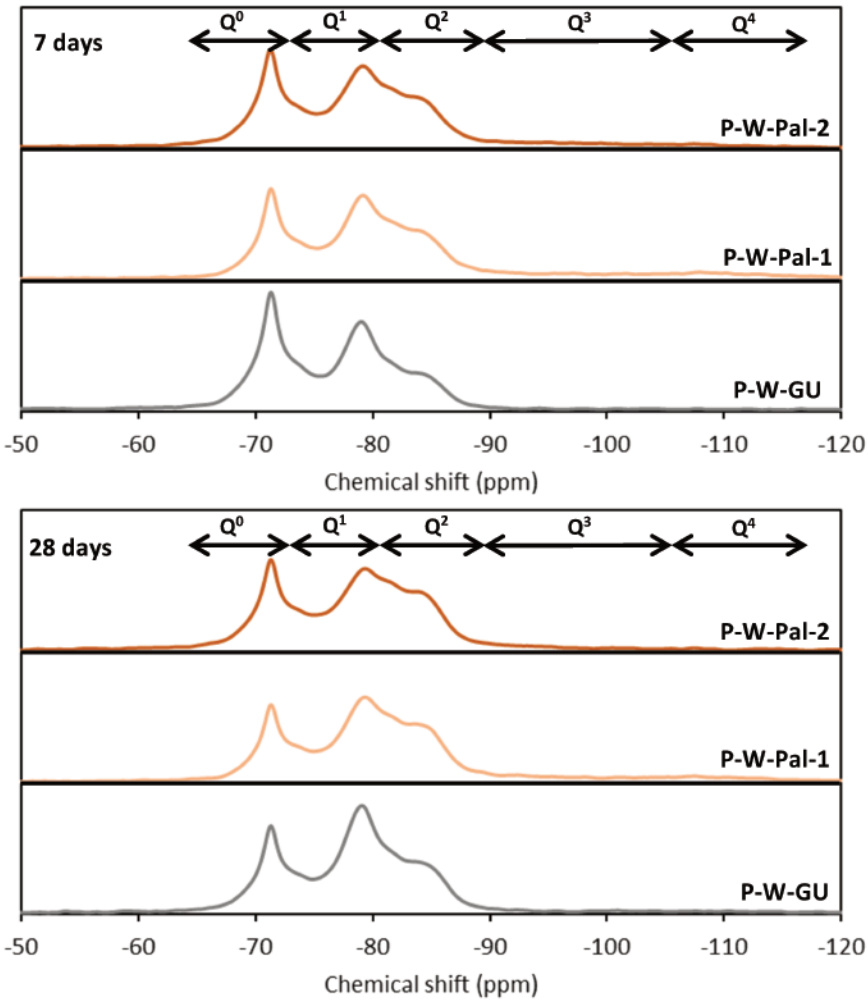

Figure 5-5: Evolution of the ^{29}Si MAS NMR spectra for the cement pastes P-W-GU (GU white cement), P-W-Pal-1 (GU white cement blended with 20% of 800°C-Pal-1) and P-W-Pal-2 (GU white cement blended with 20% of 800°C-Pal-2) hydrated during 7 and 28 days.

At 7 days, the spectrum of P-W-GU exhibit a main resonance at -71 ppm which corresponds to silicon atoms in Q^0 configuration and which can be associated with silicon from unhydrated C_2S and C_3S [37,38]. The three resonances at -79, -81 and -84 ppm correspond to silicon in Q^1, $Q^2(1Al)$ and Q^2 configurations, which can be associated with silicon in the C-(A)-S-H [35,39,40]. Between 7 and 28 days, the relative proportion of silicon in Q^0 configuration decreases and the relative proportion of silicon in Q^1, $Q^2(1Al)$ and Q^2 configurations increases. This reflects a consumption of the C_2S and C_3S associated with the formation of C-(A)-S-H.

At 7 days, the spectra of P-W-Pal-1 and P-W-Pal-2 also exhibit resonances associated with C_2S and C_3S (-71 ppm) as well as with the C-(A)-S-H (Q^1, $Q^2(1Al)$ and Q^2 at -79, -81 and -84 ppm,

respectively). The main difference is the presence of a broad resonance in the Q^3 & Q^4 spectral region which can be associated with the silicon from the calcined clay phases (palygorskite and smectite) [27]. From 7 to 28 days of hydration, the relative proportion of C_3S+C_2S (Q^1) and calcined clay phases (Q^3 and Q^4) decreases, which is associated with an increase in the relative proportion of C-(A)-S-H (Q^1, Q^2(1Al) and Q^2). These results confirm the pozzolanic reaction of Pal-1 and Pal-2 calcined at 800°C.

To accurately compare the evolution of C-(A)-S-H and calcined clay phases during hydration, a spectral integration quantification was performed (see supporting informations). The results are presented in figure 5-6.

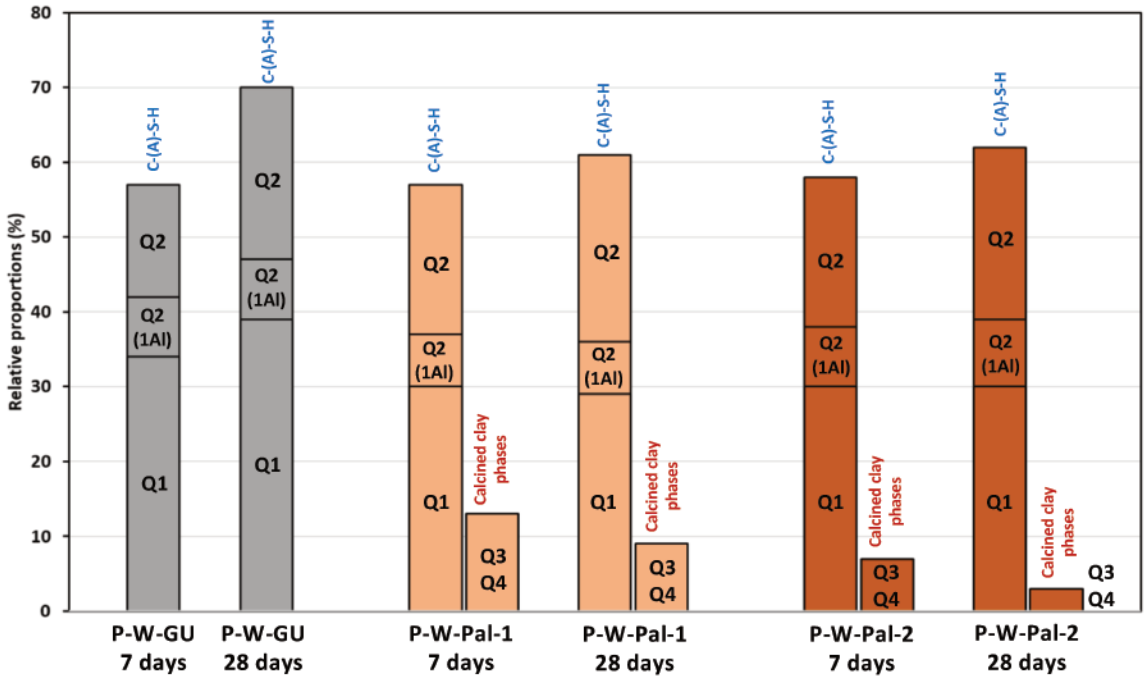

Figure 5-6: Evolution of the relative proportions of silicon contained in C-(A)-S-H and calcined clay phases of P-W-GU (100% white cement paste), P-W-Pal-1 (paste made from GU white cement blended with 20% of 800°C-Pal-1) and P-W-Pal-2 (paste made from GU white cement blended with 20% of 800°C-Pal-2) hydrated during 7 and 28 days.

For P-W-GU, the relative proportion of C-(A)-S-H increases with the hydration time, which is due to the hydration of the anhydrous phases. For P-W-Pal-1 and P-W-Pal-2, the increase in the relative proportion of C-(A)-S-H correlates with the consumption of the calcined clay

phases. After 28 days of hydration, the relative proportion of C-(A)-S-H is higher for P-W-GU- than for P-W-Pal-1 and P-W-Pal-2, however, the two blends exhibit higher compressive strength values. This could be explained by the type of C-(A)-S-H formed in the blends and/or by the filler role of the unreacted calcined clays.

By comparing the two, it appears that the consumption of calcined clay phases is higher for P-W-Pal-2 than P-W-Pal-1. Despite the greater consumption of calcined clay phases in Pal-2, there is no any particular impact on the relative proportion of C-(A)-S-H compared to Pal-1.

The average chain length of aluminosilicate tetrahedra (CL) of the C–(A)-S–H structure can be calculated with the following equation using the model of Richardson et al. [41] :

$$\overline{CL} = \frac{2\left[Q^1 + Q^2 + \frac{3}{2}Q^2(1Al)\right]}{Q^1}$$

Table 5-6 displays the evolution of the CL parameter for P-W-GU, P-W-Pal-1 and P-W-Pal-2 as function of the hydration time.

Table 5-6: Evolution of CL of the C-(A)-S-H as function of the hydration time for P-W-GU, P-W-Pal-1 and P-W-Pal-2

	P-W-GU 7 days	P-W-GU 28 days	P-W-Pal-1 7 days	P-W-Pal-1 28 days	P-W-Pal-2 7 days	P-W-Pal-2 28 days
CL	3,46	3,53	3,59	3,94	3,78	4,10

The average aluminosilicate chain length (CL) is increasing with increasing hydration times for the three systems (P-W-GU, P-W-Pal-1 and P-W-Pal-2). However, this increase is more pronounced for P-W-Pal-1 and P-W-Pal-2 than for P-W-GU. The increase in CL for the blends P-W-Pal-1 and P-W-Pal-2 in comparison to P-W-GU reveals that the increased amount of aluminium in the hydrating system leads to higher amount of aluminium incorporated into the C-(A)-S-H structure [39]. The increase in CL correlate well with the ^{27}Al MAS NMR results

which showed an increase in the amount of aluminium incorporated into the C-(A)S-H for P-W-Pal-1 and P-W-Pal-2. This increase in CL caused by the addition of calcined clay is in agreement with the results of Love et al. [42].

5.4.2.3. Electrical resistivity on calcined palygorskite grey and white cement mortars

Figure 5-7 displays the electrical resistivity at 28 days of the two references (M-G-GU and M-W-GU) and their respective blends (M-G-Pal-1, M-G-Pal-2, M-W-Pal-1 and M-W-Pal-2)

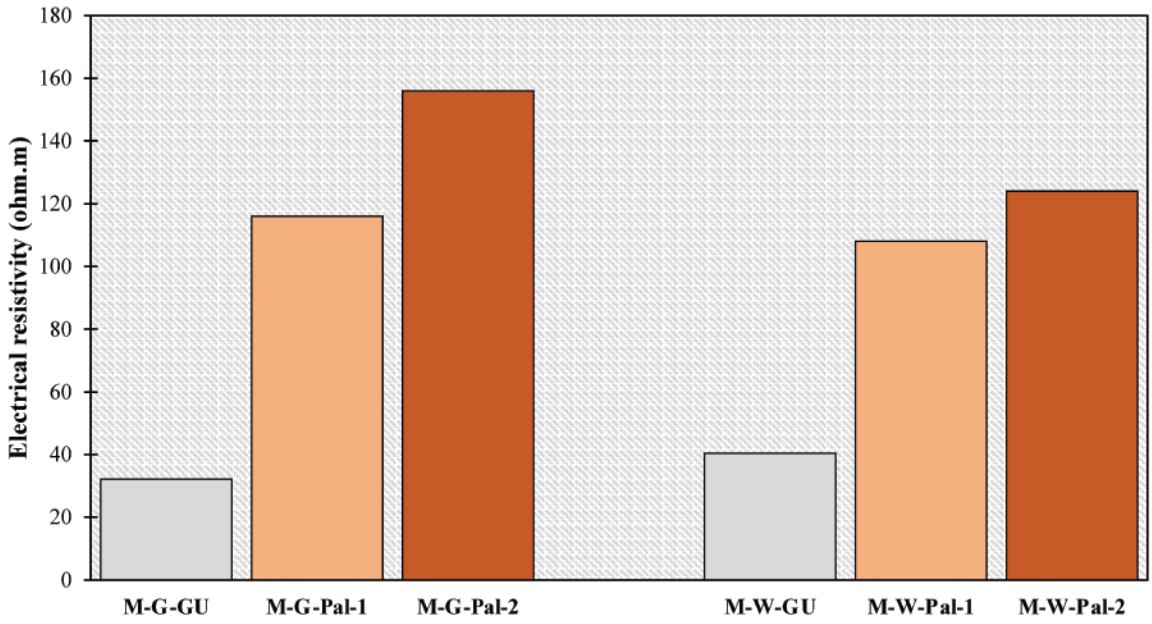

Figure 5-7: Electrical resistivity at 28 days of M-G-GU, M-W-GU, M-G-Pal-1, M-G-Pal-2, M-W-Pal-1 and M-W-Pal-2.

For both grey and white cement, there is a significant increase in the electrical resistivity when blended with 20 wt.% of 800°C calcined Pal-1 and Pal-2. This gain is electrical resistivity is mainly due to the dilution effect of the clinker with the SCM, which leads to a decrease in the total amount of alkalis [43]. Although white cement contains less alkali, it appears that the resistivity values are lower than for grey cement. This can be explained by a more connected porosity, favoring the passage of ions, and decreasing the resistivity. In all cases, the addition of 800°C Pal-1 and Pal-2 allows a significant improvement of the resistivity, suggesting an increased durability for this type of palygorskite blended cements.

5.5. Conclusion

In this paper, the comparative study of the use of two commercial palygorskite (containing different percentages of palygorskite) as supplementary cementitious materials once calcined has been carried out. Based on the results, the following conclusions can be drawn:

-A calcination temperature of 800°C is optimal for Pal-1 and Pal-2 and results in the highest pozzolanic reactivity.

-The preparation mortars with cements incorporating 20% of Pal-1 and Pal-2 calcined at 800°C showed a significant increase in compressive strength compared to the reference (GU cement-based mortars).

-Pal-2 has a higher pozzolanic reactivity and allows higher compressive strength values in mortars than Pal-1. This difference can either be due to the higher proportion of clay phases or the higher proportion of palygorskite or its greater finesse.

-In general, palygorskite is a clay with a high potential for use as a supplementary cementitious material after calcination at 800°C.

- Pal-1, the sample with the lowest percentage of palygorskite allows a significant increase in mechanical performance compared to the reference. This demonstrates that it is not necessary to use pure samples and opens new ways of valorisation for this type of material.

Further experimentation will continue with the study of samples that contain low proportions of palygorskite (between 20 and 50%) to determine whether it is possible to proposer new way of recovery of these so-called low-grade samples.

5.6. References

[1] Y. Cancio Díaz, S. Sánchez Berriel, U. Heierli, A.R. Favier, I.R. Sánchez Machado, K.L. Scrivener, J.F. Martirena Hernández, G. Habert, Limestone calcined clay cement as a low-carbon solution to meet expanding cement demand in emerging economies, Development Engineering. 2 (2017) 82–91. https://doi.org/10.1016/j.deveng.2017.06.001.

[2] P.J.M. Monteiro, S.A. Miller, A. Horvath, Towards sustainable concrete, Nature Mater. 16 (2017) 698–699. https://doi.org/10.1038/nmat4930.

[3] D.N. Huntzinger, T.D. Eatmon, A life-cycle assessment of Portland cement manufacturing: comparing the traditional process with alternative technologies, Journal of Cleaner Production. 17 (2009) 668–675. https://doi.org/10.1016/j.jclepro.2008.04.007.

[4] S.A. Miller, V.M. John, S.A. Pacca, A. Horvath, Carbon dioxide reduction potential in the global cement industry by 2050, Cement and Concrete Research. 114 (2018) 115–124. https://doi.org/10.1016/j.cemconres.2017.08.026.

[5] B. Bajželj, J.M. Allwood, J.M. Cullen, Designing Climate Change Mitigation Plans That Add Up, Environ. Sci. Technol. 47 (2013) 8062–8069. https://doi.org/10.1021/es400399h.

[6] Rapport final du Plan de transition sectoriel de l'industrie cimentière en France - La librairie ADEME, (n.d.). https://librairie.ademe.fr/changement-climatique-et-energie/5234-rapport-final-du-plan-de-transition-sectoriel-de-l-industrie-cimentiere-en-france.html#/44-type_de_produit-format_electronique (accessed May 19, 2022).

[7] A. Rahman, M.G. Rasul, M.M.K. Khan, S. Sharma, Impact of Alternative Fuels on the Cement Manufacturing Plant Performance: An Overview, Procedia Engineering. 56 (2013) 393–400. https://doi.org/10.1016/j.proeng.2013.03.138.

[8] D.J. Barker, S.A. Turner, P.A. Napier-Moore, M. Clark, J.E. Davison, CO2 Capture in the Cement Industry, Energy Procedia. 1 (2009) 87–94. https://doi.org/10.1016/j.egypro.2009.01.014.

[9] T. Staněk, P. Sulovský, Active low-energy belite cement, Cement and Concrete Research. 68 (2015) 203–210. https://doi.org/10.1016/j.cemconres.2014.11.004.

[10] E. Crossin, The greenhouse gas implications of using ground granulated blast furnace slag as a cement substitute, Journal of Cleaner Production. 95 (2015) 101–108. https://doi.org/10.1016/j.jclepro.2015.02.082.

[11] Z.T. Yao, X.S. Ji, P.K. Sarker, J.H. Tang, L.Q. Ge, M.S. Xia, Y.Q. Xi, A comprehensive

review on the applications of coal fly ash, Earth-Science Reviews. 141 (2015) 105–121. https://doi.org/10.1016/j.earscirev.2014.11.016.

[12] K. Scrivener, F. Martirena, S. Bishnoi, S. Maity, Calcined clay limestone cements (LC3), Cement and Concrete Research. 114 (2018) 49–56. https://doi.org/10.1016/j.cemconres.2017.08.017.

[13] T. Danner, G. Norden, H. Justnes, Calcareous smectite clay as a pozzolanic alternative to kaolin, European Journal of Environmental and Civil Engineering. 25 (2021) 1647–1664. https://doi.org/10.1080/19648189.2019.1590741.

[14] R. Fernandez, F. Martirena, K.L. Scrivener, The origin of the pozzolanic activity of calcined clay minerals: A comparison between kaolinite, illite and montmorillonite, Cement and Concrete Research. 41 (2011) 113–122. https://doi.org/10.1016/j.cemconres.2010.09.013.

[15] V. Poussardin, M. Paris, W. Wilson, A. Tagnit-Hamou, D. Deneele, Calcined palygorskite and smectite bearing marlstones as supplementary cementitious materials, (n.d.).

[16] Q. Xie, T. Chen, H. Zhou, X. Xu, H. Xu, J. Ji, H. Lu, W. Balsam, Mechanism of palygorskite formation in the Red Clay Formation on the Chinese Loess Plateau, northwest China, Geoderma. 192 (2013) 39–49. https://doi.org/10.1016/j.geoderma.2012.07.021.

[17] M.P.S. Krekeler, E. Hammerly, J. Rakovan, S. Guggenheim, Microscopy Studies of the Palygorskite-to-Smectite Transformation, Clays Clay Miner. 53 (2005) 92–99. https://doi.org/10.1346/CCMN.2005.0530109.

[18] T. Danner, G. Norden, H. Justnes, Characterisation of calcined raw clays suitable as supplementary cementitious materials, Applied Clay Science. 162 (2018) 391–402. https://doi.org/10.1016/j.clay.2018.06.030.

[19] N. Garg, J. Skibsted, Thermal Activation of a Pure Montmorillonite Clay and Its Reactivity in Cementitious Systems, The Journal of Physical Chemistry C. 118 (2014) 11464–11477. https://doi.org/10.1021/jp502529d.

[20] N. Garg, J. Skibsted, Pozzolanic reactivity of a calcined interstratified illite/smectite (70/30) clay, Cement and Concrete Research. 79 (2016) 101–111. https://doi.org/10.1016/j.cemconres.2015.08.006.

[21] S. Krishnan, A.C. Emmanuel, V. Shah, A. Parashar, G. Mishra, S. Maity, S. Bishnoi, Industrial production of limestone calcined clay cement: experience and insights, Green

Materials. 7 (2019) 15–27. https://doi.org/10.1680/jgrma.18.00003.

[22] A. Trümer, H.-M. Ludwig, M. Schellhorn, R. Diedel, Effect of a calcined Westerwald bentonite as supplementary cementitious material on the long-term performance of concrete, Applied Clay Science. 168 (2019) 36–42. https://doi.org/10.1016/j.clay.2018.10.015.

[23] D. Massiot, F. Fayon, M. Capron, I. King, S. Le Calvé, B. Alonso, J.-O. Durand, B. Bujoli, Z. Gan, G. Hoatson, Modelling one- and two-dimensional solid-state NMR spectra: Modelling 1D and 2D solid-state NMR spectra, Magn. Reson. Chem. 40 (2002) 70–76. https://doi.org/10.1002/mrc.984.

[24] Standard Test Methods for Measuring the Reactivity of Supplementary Cementitious Materials by Isothermal Calorimetry and Bound Water Measurements, (n.d.). https://www.astm.org/c1897-20.html (accessed May 19, 2022).

[25] C01 Committee, Test Method for Compressive Strength of Hydraulic Cement Mortars (Using 2-in. or [50-mm] Cube Specimens), ASTM International, n.d. https://doi.org/10.1520/C0109_C0109M-16A.

[26] L.C. Carniel, R.V. Conceição, N. Dani, V.F. Stefani, N.M. Balzaretti, R. dos Reis, Structural changes of potassium-saturated smectite at high pressures and high temperatures: Application for subduction zones, Applied Clay Science. 102 (2014) 164–171. https://doi.org/10.1016/j.clay.2014.09.037.

[27] V. Poussardin, W. Wilson, M. Paris, A. Tagnit-Hamou, D. Deneele, Calcined clays as supplementary cementitious materials: a comparison between palyorskite and kaolinite, (n.d.).

[28] D. Londono-Zuluaga, A. Gholizadeh-Vayghan, F. Winnefeld, F. Avet, M. Ben Haha, S.A. Bernal, Ö. Cizer, M. Cyr, S. Dolenec, P. Durdzinski, J. Haufe, D. Hooton, S. Kamali-Bernard, X. Li, A.T.M. Marsh, M. Marroccoli, M. Mrak, Y. Muy, C. Patapy, M. Pedersen, S. Sabio, S. Schulze, R. Snellings, A. Telesca, A. Vollpracht, G. Ye, S. Zhang, K.L. Scrivener, Report of RILEM TC 267-TRM phase 3: validation of the R3 reactivity test across a wide range of materials, Mater Struct. 55 (2022) 142. https://doi.org/10.1617/s11527-022-01947-3.

[29] V. Poussardin, M. Paris, A. Tagnit-Hamou, D. Deneele, Potential for calcination of a palygorskite-bearing argillaceous carbonate, Applied Clay Science. 198 (2020) 105846. https://doi.org/10.1016/j.clay.2020.105846.

[30] Y. Kawabata, K. Yamada, Evaluation of Alkalinity of Pore Solution Based on the Phase

Composition of Cement Hydrates with Supplementary Cementitious Materials and its Relation to Suppressing ASR Expansion, Journal of Advanced Concrete Technology. 13 (2015) 538–553. https://doi.org/10.3151/jact.13.538.

[31] M.D. Andersen, H.J. Jakobsen, J. Skibsted, Characterization of white Portland cement hydration and the C-S-H structure in the presence of sodium aluminate by 27Al and 29Si MAS NMR spectroscopy, Cement and Concrete Research. 34 (2004) 857–868. https://doi.org/10.1016/j.cemconres.2003.10.009.

[32] M.D. Andersen, H.J. Jakobsen, J. Skibsted, A new aluminium-hydrate species in hydrated Portland cements characterized by 27Al and 29Si MAS NMR spectroscopy, Cement and Concrete Research. 36 (2006) 3–17. https://doi.org/10.1016/j.cemconres.2005.04.010.

[33] A. Kunhi Mohamed, P. Moutzouri, P. Berruyer, B. Walder, J. Siramanont, M. Harris, M. Negroni, S. Galmarini, S. Parker, K. Scrivener, L. Emsley, P. Bowen, The Atomic-Level Structure of Cementitious Calcium Aluminate Silicate Hydrate, Journal of the American Chemical Society. XXXX (2020). https://doi.org/10.1021/jacs.0c02988.

[34] I.G. Richardson, A.R. Brough, R. Brydson, G.W. Groves, C.M. Dobson, Location of Aluminum in Substituted Calcium Silicate Hydrate (C-S-H) Gels as Determined by 29Si and 27Al NMR and EELS, Journal of the American Ceramic Society. 76 (1993) 2285–2288. https://doi.org/10.1111/j.1151-2916.1993.tb07765.x.

[35] M.D. Andersen, H.J. Jakobsen, J. Skibsted, Incorporation of Aluminum in the Calcium Silicate Hydrate (C−S−H) of Hydrated Portland Cements: A High-Field ^{27} Al and ^{29} Si MAS NMR Investigation, Inorganic Chemistry. 42 (2003) 2280–2287. https://doi.org/10.1021/ic020607b.

[36] P. Faucon, A. Delagrave, J. C. Petit, C. Richet, J.M. Marchand, H. Zanni, Aluminum Incorporation in Calcium Silicate Hydrates (C−S−H) Depending on Their Ca/Si Ratio, J. Phys. Chem. B. 103 (1999) 7796–7802. https://doi.org/10.1021/jp990609q.

[37] G. Cardinaud, E. Rozière, O. Martinage, A. Loukili, L. Barnes-Davin, M. Paris, D. Deneele, Calcined clay – Limestone cements: Hydration processes with high and low-grade kaolinite clays, Construction and Building Materials. 277 (2021) 122271. https://doi.org/10.1016/j.conbuildmat.2021.122271.

[38] J. Skibsted, H.J. Jakobsen, C. Hall, Quantification of calcium silicate phases in Portland cements by 29Si MAS NMR spectroscopy, Faraday Trans. 91 (1995) 4423. https://doi.org/10.1039/ft9959104423.

[39] Z. Dai, T.T. Tran, J. Skibsted, Aluminum Incorporation in the C-S-H Phase of White Portland Cement-Metakaolin Blends Studied by ^{27}Al and ^{29}Si MAS NMR Spectroscopy, J. Am. Ceram. Soc. 97 (2014) 2662–2671. https://doi.org/10.1111/jace.13006.

[40] X. Pardal, F. Brunet, T. Charpentier, I. Pochard, A. Nonat, 27 Al and 29Si Solid-State NMR Characterization of Calcium-Aluminosilicate-Hydrate, Inorg. Chem. 51 (2012) 1827–1836. https://doi.org/10.1021/ic202124x.

[41] I.G. Richardson, G.W. Groves, The incorporation of minor and trace elements into calcium silicate hydrate (C-S-H) gel in hardened cement pastes, Cement and Concrete Research. 23 (1993) 131–138. https://doi.org/10.1016/0008-8846(93)90143-W.

[42] C.A. Love, I.G. Richardson, A.R. Brough, Composition and structure of C–S–H in white Portland cement–20% metakaolin pastes hydrated at 25 °C, Cement and Concrete Research. 37 (2007) 109–117. https://doi.org/10.1016/j.cemconres.2006.11.012.

[43] L. Huang, P. Yan, Effect of alkali content in cement on its hydration kinetics and mechanical properties, Construction and Building Materials. 228 (2019) 116833. https://doi.org/10.1016/j.conbuildmat.2019.116833.

5.7. Bilan scientifique du chapitre 5

Cette dernière partie dresse un bilan scientifique de ce chapitre 5 qui s'intéresse à l'utilisation de deux palygorskites calcinées comme ajouts cimentaires. L'étude de la calcination et de la réactivité pouzzolanique a permis de démontrer que la température de calcination optimale (qui entraine la plus grande réactivité) de ces deux matériaux est de 800°C. Par la suite, l'utilisation de ces deux argiles calcinées à 800°C comme ajout cimentaire a permis une importante augmentation de la résistance à la compression sur des mortiers. Pal-2, qui est l'argile contenant la plus grande proportion de palygorskite présente la meilleure réactivité, cependant les résultats sur Pal-1 sont également excellents. Cela confirme donc que la palygorskite est une argile d'intérêt pour une utilisation comme ajout cimentaire après calcination, notamment du fait de sa forte réactivité pouzzolanique, confirmant ainsi les résultats des chapitres précédents.

Chapitre 6 – Utilisation de palygorskite calcinée comme ajout cimentaire : une étude comparative avec le métakaolin

6.1. Avant-propos

Note : Ce chapitre est basé sur un article soumis dans un journal international à comité de lecture.

Titre de l'article : **Calcined clays as supplementary cementitious materials : a comparison between palygorskite and kaolinite**

Victor Poussardin, William Wilson, Michael Paris, Arezki Tagnit-Hamou, Dimitri Deneele

Soumis à : Cement and concrete research

Contribution à la thèse

Dans le chapitre 5 nous avons pu mettre en avant que la palygorskite calcinée est une argile avec un fort potentiel pour une utilisation comme ajout cimentaire. Notamment du fait de sa haute réactivité pouzzolanique qui permet une nette augmentation des performances mécaniques en système cimentaire en comparaison d'un ciment portland classique. Afin de compléter cette étude, l'objectif est désormais de comprendre quels sont les facteurs qui sont à l'origine de cette forte réactivité. Pour cela, ce chapitre 6 s'intéresse à l'utilisation d'une palygorskite calcinée comme ajout cimentaire et compare les résultats avec la référence actuelle qu'est le métakaolin. Au travers de cette étude, le premier objectif est de situer la forte réactivité (mis en avant dans le chapitre 5) de la palygorskite calcinée en comparaison du métakaolin. Le second objectif est de déterminer quel est le lien entre les modifications physico-chimiques induites par la calcination, la réactivité pouzzolanique et les performances mécaniques en système cimentaire.

Résumé en français

L'utilisation d'argiles calcinées ajouts cimentaires peut permettre d'atteindre les objectifs de la COP26 tout en stimulant l'économie, assurant ainsi une transition écologique viable. Le métakaolin est l'argile calcinée qui présente le plus grand potentiel d'utilisation comme ajout cimentaire, notamment en raison de sa grande réactivité et de sa disponibilité dans le monde entier. Ces dernières années, l'utilisation du métakaolin en tant qu'ajout cimentaire a constitué un axe de recherche important, tandis que les autres types d'argiles ont été négligés. Cependant, l'utilisation de nouvelles argiles comme ajouts cimentaires est essentielle pour développer des ciments plus durables dans les régions où la kaolinite n'est pas disponible. Cette étude examine et compare l'utilisation de deux argiles commerciales comme ajouts cimentaires : une palygorskite calcinée (dont la réactivité dans les milieux cimentaires n'a pas encore été étudiée) et un métakaolin. Les modifications physico-chimiques induites par le traitement thermique ont d'abord été étudiées par diffraction des rayons X et par des analyses de RMN MAS ^{27}Al et ^{29}Si. La réactivité a ensuite été étudiée en réalisant des tests d'activité pouzzolanique et des mesures de performances mécaniques en système cimentaire. Les résultats montrent que la palygorskite se comporte très différemment de la kaolinite pendant la calcination, elle présente une cinétique de déshydroxylation plus longue et graduelle. La quantification de l'évolution des proportions relatives d'aluminium 4, 5 et 6 a démontré que l'augmentation de la réactivité pouzzolanique est directement liée à l'apparition d'aluminium 4 et 5 durant la calcination. Bien que la palygorskite calcinée présente une pouzzolanicité inférieure à celle du métakaolin, elle se classe parmi les ajouts cimentaires hautement réactifs. Les résultats ont montré une augmentation significative des performances mécaniques des pâtes incorporant seulement 10% de palygorskite calcinée par rapport à la référence (100% de ciment portland). Il apparaît donc que la palygorskite calcinée peut être un ajout cimentaire approprié une fois calcinée, ce qui ouvre une nouvelle voie de développement de ciments composés bas carbone dans les régions où la kaolinite n'est pas disponible.

Résumé en anglais

The use of calcined clays as Supplementary Cementitious Materials (SCMs) can help to achieve the COP26 objectives while also boosting the economy and thus ensuring a viable ecological transition. Metakaolin is the calcined clay with the highest potential for a use as SCM, especially because of its high reactivity, the relatively low calcination temperature and the availability across the world. In recent years, the use of calcined kaolinite-based clays as SCM has been an important research focus while the other types of clays have been neglected. However, using new clays as SCMs is essential to develop more sustainable cements in regions where kaolinite is not available. This study investigates and compares the calcination and the use as SCMs of two commercial clays: a palygorskite (whose reactivity in cementitious media has not yet been studied) and a kaolinite. The physico-chemical modifications induced by the thermal treatment were first investigated by X-ray diffraction, ^{27}Al and ^{29}Si MAS NMR analyses. The reactivity was then studied with pozzolanic activity tests and mechanical performance measurements in cementitious systems. The results show that palygorskite behaves quite differently from kaolinite during calcination, it exhibits longer and gradual dehydroxylation kinetics. The quantification of the evolution of the relative proportion of 4-fold, 5-fold and 6-fold aluminium has shown that the increase in pozzolanic reactivity can be linked to the formation of 4-fold and 5-fold aluminium during the calcination. Although calcined palygorskite exhibits pozzolanicity lower than metakaolin, it ranks in the highly reactive SCMs. The results showed a significant increase of mechanical performance on pastes incorporating only 10% of calcined palygorskite in comparison to the reference (100% Portland cement) which indicates that calcined palygorskite can be a suitable SCM once calcined. This open new ways of development of blended cement in locations where kaolin is not available.

6.2. Introduction

The COP26 in Glasgow set the objective of limiting the global temperature increase to +1.5°C compared to pre-industrial levels by 2050 [1]. This will require strong mitigation measures across all economic sectors, including the cement industry, which is estimated to be responsible of about 8% of global anthropogenic CO_2 emissions [2].

Paradoxically, concrete (of which cement is the main component) remains one of the least carbon-intensive construction material, since 1kg of concrete emits an average of 0.13 kg of CO_2. In comparison, 1 kg of wood or steel emits 0.46 and 2.8 kg of CO_2 respectively [3]. The fact that the cement industry is responsible for so much CO_2 emissions is explained by the quantities involved. The widespread urbanization that accompanies economic development results in the rapid construction of industrial and transport infrastructure, which leads to a significant increase in cement demand [4]. In 2019, 4.2 billion tons of cement were produced worldwide, suggesting that it is not the cement itself but its intensive use that makes it a polluting construction material [5]. In this context, the cement industries are turning to research and development of new innovations that can reduce the environmental cost of cement to achieve the COP26 objectives while also boosting the economy and thus ensuring a proper ecological transition. A few percent reduction in the amount of CO_2 emitted during the manufacture of 1kg of cement would have a significant impact on global anthropogenic CO_2 emissions, provided that these innovations are implemented on a large scale.

The use of Supplementary Cementitious Materials (SCMs) as a substitute for clinker is a well-known technology that can be used to reduce the environmental cost of cement. These supplementary cementitious materials (SCMs) allow the proportion of clinker (the main component of cement which causes most of the CO_2 emissions) to be reduced without significantly affecting the mechanical properties or durability of cementitious products. Among the SCMs widely used today are blast furnace slag [6] and coal power plant fly ash [7]. Unfortunately, blast furnace slag resources are not abundant enough to be used sustainably and the energy transition rightly limits the availability of fly ash resources from coal combustion [8]. The use of calcined clays as SCMs is now gaining popularity, as the reserves of clays with calcination potential are considerable and evenly distributed [9], making them a

first-choice resource for use as SCM. Numerous studies have been carried out in recent years on the reactivity of different types of calcined clays in cementitious systems and the results are unanimous: kaolinitic calcined clays is the most promising [10–13] while calcined smectites [14–17] and illites [16,18–20] show much fewer encouraging results. However, it is worth remembering that clays are not limited to kaolinite, smectite and illite families. There are other clays which are less conventional and less abundant, but which should be studied to propose new alternatives to kaolinitic clays.

Previous publications investigating the calcination and reactivity of dolomitic marlstones containing palygorskite [21–23] showed that this clay can have a potentially high pozzolanic reactivity. This hypothesis was confirmed in a subsequent publication which highlighted the high potential of calcined palygorskite for a use as SCM [24]. The objective is now to identify the factors that explain this strong reactivity and to place this calcined clay in comparison to metakaolin (which is the current reference in term of calcined clays). This paper includes the quantification of the relative proportion of 4-fold, 5-fold and 6-fold aluminium as function of the calcination temperature as well as the evolution of the silicon environment, the pozzolanic activity and compressive strength in cementitious systems. The main objective is to characterize precisely the physico-chemical modifications taking place during calcination, to relate these modifications to the pozzolanic reactivity and to the mechanical performance in a cementitious system.

6.3. Materials and experimental methods

6.3.1. Materials

The palygorskite (PFl-1) and kaolinite (KGa-1b) samples are references clays provided by the Clay Minerals Society from their repository of Source Clays. Baseline studies have been done by Chipera and Bish [25] on these two commercial samples by semi quantitative X-ray Diffraction (XRD) analysis. The mineralogical compositions of PFl-1 and KGa-1b are presented in table 6-1.

PFl-1					
Phase	**Palygorskite**	**Smectite**	**Quartz**	**Feldspar**	**Other**
wt.%	79	11	6	4	1
KGa-1b					
Phase	**Kaolinite**	**Anatase**	**Crandallite**		
wt.%	96	3	1		

Table 6-1: Mineralogical composition of PFl-1 and KGa-1b

PFl-1 contains 79% palygorskite associated with 11% smectite. The joint occurrence of palygorskite and smectite is typical, as one mechanism of palygorskite formation is based on the alteration of smectite [26–28]. The rest of the sample is composed of common minerals such as quartz and feldspar. KGa-1b contains 96% kaolinite associated with 3% of anatase and 1% of crandallite.

The chemical analysis of the raw materials was carried out by X-Ray Fluorescence (XRF), the proportions of oxides (expressed in weight %) are presented in table 6-2.

Table 6-2: Chemical analysis of PFl-1 and KGa-1b

	Oxydes	**SiO_2**	**Al_2O_3**	**MgO**	**Fe_2O_3**	**CaO**	**P_2O_5**	**K_2O**	**TiO_2**	**Cr_2O_3**	**LOI (1050°C)**
PFl-1	wt. %	57.6	10.2	9.3	3.1	1.7	0.8	0.8	0.4	0.2	16.7
KGa-1b	wt. %	46.0	40.0		0.2		0.1		1.6	0.2	13

The main oxides are SiO_2 and Al_2O_3 for KGa-1b and SiO_2, Al_2O_3 and MgO for PFl-1. The occurrence of MgO and Fe_2O_3 in PFl-1 comes from palygorskite, which is a TOT clay that incorporates magnesium and iron in its octahedral sheets in substitution of aluminium. KGa-1b contains a proportion of aluminium almost 4 times higher than that of PFl-1.

Table 6-3 display the particle size distributions of the general use cement (GU cement), PFl-1 and KGa-1b before and after calcination at 800°C

Table 6-3: Particle size distributions of the general use cement (GU cement), PFl-1 and KGa-1b before and after calcination at 800°C.

Label	d10 (μm)	d50 (μm)	d90 (μm)
PFl-1	4,6	19.1	70,2
800°C-PFl-1	5,3	22,1	98,7
KGa-1b	1,0	3,6	26,8
800°C-KGa-1b	1,0	3,8	25,4
GU cement	3.5	20.5	59.7

6.3.2. Thermogravimetric analysis and Differential Scanning Calorimetry (TGA/DSC)

TGA/DSC analysis were carried out with a SETARAM SESTYS 24 thermal analyzer from 30°C to 1200°C with a heating rate of 10°C/min under atmospheric conditions.

6.3.4. Calcination

The calcination was carried out in alumina crucibles using a silicon carbide laboratory furnace chamber without atmosphere control. The PFl-1 sample was heated at the same temperatures plus 525 and 550°C. After calcination, the samples were left overnight to cool down to 20°C (door closed). This calcination protocol was performed in accordance with the existing bibliography [15,16,21,29–31].

6.3.5. X-ray diffraction analysis

The X-ray diffraction measurements were carried out on a Bruker D8 powder diffractometer using a Bragg-Brentano geometry. The X-ray was generated by a copper anode tube (40 kV / 40 mA) that emits Cu Kα1 radiation (8 keV) of a wavelength λ = 1.5418 Å. The diffractograms

were acquired between 5° and 60° 2θ, with a step size of 0.017° 2θ and a measurement time of 1 second per step.

6.3.6. Nuclear magnetic resonance

The ^{27}Al MAS NMR spectra were acquired using a MAS probe of 2.5 mm on a Bruker Avance III 500 MHz spectrometer. The length of the excitation pulse used was π/13 for a radio frequency field of 11 kHz. The MAS frequency was 30 kHz and the repetition time was 1 second. For all the acquisitions a ^{1}H decoupling was performed, and an aqueous solution of $Al(NO_3)_3$ was used as the reference for the ^{27}Al MAS NMR spectra. The quantification by spectral decompositions was done using the dmfit software [32].

The ^{29}Si MAS NMR spectra were acquired using a MAS probe of 7 mm on a Bruker NEO 300 MHz spectrometer. The length of the excitation pulse used was π/2 and the MAS frequency was 5 kHz with a repetition time of 10s. Spectra were referenced against TMS (Tetramethylsilane).

6.3.7. Pozzolanic activity: a modified Chapelle test

The pozzolanic activity of each material (raw and calcined) was assessed by using the modified Chapelle test according to the NF P18-513 standard (annex A) [33]: 1g of dry SCM was mixed with 2g of CaO in 250 ml of CO_2-free distilled water. The suspension was then heated to 85°C (+/- 5°C) with continuous stirring for 16 hours. After 16 hours the solution was cooled to room temperature with tap water and the amount of remaining portlandite was determined by sucrose extraction and acid titration. The results is expressed in mg $Ca(OH)_2$ fixed /g calcined clay.

6.3.8. Pozzolanic activity: isothermal calorimetry

The reactivity of each materials (raw and calcined) was assessed by measuring the cumulative heat release according to ASTM C1897 [34] : 10g of dry SCM was mixed at 40°C with 30g of $Ca(OH)_2$, 5g of $CaCO_3$ and 54g of potassium solution. 15g of the freshly mixed paste was then cast and placed into the calorimeter measurement chamber. The heat release was recorded

at 40°C for 168h (7 days) after mixing. The cumulative heat was assessed by integrating the recorded heat release and converted in units of J/g of SCM.

6.3.9. Calcined clay-cement blends and compressive strength measurements

The compressive strength was assessed on paste cubes (20 x 20 x 20 mm^3) made with a water to binder ratio (w/b) of 0.4. Calcined clay-cement blends were obtained by mixing 90 wt.% of general use grey Portland cement (GU) with 10 wt.% of 800°C calcined PFl-1 (for P-PFl-1 paste) or 10 wt.% of 800°C calcined KGa-1b (for P-KGa-1b paste). The choice of this percentage of replacement was made in order to ensure workable mixtures, as higher clay contents of PFl-1 and KGa-1b would lead to high water demand. The particle size distributions of the GU cement, PFl-1 and KGa-1b (before and after calcination) are shown in Table 6-3.

Control cement paste (labelled P-Ref) were prepared using 100 wt.% GU cement as cementing material. A polycarboxylate (PC) superplasticizer was used to obtain a slump flow of the blended systems equivalent to that of the control mixture.

Pastes were mixed and specimens were molded in 20x20x20 cm^3 molds after which they were placed in plastic bags for 20h-24h until demolding. The demolded pastes cubes were stored in saturated lime water until testing. At 7 and 28 days the compressive strength was assessed with a loading procedure adapter from the ASTM C109 loading procedure [35].

6.3.10. Calcined clay-cement blends and x-ray diffraction analysis

Cementitious pastes were prepared following the same protocol as for compressive strength measurements and cast in cylindrical molds. Samples were demolded after 24h (first analysis) and stored in small volume of water (to avoid leaching) until testing. X-ray diffraction analyses were conducted on fresh discs after 1, 3, 7 and 28 days of hydration using a PANalytical X'Pert pro MPD diffractometer equipped with a PIXcel 1D detector (active length of 3.347°2θ). The tube voltage and current were 40 kv and 50 mA respectively. Measurements were carried out using a Bragg-Brentano geometry with 0.04 rad Soller slits, an anti-scatter slit of ½° and incident divergence slit of ½°. The diffractograms were acquired between 5° and 70° 2θ, with

a step size of 0.0267° 2θ and a measurement time of 0.3 second per step. Samples were rotated at 2 rotations per second during the acquisition. Rietveld refinements were performed using the PANalytical software HighScore Plus 4.7a. An external standard (Alfa Aesar, α-Al_2O_3 corundum) was also scanned and analyzed to allow quantification of the non-crystalline content.

6.4. Results and discussion

6.4.1. Thermogravimetric analysis and differential scanning calorimetry

Figure 6-1 displays the TGA/DSC analysis of the palygorskite (PFl-1) and kaolinite (KGa-1b) samples as function of the temperature.

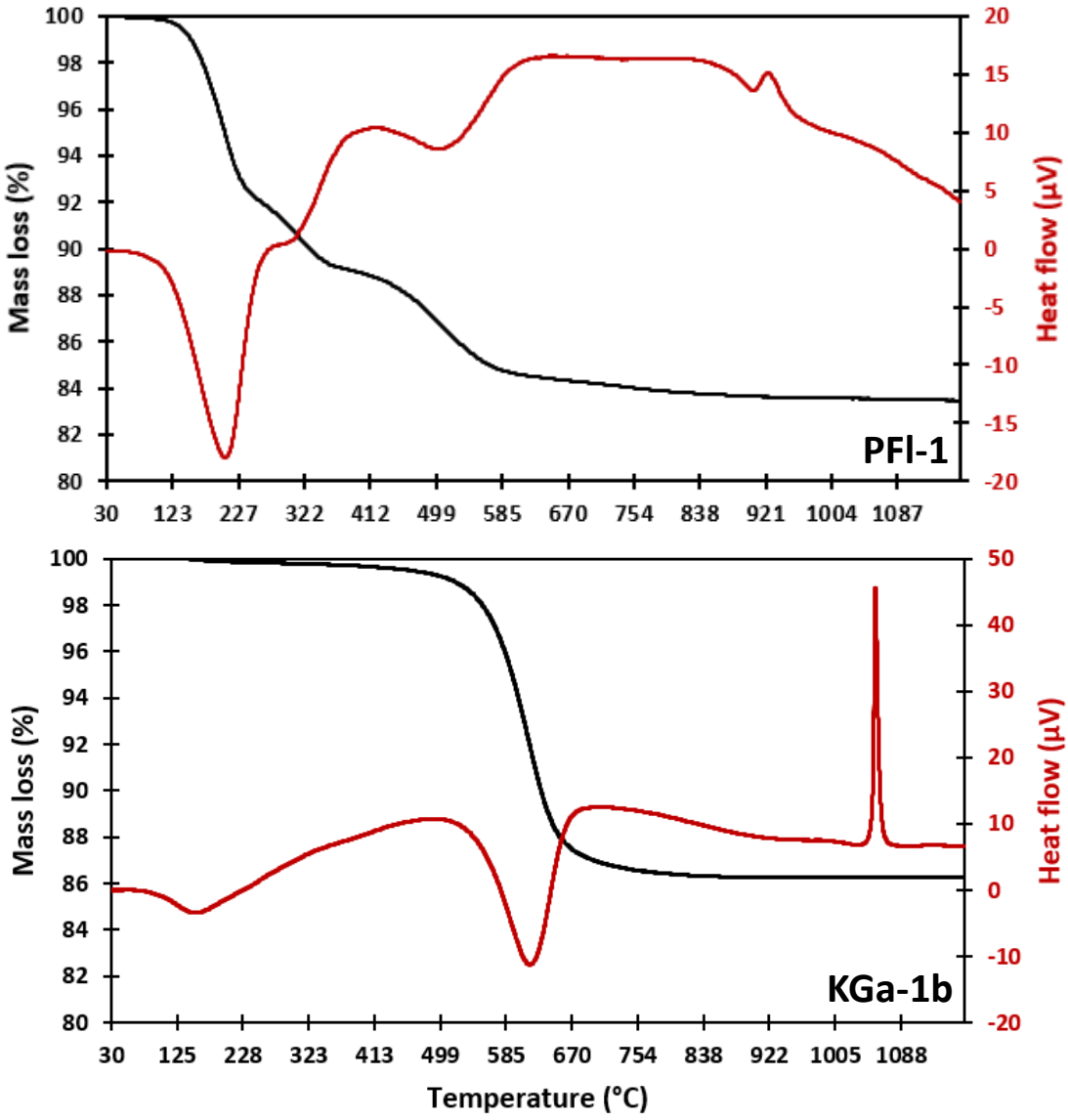

Figure 6-1: Thermogravimetric analysis and differential scanning calorimetry curves of the palygorskite (PFl-1) and kaolinite (KGa-1b) samples.

The TGA and DSC curves of PFl-1 can be separated in four steps:

- 30 – 230°C : a mass loss of 8% is associated with an endothermic peak, which corresponds to the dehydration of interparticle and interlayer water of smectite and part of zeolitic water of palygorskite [36].
- 230 – 330°C : a mass loss of 3% is associated with an endothermic peak, which corresponds to the dehydration of the remaining zeolitic water of palygorskite [36].
- 330 – 580°C : a mass loss of 4% is associated with an endothermic peak, which corresponds to the dehydroxylation of palygorskite and smectite [37,38].
- 900°C : an exothermic peak corresponds to a recrystallization phenomenon [39].

The TGA and DSC curves of KGa-1b can be separated in three steps:

- 30-180°C : a mass loss of 0.2% is associated with an endothermic peak, which corresponds to the desorption of surface water of kaolinite [40].
- 470 – 670 : a mass loss of 14% is associated with an endothermic peak, which corresponds to the dehydroxylation of kaolinite [41].
- 1050°C : an exothermic peak corresponds to a recrystallization phenomenon [42].

It appears that PFl-1 and KGa-1b have a different sensitivity to heat treatment. For PFl-1, there several dehydration steps can be explained by the occurrence of palygorskite and smectite. Palygorskite has a particular TOT structure in channels which allows storage of zeolitic water. By the nature of its interfoliar cations, smectite can store water molecules in the interfoliar space. The occurrence of these two clay minerals in PFl-1 explains the existence of these different phases of dehydration of the interfoliar space and the zeolitic channels. In contrast, kaolinite has a TO structure that limits water retention, which will only occur through adsoprtion on the surfaces. The dehydroxylation of KGa-1b occurs at slightly higher temperatures (470-670°C) than PFl-1 (330-580°C) but is also much more significant, with a mass loss of 14% compared to only 4% for PFl-1. This can be explained by the ratio of octahedral to tetrahedral cations, which is higher for kaolinite than for palygorskite and smectite. Knowing that dehydroxylation takes place on the octahedral cations, it is expected that dehydroxylation will be higher for KGa-1b than for PFl-1. These results are in accordance with the existing literature on the TGA/DSC analysis of kaolinite and palygorskite [36–42].

In order to characterize the evolution of the crystalline phases during calcination it was decided to carry out an X-ray diffraction analysis.

6.4.2. X-ray diffraction analysis

Figure 6-2 displays the evolution of the diffractograms of the palygorskite (PFl-1) and kaolinite (KGa-1b) samples as function of the calcination temperature.

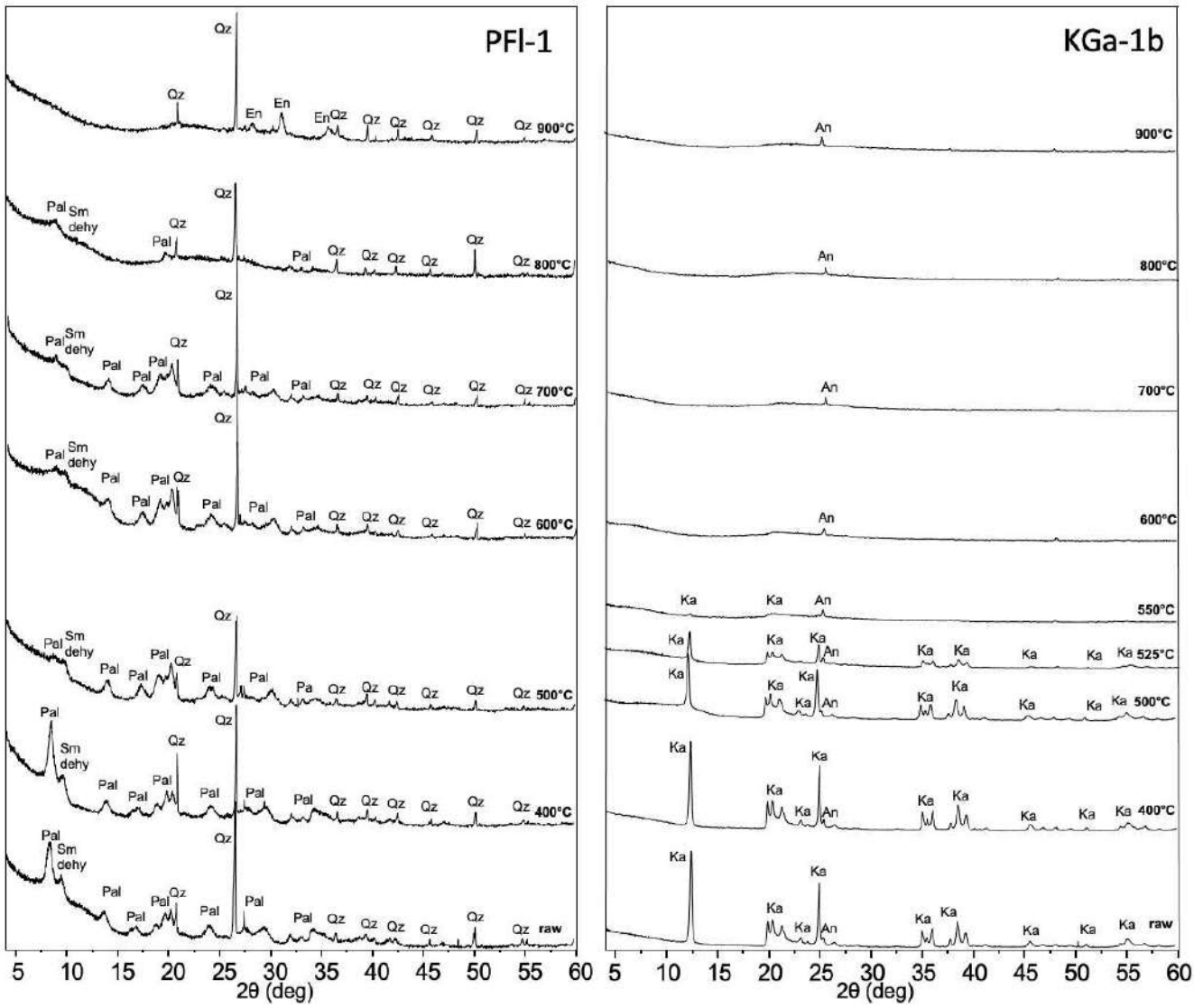

Figure 6-2: Evolution of the X-ray diffractograms of the palygorskite (PFl-1) and kaolinite (KGa-1b) samples as a function of the calcination temperature. Pal = palygorskite ; Sm dehy = dehydrated smectite ; Ka = kaolinite ; An = anatase ; Qz = quartz ; En = enstatite.

The diffractogram of the raw PFl-1 shows the characteristic peaks of palygorskite, smectite and quartz. From 500°C and with increasing calcination temperature, the intensity of the

peaks associated with palygorskite and smectite is decreasing gradually. These peaks are no longer detectable above 900°C and there is the apparition of new peaks associated with enstatite. The recrystallization of enstatite at 900°C is in accordance with TGA/DSC results. This phenomenon could reduce the reactivity of calcined PFl-1 as Si and Al will be trapped into a metastable neoformed phase. With increasing the calcination temperature, the peaks associated with quartz do not evolve and are still detectable after 900°C, meaning that this phase resist well to the heat treatment.

The diffractogram of the raw KGa-1b shows the characteristic peaks of kaolinite and anatase. From 500°C and with increasing calcination temperature, there is a decrease in the intensity of peaks associated with kaolinite until they are no longer detectable after 600°C. Anatase is not affected by the heat treatment and its XRD signature is still detectable after 900°C. Furthermore, the high temperature calcination of KGa-1b does not lead to recrystallisation phenomena which could reduce the reactivity. This agrees with the TGA/DSC results, which state that a temperature of 1050°C is required to achieve recrystallisation.

Comparison of the two samples shows that they do not behave in the same way when subjected to heat treatment. For PFl-1, the crystal structures of palygorskite and smectite resists well to heat treatment (up to more than 800°C) and their loss of crystallinity is gradual. On the other hand, for KGa-1b, the loss of crystallinity of kaolinite is very fast and occurs entirely between 500 and 600°C of calcination temperature. Thus, PFl-1 and KGa-1b have has completely different calcination behaviors.

6.4.3. ^{27}Al Nuclear magnetic resonance analysis

Figure 6-3 displays the evolution of the ^{27}Al MAS NMR spectra of the palygorskite (PFl-1) and kaolinite (KGa-1b) samples as a function of the calcination temperature.

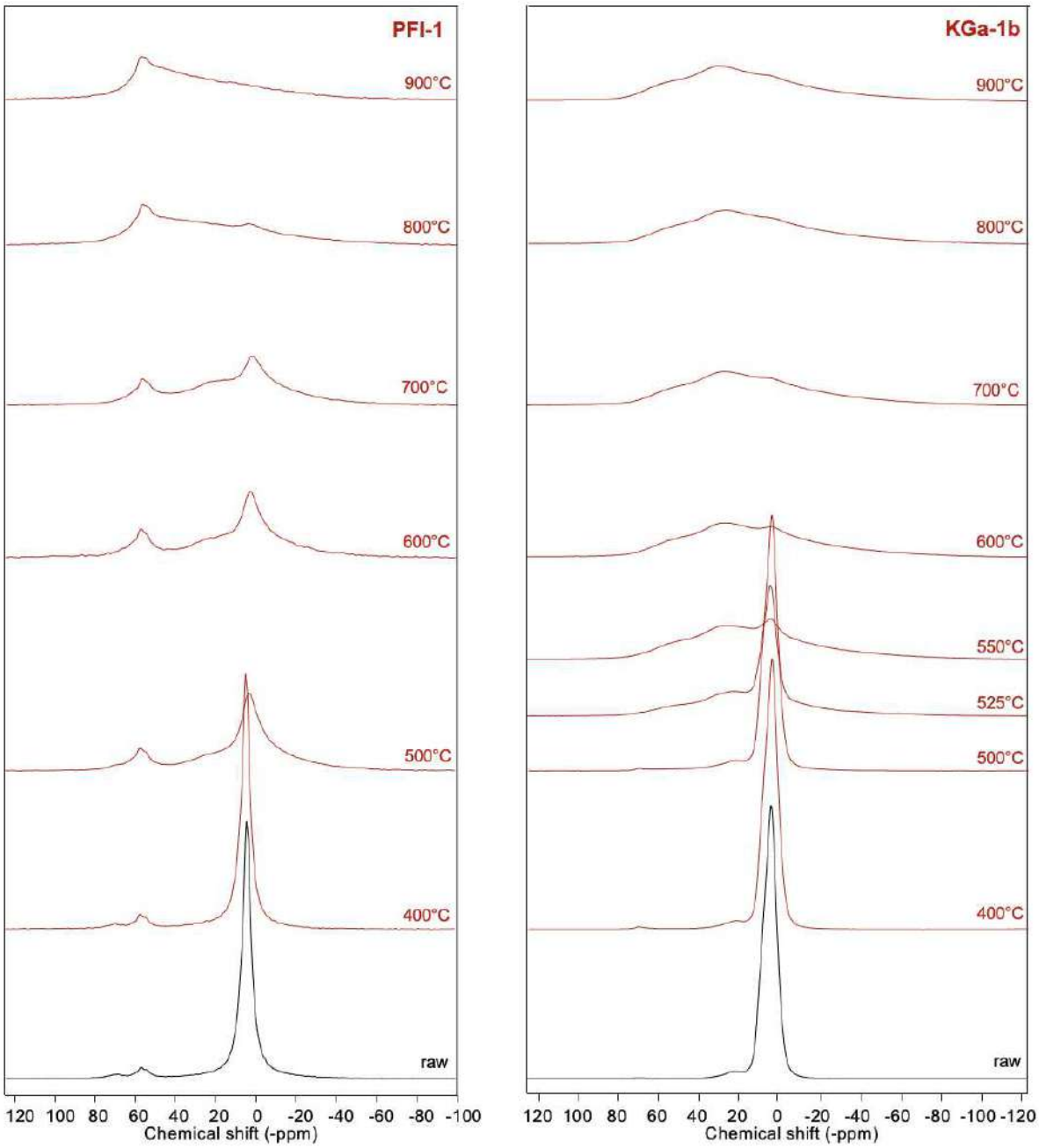

Figure 6-3: Evolution of the ^{27}Al MAS NMR spectra of the palygorskite (PFl-1) and kaolinite (KGa-1b) samples as a function of the calcination temperature.

The ^{27}Al MAS NMR spectrum of the raw PFl-1 sample exhibits three main resonances at 3, 58 and 70 ppm. The 3 ppm line corresponds to 6-fold aluminium [42] and can be associated with octahedral aluminium present within the palygorskite and smectite structures. The 70 ppm line corresponds to 4-fold aluminium [42] and can be associated with isomorphic substitutions within the palygorskite and/or smectite tetrahedra [43]. The 57 ppm line corresponds to AlO_4 $q^4(4Si)$ [44] and can be associated with the feldspar phase detected by Chipera and Bish [24].

The increase in calcination temperature leads to a diminution of the 6-fold aluminium line intensity (70 ppm). This diminution is accompanied by the appearance of two new resonances at 30 ppm and 59 ppm, which correspond to 5-fold and 4-fold aluminium, respectively [42]. The change in the coordination of aluminium atoms is a consequence of the dehydroxylation of the clay phases. From a ^{27}Al MAS NMR perspective, the dehydroxylation of palygorskite (and smectite) takes place progressively from 500°C up to 900°C.

The ^{27}Al MAS NMR spectrum of the raw KGa-1b sample exhibits two main resonances at 3 and 70 ppm, which correspond to 6-fold and 4-fold aluminium, respectively [42]. They can be associated with octahedral and tetrahedral aluminium present within the kaolinite structure. The shoulder at ~25 ppm comes from the external satellite transition (ST2) of the 6-fold aluminium [45]. As for the PFl-1 sample, the increase in calcination temperature leads to a dehydroxylation of the clay phase. This results in a decrease of intensity of the 6-fold aluminium resonance associated with the appearance of two new resonances at 30 and 59 ppm, which correspond to 5-fold and 4-fold aluminium, respectively [42]. In contrast to palygorskite and smectite, the dehydroxylation of kaolinite is occurring almost entirely in between 500 and 600°C.

These results confirm the XRD results and demonstrate that the two samples have a completely different behavior during the heat treatment. According to the ^{27}Al MAS NMR results, kaolinite dehydroxylates very easily at temperatures between 500 and 600°C, whereas palygorskite (and smectite) has more inertia and dehydroxylates progressively from 500°C up to 900°C.

The comparison of TGA/DSC and ^{27}Al MAS NMR results shows an inconsistency in the optimum calcination temperature. On the one hand, TGA/DSC results suggest that most of the dehydroxylation of palygorskite takes place between 330 and 580°C (see figure 6-1). At higher temperatures, no significant mass changes or heat flow is recorded until recrystallisation at 900°C. Similar results were obtained by Snellings et al [46] who observed a dehydroxylation of palygorskite (by differential thermal analysis) between 380 and 580°C.

On the other hand, the ^{27}Al MAS NMR analyses suggest that the dehydroxylation of palygorskite occurs gradually between 400 and 800°C. There is a change in coordination of the aluminium atoms well after 600°C of calcination temperature. Therefore, it is questionable whether the change in coordination of the aluminium atoms is a direct consequence of dehydroxylation. In such case, there should be a TGA/DSC a variation in the signal even after 600°C. It is also important to note that for the kaolinite sample, the TGA/DSC and ^{27}Al MAS NMR results correlate well and both support that dehydroxylation occurs between 500 and 600°C. Although the two techniques do not operate on the same scale, it is very surprising to have this divergence of results for palygorskite and not for kaolinite. Further investigations are therefore needed.

6.4.4. ^{29}Si Nuclear magnetic resonance

Figure 6-4 displays the evolution of the ^{29}Si MAS NMR spectra of the palygorskite (PFl-1) and kaolinite (KGa-1b) samples as function of the calcination temperature.

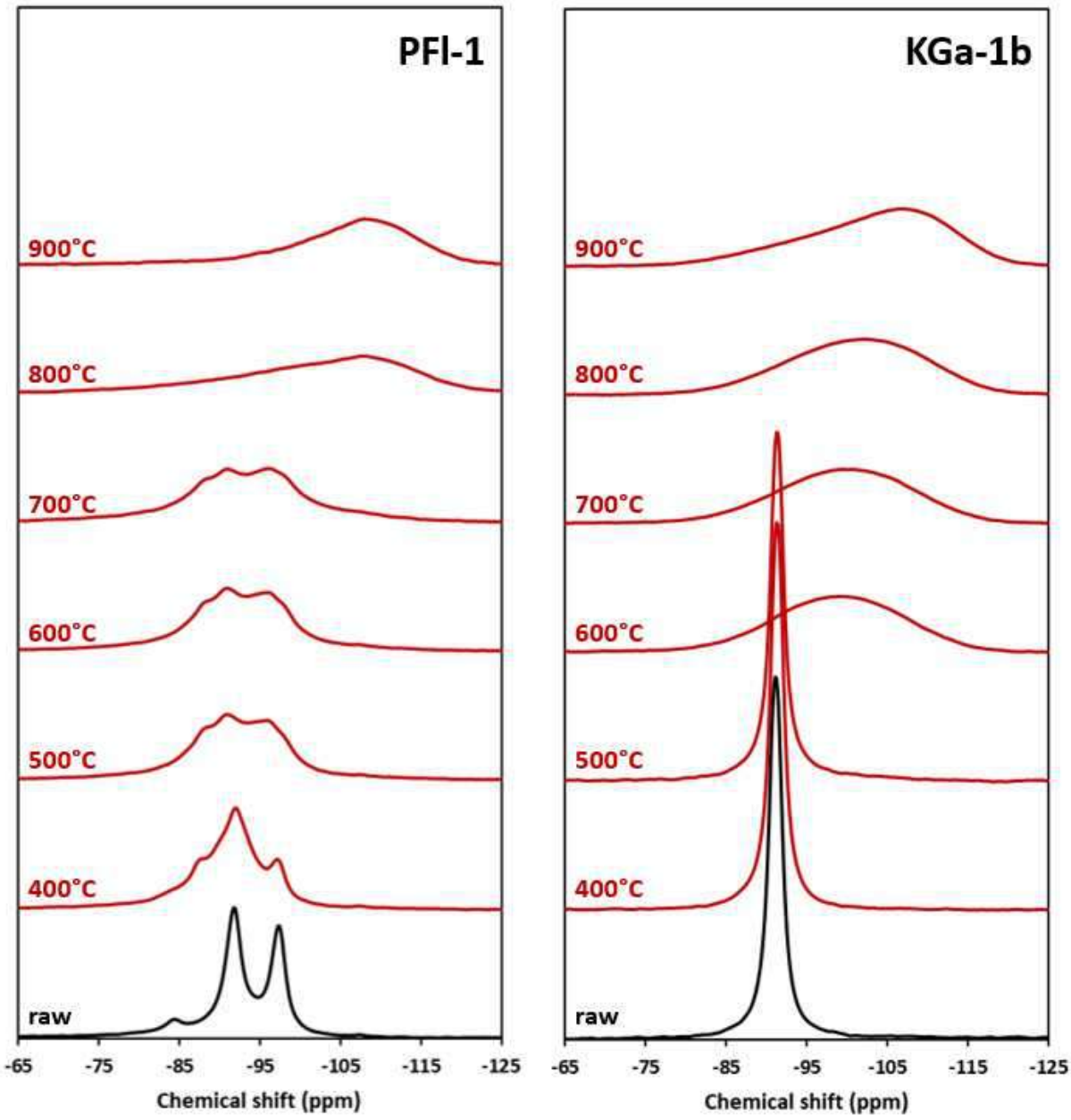

Figure 6-4: Evolution of the ^{29}Si MAS NMR spectra of the palygorskite (PFl-1) and kaolinite (KGa-1b) samples as a function of the calcination temperature.

The ^{29}Si MAS NMR spectra of the raw PFl-1 shows two main resonances at -92 and -97 ppm, which corresponds to Q^3 silicon sites that can be associated with silicon from the edges and the center of palygorskite tetrahedra, respectively [47]. The weak band at -84 ppm can be assigned to Q^3(1Al) of palygorskite as suggested by Komarnemi et al [48] (in this case, the intensity of this Q^3(1Al) resonance can be related to the amount of tetrahedral aluminium, higher is the intensity, higher is the incorporation of aluminium in tetrahedral position). On

the other hand, this resonance could also be assigned to terminal SiOH in the micropores (generated by the channels of palygorskite), as suggested by Barron et al [49].

The ^{29}Si MAS NMR spectrum of raw KGa-1b exhibit one main resonance at -91 ppm, which is characteristic of silicon in Q^3 configuration that can be associated with silicon of kaolinite tetrahedra [42,50].

For PFl-1, the increase of the calcination temperature leads to a broadening of the resonances associated with the Q^3 of palygorskite, which reflects a larger distribution of the local environments of silicon atoms and indicates a structural loss of palygorskite [51]. Between 700 and 800°C, a low-frequency shift of the Q^3 resonances is observed. This shift indicates an evolution of the silicon environment, from Q^3 amorphous silica to condensed Q^4 silica [16]. Two main stages are therefore distinguished during the calcination of PFl-1. A first step of progressive amorphisation between 400 and 700°C followed by a silicon condensation after 700°C.

For KGa-1b, there are no major differences up to 500°C of calcination temperature. From 600 °C, however, the spectra change completely. The width of the signal increases (reflecting the presence of amorphous material) and the center of gravity of the signal is now located between -99 and -101 ppm. From 600°C to 900°C, this low-frequency shift will continue until -107 ppm which is characteristic of condensed Q^4 silica. This condensation phenomenon has already been described in the literature [42,50].

For both PFl-1 and KGa-1b the appearance of silicon in the Q^4 configuration can be explain by the formation of an amorphous silica gel. The formation of this sillica gel is due to the segregation of silicon (as evidenced by the low-frequency position of the resonance) from the calcined clay phases [50]. The absence of recrystallisation of new phases detectable by XRD (whose ^{29}Si MAS NMR signature is in this chemical shift range) tends to confirm this hypothesis. By comparing KGa-1b and PFl-1, it appears that this segregation phenomenon starts from 600°C for KGa-1b while 800°C is necessary for PFl-1. The segregation of silicon from the calcined clay phases will result in a change in the coordination of the aluminium atoms from the calcined clay phases, which is verified by the ^{27}Al MAS NMR spectra (see figure 6-3).

6.4.5. Dehydroxylation and pozzolanic reactivity

To better understand the role of the dehydroxylation in the reactivity of these calcined clays, the different aluminium coordinations were quantified by spectral integration (see supporting informations). The relative proportions of 4, 5 and 6-fold aluminium are then compared with the $Ca(OH)_2$ consumption (modified Chapelle test) and the cumulative heat release (isothermal calorimetry) for both PFl-1 and KGa-1b samples. The main objective is to determine whether there is a link between the appearance of aluminium 4 and 5 and the increase in pozzolanic reactivity.

Figure 6-5 displays the evolution of the relative proportions (%) of Al(IV), Al(V) and Al(VI) and the $Ca(OH)_2$ consumption ($mg(Ca(OH)_2/g$ calcined clay) of the palygorskite (PFl-1) and kaolinite (KGa-1b) samples as function of the calcination temperature.

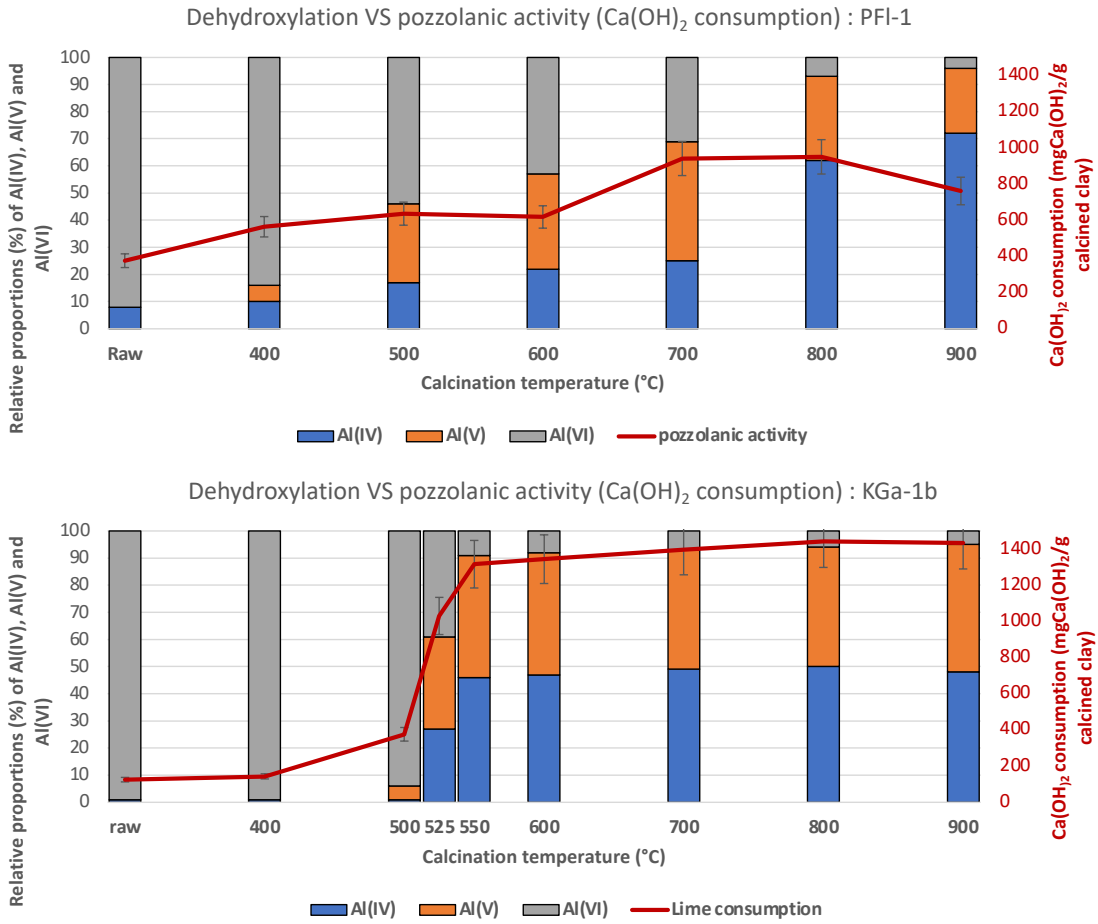

Figure 6-5: Evolution of the relative proportions of Al(IV), Al(V) and Al(VI) and the pozzolanic activity ($Ca(OH)_2$ consumption) of the palygorskite (PFl-1) and kaolinite (KGa-1b) samples as a function of the calcination temperature.

For the KGa-1b sample the evolution of the $Ca(OH)_2$ consumption seems to closely follows the evolution of the aluminium environment (diminution of the proportion of Al-6 and apparition of Al-4 and Al-5). The $Ca(OH)_2$ consumption increases abruptly from 500°C and reaches a plateau at 550°C. It is in this temperature range that most of the dehydroxylation of kaolinite occurs. From 550°C, it could be possible that the heat treatment allowed the creation of enough defects (dehydroxylated aluminium) to trigger a complete dissolution process. These defects are points of weakness in the structure of the kaolinite which will facilitate the releases of the aluminium, followed by the silicon and allow their reaction with the calcium from the $Ca(OH)_2$.

For the PFl-1 sample, the evolution of the $Ca(OH)_2$ consumption is completely different. Firstly, the raw PFl-1 has three time the $Ca(OH)_2$ consumption of the raw KGa-1b (376 against 125 mg $Ca(OH)_2$/g). This could be explained by the particular structure of palygorskite, which is three-dimensional and therefore has a higher specific surface area, facilitating its dissolution and reaction with $Ca(OH)_2$. Secondly, as the calcination temperature increase, the $Ca(OH)_2$ consumption gradually increases and reaches its maximum at a temperature of 800°C (950 mg $Ca(OH)_2$/g). Between 500°C and 600°C, the relative proportions of 4 and 5-fold aluminium increase (as confirmed by the loss of mass on TGA/DSC results in figure 6-1), but the pozzolanic activity remains constant at around 625 mg $Ca(OH)_2$/g. The same observation can be done between 700°C and 800°C (but this time, the pozzolanic activity increase). The decrease in pozzolanic activity between 800°C and 900°C can be explained by the precipitation of the enstatite observed by XRD. It therefore seems that the $Ca(OH)_2$ consumption by PFl-1 does not closely follows the apparition of 4 and 5-fold aluminium (especially at 600 and 800°C).

It is difficult to characterize the pozzolanic reactivity of a calcined clay by its $Ca(OH)_2$ consumption only. Indeed, the modified Chapelle test does not take into account the influence of the pore solution on the kinetics of the pozzolanic reaction. Pozzolanic activity was therefore also measured by using the ASTM C1897 standard [52].

Figure 6-6 displays the evolution of the relative proportions (%) of Al(IV), Al(V) and Al(VI) and the 7 days cumulative heat release (J/g calcined clay) of the palygorskite (PFl-1) and kaolinite (KGa-1b) samples as function of the calcination temperature.

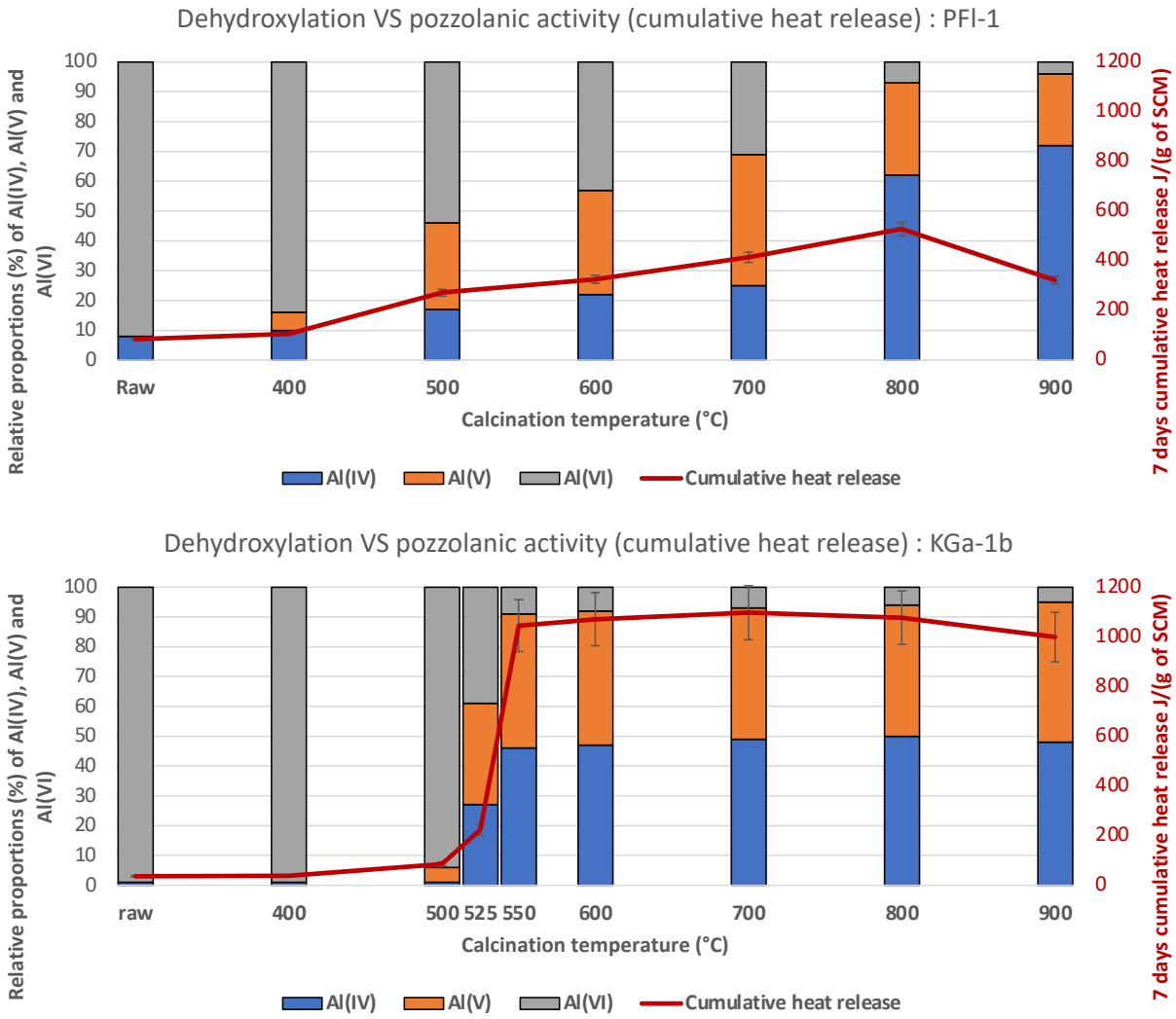

Figure 6-6: Evolution of the relative proportions of Al(IV), Al(V) and Al(VI) and the pozzolanic activity (cumulative heat release) of the palygorskite (PFl-1) and kaolinite (KGa-1b) samples as a function of the calcination temperature.

As with the $Ca(OH)_2$ consumption measurements (figure 6-5), for KGa-1b, the evolution of the cumulative heat release closely follows the evolution of 4 and 5-fold aluminium proportions : A significant increase in cumulative heat release occurs between 500 and 600°C, temperatures between which most of the dehydroxylation of kaolinite takes place.

For PFl-1, unlike with the $Ca(OH)_2$ consumption measurements (figure 6-5), the evolution of the cumulative heat released this time closely follows the evolution of 4 and 5-fold aluminium proportions. The increase in cumulative heat release is gradual, reaching a maximum at 800°C,

and then decreases sharply at 900°C due to recrystallization phenomena. The results of the Chapelle test and the cumulative heat release measurements are therefore similar for KGa-1b but there are some differences for PFl-1. It seems that, despite a constant $Ca(OH)_2$ consumption between 700 and 800°C (figure 6-5), there is still an increase in the cumulative heat release (figure 6-6), which reflects an increase in pozzolanic reactivity for PFl-1. ASTM C1897 standard test therefore seems to best represent the pozzolanic reactivity of the aluminous phases (in comparison to the modified Chapelle test) and should be taken into account to simulate the pozzolanic reactivity.

Cement pastes incorporating 10% of each of the two clays, calcined at 500, 600, 700 and 800°C were then made and their compressive strength measured. The main objective being to determine more accurately the best calcination temperature for KGa-1b and PFl-1 and to verify if there is a link between $Ca(OH)_2$ consumption, cumulative heat release and mechanical performance in cementitious systems.

6.4.6. Compressive strength measurements

Figure 6-7 displays the evolution of the compressive strength (MPa) at 7 and 28 days of the reference cement paste (P-Ref) and the cement pastes blended with 10% of PFl-1 (P-PFl-1) and 10% of KGa-1b (P-KGa-1b) calcined at 500, 600, 700 and 800°C.

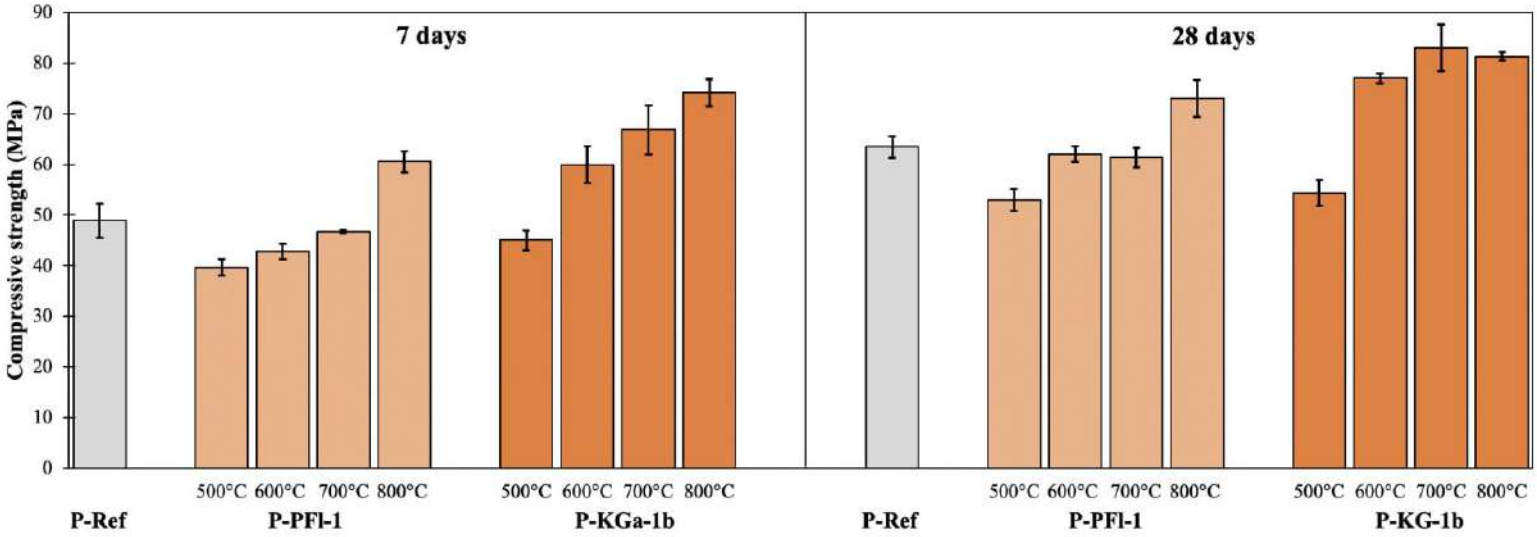

Figure 6-7: Compressive strength at 7 and 28 days of P-Ref, P-PFl-1 (incorporating PFl-1 calcined at 500, 600, 700 and 800°C) and P-KGa-1b (incorporating KGa-1b calcined at 500, 600, 700 and 800°C).

After 7 days of hydration, both P-PFl-1 and P-KGa-1b exhibit an increase in compressive strength with the increase of the calcination temperature. PFl-1 must be calcined at 700°C or 800°C to obtain an equivalent (47 MPa at 700°C) or higher compressive strength value (61 MPa at 800°C) compared to the reference (49 MPa). A calcination at 600°C is sufficient for KGa-1b to provide significant strength improvement (60 MPa).

There is a good correlation between the evolution of compressive strength measurements (figure 6-7) and the evolution of cumulative heat release (figure 6-6) for PFl-1 and KGa-1b. On the other hand, the correlation with the $Ca(OH)_2$ consumption (figure 6-5) is much less obvious, especially for PFl-1 between 700°C and 800°C.

After 28 days of hydration, the compressive strength of pastes incorporating PFl-1 calcined at 600°C and 700°C is equivalent (62 and 61 MPa) to that of the reference (63 MPa). A calcination temperature of 800°C is necessary to achieve a significant increase in compressive strength (73 MPa) on pastes incorporating calcined PFl-1. For KGa-1b, a calcination temperature of 600°C is sufficient to obtain a higher compressive strength (77 MPa) than the reference, and

the difference between 600°C (77 MPa), 700°C (83 MPa) and 800°C (80 MPa) is not significant regarding the standard deviation.

For P-KGa-1b, the compressive strength increase abruptly between 500 and 600°C and remains constant until 800°C which is in good correlation with the evolution of the cumulative heat release (figure 6-6), the $Ca(OH)_2$ consumption (figure 6-5), the dehydroxylation evidenced by ^{27}Al MAS NMR (figure 6-3) and the formation of the silica gel evidenced by ^{29}Si MAS NMR (figure 6-4).

For P-PFl-1, the compressive strength increases more gradually which is also consistent with pozzolanic activity results (figures 6-3 and 6-4). The significant increase in compressive strength between 700 and 800°C (at 7 and 28 days) correlates well with the ^{29}Si MAS NMR results. It seems that the sillica gel formed between 700 and 800°C (highlighted by the formation of Q^4 on figure 6-4) is responsible for the increase in mechanical performance due to a high pozzolanic reactivity. Based on the compressive strength evolution, both calcined PFl-1 and KGa-1b are suitable for a use as SCM and a calcination temperature of 800°C is required for PFl-1 while KGa-1b can be calcined at only 600°C. Furthermore, the compressive strength seems to closely follow the increase of cumulative heat release, the appearance of 4- and 5- fold aluminium and the formation of an amorphous silica gel.

6.4.7. Hydration kinetics analysis

To understand the influence of these supplementary cementitious materials on the hydration kinetics of the cement, the evolution of the crystalline phases has been investigated by X-ray diffraction on two blended cement pastes incorporating 10% of 800°C-PFl-1 and 10% of 800°C-KGa-1b. Figure 6-7 displays the evolution of the crystalline phases of the GU cement paste as a function of the hydration time.

Figure 6-7 displays the evolution of the crystalline phases of GU cement paste as function of the hydration time.

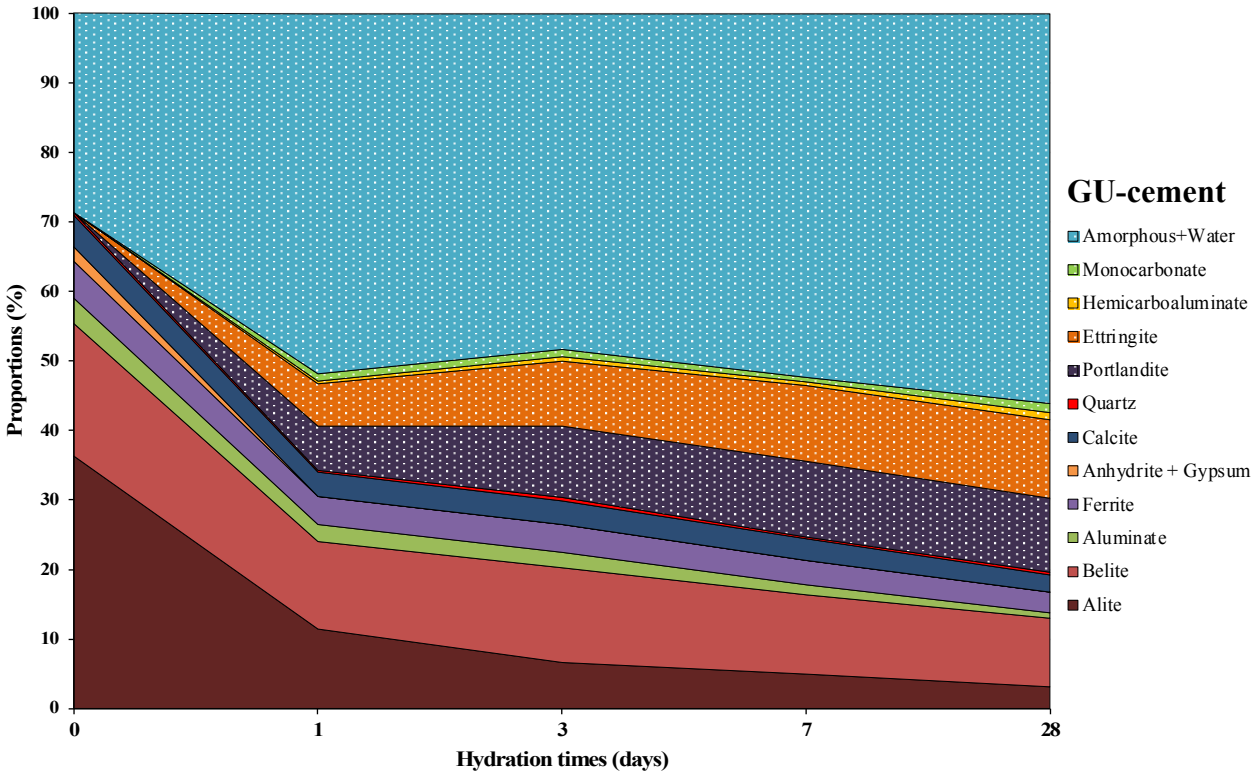

Figure 6-7: Evolution of the crystalline phases of GU cement paste as function of the hydration time.

With the increase of the hydration time, there is a decrease of the proportion of anhydrous phases (alite, belite, aluminate, ferrite) associated with the appearance of hydrates such as portlandite, ettringite and C-S-H (which is amorphous). It is important to note the formation of carboaluminates, which result from the reaction of the aluminous phases of the clinker with the calcite contained in the cement [53]. After 1 day of hydration, all the gypsum and anhydrite have already been consumed to form ettringite and control the hydration of the aluminate phase.

Figure 6-8 displays the evolution of the crystalline phases of 800°C-KGa-1b and 800°C-PFl-1 cement blends pastes as function of the hydration time.

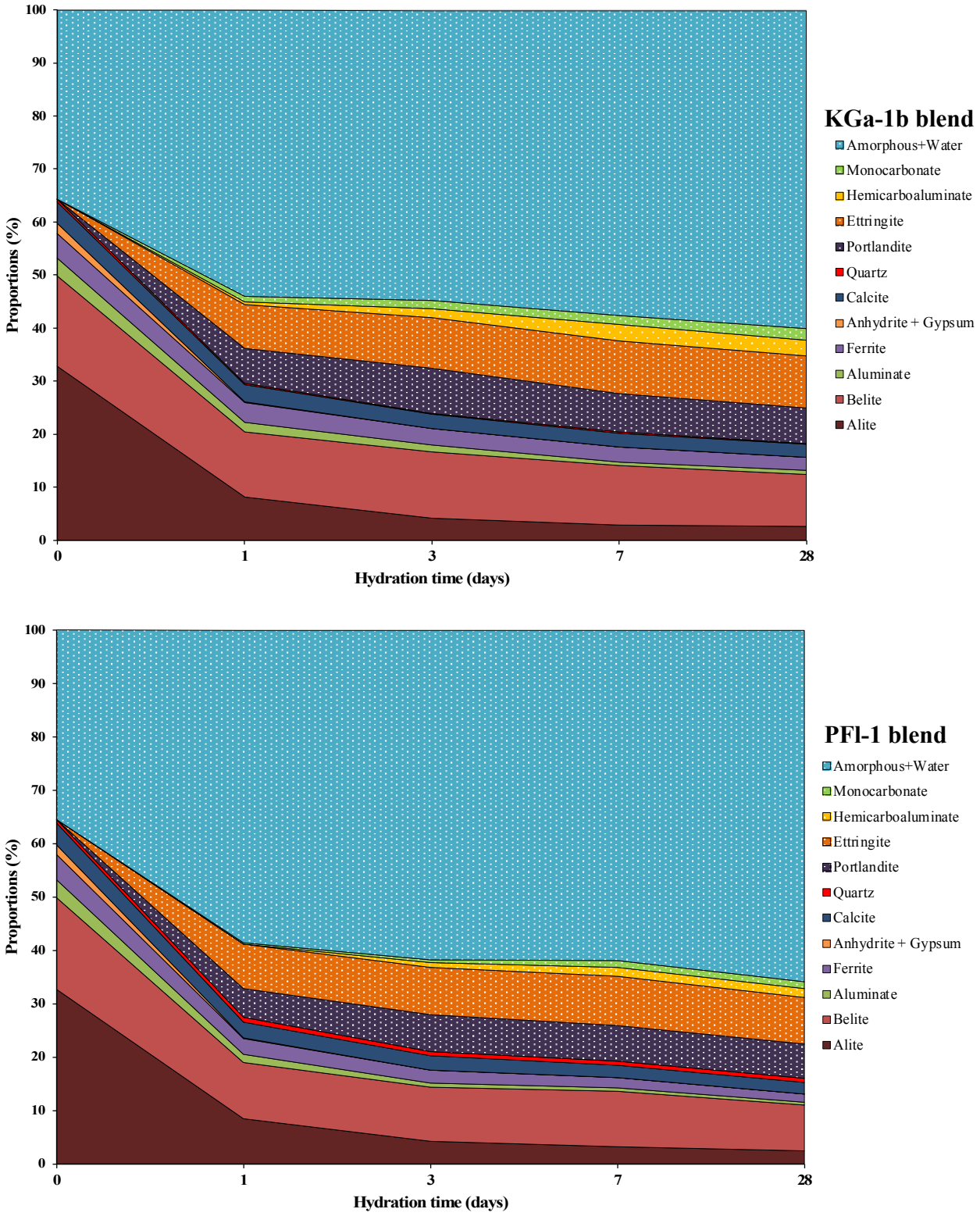

Figure 6-8: Evolution of the crystalline phases of 800°C-KGa-1b-cement blend (KGa-1b blend) and 800°C-PFl-1-cement blend (PFl-1 blend) pastes as a function of the hydration time.

The first important difference with figure 6-7 is that the hydration of the 800°C-KGa-1b and 800°C-PFl-1 cement blends results in the formation of a larger amount of carboaluminates. In these systems, additional carboaluminates are produced by the reaction of the aluminium in the calcined clay phases with the calcium and carbonates available in the system (from portlandite and calcite). The precipitation of these compounds has been shown to have a significant effect on porosity refinement and strength development [54]. Figure 6-8 also shows higher formation of carboaluminates for the mixture incorporating metakaolin rather than calcined palygorskite. This is due to the total amount of aluminium of the clay, which is sighificantly higher for kaolinite (40% Al_2O_3) compared to palygorskite (10% Al_2O_3). As a consequence, the SiO_2 content of calcined palygorskite is higher and thus have a higher contribution to the C-(A)-S-H. The addition of palygorskite or calcined kaolinite does not seem to have an influence on the amount of ettringite formed. This can be explained by the presence of carbonates which limits the sulfate inclusion in AFm phases, as the carboaluminates will be preferentially formed and most sulfate will be in ettringite [55].

6.5. Conclusion

This study compared the use of a calcined palygorskite and calcined kaolinite as supplementary cementitious materials. The investigated parameters include the calcination temperature, the pozzolanic reactivity and the mechanical performance in cementitious systems. Based on the results, the following conclusions can be drawn:

1- The calcination of palygorskite and kaolinite leads to a change in the coordination of the aluminium atoms from 6-fold to 4-fold and 5-fold coordinations. This phenomenon is very abrupt between 500 and 600°C for kaolinite, whereas it is gradual between 400 and 800°C for palygorskite.

2- The calcination of palygorskite and kaolinite leads to the segregation of the silicon from the calcined clay phases into an amorphous silica gel. The formation of this gel occurs at 600°C for kaolinite whereas 800°C is required for palygorskite.

3- A direct correlation was observed between the formation of the silica gel, the apparition of aluminium 4 and 5, the increase in pozzolanic reactivity and the increase in mechanical performance in cementitious system for both calcined palygorskite and calcined kaolinite.

4- Contrary to what is usually argued in the literature, the proportion of aluminium 5 cannot be used as a stand-alone criterion to assess the pozzolanic activity of an Al-rich SCM. It is also necessary to monitor aluminium 4 and the evolution of silicon (amorphous silica gel).

5- The calcined palygorskite has a high pozzolanic reactivity after calcination at 800°C and allows an improvement in compressive strength (already at 7 days). It can therefore be considered as a highly reactive pozzolan like metakaolin.

The next stage of the experiment will involve the study of “low grade” palygorskite samples to verify the observations made in this study and to propose new ways of adding value to this type of materials. Furthermore, dissolution studies in cementitious media of those calcined clays would make it possible to determine which type of aluminium is the most reactive.

6.6. References

[1] P. Smith, L. Beaumont, C.J. Bernacchi, M. Byrne, W. Cheung, R.T. Conant, F. Cotrufo, X. Feng, I. Janssens, H. Jones, M.U.F. Kirschbaum, K. Kobayashi, J. LaRoche, Y. Luo, A. McKechnie, J. Penuelas, S. Piao, S. Robinson, R.F. Sage, D.J. Sugget, S.J. Thackeray, D. Way, S.P. Long, Essential outcomes for COP26, Glob.Change Biol. (2021). https://doi.org/10.1111/gcb.15926.

[2] D.N. Huntzinger, T.D. Eatmon, A life-cycle assessment of Portland cement manufacturing: comparing the traditional process with alternative technologies, Journal of Cleaner Production. 17 (2009) 668–675. https://doi.org/10.1016/j.jclepro.2008.04.007.

[3] G.P. Hammond, C.I. Jones, Embodied energy and carbon in construction materials, Proceedings of the Institution of Civil Engineers - Energy. 161 (2008) 87–98. https://doi.org/10.1680/ener.2008.161.2.87.

[4] Y. Cancio Díaz, S. Sánchez Berriel, U. Heierli, A.R. Favier, I.R. Sánchez Machado, K.L. Scrivener, J.F. Martirena Hernández, G. Habert, Limestone calcined clay cement as a low-carbon solution to meet expanding cement demand in emerging economies, Development Engineering. 2 (2017) 82–91. https://doi.org/10.1016/j.deveng.2017.06.001.

[5] Global Cement Magazine, (n.d.) 11.

[6] M. Behim, B. Redjel, R. Jauberthie, Réactivitié du laitier de hauts fourneaux d’Annaba

(Algérie) en substitution partielle du ciment, (2002).

[7] Z.T. Yao, X.S. Ji, P.K. Sarker, J.H. Tang, L.Q. Ge, M.S. Xia, Y.Q. Xi, A comprehensive review on the applications of coal fly ash, Earth-Science Reviews. 141 (2015) 105–121. https://doi.org/10.1016/j.earscirev.2014.11.016.

[8] K. Scrivener, F. Martirena, S. Bishnoi, S. Maity, Calcined clay limestone cements (LC3), Cement and Concrete Research. 114 (2018) 49–56. https://doi.org/10.1016/j.cemconres.2017.08.017.

[9] K.L. Scrivener, V.M. John, E.M. Gartner, Eco-efficient cements: Potential economically viable solutions for a low-CO2 cement-based materials industry, Cement and Concrete Research. 114 (2018) 2–26. https://doi.org/10.1016/j.cemconres.2018.03.015.

[10] R.S. Almenares, L.M. Vizcaíno, S. Damas, A. Mathieu, A. Alujas, F. Martirena, Industrial calcination of kaolinitic clays to make reactive pozzolans, Case Studies in Construction Materials. 6 (2017) 225–232. https://doi.org/10.1016/j.cscm.2017.03.005.

[11] A. Alujas, R. Fernández, R. Quintana, K.L. Scrivener, F. Martirena, Pozzolanic reactivity of low grade kaolinitic clays: Influence of calcination temperature and impact of calcination products on OPC hydration, Applied Clay Science. 108 (2015) 94–101. https://doi.org/10.1016/j.clay.2015.01.028.

[12] H. El-Diadamony, A.A. Amer, T.M. Sokkary, S. El-Hoseny, Hydration and characteristics of metakaolin pozzolanic cement pastes, HBRC Journal. 14 (2018) 150–158. https://doi.org/10.1016/j.hbrcj.2015.05.005.

[13] C. He, E. Makovicky, B. Osbæck, Thermal stability and pozzolanic activity of calcined kaolin, Applied Clay Science. 9 (1994) 165–187. https://doi.org/10.1016/0169-1317(94)90018-3.

[14] I.W. Brown, K.J.D. MacKenzie, R.H. Meinhold, The thermal reactions of montmorillonite studied by high-resolution solide-state 29Si and 27Al NMR, (1987).

[15] N. Garg, J. Skibsted, Thermal Activation of a Pure Montmorillonite Clay and Its Reactivity in Cementitious Systems, The Journal of Physical Chemistry C. 118 (2014) 11464–11477. https://doi.org/10.1021/jp502529d.

[16] N. Garg, J. Skibsted, Pozzolanic reactivity of a calcined interstratified illite/smectite (70/30) clay, Cement and Concrete Research. 79 (2016) 101–111. https://doi.org/10.1016/j.cemconres.2015.08.006.

[17] R. Kaminskas, R. Kubiliute, B. Prialgauskaite, Smectite clay waste as an additive for Portland cement, Cement and Concrete Composites. 113 (2020) 103710. https://doi.org/10.1016/j.cemconcomp.2020.103710.

[18] S. Hollanders, R. Adriaens, J. Skibsted, Ö. Cizer, J. Elsen, Pozzolanic reactivity of pure calcined clays, Applied Clay Science. 132–133 (2016) 552–560. https://doi.org/10.1016/j.clay.2016.08.003.

[19] R. Fernandez, F. Martirena, K.L. Scrivener, The origin of the pozzolanic activity of calcined clay minerals: A comparison between kaolinite, illite and montmorillonite, Cement and Concrete Research. 41 (2011) 113–122. https://doi.org/10.1016/j.cemconres.2010.09.013.

[20] E.F. Irassar, V.L. Bonavetti, C.C. Castellano, M.A. Trezza, V.F. Rahhal, G. Cordoba, R.

Lemma, Calcined illite-chlorite shale as supplementary cementing material: Thermal treatment, grinding, color and pozzolanic activity, Applied Clay Science. 179 (2019) 105143. https://doi.org/10.1016/j.clay.2019.105143.

[21] V. Poussardin, M. Paris, A. Tagnit-Hamou, D. Deneele, Potential for calcination of a palygorskite-bearing argillaceous carbonate, Applied Clay Science. 198 (2020) 105846. https://doi.org/10.1016/j.clay.2020.105846.

[22] V. Poussardin, M. Paris, W. Wilson, A. Tagnit-Hamou, D. Deneele, Self-reactivity of a calcined palygorskite-bearing marlstone for potential use as supplementary cementitious material, Applied Clay Science. 216 (2022) 106372. https://doi.org/10.1016/j.clay.2021.106372.

[23] V. Poussardin, M. Paris, W. Wilson, A. Tagnit-Hamou, D. Deneele, Calcined palygorskite and smectite bearing marlstones as supplementary cementitious materials, (n.d.).

[24] V. Poussardin, W. Wilson, M. Paris, A. Tagnit-Hamou, D. Deneele, Calcined palygorskites as supplementary cementitious materials, (n.d.).

[25] S. Chipera, D. Bish, Baseline Studies of the Clay Minerals Society Source Clays: Powder X-ray Diffraction Analyses, Copyright Clays and Clay Minerals. 49 (2001) 398–409. https://doi.org/10.1346/CCMN.2001.0490507.

[26] M.P.S. Krekeler, E. Hammerly, J. Rakovan, S. Guggenheim, Microscopy Studies of the Palygorskite-to-Smectite Transformation, Clays Clay Miner. 53 (2005) 92–99. https://doi.org/10.1346/CCMN.2005.0530109.

[27] Direct evidence of transformation from smectite to palygorskite: TEM investigation | SpringerLink, (n.d.). https://link.springer.com/article/10.1360/03yd0509 (accessed June 13, 2022).

[28] Microscopy Studies of the Palygorskite-to-Smectite Transformation: Ingenta Connect, (n.d.). https://www.ingentaconnect.com/contentone/cms/ccm/2005/00000053/00000001/art00009 (accessed June 13, 2022).

[29] T. Danner, G. Norden, H. Justnes, Characterisation of calcined raw clays suitable as supplementary cementitious materials, Applied Clay Science. 162 (2018) 391–402. https://doi.org/10.1016/j.clay.2018.06.030.

[30] S. Krishnan, A.C. Emmanuel, V. Shah, A. Parashar, G. Mishra, S. Maity, S. Bishnoi, Industrial production of limestone calcined clay cement: experience and insights, Green Materials. 7 (2019) 15–27. https://doi.org/10.1680/jgrma.18.00003.

[31] A. Trümer, H.-M. Ludwig, M. Schellhorn, R. Diedel, Effect of a calcined Westerwald bentonite as supplementary cementitious material on the long-term performance of concrete, Applied Clay Science. 168 (2019) 36–42. https://doi.org/10.1016/j.clay.2018.10.015.

[32] N. Doebelin, R. Kleeberg, *Profex* : a graphical user interface for the Rietveld refinement program *BGMN*, Journal of Applied Crystallography. 48 (2015) 1573–1580. https://doi.org/10.1107/S1600576715014685.

[33] E. Ferraz, S. Andrejkovičová, W. Hajjaji, A. Velosa, A. Santos Silva, F. Rocha, Pozzolanic

activity of metakaolins by the French standard of the modified Chapelle test: A direct methology, Acta Geodynamica et Geomaterialia. 12 (2015) 289–298. https://doi.org/10.13168/AGG.2015.0026.

[34] Standard Test Methods for Measuring the Reactivity of Supplementary Cementitious Materials by Isothermal Calorimetry and Bound Water Measurements, (n.d.). https://www.astm.org/c1897-20.html (accessed March 24, 2022).

[35] C01 Committee, Test Method for Compressive Strength of Hydraulic Cement Mortars (Using 2-in. or [50-mm] Cube Specimens), ASTM International, n.d. https://doi.org/10.1520/C0109_C0109M-16A.

[36] M. Önal, Y. Sarıkaya, Some physicochemical properties of a clay containing smectite and palygorskite, Applied Clay Science. 44 (2009) 161–165. https://doi.org/10.1016/j.clay.2009.01.012.

[37] S. Guggenheim, Baseline Studies of the Clay Minerals Society Source Clays: Thermal Analysis, Clays and Clay Minerals. 49 (2001) 433–443. https://doi.org/10.1346/CCMN.2001.0490509.

[38] C.M. Earnest, Thermal analysis of selected illite and smectite clay minerals. Part II. Smectite clay minerals, in: W. Smykatz-Kloss, S.St.J. Warne (Eds.), Thermal Analysis in the Geosciences, Springer, Berlin, Heidelberg, 1991: pp. 288–312. https://doi.org/10.1007/BFb0010272.

[39] W. Hirsiger, M. Müller-Vonmoos, H.G. Wiedemann, Thermal analysis of palygorskite, Thermochimica Acta. 13 (1975) 223–230. https://doi.org/10.1016/0040-6031(75)80083-9.

[40] T. Jacobs, Kinetics of the Thermal Dehydration of Kaolinite, Nature. 182 (1958) 1086–1087. https://doi.org/10.1038/1821086a0.

[41] M. Bellotto, A. Gualtieri, G. Artioli, S.M. Clark, Kinetic study of the kaolinite-mullite reaction sequence. Part I: Kaolinite dehydroxylation, Phys Chem Minerals. 22 (1995) 207–217. https://doi.org/10.1007/BF00202253.

[42] G. Qiu, T. Jiang, G. Li, X. Fan, Z. Huang, Activation and removal of silicon in kaolinite by thermochemical process, Scandinavian Journal of Metallurgy. 33 (2004) 121–128. https://doi.org/10.1111/j.1600-0692.2004.00677.x.

[43] A.Á.B. Maia, R.S. Angélica, R. de Freitas Neves, H. Pöllmann, C. Straub, K. Saalwächter, Use of 29Si and 27Al MAS NMR to study thermal activation of kaolinites from Brazilian Amazon kaolin wastes, Applied Clay Science. 87 (2014) 189–196. https://doi.org/10.1016/j.clay.2013.10.028.

[44] J. Sanz, J.M. Serratosa, Silicon-29 and aluminum-27 high-resolution MAS-NMR spectra of phyllosilicates, Journal of the American Chemical Society. 106 (1984) 4790–4793. https://doi.org/10.1021/ja00329a024.

[45] D. Muller, W. Gessner, A. Samoson, E. Lippmaa, Solid-state Aluminium-27 Nuclear Magnetic Resonance Chemical Shift and Quadrupole Coupling Data for Condensed AlO4, Tetrahedra, J. Chem. Soc. Dalton Trans. (1986) 5.

[46] M. Paris, The two aluminum sites in the 27Al MAS NMR spectrum of kaolinite: Accurate determination of isotropic chemical shifts and quadrupolar interaction parameters, American Mineralogist. (2014) 393–400.

[47] R. Snellings, G. Mertens, J. Elsen, Supplementary Cementitious Materials, Reviews in Mineralogy and Geochemistry. 74 (2012) 211–278. https://doi.org/10.2138/rmg.2012.74.6.

[48] J.-B. D'Espinose de la Caillerie, J.J. Fripiat, A reassessment of the ^{29} Si MAS-NMR spectra of sepiolite and aluminated sepiolite, Clay Miner. 29 (1994) 313–318. https://doi.org/10.1180/claymin.1994.029.3.02.

[49] S. Komarneni, C.A. Fyfe, G.J. Kennedy, Detection of Nonequivalent Si Sites in Sepiolite and Palygorskite by Solid-state 29Si Magic Angle Spinning-Nuclear Magnetic Resonance, Clays & Clay Minerals. 34 (1986) 99–102. https://doi.org/10.1346/CCMN.1986.0340113.

[50] P.F. Barron, R.L. Frost, N. Qlil, Solid state 29Si NMR examination of the 2:1 ribbon magnesium silicates, sepiolite and palygorskite, American Mineralogist. 70 (1985) 758–766.

[51] J. Rocha, J. Klinowski, 29Si and 27Al magic-angle-spinning NMR studies of the thermal transformation of kaolinite, Phys Chem Minerals. 17 (1990) 179–186. https://doi.org/10.1007/BF00199671.

[52] K.J.D. MacKenzie, M.E. Smith, Multinuclear Solid-State NMR of Inorganic Materials, Pergamon Materials Series, n.d.

[53] ASTMC1897, (n.d.).

[54] P. Klieger, Carbonate Additions to Cement, ASTM International, 1990.

[55] The reaction between metakaolin and limestone and its effect in porosity refinement and mechanical properties - ScienceDirect, (n.d.). https://www.sciencedirect.com/science/article/pii/S0008884620315878 (accessed July 7, 2022).

[56] V.L. Bonavetti, V.F. Rahhal, E.F. Irassar, Studies on the carboaluminate formation in limestone filler-blended cements, Cement and Concrete Research. 31 (2001) 853–859. https://doi.org/10.1016/S0008-8846(01)00491-4.

6.7. Bilan scientifique du chapitre 6

Cette dernière partie dresse un bilan scientifique de ce chapitre 6 qui s'intéresse à la comparaison de la réactivité pouzzolanique de deux échantillons argileux calcinés fortement concentrés, une palygorskite et un kaolin. Ces deux échantillons proviennent de la Clay Mineral Society (PFl-1 (Palygorskite) et KGa-1b (Kaolinite)).

Il a été démontré que les deux argiles ont un comportement radicalement différent lors de leur calcination. Les modifications physico-chimiques se font de manière progressive pour la palygorskite (400 et 800°C) alors que ce phénomène est beaucoup plus brutal pour la kaolinite (entre 500 et 600°C). Un lien direct entre ces modifications physico-chimiques, la réactivité pouzzolanique et les performances mécaniques en système cimentaire a été mis en évidence. Plus précisément, il a été démontré que l'évolution de l'environnement du silicium des phases argileuses lors de la calcination (phénomène de ségrégation du silicium qui se condense) ainsi que le changement de coordination des atomes d'aluminium (lié à la déshydroxylation des phases argileuses) corrèlent parfaitement avec l'augmentation de la réactivité pouzzolanique et des performances mécaniques en système cimentaire de ces deux matériaux.

Plusieurs observations ont pu être relevées lors de la comparaison des données de RMN ^{27}Al et ATG/DSC. Malgré un changement de coordination des atomes d'aluminium après 600°C pour la palygorskite, il n'y a aucune variation de masse ni de flux de chaleur détecté par ATG/DSC. Il semble donc que le changement de coordination des atomes d'aluminium ne soit pas uniquement dû à un phénomène de déshydroxylation, mais également à un réarrangement de la structure de l'argile. Ce réarrangement entraine une modification de l'environnement de l'aluminium bien après la déshydroxylation.

Ce chapitre 6 a permis de démontrer que malgré sa plus faible réactivité pouzzolanique en comparaison du métakaolin, la palygorskite calcinée est une argile qui peut être classée dans la famille des pouzzolanes hautement réactives.

Conclusion générale

Ce projet de de thèse consistait donc en une étude expérimentale multi-échelle de l'utilisation d'argiles et de marnes calcinées dans le développement de ciments composés. L'objectif principal était d'évaluer le potentiel de nouveaux matériaux à base d'argiles non conventionnelles pour une utilisation comme ajouts cimentaires, dans le but de réduire la part de clinker des ciments composés. Associé à cet objectif principal, il y avait la nécessité d'apporter de nouvelles connaissances fondamentales sur la calcination et la réactivité en système cimentaire de ces argiles puis d'identifier les liens existants entre les observations faites à l'échelle micro et macro.

Tout a débuté avec l'étude de la calcination de deux marnes dolomitiques, contenant toutes les deux de la smectite mais dont l'une contenait également de la palygorskite. Il a été possible de démontrer que ces matériaux multiphasés complexes présentent un potentiel d'utilisation comme ajout cimentaire après calcination, et ce, malgré leur faible proportion d'argiles. Du fait de leur composition minéralogique complexe, et notamment de la présence de carbonates, il y a la formation de plusieurs phases réactives après calcination qui ont un potentiel impact sur l'hydratation et qui doivent donc être contrôlées. En comparant la réactivité pouzzolanique et les performances mécaniques en système cimentaire, il est apparu que la marne contenant de la palygorskite présentait les meilleurs résultats. Ceci démontre l'effet bénéfique de la présence de palygorskite et laisse présager que cette argile présente un certain potentiel pour une utilisation comme SCM après calcination. Cependant, la présence de synergies avec les autres phases réactives néoformées durant la calcination ne peut pas être écartée et pourrait expliquer la forte réactivité de la marne contenant de la palygorskite.

Afin d'affirmer et/ou d'infirmer ces hypothèses nous nous sommes intéressés à des échantillons présentant des teneurs plus élevées en palygorskite (Pal-1 et Pal-2 contenant 61% et 73% de palygorskite respectivement) et ne possédant pas de carbonates, ni de minéraux accessoires pouvant entrainer la formation de phases réactives après calcination. L'étude de la calcination, de la réactivité pouzzolanique et des performances mécaniques en système cimentaire a confirmé le fort potentiel pour une utilisation comme ajout cimentaire de ce type

d'argile. L'incorporation de 20% de ces matériaux calcinés à 800°C dans des ciments composés permet une augmentation de 28% de la résistance à la compression sur mortiers (pour l'argile avec 61% de palygorskite et 25% de smectite) et de 44% (pour l'argile avec 73% de palygorskite et 21% de smectite). Cette différence de réactivité entre les deux matériaux utilisés peut être aussi bien expliquée par la plus haute proportion de palygorskite que par la plus haute proportion globale d'argile (palygorskite + smectite) ou encore la plus grande finesse de Pal-2 en comparaison de Pal-1.

En raison du potentiel intéressant de la palygorskite, il est ensuite apparu nécessaire d'étudier de manière plus poussée un échantillon ayant une teneur élevée en palygorskite afin d'identifier quels sont les paramètres clés qui influent sur sa réactivité, puis de le comparer avec un kaolin. Pour ce faire nous nous sommes procurés une palygorskite et un kaolin auprès de la Clay Mineral Society. Ainsi, une étude détaillée a permis de comparer les modifications physico-chimiques qui se déroulent lors de la calcination, puis de comparer leur réactivité pouzzolanique et enfin leurs performances mécaniques en système cimentaire. Il a été démontré que la calcination de la palygorskite et de la kaolinite induit de nombreux changements dans la structure de ces argiles. Il y a un phénomène de déshydroxylation ainsi que la formation d'un gel de silice amorphe à différentes températures de calcination. Ce phénomène se produit de manière très brutale entre 500 et 600°C pour la kaolinite alors qu'il est beaucoup plus progressif (entre 400 et 800°C) pour la palygorskite. Ces deux phénomènes (déshydroxylation et formation du gel de silice amorphe) corrèlent avec l'augmentation de la réactivité pouzzolanique et des performances mécaniques en système cimentaire. En comparant ces deux échantillons modèles, il apparaît que la palygorskite calcinée peut être considérée comme une pouzzolane hautement réactive, et représente une alternative au métakaolin dans les régions du monde où ce dernier n'est pas disponible.

Ce travail de thèse a permis dans un premier temps de démontrer que les marnes, malgré leur minéralogie complexe présentent un fort potentiel d'utilisation comme SCM après calcination, permettant ainsi d'ouvrir de nouvelles voies de valorisation de ce types de matériaux. Par la suite, il a été démontré que la palygorskite est une argile à haut potentiel pour une utilisation comme ajout cimentaire après calcination, et peut être considérée comme une alternative viable au métakaolin. L'étude poussée de l'utilisation de palygorskites

calcinées comme ajouts cimentaires a également permis d'apporter de nouvelles connaissances fondamentales sur la compréhension des mécanismes impliqués lors de la calcination de ce type de matériaux. L'évolution de la coordination des atomes d'aluminium ainsi que la formation d'un gel de silice amorphe lors de la calcination sont les deux éléments clés en terme de réactivité pouzzolanique et de performances mécaniques en système cimentaire.

De nombreuses questions restent cependant en suspens. D'un point de vue fondamental il serait intéressant de déterminer quel type d'aluminium (coordination 4 ou 5) va avoir la plus grande influence sur la réactivité de l'argile calcinée. Pour cela, des tests de vitesse de dissolution en milieu cimentaire des argiles calcinées pourraient s'avérer pertinents et permettraient de déterminer quelles sont les éléments clés qui vont influer la réactivité pouzzolanique. Du point de vue ingénierie il serait pertinent d'étudier la formulation de bétons avec des ciments composés incorporant de la palygorskite calcinée afin d'avoir une vision complète des performances de ce nouveau SCM. Cela passerait par une première étape de formulation d'un ciment composé à base de palygorskite calcinée, d'une étude de la compatibilité avec différents types de superplastifiants et finalement de la réalisation de bétons. En parallèle de tout ça, la recherche de nouveaux échantillons avec différentes teneurs en palygorskite est également nécessaire, notamment dans une optique de détermination de la proportion de palygorskite minimale qui permet d'obtenir un ciment composé présentant des performances similaires à un ciment portland classique.

Annexes

Informations complémentaires du chapitre 2

Spectral decompositions of the ^{27}Al MAS spectra were done by using the dmfit software. The initial fit was constructed from the spectrum of the argillaceous-carbonate calcined at 600°C. The relevance of this fit is supported by ^{27}Al 3QMAS spectrum of the same sample. Signal from 6-fold aluminium that resisted calcination are represented by a Lorentzian line (labelled L6_hatched). In order to account for the asymmetry of the ^{27}Al resonances (due to the presence of Electric Field Gradient distributions) in this amorphous sample, we chose the 'Czsimple' shape implemented in dmfit with d=5 to use the Gaussian Isotropic Model. The isotropic chemical shift distribution is described by an independent Gaussian distribution. Thus, a 'Czsimple' line (labelled C6_dotted) was used to complete the description of the 6-fold aluminium resonance. A single 'Czsimple' line (labelled C5) was used for the 5-fold aluminium resonance. Finally, two 'Czsimple' lines (labelled C4_hatched and C4_dotted) were mandatory to fully describe the 4-fold aluminium resonance. Parameters for the five lines are gathered in Table S1. Except amplitudes, all other parameters were kept constant when fitting the ^{27}Al MAS spectra of the argillaceous-carbonate samples calcined at 700, 800 and 900°C. Table S2 gives the relative proportions of the lines as a function of the calcination temperature.

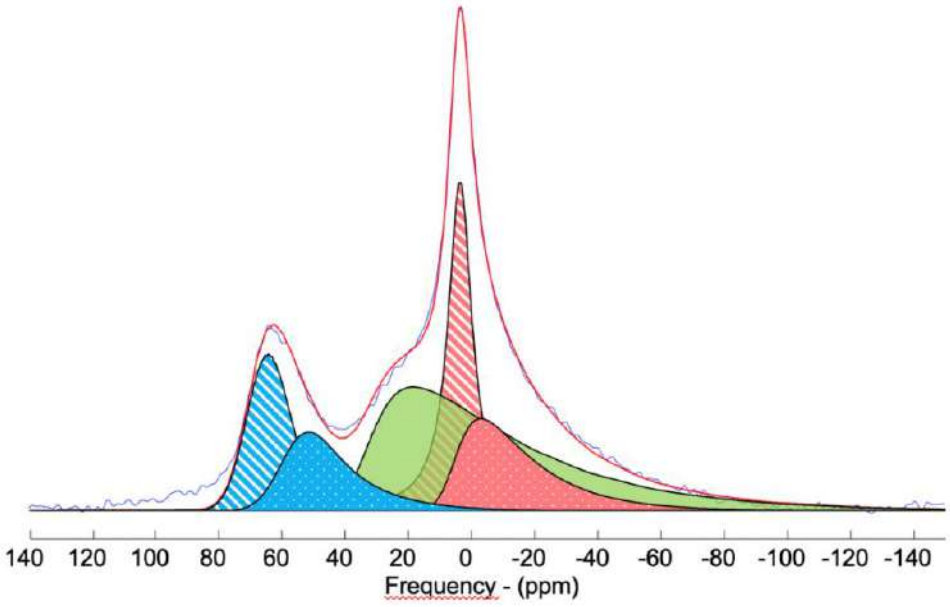

Figure S1: Spectral integration of the ^{27}Al MAS NMR spectrum of the argillaceous-carbonate calcined at 600°C.

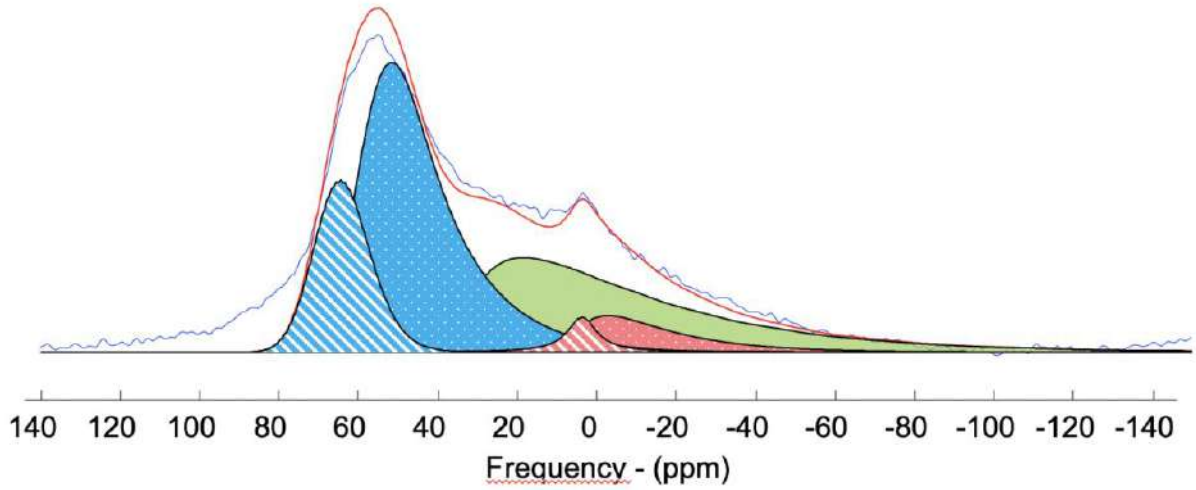

Figure S2: Spectral integration of the ^{27}Al MAS NMR spectrum of the argillaceous-carbonate calcined at 700°C.

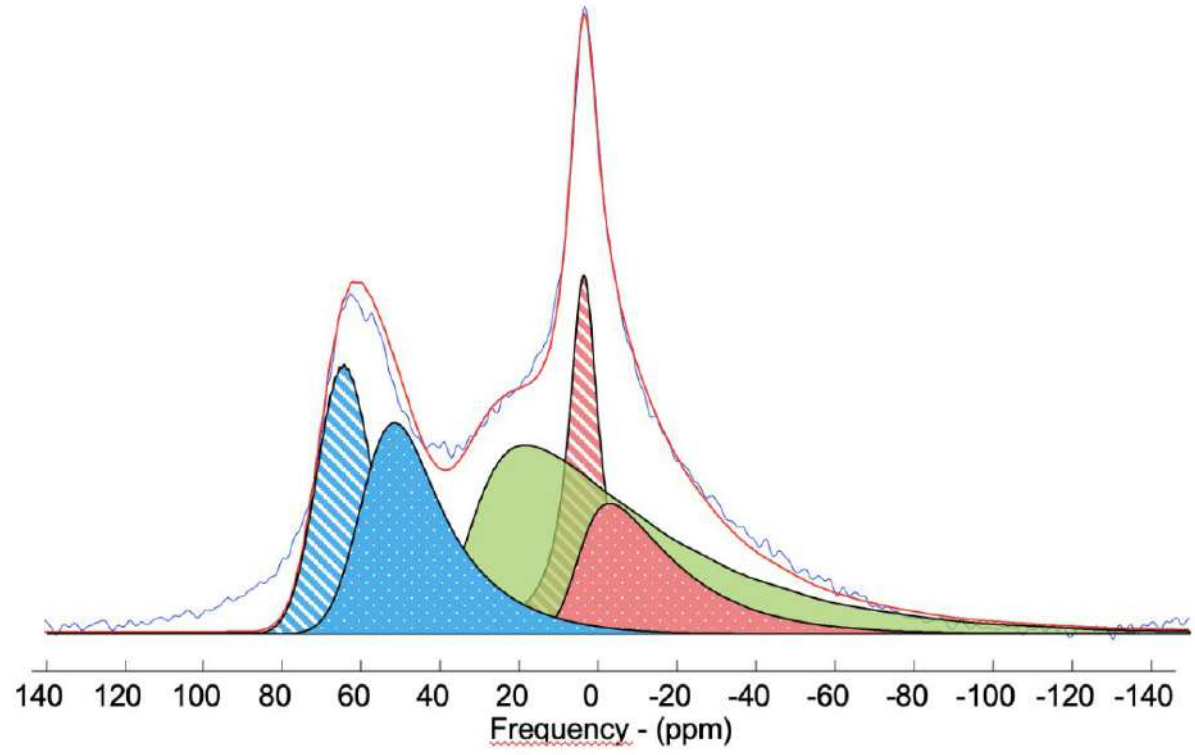

Figure S3: Spectral integration of the ^{27}Al MAS NMR spectrum of the argillaceous-carbonate calcined at 800°C.

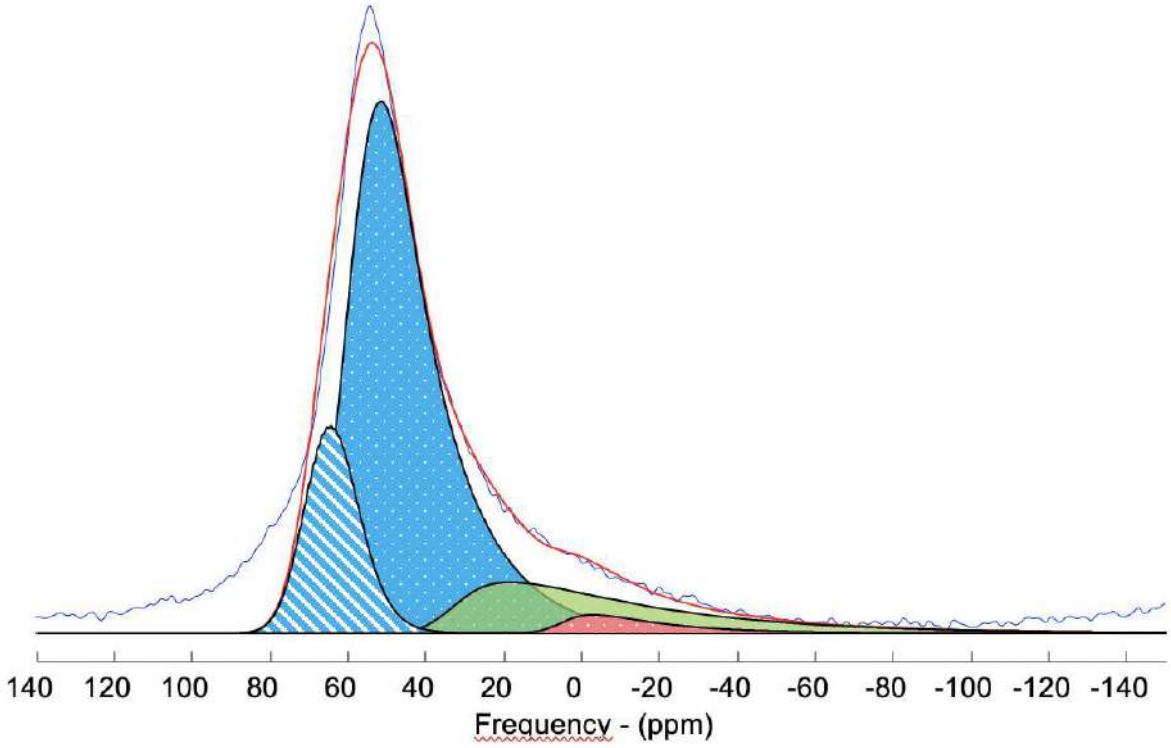

Figure S4: Spectral integration of the ^{27}Al MAS NMR spectrum of the argillaceous-carbonate calcined at 900°C.

Table S1: Parameters for the ^{27}Al MAS NMR spectral decompositions. diso is the isotropic chemical shift, C_Q is the mean quadrupolar product (GIM) and FWHM CS is the full width at half maximum of the Gaussian distribution of isotropic chemical shift.

Component	Shape	d_{iso} (ppm)	Width (ppm)	C_Q (MHz)	FWHM CS (ppm)
L6_hatched	Lorentzienne	3.8	9.0		
C6_dotted	CzSimple	6.5		7.0	10.0
C5	CzSimple	35.0		10.0	14.0
C4_dotted	CzSimple	61.0		6.5	15.0
C4_hatched	CzSimple	69.0		3.5	14.0

Table S2: Relative Proportions of the components of ^{27}Al MAS NMR spectra as function of the calcination temperature.

	C4_hatched	C4_dotted	C5	L6_hatched	C6_dotted
600°C	14	11	38	22	15
700°C	15	19	37	16	13
800°C	16	44	31	3	6
900°C	16	67	14	0	3

The Rietveld quantification of the raw and calcined material at 800°C was performed using the Profex Rietveld refinement program [19]. Ideal structural phases have been used and refined as best as possible. The sample is a natural sample made of a mixture of several phases, which explains the difficulty in obtaining a perfect fit. For the raw sample two different palygorskite crystal structures (Palygorskite1 and Palygorskite2) and two Dolomite (Dolomite and Dolomite2) have been necessary to optimize the fit. The high R_{wp} value for the refinement of the raw sample is explained by a difficulty to fit the shape of the characteristic peaks of Dolomite. The presence of a low proportion of Ankerite may explain this difficulty. Concerning the refinement of the 800°C calcined material, to simulate the dehydrated smectite, crystalline structure of a zero-water layer potassium smectite was used.

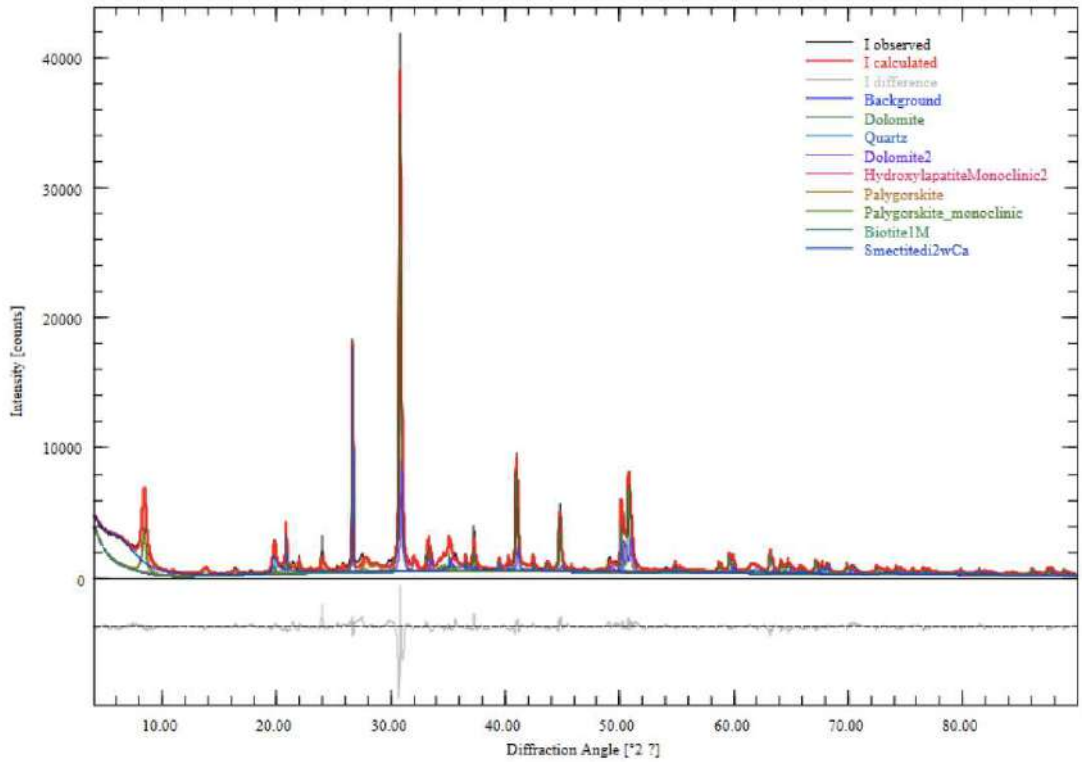

Figure S5: Rietveld refinement of the raw argillaceous-carbonate (with peaks of phases).

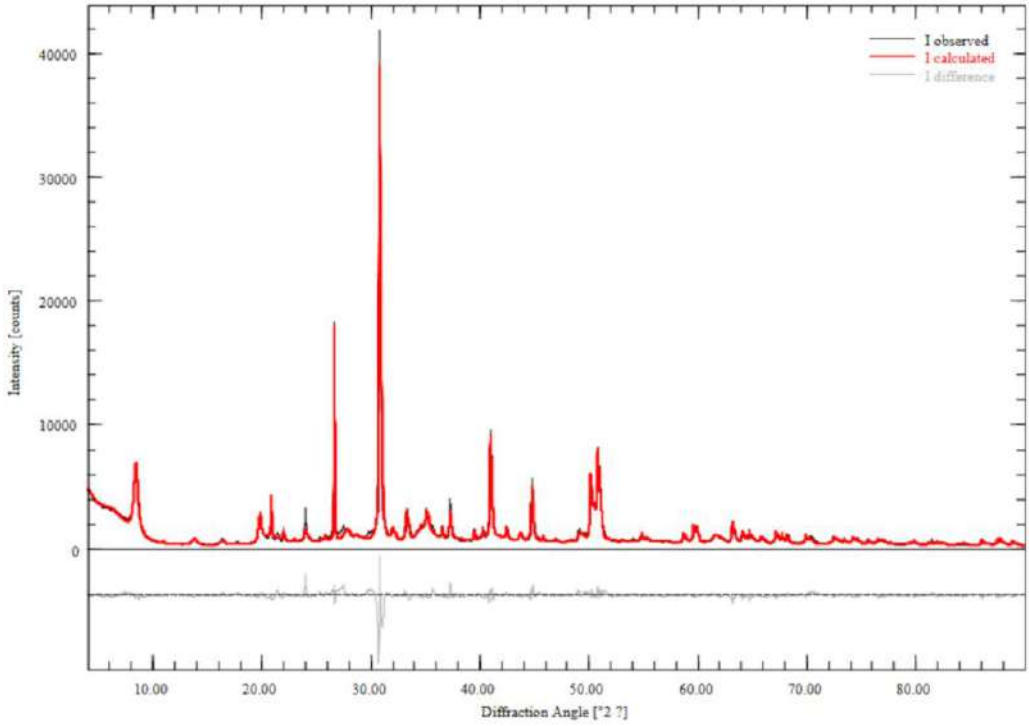

Figure S6 : Rietveld refinement of the raw argillaceous-carbonate (without peaks of phases).

Table S3: Statistics of the Rietveld refinement of the raw argillaceous-carbonate.

Statistics	R_{wp} = 10.24	R_{exp} = 3.14	X^2 = 10.63	GoF = 3.26

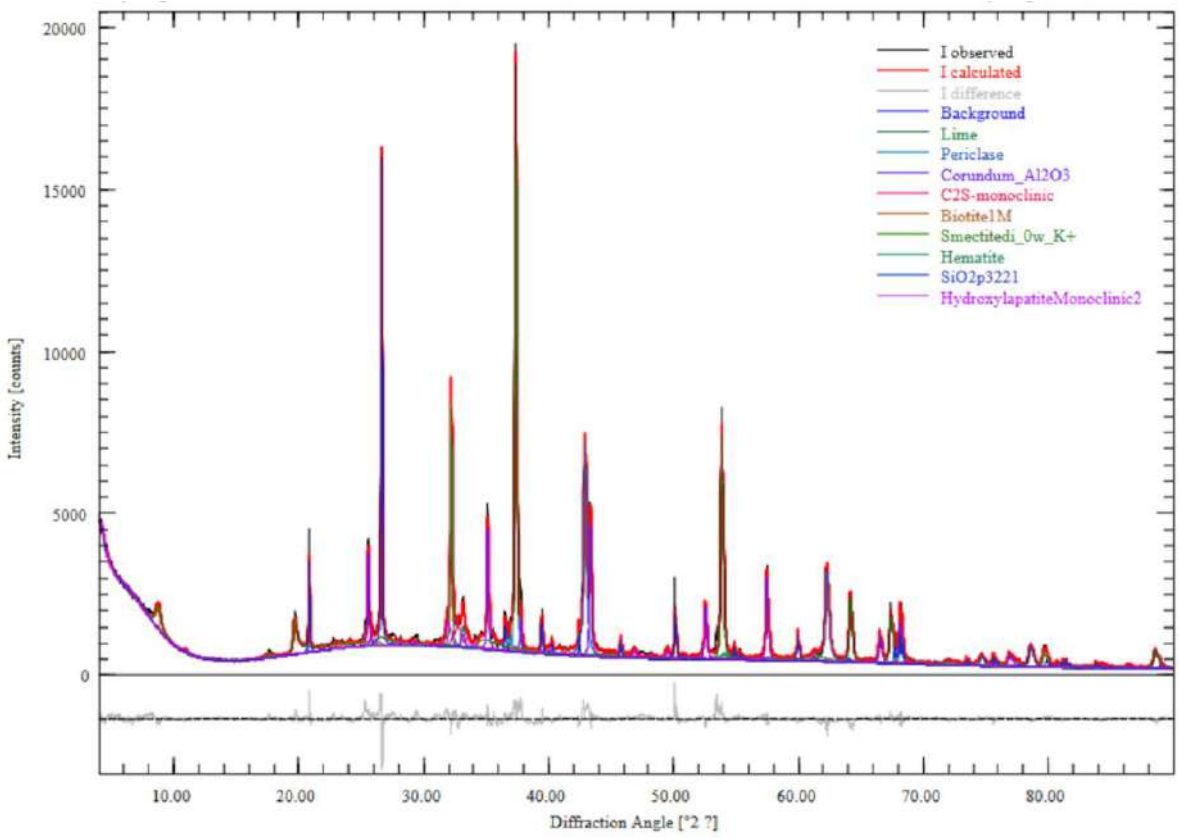

Figure S7: Rietveld refinement of the argillaceous-carbonate calcined at 800°C (with peaks of phases).

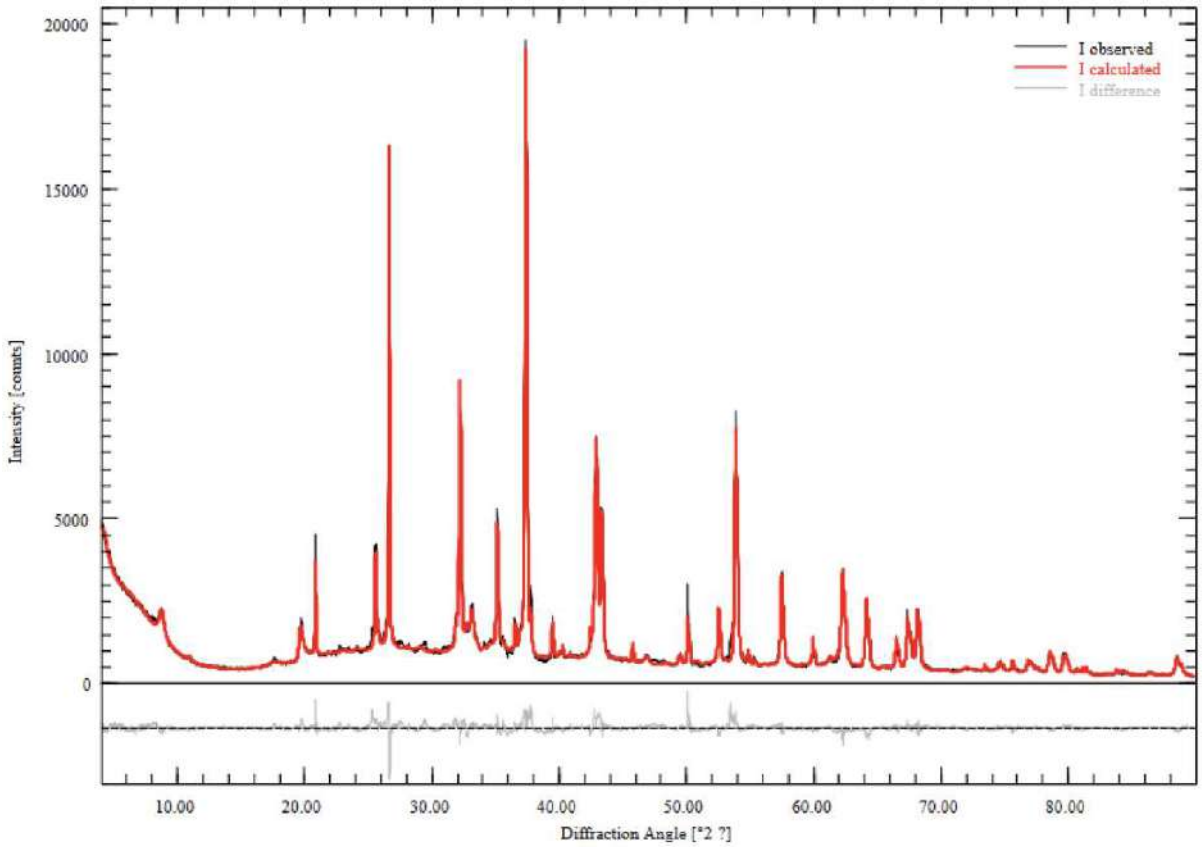

Figure S8: Rietveld refinement of the argillaceous-carbonate calcined at 800°C (without peaks of phases).

Table S4: Statistics of the Rietveld refinement of the argillaceous-carbonate calcined at 800°C.

Statistics	R_{wp} = 6.74	R_{exp} = 3.26	X^2 = 4.27	GoF = 2.07

Informations complémentaires du chapitre 3

Spectral decompositions of ^{29}Si MAS NMR spectra have been done by using the dmfit software [1]. The initial fit was constructed from the spectrum of the calcined marlstone hydrated for 7 days. For the line at -107.8 ppm associated with quartz, we used a Lorentzian lineshape. For the lineshapes of all other lines, we used an equally weighted sum of Gaussian and Lorentzian of same widths ('Gaus/Lor' model in dmfit). One line (labelled Q^0/Q^1) was used to describe the resonance associated with Q^0/Q^1 of belite and/or akermanite/gehlenite. Four lines (labelled Q^1 CSH 1, Q^1 CSH 2, Q^2(1Al) CSH and Q^2 CSH) were used to describe the resonances associated with Q^1, Q^2(1Al) and Q^2 of C-(A)-S-H. Two lines (labeled Q^3 calcined clay 1 and Q^3 calcined clay 2) were used to describe the resonance associated with Q^3 of calcined clay phases. Finally, one line (labeled Q^4 Silica) and one Lorentzian line (labeled Q^4 Quartz) were used to described the resonance associated with Q^4 of silica polymorphs. The parameters of the lines are gathered in table S1. All parameters except amplitude were kept constant for the fitting of the ^{29}Si MAS spectra of the calcined argillaceous carbonate hydrated during 14, 28 and 180 days.

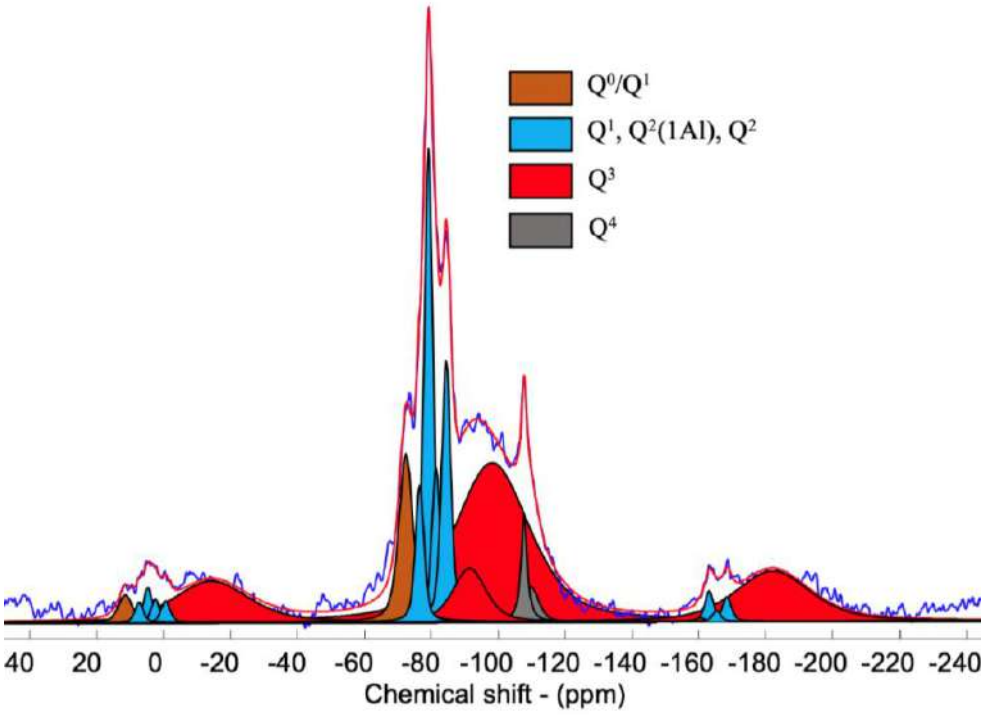

Figure S1: Spectral integration of the ^{29}Si MAS NMR spectrum of the marlstone calcined at 800°C and hydrated during 7d.

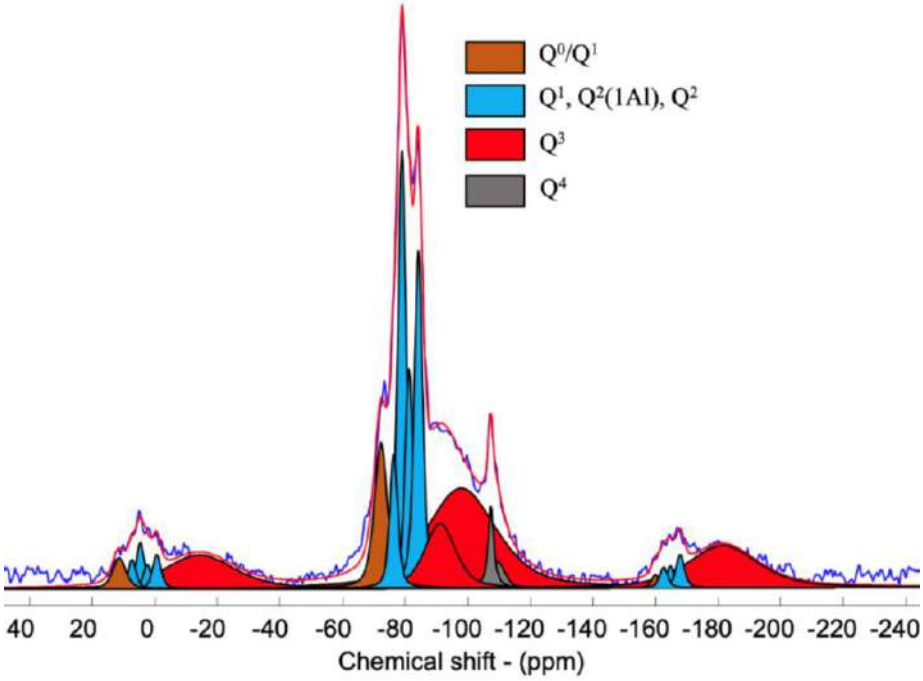

Figure S2: Spectral integration of the ^{29}Si MAS NMR spectrum of the marlstone calcined at 800°C and hydrated during 14d.

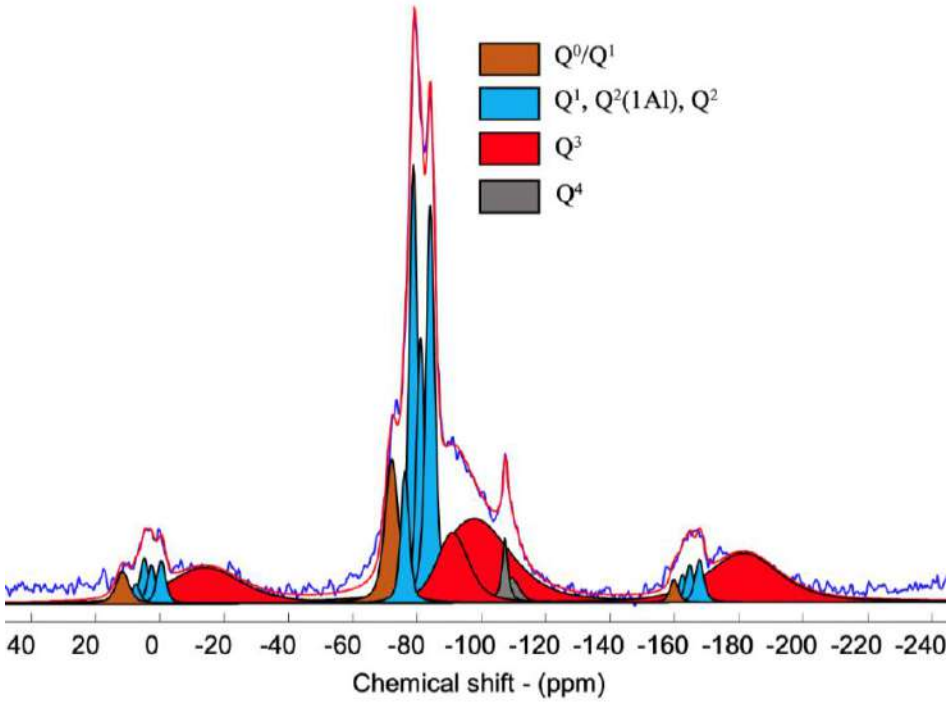

Figure S3: Spectral integration of the ^{29}Si MAS NMR spectrum of the marlstone calcined at 800°C and hydrated during 28d.

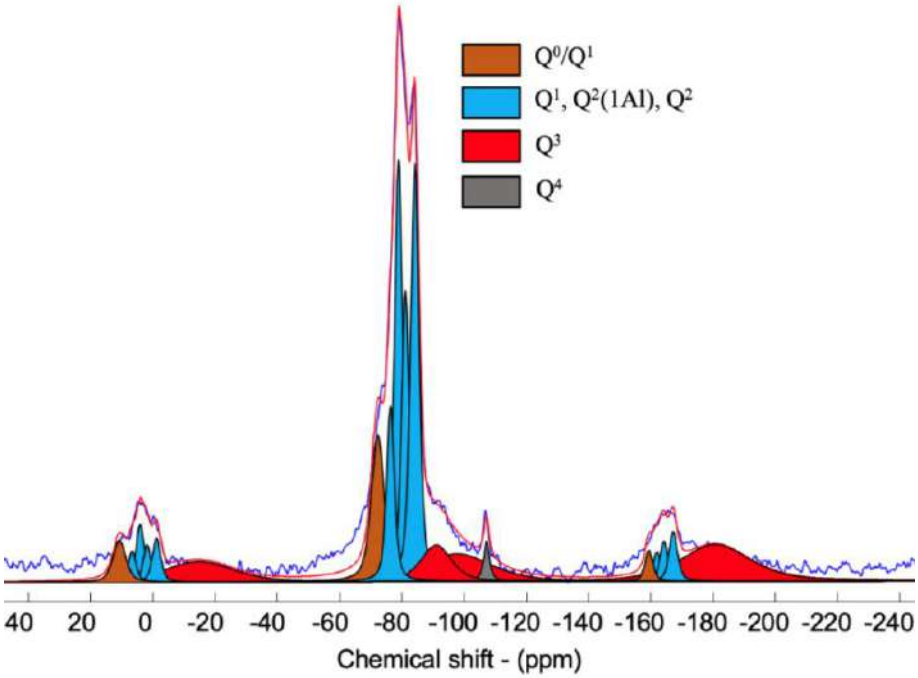

Figure S4: Spectral integration of the ^{29}Si MAS NMR spectrum of the marlstone calcined at 800°C and hydrated during 180d.

Table S1: Parameters and relative proportions for the ^{29}Si MAS NMR spectral decompositions. diso is the isotropic chemical shift and f.w.h.m the full width at half maximum.

Parameters			Relative proportions			
Component	**d_{iso} (ppm)**	**f.w.h.m. (ppm)**	**7d**	**14d**	**28d**	**180d**
Q^4 Silica	-109.9	5.4	1.5	1.3	1.2	1.2
Q^4 Quartz 2	-107.8	2.1	2.2	1.9	1.5	0
Q^3 Calcined-clay 1	-98.2	26.5	52.9	42.4	39.4	25.1
Q^3 Calcined-clay 2	-91.4	11.7	5.1	7.1	7.4	4.9
Q^2 CSH	-84.5	3.2	8.0	12.1	14.1	18.9
Q^2(1Al) CSH	-81.4	3.0	4.6	7.4	9.2	12.6
Q^1 CSH 1	-79.2	3.1	13.7	14.6	14.4	18.2
Q^1 CSH 2	-76.6	3.0	4.0	5.0	4.8	8.3
Q^0/Q^1	-72.5	4.97	8.0	8.2	8.0	10.8

Table S2: MCL and Al/Si values as function of the hydration time calculated by using a fully cross-linked tobermorite model.

Fully cross-linked C-(A)-S-H structure		
Hydration time (days)	**MCL**	**Al/Si**
7	9,16	0,143
14	10,87	0,153
28	11,95	0,149
180	10,24	0,078

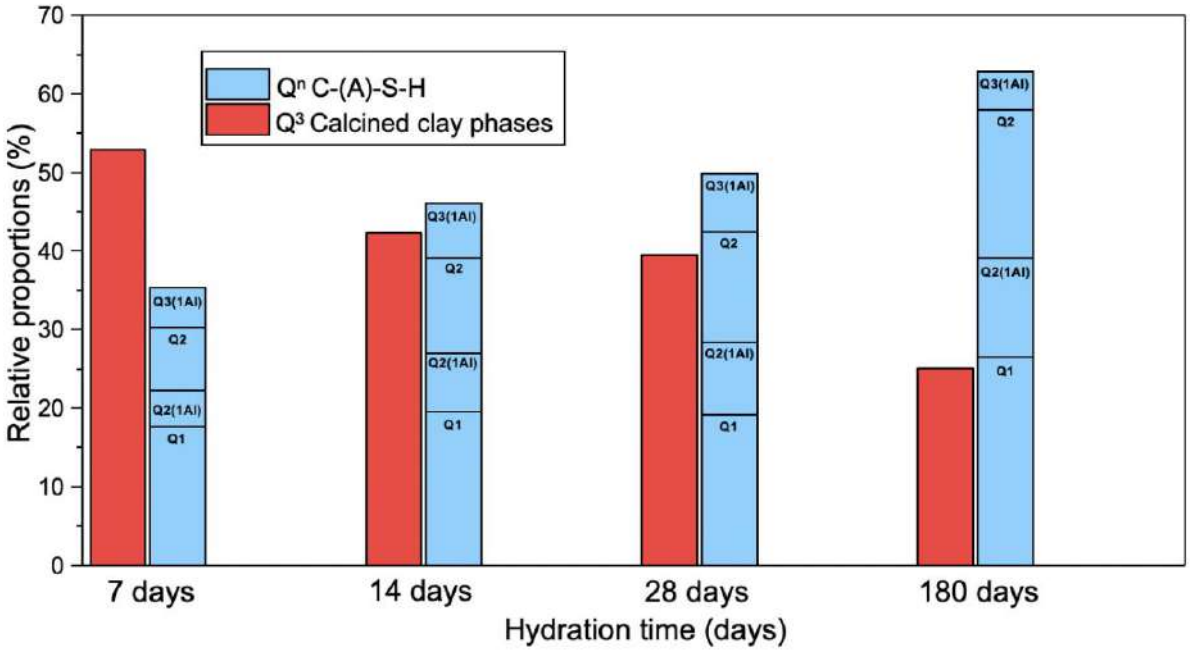

Figure S5: Relative proportions (with Q^3 Calcined clay-2 associated with Q^3(1Al) C-(A)-S-H) of silicon-containing phases (from the perspective of silicon content) as function of the hydration time obtained from ^{29}Si NMR spectra.

References

[1] N. Doebelin, R. Kleeberg, *Profex* : a graphical user interface for the Rietveld refinement program *BGMN*, Journal of Applied Crystallography. 48 (2015) 1573–1580. https://doi.org/10.1107/S1600576715014685.

Informations complémentaires du chapitre 4

Spectral decomposition MS1

Dmfit software [1] has been used to perform the spectral decompositions of ^{29}Si MAS NMR spectra. The 800°C-MS1 hydrated during 7 days has been used to construct the initial fit. All the lines were modeled using an equally weighted sum of Gaussian and Lorentzian of same widths ('Gaus/Lor' model in dmfit). Q^0/Q^1 of C2S and/or akermanite/gehlenite resonance was described using one line (labelled Q^0/Q^1). Q^1, Q^2(1Al) and Q^2 resonances of C-(A)-S-H were described using four lines (labelled Q^1 CSH 1, Q^1 CSH 2, Q^2(1Al) CSH and Q^2 CSH). Q^3 resonance of calcined clay phases was described using two lines (labeled Q^3 calcined clay 1 and Q^3 calcined clay 2). Finaly, Q^4 resonance of silica polymorphs was described using one line (labeled Q^4 Silica) and one Lorentzian line (labeled Q^4 Quartz). Table S1 gathered the parameters of the lines used. All parameters except amplitude were kept constant for the fitting of the ^{29}Si MAS spectra of the 800°C-MS1 hydrated during 14, 28 and 180 days.

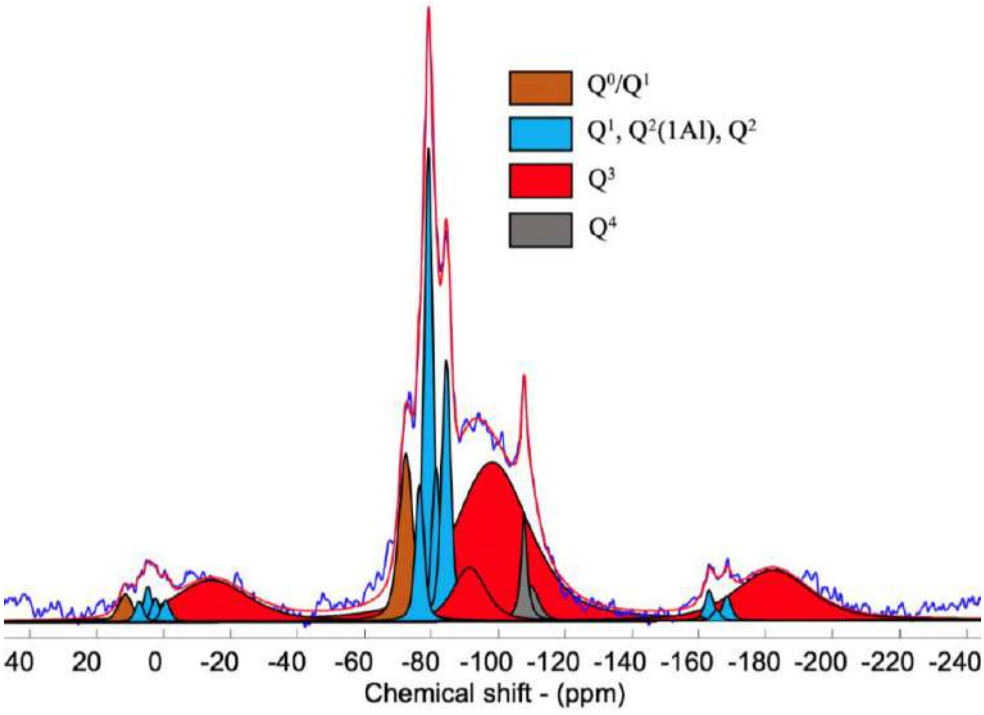

Figure S1: Spectral integration of the ^{29}Si MAS NMR spectrum of MS1 calcined at 800°C and hydrated during 7d.

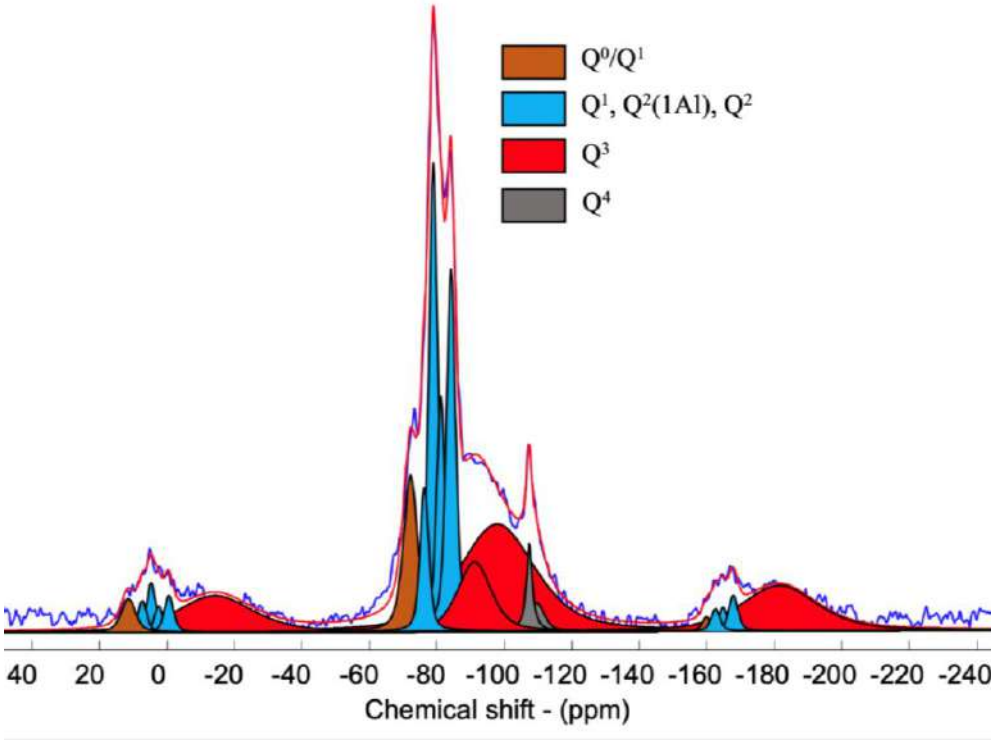

Figure S2: Spectral integration of the ^{29}Si MAS NMR spectrum of MS1 calcined at 800°C and hydrated during 14d.

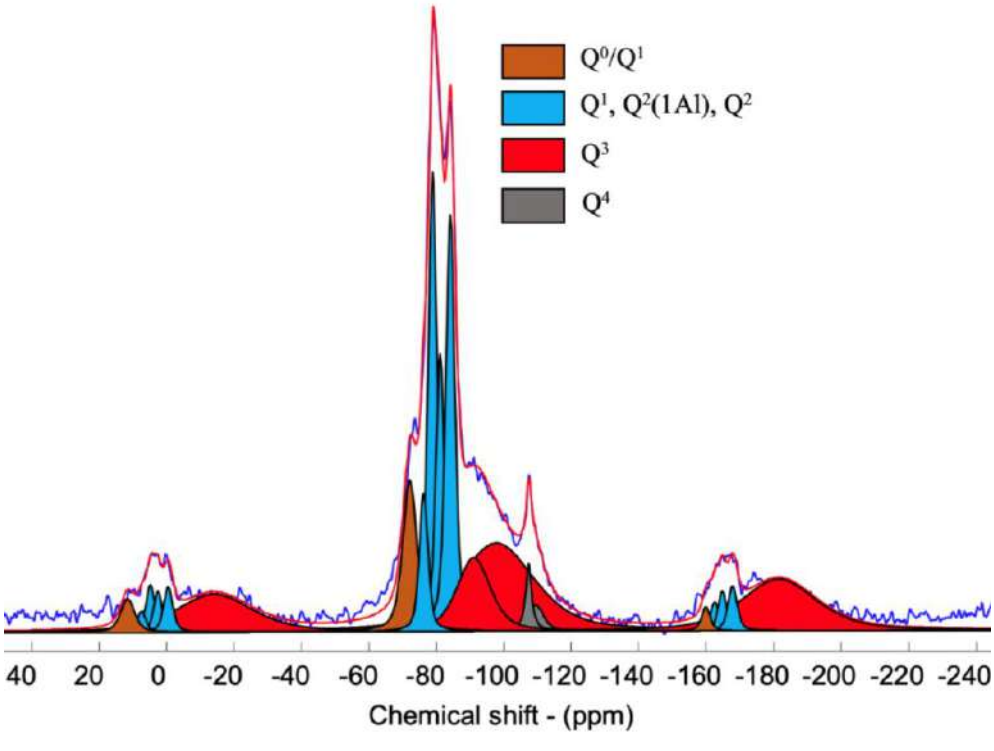

Figure S3: Spectral integration of the ^{29}Si MAS NMR spectrum of MS1 calcined at 800°C and hydrated during 28d.

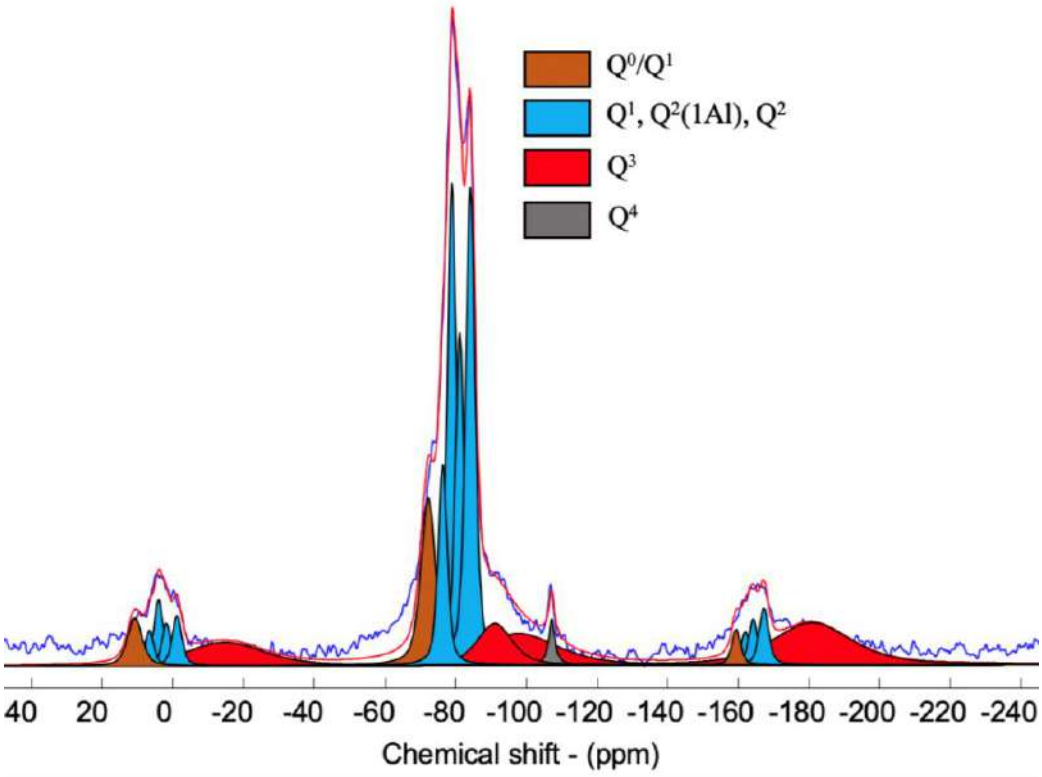

Figure S4: Spectral integration of the ^{29}Si MAS NMR spectrum of MS1 calcined at 800°C and hydrated during 180d.

Table S1: Parameters and relative proportions for the ^{29}Si MAS NMR spectral decompositions of hydrated 800°C-MS1. diso is the isotropic chemical shift and f.w.h.m the full width at half maximum.

Parameters			Relative proportions			
Component	**d_{iso} (ppm)**	**f.w.h.m. (ppm)**	**7d**	**14d**	**28d**	**180d**
Q^4 Silica	-109.9	5.4	1.5	1.3	1.2	0
Q^4 Quartz 2	-107.8	2.1	2.2	1.9	1.5	1,2
Q^3 Calcined-clay 1	-98.2	26.5	52.9	42.4	39.4	25.1
Q^3 Calcined-clay 2	-91.4	11.7	5.1	7.1	7.4	4.9
Q^2 CSH	-84.5	3.2	8.0	12.1	14.1	18.9
Q^2(1Al) CSH	-81.4	3.0	4.6	7.4	9.2	12.6
Q^1 CSH 1	-79.2	3.1	13.7	14.6	14.4	18.2
Q^1 CSH 2	-76.6	3.0	4.0	5.0	4.8	8.3
Q^0/Q^1	-72.5	4.97	8.0	8.2	8.0	10.8

Spectral decomposition MS2

Dmfit software [2] has been used to perform the spectral decompositions of ^{29}Si MAS NMR spectra. The 800°C-MS2 hydrated during 7 days has been used to construct the initial fit. All the lines were modeled using an equally weighted sum of Gaussian and Lorentzian of same widths ('Gaus/Lor' model in dmfit). Q^0/Q^1 of C2S and/or akermanite/gehlenite resonance was described using one line (labelled Q^0/Q^1). Q^1, Q^2(1Al) and Q^2 resonances of C-(A)-S-H were described using four lines (labelled Q^1 CSH 1, Q^1 CSH 2, Q^2(1Al) CSH and Q^2 CSH). Q^3/Q^4 resonances of calcined clay phases was describe using three lines (labeled Q^3 calcined clay 1, Q^3 calcined clay 2 and Q^4 calcined clay). Finally, Q^4 resonance of quartz was described using one Lorentzian line (labeled Q^4 Quartz). Table S2 gathered the parameters of the lines used. All parameters except amplitude were kept constant for the fitting of the ^{29}Si MAS spectra of the 800°C-MS1 hydrated during 14, 28 and 180 days.

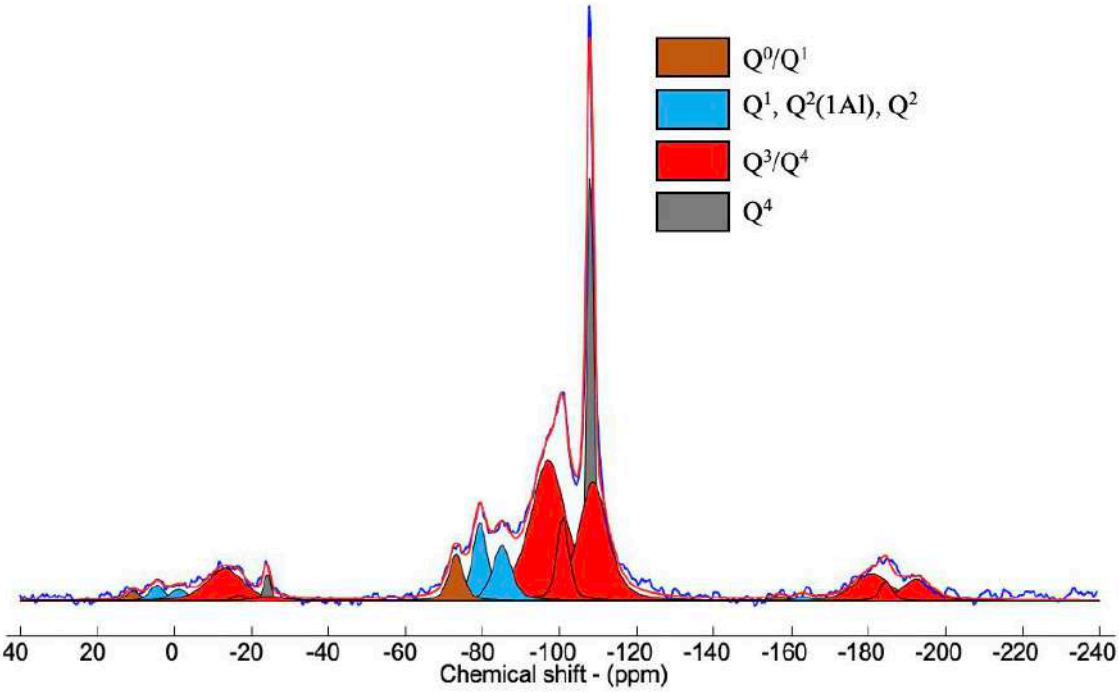

Figure S5: Spectral integration of the ^{29}Si MAS NMR spectrum of MS2 calcined at 800°C and hydrated during 7d.

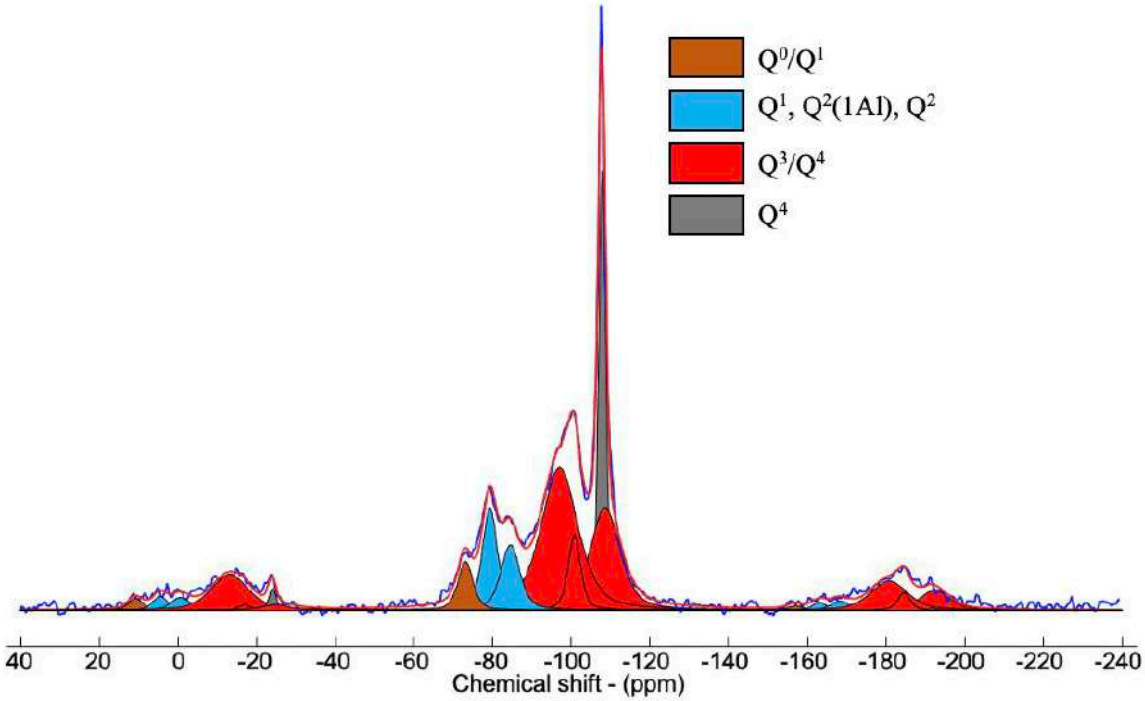

Figure S6: Spectral integration of the ^{29}Si MAS NMR spectrum of MS2 calcined at 800°C and hydrated during 14d.

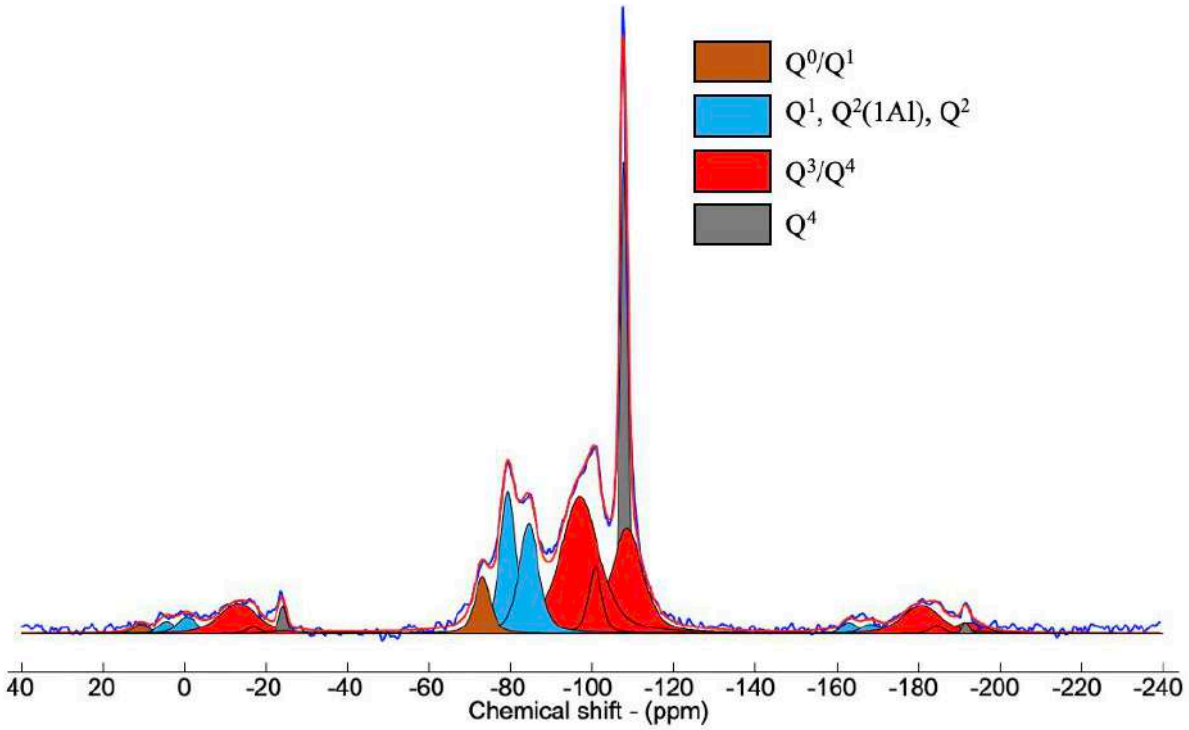

Figure S7: Spectral integration of the ^{29}Si MAS NMR spectrum of MS2 calcined at 800°C and hydrated during 28d.

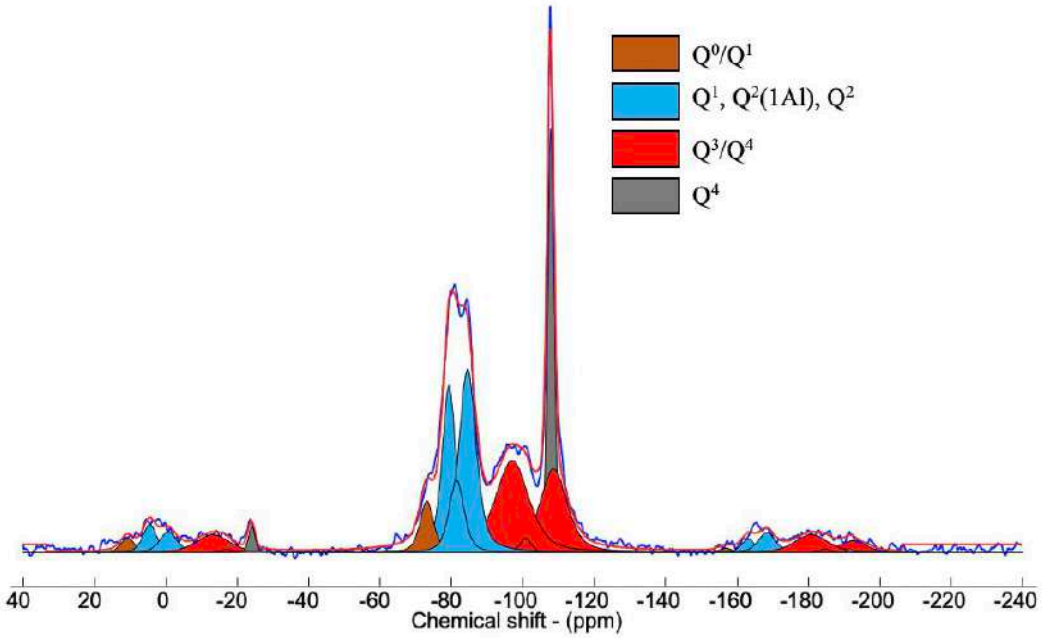

Figure S8: Spectral integration of the ^{29}Si MAS NMR spectrum of MS1 calcined at 800°C and hydrated during 180d.

Table S2: Parameters and relative proportions for the ^{29}Si MAS NMR spectral decompositions of hydrated 800°C-MS2. diso is the isotropic chemical shift and f.w.h.m the full width at half maximum.

Parameters			Relative proportions			
Component	**d_{iso} (ppm)**	**f.w.h.m. (ppm)**	**7d**	**14d**	**28d**	**180d**
Q^4 quartz	-107.89	2.2	13,64	13,75	14,44	13,37
Q^4 Calcined-clay	-108,6	9	22,30	19,13	17,05	14,31
Q^3 Calcined-clay 1	-100,8	3,75	6,98	6,19	4,94	1,31
Q^3 Calcined-clay 2	-97	11.11	37,95	38,32	34,41	23,13
Q^2 CSH	-85	5,7	6,72	8,32	12,30	21,11
Q^2(1Al) CSH	-81.4	5	0	0	0	5,94
Q^1 CSH 1	-79.3	4,5	7,69	9,36	11,94	15,58
Q^0/Q^1	-73,1	4,50	4,71	4,93	4,92	5,25

Rietveld quantification

The Rietveld quantification of MS1 and MS2 was performed using the Profex Rietveld refinement program [2]. Ideal structural phases have been used and refined as best as possible. The samples are natural samples made of a mixture of several phases, which explains the difficulty in obtaining a perfect fit.

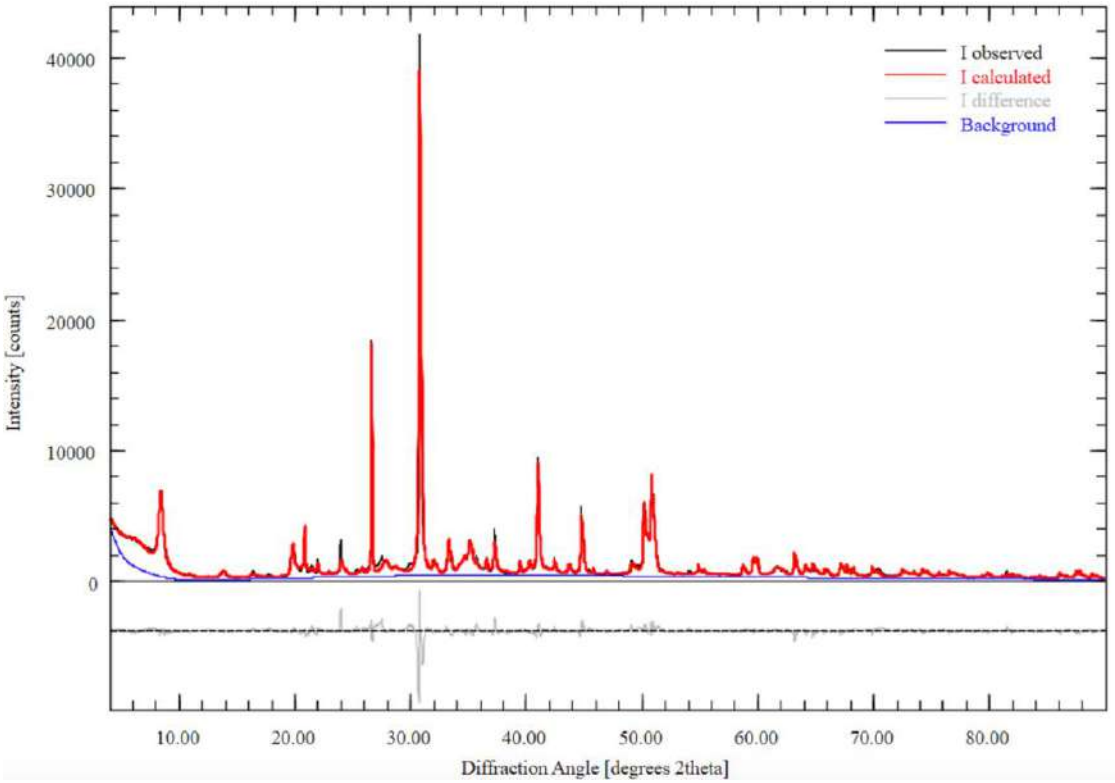

Figure S9 : Rietveld refinement of MS1 (without peaks of phases).

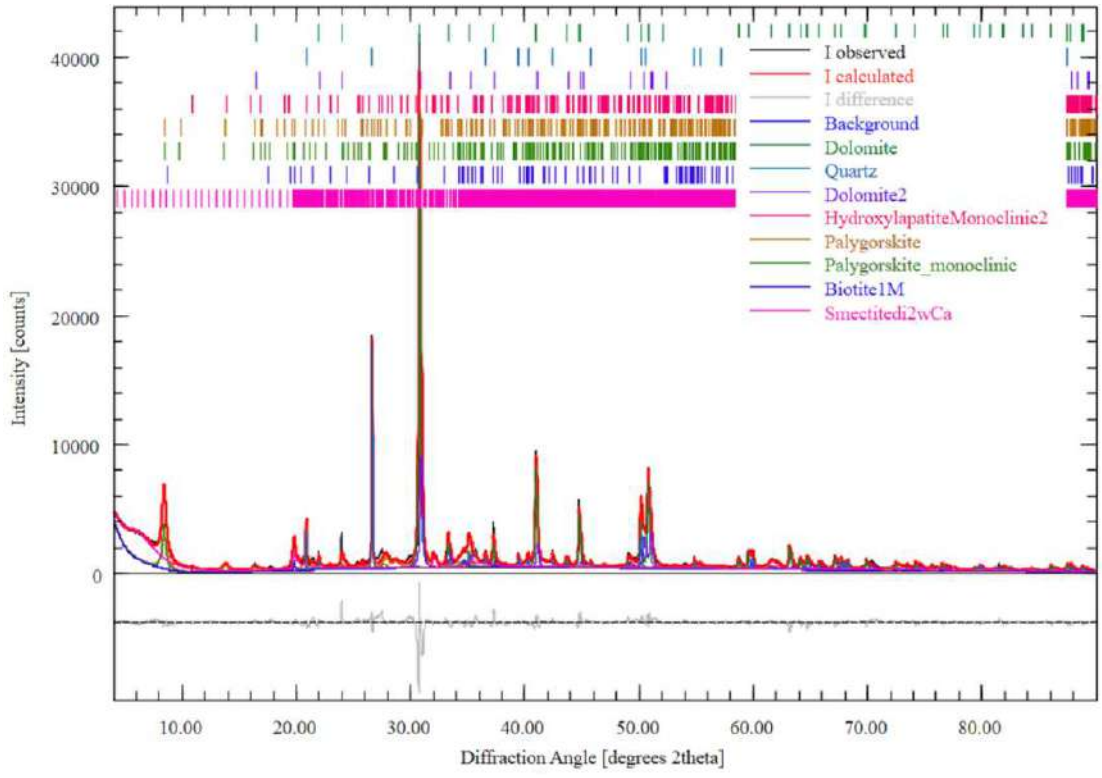

Figure S10 : Rietveld refinement of MS1 (with peaks of phases).

Table S3: Statistics of the Rietveld refinement of MS1.

Statistics	R_{wp} = 10,24	R_{exp} = 3.14	X^2 = 10,6	GoF = 3,26

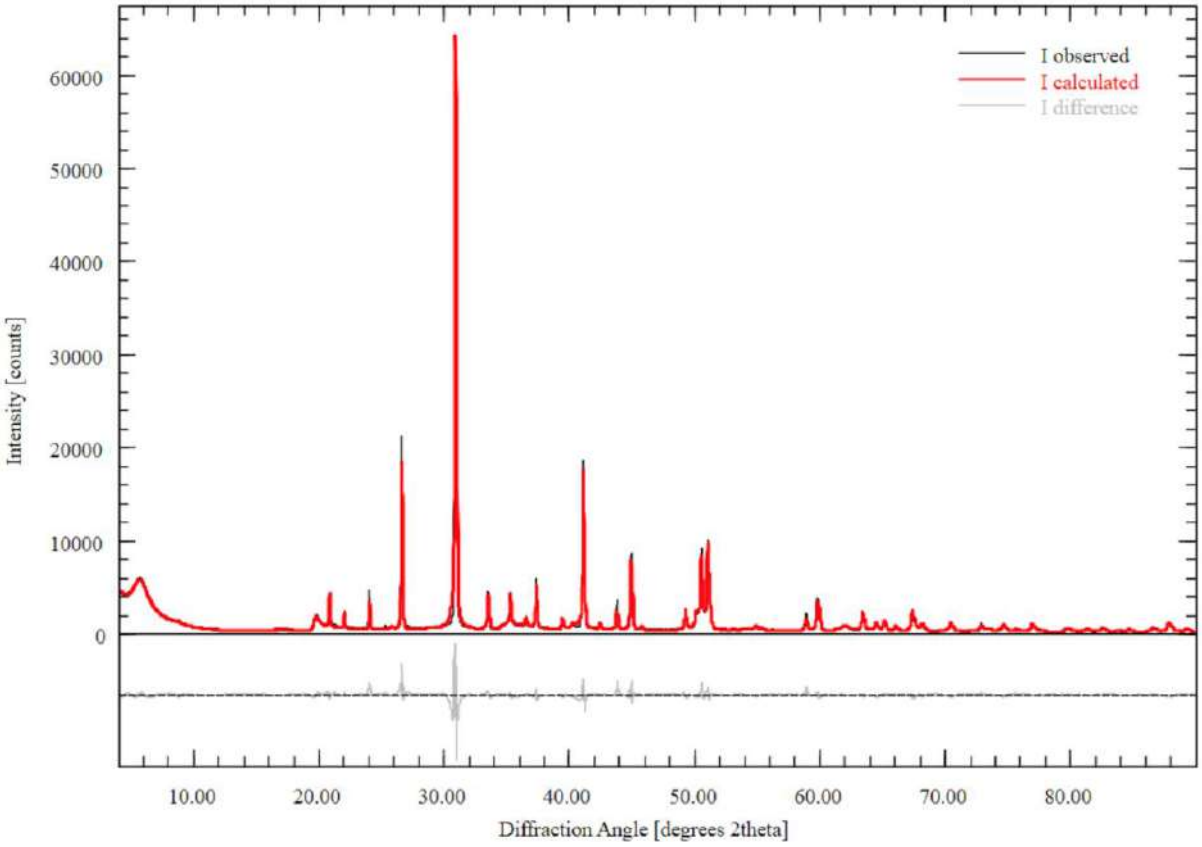

Figure S11 : Rietveld refinement of MS2 (without peaks of phases).

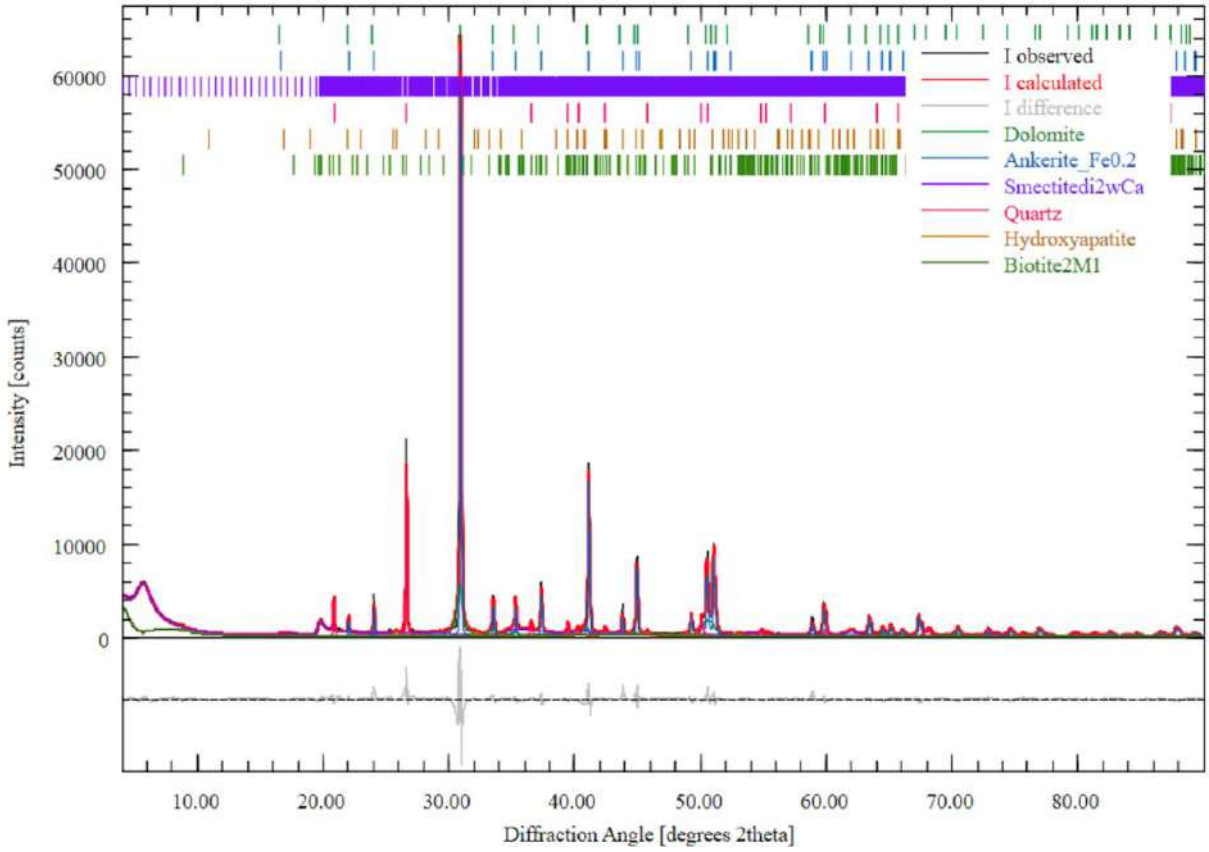

Figure S12 : Rietveld refinement of MS2 (with peaks of phases).

Table S4: Statistics of the Rietveld refinement of MS2.

Statistics	R_{wp} = 9,67	R_{exp} = 3.47	X^2 = 7,76	GoF = 2.78

References

[1] D. Massiot, F. Fayon, M. Capron, I. King, S. Le Calvé, B. Alonso, J.-O. Durand, B. Bujoli, Z. Gan, G. Hoatson, Modelling one- and two-dimensional solid-state NMR spectra: Modelling 1D and 2D solid-state NMR spectra, Magn. Reson. Chem. 40 (2002) 70–76. https://doi.org/10.1002/mrc.984.

[2] N. Doebelin, R. Kleeberg, *Profex* : a graphical user interface for the Rietveld refinement program *BGMN*, Journal of Applied Crystallography. 48 (2015) 1573–1580. https://doi.org/10.1107/S1600576715014685.

Informations complémentaires du chapitre 5

Spectral decompositions of ^{29}Si MAS NMR spectra have been done by using the dmfit software. The initial fit was constructed from the spectrum of the raw white Portland cement. For the lineshapes of all lines, we used an equally weighted sum of Gaussian and Lorentzian of same widths ('Gaus/Lor' model in dmfit). One line (labelled Q^0/Q^1) was used to describe the resonance associated with Q^0/Q^1 of belite and three lines were used to describe the resonance associated with Q^0/Q^1 of alite.

The fits of the hydrated cement at 7 and 28 days were constructed using lines previously constructed for alite and belite. Two Gaussian lines (labeled as Q^1) were used to describe the C-S-H in Q^1 configuration, one Gaussian line to describe the C-S-H in Q^2 configuration and one line to describe the C-S-H in Q^2(1Al) configuration.

The fits of Min-U-400 and Min-U-FG calcined at 800°C were constructed using one Gaussian line to describe the silicon in Q^4 configuration associated to quartz at -108 ppm. Four Gaussian lines were used to describe the silicon in Q^3 configuration associated with the calcined clay.
The fits of the blendings 0.2wPc + 0.8Min-U-400-800°C and 0.2wPc + 0.8Min-U-FG-800°C were constructed using the preceding lines constructed for the raw cement and the calcined clay. The silicon in Q^1, Q^2 and Q^2(1Al) in the same way than for the pure cement paste.

The parameters of the lines are gathered in table S-1. At first, all parameters except amplitude were kept constant for the fitting of the ^{29}Si MAS spectra of the three mixings, then the full width at half maximum (f.w.m.h.) has been allowed to vary.

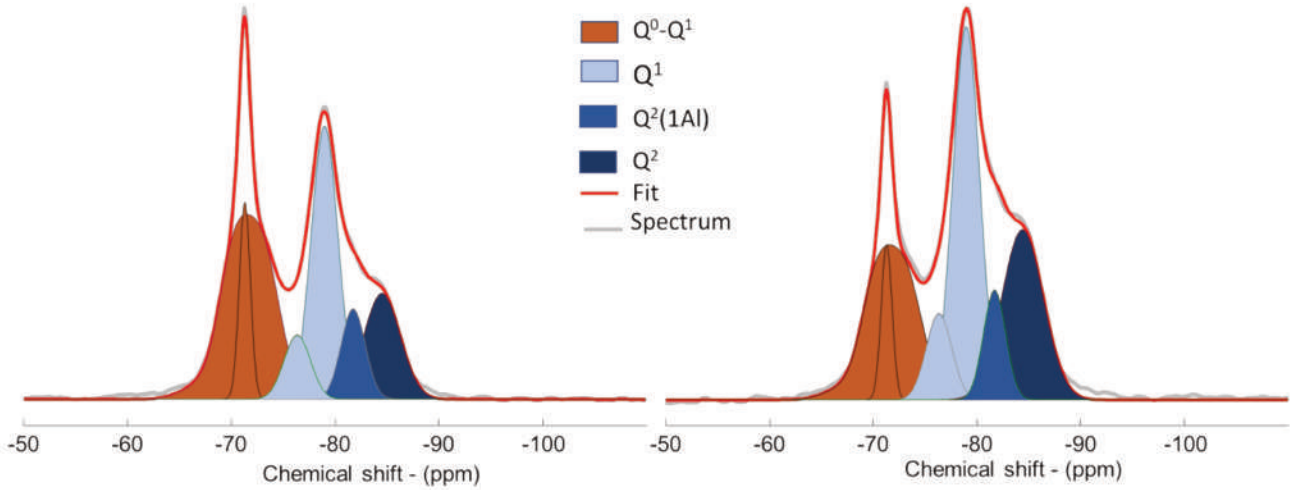

Figure S1 : Spectral integration of the 29Si MAS NMR spectra of the white Portland cement hydrated during 7 and 28 days.

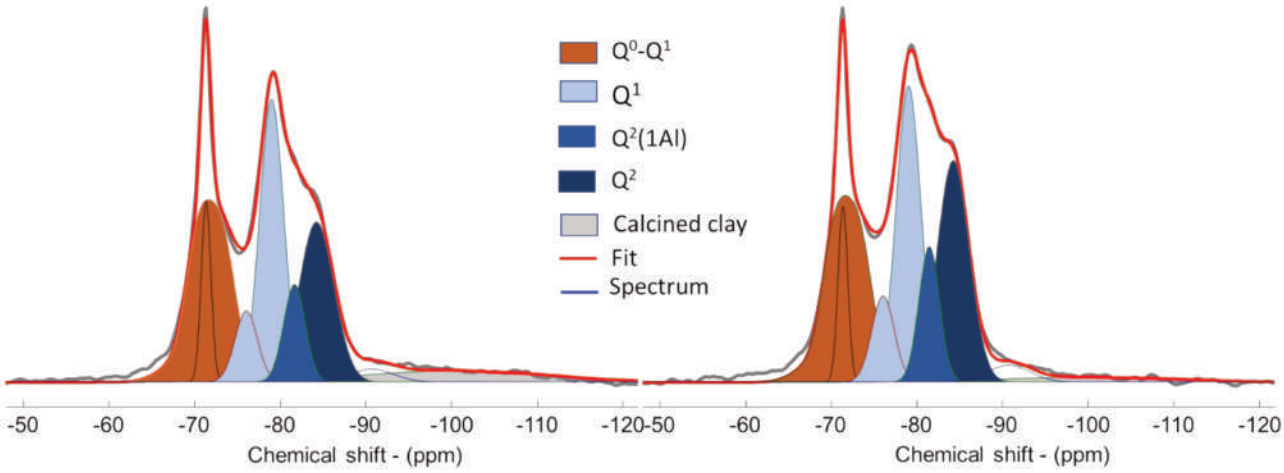

Figure S2 : Spectral integration of the 29Si MAS NMR spectra of the blendings 80% white Portland cement + 20% Min-U-400-800°C hydrated during 7 and 28 days.

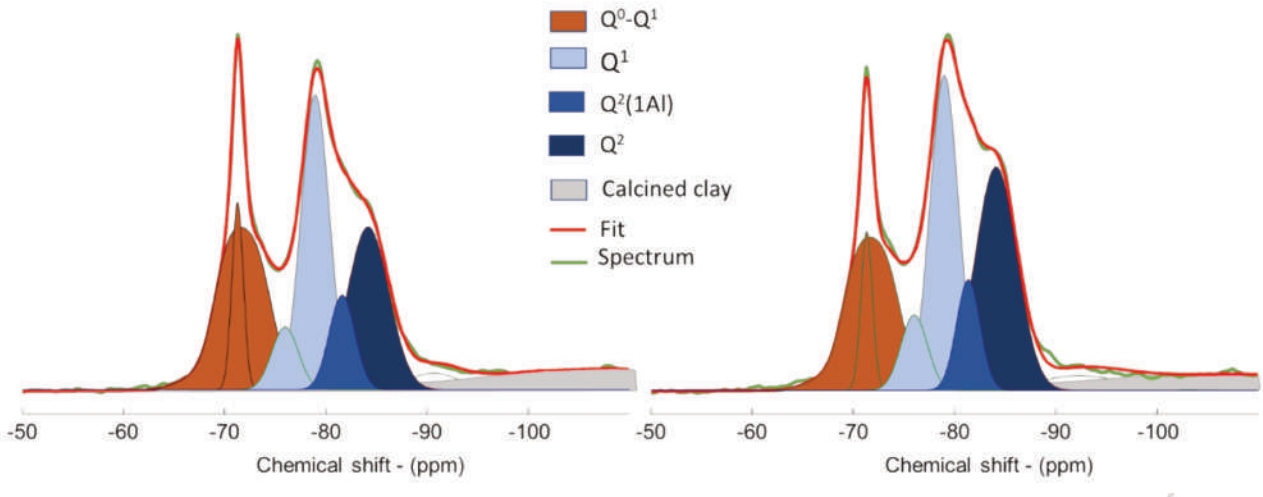

Figure S3 : Spectral integration of the ^{29}Si MAS NMR spectra of the blendings 80% white Portland cement + 20% Min-U-FG-800°C hydrated during 7 and 28 days.

Table S1: Parameters and relative proportions for the ^{29}Si MAS NMR spectral decompositions. δiso is the isotropic chemical shift.

Parameters		Relative proportions					
Component	d_{iso} (ppm)	Cement		80% Cement + 20% Min-U-400-800°C		80% Cement + 20% Min-U-FG-800°C	
		7d	28d	7d	28d	7d	28d
Q^3 Min-U-400-800°C 1	-99,5			7,4	3,1		
Q^3 Min-U-FG-800°C 1	-107,5					12,8	9,2
Q^3 Calcined clay 2	-90,7			1,9	2,4	2,4	3,4
Q^2 CSH	-84,2	14,6	22,6	19,9	23,4	19,4	25,1
Q^2(1Al) CSH	-81,5	8,2	7,8	7,6	9,3	7,1	7,1
Q^1 CSH 1	-79,0	27,1	31,7	24,0	23,9	23,9	24,0
Q^1 CSH 2	-76,0	6,4	7,1	5,7	6,4	4,8	5,4
Q^0/Q^1(Alite)	-71,5	35,5	25,4	27,5	26,0	23,5	20,8
Q^0/Q^1(Bélite)	-71,3	8,1	5,4	6,2	5,6	6,2	4,9

Rietveld quantification

The Rietveld quantification of Pal-1 and Pal-2 was performed using the Profex Rietveld refinement program [2]. Ideal structural phases have been used and refined as best as possible.

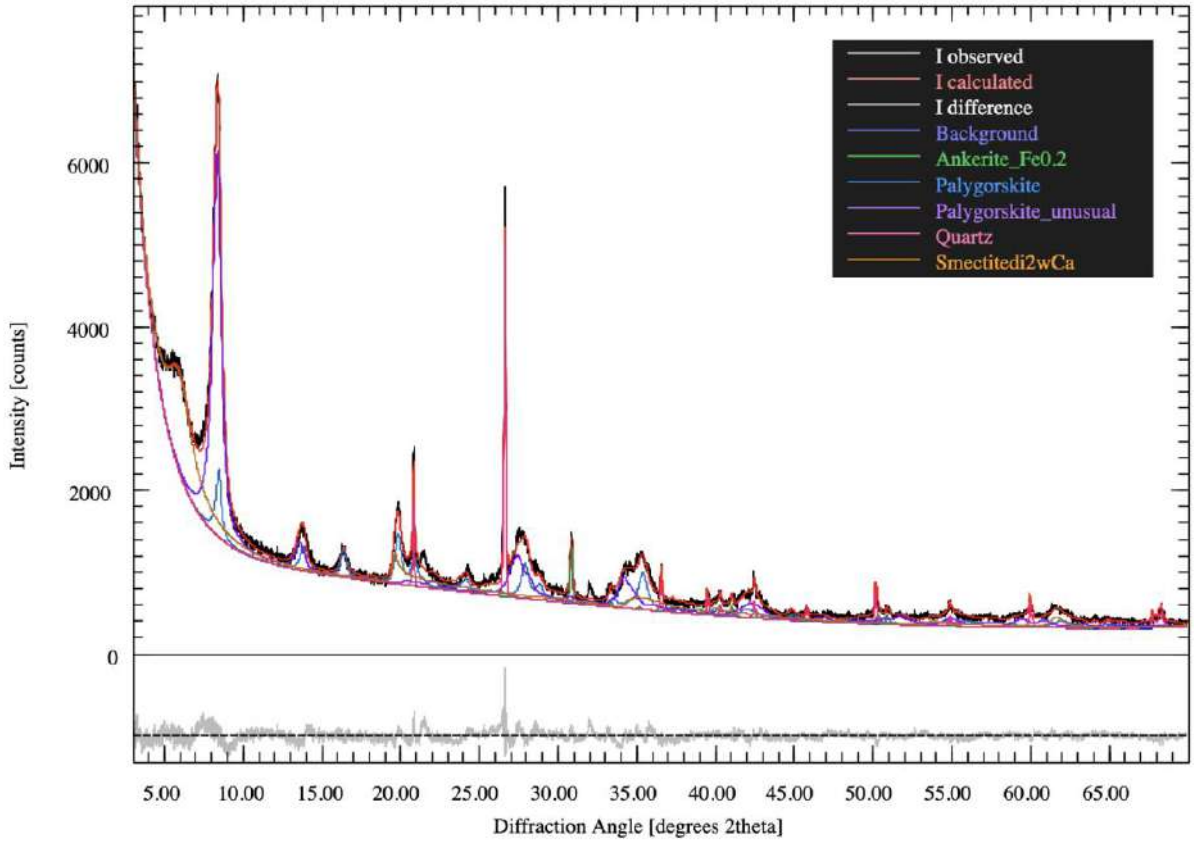

Figure S4 : Rietveld refinement of Pal-1.

Table S2: Statistics of the Rietveld refinement of Pal-1.

Statistics	R_{wp} = 5.03	R_{exp} = 3.07	X^2 = 12.68	GoF = 1.63

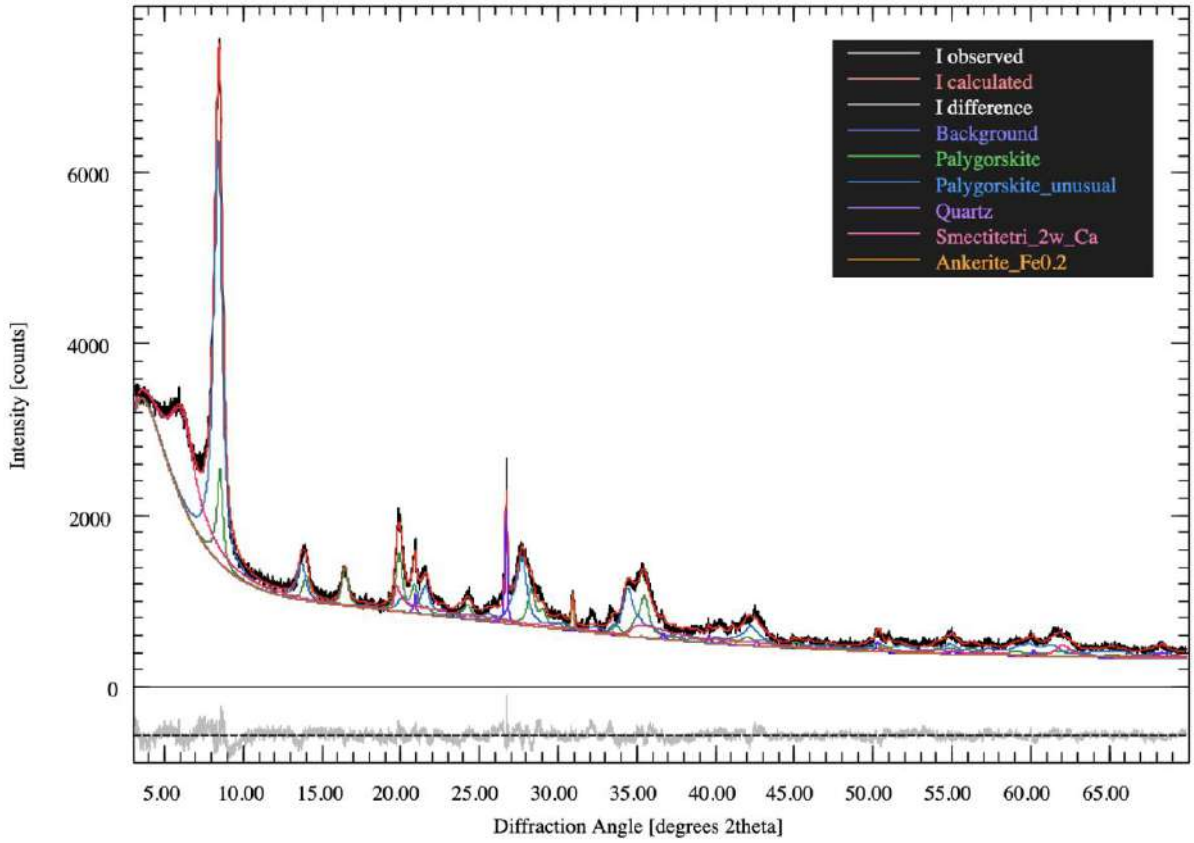

Figure S4 : Rietveld refinement of Pal-2.

Table S2: Statistics of the Rietveld refinement of Pal-2.

Statistics	R_{wp} = 4.99	R_{exp} = 3.08	X^2 = 2.62	GoF = 1.62

Informations complémentaires du chapitre 6

Spectral decompositions of the ^{27}Al MAS spectra were done by using the dmfit software (Massiot et al., 2002).

PFl-1 spectral decomposition

PFl-raw

Table S1: Parameters for PFl-raw ^{27}Al MAS NMR spectral decompositions. diso is the isotropic chemical shift, C_Q is the mean quadrupolar product (GIM) and FWHM CS is the full width at half maximum of the Gaussian distribution of isotropic chemical shift.

Component	Shape	δ_{iso} (ppm)	Width (ppm)	C_Q (MHz)	FWHM CS (ppm)	Proportions (%)
Al-6	Lorentzienne	4.22	5.20			92
Al-4	CzSimple	70.0		7.0	15.0	6
Al-4	Q mas 1/2	59.75		3.521		2

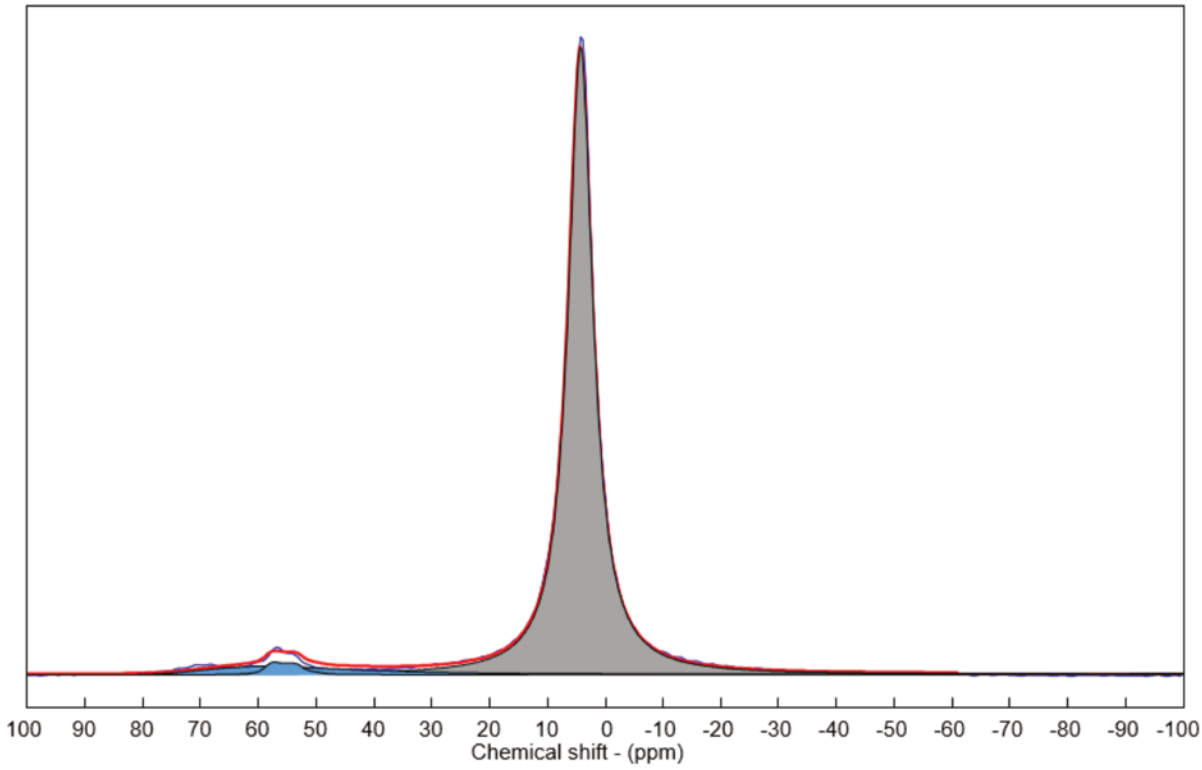

Figure S1: Spectral decomposition of PFl-raw ^{27}Al MAS NMR spectrum.

PFI-400

Table S2: Parameters for PFI-400 ^{27}Al MAS NMR spectral decompositions. diso is the isotropic chemical shift, C_Q is the mean quadrupolar product (GIM) and FWHM CS is the full width at half maximum of the Gaussian distribution of isotropic chemical shift.

Component	Shape	δ_{iso} (ppm)	Width (ppm)	C_Q (MHz)	FWHM CS (ppm)	Proportions (%)
Al-6	Lorentzienne	4.16	4.67			84
Al-6	CzSimple	6.50		7.0	10.0	0
Al-5	CzSimple	33.0		8.5	17.0	6
Al-4	CzSimple	70.0		7.0	15.0	7
Al-4	CzSimple	60.0		6.5	12.0	0
Al-4	Q mas 1/2	59.75		3.521		3

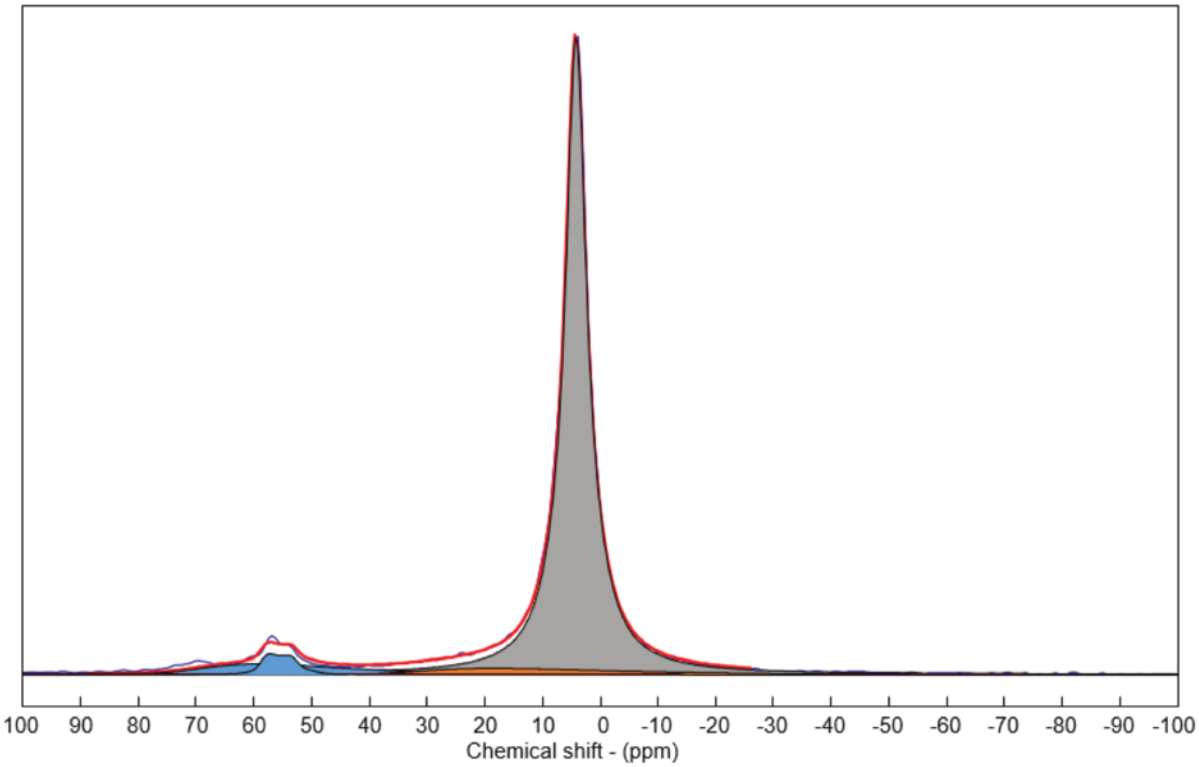

Figure S2: Spectral decomposition of PFI-400 ^{27}Al MAS NMR spectrum.

PFL-500

Table S3: Parameters for PFl-500 ^{27}Al MAS NMR spectral decompositions. diso is the isotropic chemical shift, C_Q is the mean quadrupolar product (GIM) and FWHM CS is the full width at half maximum of the Gaussian distribution of isotropic chemical shift.

Component	Shape	δ_{iso} (ppm)	Width (ppm)	C_Q (MHz)	FWHM CS (ppm)	Proportions (%)
Al-6	Lorentzienne	4.16	4.67			34
Al-6	CzSimple	6.50		7.0	10.0	20
Al-5	CzSimple	33.0		8.5	17.0	29
Al-4	CzSimple	70.0		7.0	15.0	12
Al-4	CzSimple	60.0		6.5	12.0	0
Al-4	Q mas 1/2	59.75		3.521		5

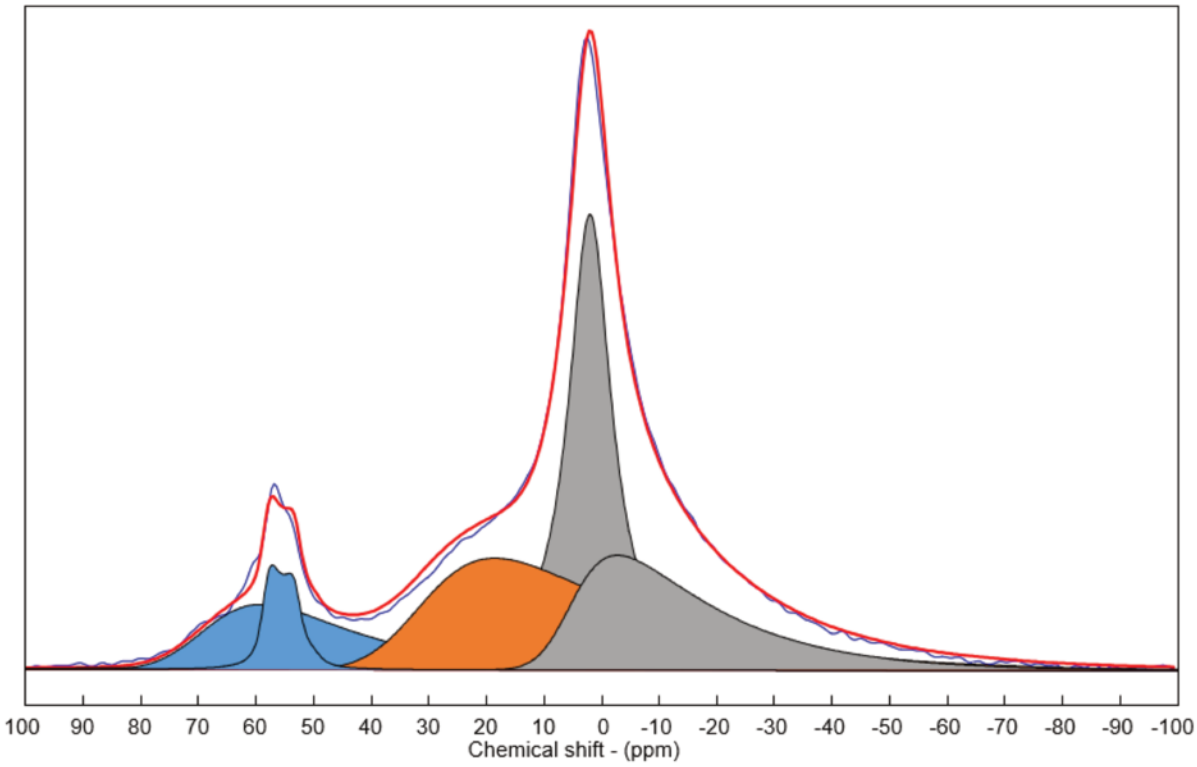

Figure S3: Spectral decomposition of PFl-500 ^{27}Al MAS NMR spectrum.

PFL-600

Table S4: Parameters for PFl-600 ^{27}Al MAS NMR spectral decompositions. diso is the isotropic chemical shift, C_Q is the mean quadrupolar product (GIM) and FWHM CS is the full width at half maximum of the Gaussian distribution of isotropic chemical shift.

Component	Shape	δ_{iso} (ppm)	Width (ppm)	C_Q (MHz)	FWHM CS (ppm)	Proportions (%)
Al-6	Lorentzienne	2.0	9.0			27
Al-6	CzSimple	6.50		7.0	10.0	16
Al-5	CzSimple	33.0		8.5	17.0	35
Al-4	CzSimple	70.0		7.0	15.0	17
Al-4	CzSimple	60.0		6.5	12.0	0
Al-4	Q mas 1/2	59.75		3.521		5

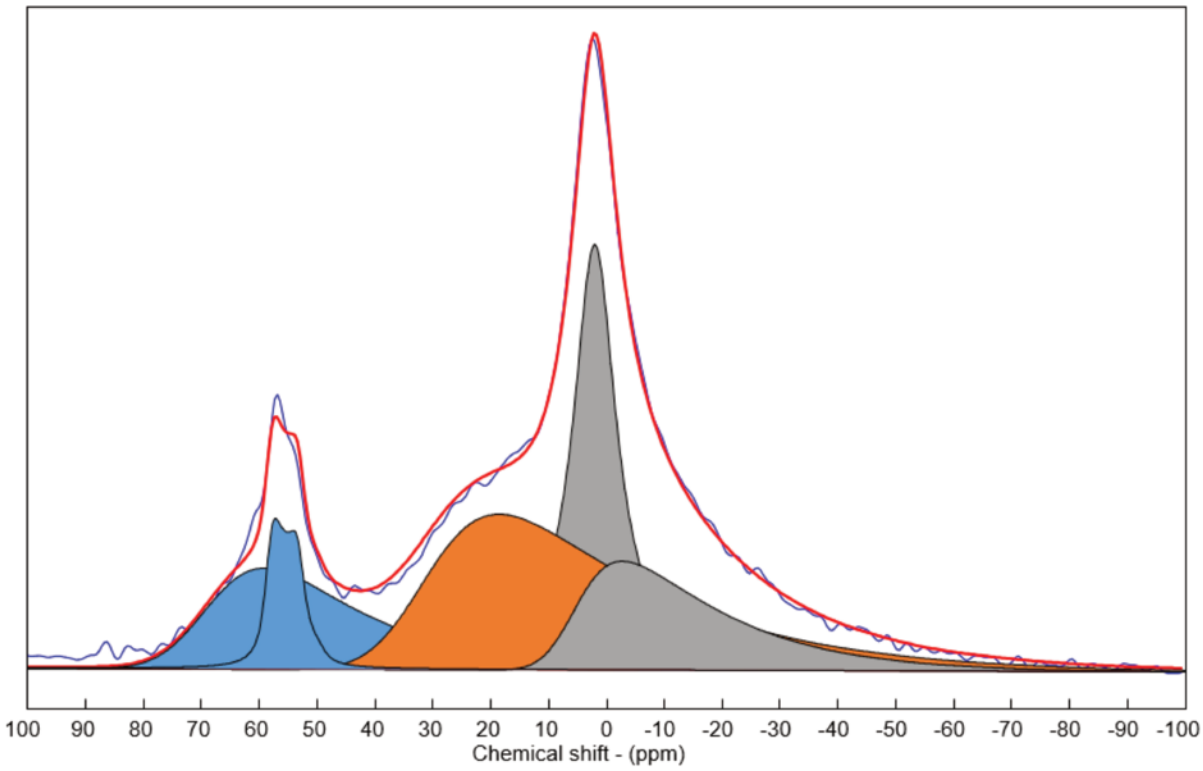

Figure S4: Spectral decomposition of PFl-600 ^{27}Al MAS NMR spectrum.

PFI-700

Table S5: Parameters for PFI-700 ^{27}Al MAS NMR spectral decompositions. diso is the isotropic chemical shift, C_Q is the mean quadrupolar product (GIM) and FWHM CS is the full width at half maximum of the Gaussian distribution of isotropic chemical shift.

Component	Shape	δ_{iso} (ppm)	Width (ppm)	C_Q (MHz)	FWHM CS (ppm)	Proportions (%)
Al-6	Lorentzienne	2.0	9.0			15
Al-6	CzSimple	6.50		7.0	10.0	16
Al-5	CzSimple	33.0		8.5	17.0	44
Al-4	CzSimple	68.0		7.0	15.0	19
Al-4	CzSimple	60.0		6.5	12.0	2
Al-4	Q mas 1/2	59.75		3.521		4

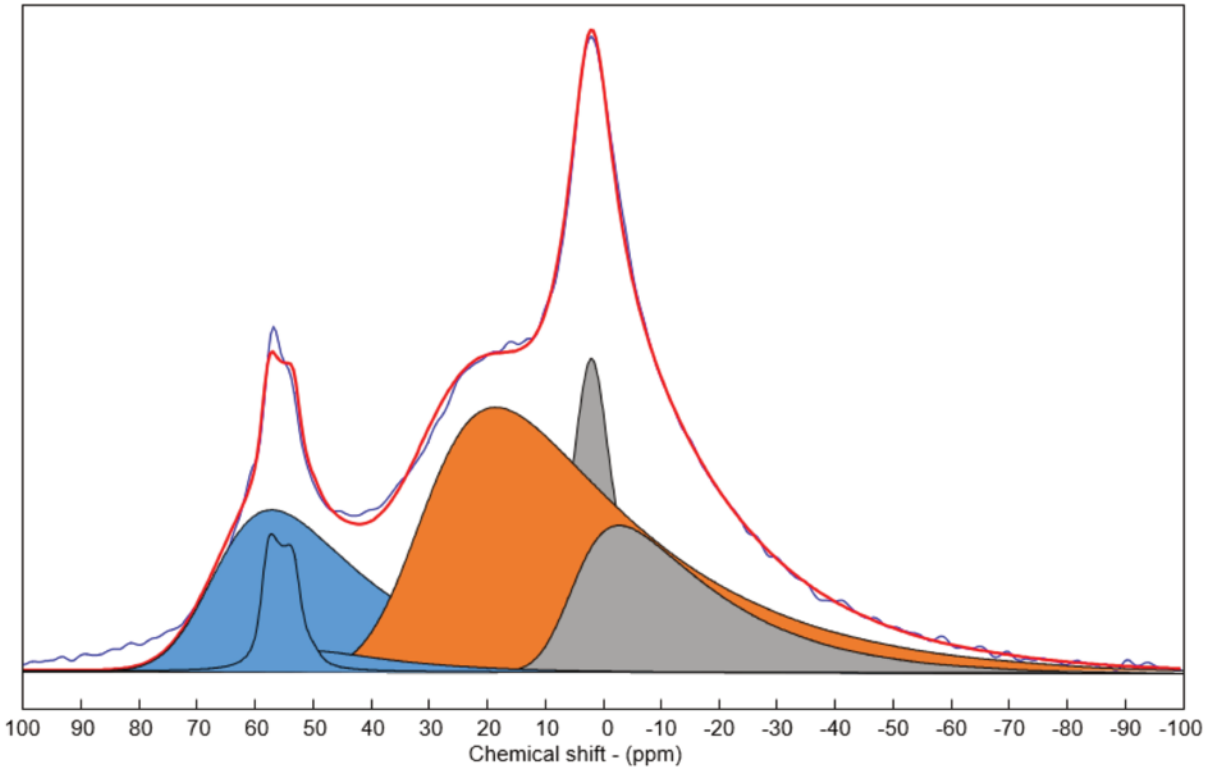

Figure S5: Spectral decomposition of PFI-700 ^{27}Al MAS NMR spectrum.

PFI-800

Table S6: Parameters for PFI-800 ^{27}Al MAS NMR spectral decompositions. diso is the isotropic chemical shift, C_Q is the mean quadrupolar product (GIM) and FWHM CS is the full width at half maximum of the Gaussian distribution of isotropic chemical shift.

Component	Shape	δ_{iso} (ppm)	Width (ppm)	C_Q (MHz)	FWHM CS (ppm)	Proportions (%)
Al-6	Lorentzienne	3.50	9.0			3
Al-6	CzSimple	6.50		7.0	10.0	4
Al-5	CzSimple	33.0		10	17.0	31
Al-4	CzSimple	68.0		7.0	15.0	34
Al-4	CzSimple	55.0		8.0	15.0	23
Al-4	Q mas 1/2	59.75		3.521		5

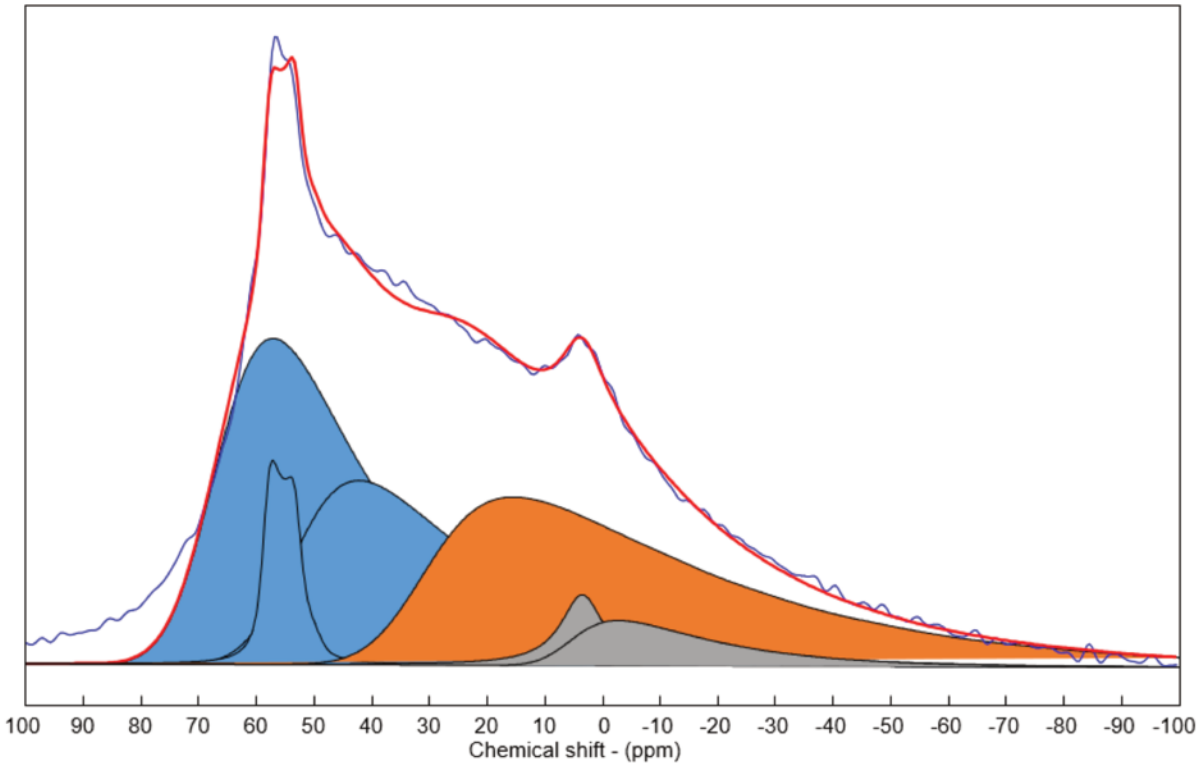

Figure S6: Spectral decomposition of PFI-800 ^{27}Al MAS NMR spectrum.

PFI-900

Table S7: Parameters for PFI-900 ^{27}Al MAS NMR spectral decompositions. diso is the isotropic chemical shift, C_Q is the mean quadrupolar product (GIM) and FWHM CS is the full width at half maximum of the Gaussian distribution of isotropic chemical shift.

Component	Shape	δ_{iso} (ppm)	Width (ppm)	C_Q (MHz)	FWHM CS (ppm)	Proportions (%)
Al-6	Lorentzienne	3.50	9.0			0
Al-6	CzSimple	6.50		7.0	10.0	4
Al-5	CzSimple	33.0		10.0	17.0	24
Al-4	CzSimple	68.0		7.0	15.0	34
Al-4	CzSimple	55.0		8.0	15.0	32
Al-4	Q mas 1/2	59.75		3.521		6

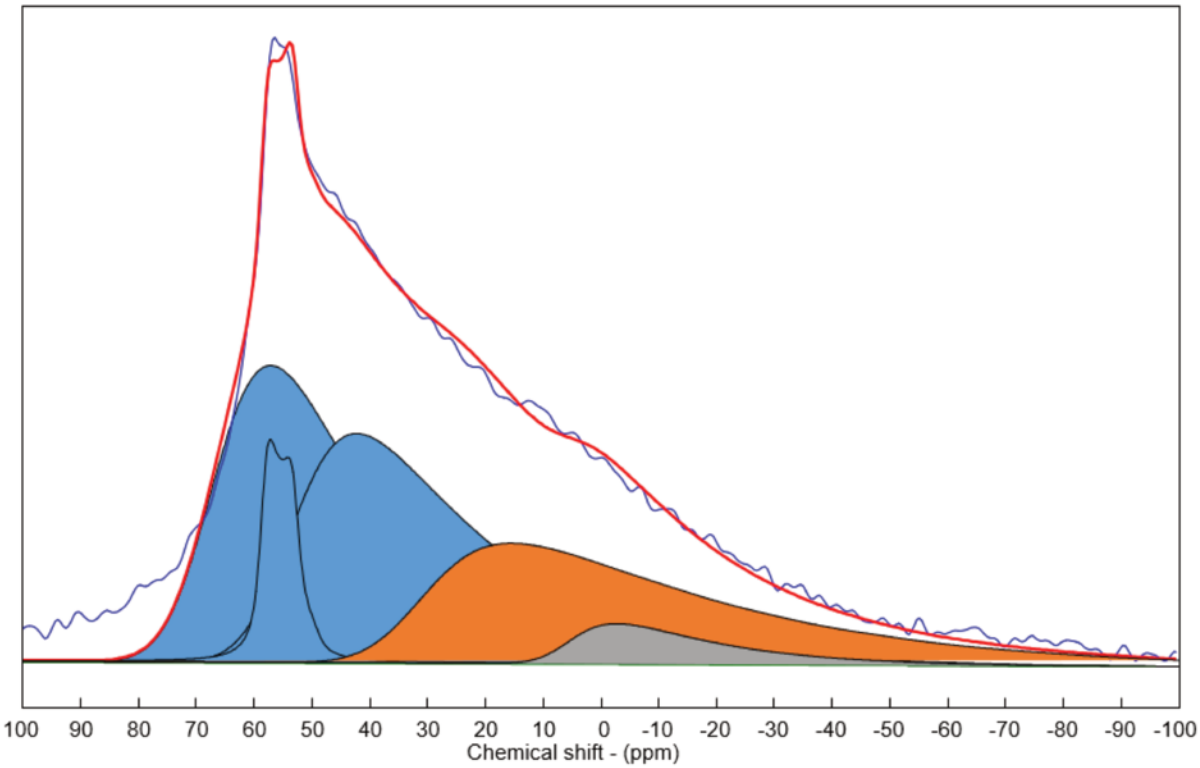

Figure S7: Spectral decomposition of PFI-900 ^{27}Al MAS NMR spectrum.

KGa-1b spectral decomposition

KGa-1b raw

Table S8: Parameters for KGa-1b-raw ^{27}Al MAS NMR spectral decompositions. diso is the isotropic chemical shift, C_Q is the mean quadrupolar product (GIM) and FWHM CS is the full width at half maximum of the Gaussian distribution of isotropic chemical shift.

Component	Shape	δ_{iso} (ppm)	Width (ppm)	C_Q (MHz)	FWHM CS (ppm)	Proportions (%)
Al-6	Int2QUAD	7.50		3.1		99
Al-4	Lorentzienne	69.42	5.56			1

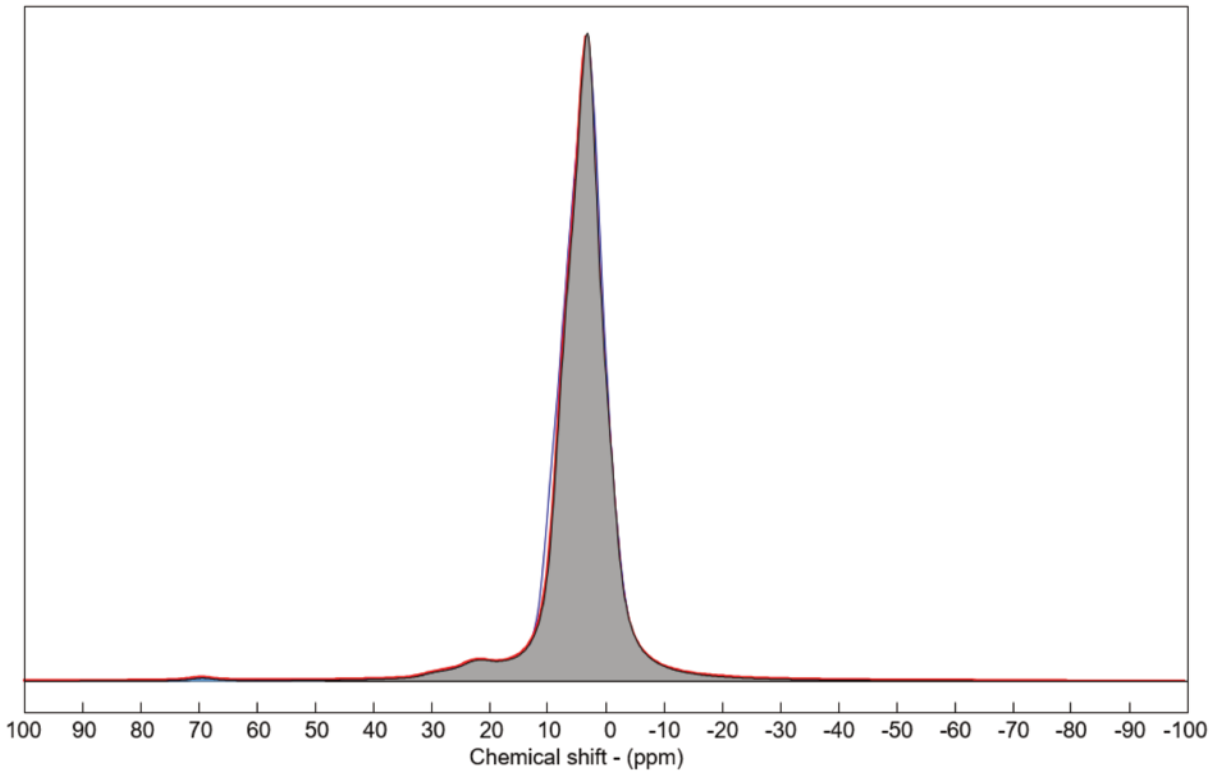

Figure S8: Spectral decomposition of KGa-1b-raw ^{27}Al MAS NMR spectrum.

KGa-1b 525

Table S9: Parameters for KGa-1b-525 ^{27}Al MAS NMR spectral decompositions. diso is the isotropic chemical shift, C_Q is the mean quadrupolar product (GIM) and FWHM CS is the full width at half maximum of the Gaussian distribution of isotropic chemical shift.

Component	Shape	δ_{iso} (ppm)	Width (ppm)	C_Q (MHz)	FWHM CS (ppm)	Proportions (%)
Al-6	Gaussienne	3.98	8.07			36
Al-6	CzSimple	5.0		8.0	12	3
Al-5	CzSimple	35.0		8.5	18	34
Al-4	CzSimple	63.92		10.0	20	27

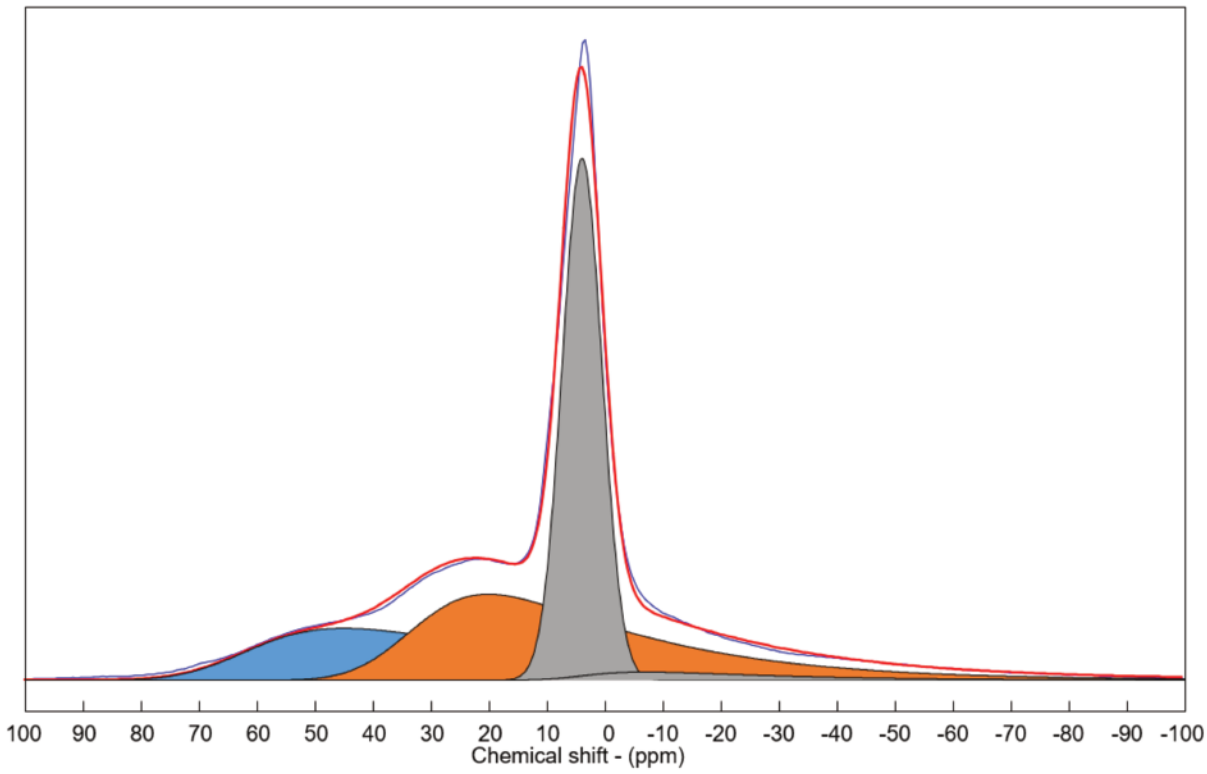

Figure S9: Spectral decomposition of KGa-1b-525 ^{27}Al MAS NMR spectrum.

KGa-1b 550

Table S10: Parameters for KGa-1b-550 ^{27}Al MAS NMR spectral decompositions. diso is the isotropic chemical shift, C_Q is the mean quadrupolar product (GIM) and FWHM CS is the full width at half maximum of the Gaussian distribution of isotropic chemical shift.

Component	Shape	δ_{iso} (ppm)	Width (ppm)	C_Q (MHz)	FWHM CS (ppm)	Proportions (%)
Al-6	Gaussienne	3.56	9.23			6
Al-6	CzSimple	5.0		8.0	12	3
Al-5	CzSimple	37.71		9.5	15	45
Al-4	CzSimple	63.92		10.0	20	46

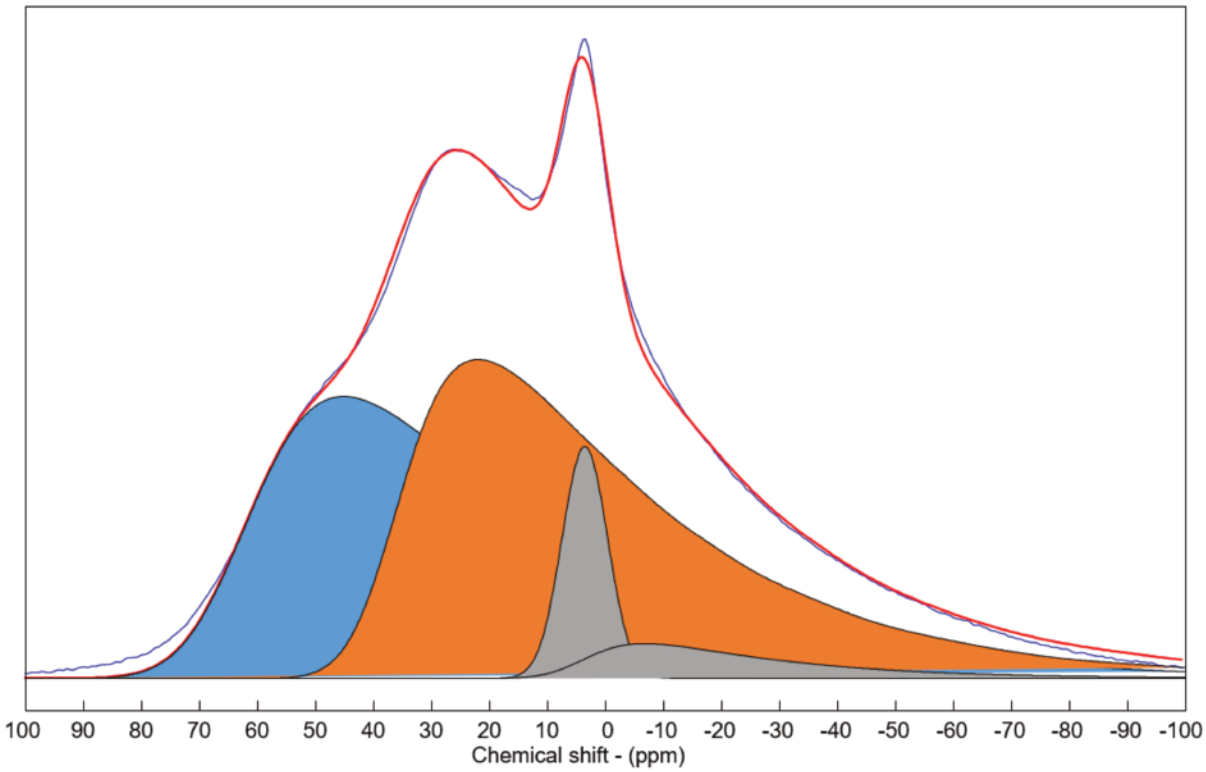

Figure S10: Spectral decomposition of KGa-1b-550 ^{27}Al MAS NMR spectrum.

KGa-1b 600

Table S11: Parameters for KGa-1b-600 ^{27}Al MAS NMR spectral decompositions. diso is the isotropic chemical shift, C_Q is the mean quadrupolar product (GIM) and FWHM CS is the full width at half maximum of the Gaussian distribution of isotropic chemical shift.

Component	Shape	δ_{iso} (ppm)	Width (ppm)	C_Q (MHz)	FWHM CS (ppm)	Proportions (%)
Al-6	Gaussienne	2.75	9.09			2
Al-6	CzSimple	5.0		8.0	12	6
Al-5	CzSimple	37.71		9.5	15	45
Al-4	CzSimple	63.92		10.0	20	47

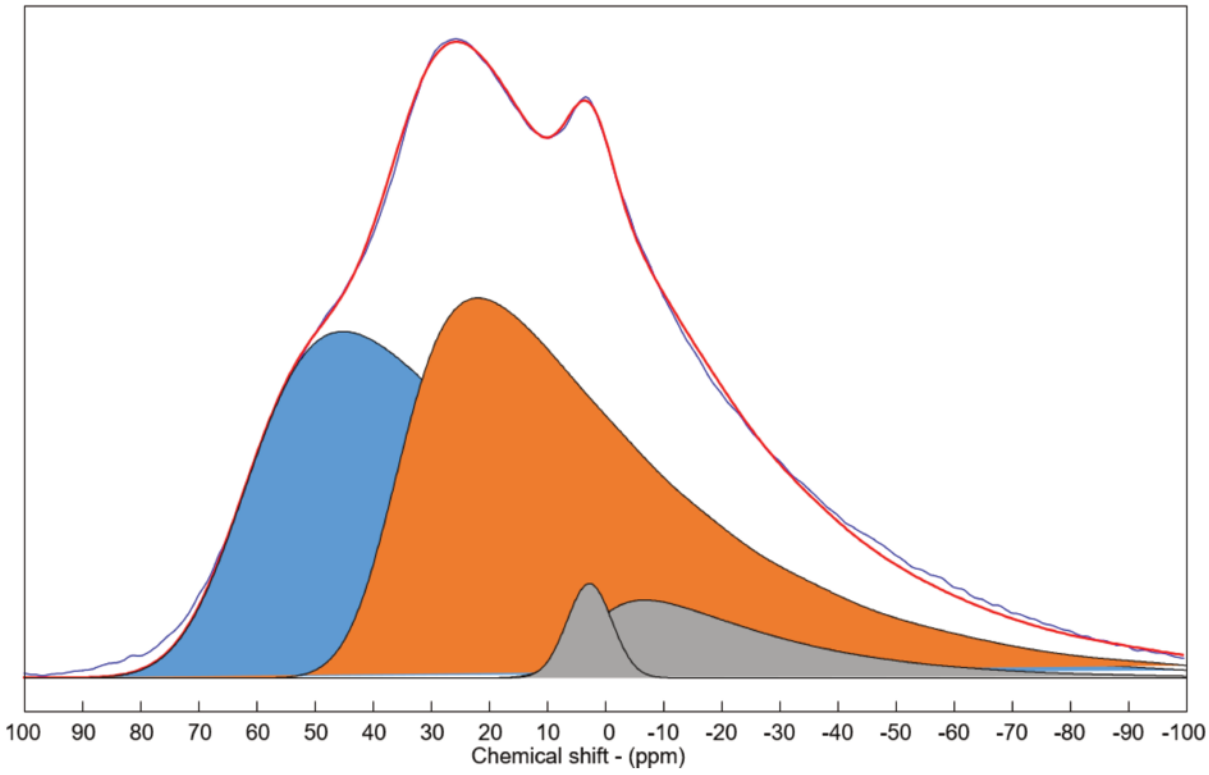

Figure S11: Spectral decomposition of KGa-1b-600 ^{27}Al MAS NMR spectrum.

KGa-1b 700

Table S12: Parameters for KGa-1b-700 ^{27}Al MAS NMR spectral decompositions. diso is the isotropic chemical shift, C_Q is the mean quadrupolar product (GIM) and FWHM CS is the full width at half maximum of the Gaussian distribution of isotropic chemical shift.

Component	Shape	δ_{iso} (ppm)	Width (ppm)	C_Q (MHz)	FWHM CS (ppm)	Proportions (%)
Al-6	Gaussienne	3.50	12.0			1
Al-6	CzSimple	5.0		8.0	12	6
Al-5	CzSimple	37.71		9.5	15	44
Al-4	CzSimple	63.92		10.0	20	49

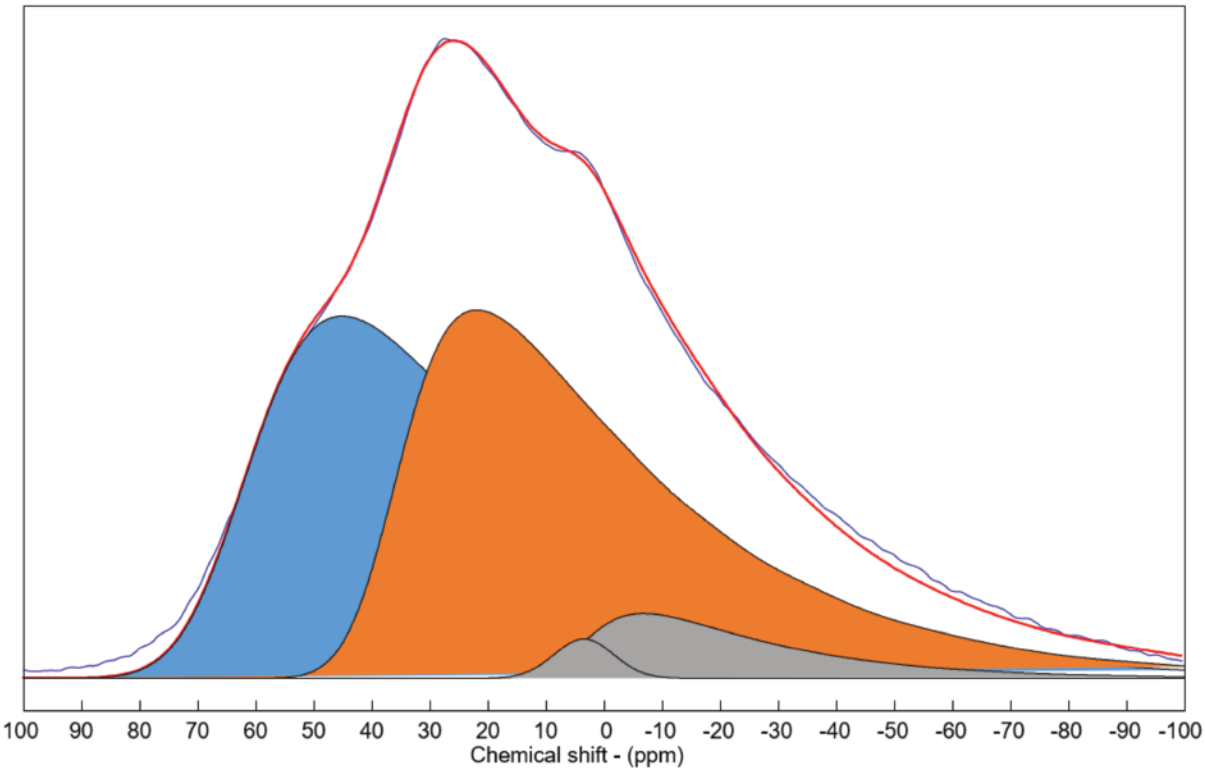

Figure S12: Spectral decomposition of KGa-1b-700 ^{27}Al MAS NMR spectrum.

KGa-1b 800

Table S13: Parameters for KGa-1b-800 ^{27}Al MAS NMR spectral decompositions. diso is the isotropic chemical shift, C_Q is the mean quadrupolar product (GIM) and FWHM CS is the full width at half maximum of the Gaussian distribution of isotropic chemical shift.

Component	Shape	δ_{iso} (ppm)	Width (ppm)	C_Q (MHz)	FWHM CS (ppm)	Proportions (%)
Al-6	Gaussienne	3.50	12.0			0
Al-6	CzSimple	5.0		8.0	12	6
Al-5	CzSimple	37.71		9.5	15	44
Al-4	CzSimple	63.92		10.0	20	50

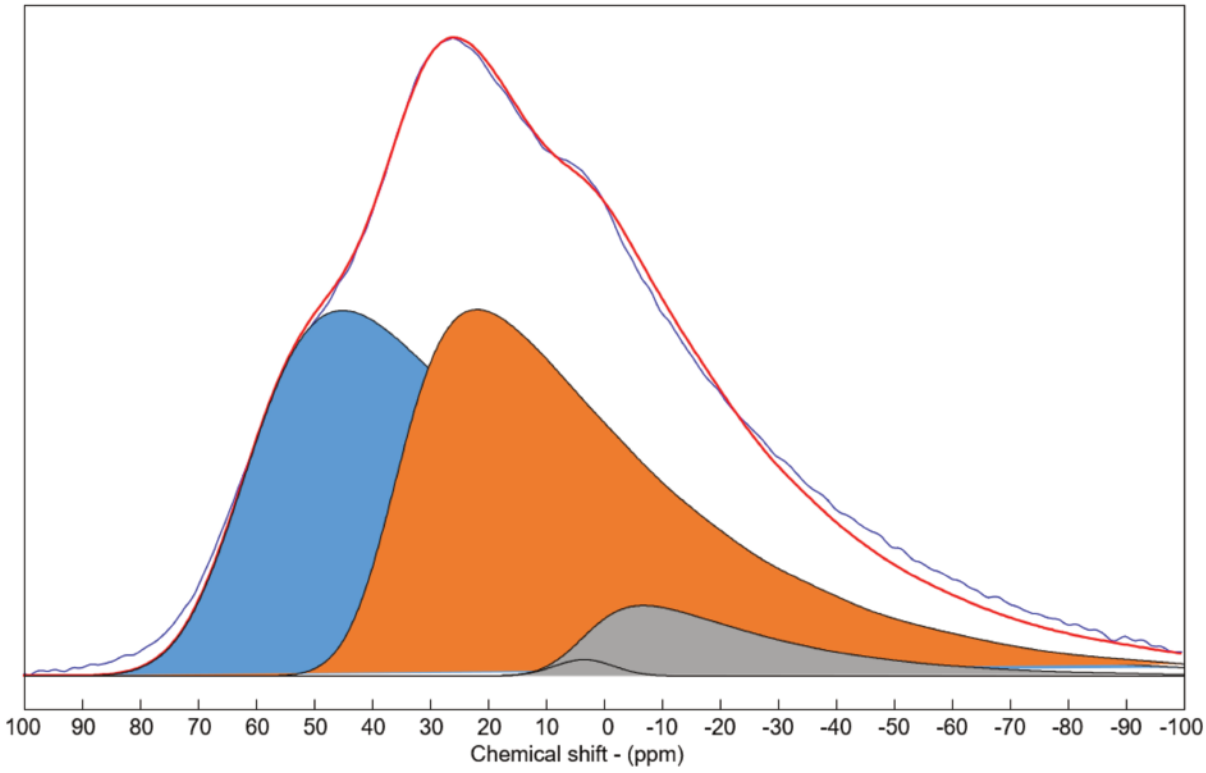

Figure S13: Spectral decomposition of KGa-1b-800 ^{27}Al MAS NMR spectrum.

KGa-1b 900

Table S14: Parameters for KGa-1b-900 ^{27}Al MAS NMR spectral decompositions. diso is the isotropic chemical shift, C_Q is the mean quadrupolar product (GIM) and FWHM CS is the full width at half maximum of the Gaussian distribution of isotropic chemical shift.

Component	Shape	δ_{iso} (ppm)	Width (ppm)	C_Q (MHz)	FWHM CS (ppm)	Proportions (%)
Al-6	Gaussienne	3.50	12.0			1
Al-6	CzSimple	5.0		8.0	12	4
Al-5	CzSimple	40.36		9.5	15	47
Al-4	CzSimple	67.55		10.0	20	48

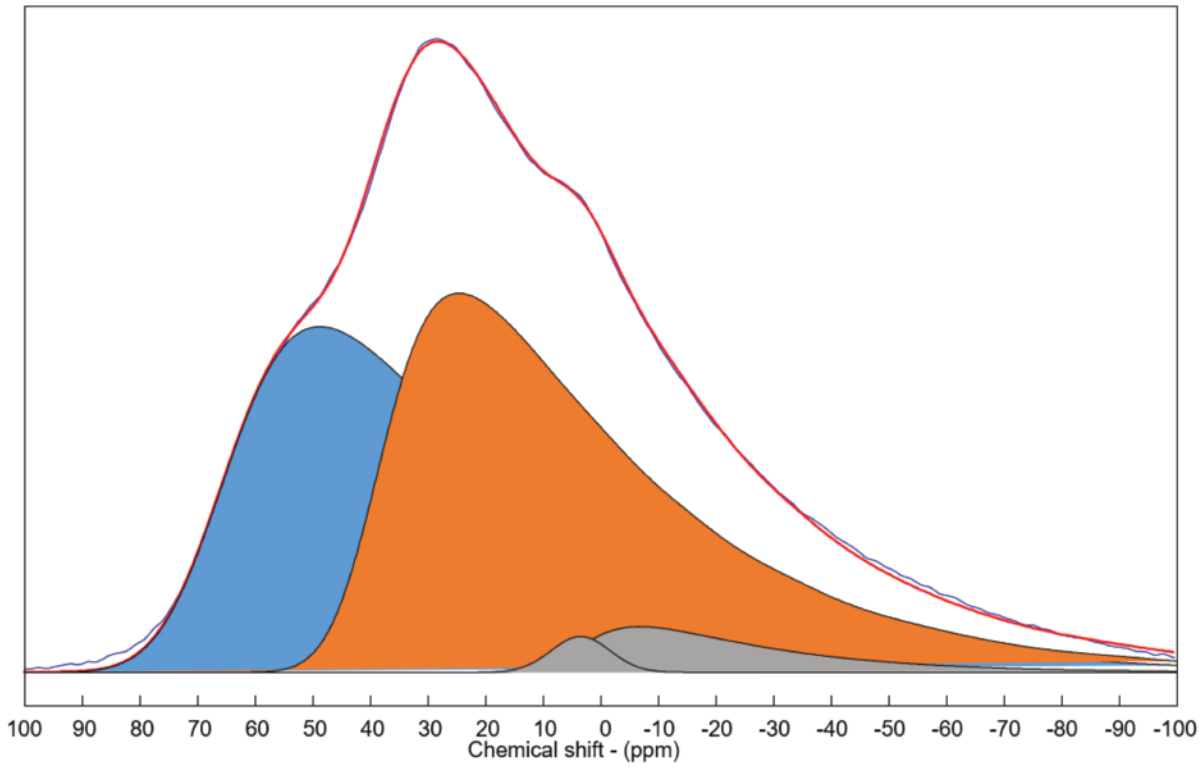

Figure S14: Spectral decomposition of KGa-1b-900 ^{27}Al MAS NMR spectrum.

References

Massiot, D., Fayon, F., Capron, M., King, I., Le Calvé, S., Alonso, B., Durand, J.-O., Bujoli, B., Gan, Z., Hoatson, G., 2002. Modelling one- and two-dimensional solid-state NMR spectra: Modelling 1D and 2D solid-state NMR spectra. Magn. Reson. Chem. 40, 70–76. https://doi.org/10.1002/mrc.984

Titre : Utilisation d'argiles et de marnes calcinées dans le développement de ciments composés.

Mots clés : argiles calcinées, pouzzolanes, ciments composés, marnes calcinées

Résumé : L'utilisation de Supplementary Cementitious Materials (SCMs) en substitution du clinker est une technologie aujourd'hui bien connue qui permet de réduire le coût environnemental du ciment. Parmi les SCMs largement utilisés on retrouve les cendres volantes, les laitiers de hauts fourneaux ou encore la poudre de verre. Dans les dernières années, un intérêt grandissant s'est développé pour l'utilisation d'argiles calcinées comme ajouts cimentaires, notamment du fait de leur forte réactivité et leur grande disponibilité. Ce projet de thèse s'intéresse à l'utilisation d'argiles et de marnes calcinées comme ajouts cimentaires. L'objectif principal est d'identifier de nouveaux échantillons susceptibles de présenter un intérêt pour une utilisation comme SCMs. Pour ce faire, une approche multi-échelle macro et micro est utilisée afin d'étudier de manière précise la calcination, la réactivité pouzzolanique et le comportement en système cimentaire de ces nouveaux échantillons. Il a été possible de démontrer que les marnes (malgré leur composition minéralogique complexe) présentent un potentiel d'utilisation comme ajout cimentaire après calcination, et ce, même avec une faible proportion d'argiles. Par la suite, il a été démontré que la palygorskite est une argile à haut potentiel pour une utilisation comme ajout cimentaire après calcination, et peut être considérée comme une alternative viable au métakaolin. L'étude poussée de l'utilisation de palygorskites calcinées comme ajouts cimentaires a également permis d'apporter de nouvelles connaissances fondamentales sur la compréhension des mécanismes impliqués lors de la calcination de ce type de matériaux.

Title : Calcined clays and marlstones as supplementary cementitious materials

Keywords : calcined clays, pozzolanes, blended cements, calcined marlstones

Abstract : The use of Supplementary Cementitious Materials (SCMs) as a substitute for clinker is a well-known technology that can reduce the environmental cost of cement. Among the SCMs widely used today are fly ash, blast furnace slag and glass powder. In recent years, there has been a growing interest in the use of calcined clays as SCMs, particularly due to their high reactivity and availability.This thesis project focuses on the use of calcined clays and marlstones as supplementary cementitious materials. The main aim is to identify new materials that could be of interest for use as SCMs. To this end, a multi-scale macro/micro approach is used to study the calcination, pozzolanic reactivity and performance in cementitious systems of these new materials. It was possible to demonstrate that marlstones (despite their complex mineralogical composition) have the potential to be used as supplementary cementitious materials after calcination, even with a low proportion of clays. Subsequently, it was shown that palygorskite is a high potential clay for use as a supplementary cementitious material after calcination, and can be considered as a viable alternative to metakaolin. The extensive study of the use of calcined palygorskites as SCMs has also provided new fundamental insights into the understanding of the mechanisms involved in the calcination of this type of material.